Receiver synchronisation techniques for CDMA mobile radio communications based on the use of *a priori* information

George Vardoulias

A thesis submitted for the Degree of Doctor of Philosophy.
The University of Edinburgh.
September 2000

Στους γονεὶς μου Γεωργία και Θανὰση

Abstract

Receiver synchronisation can be a major problem in a mobile radio environment where the communication channel is subject to rapid changes. Communication in spread spectrum systems is impossible unless the received spreading waveform and receiver-generated replica of the spreading waveform are initially synchronised in both phase and frequency. Phase and frequency synchronisation is usually accomplished by performing a two-dimensional search in the time/frequency ambiguity area. Generally, this process must be accomplished at very low SNRs, as quickly as possible, using the minimum amount of hardware.

This thesis looks into techniques for improving spread spectrum receiver synchronisation in terms of the mean acquisition time. In particular, *the thesis is focused on receiver structures that provide and/or use a priori information in order to minimise the mean acquisition time.*

The first part of this work is applicable to synchronisation scenarios involving LEO satellites. In this case, the receiver faces large Doppler shifts and must be able to search a large Doppler ambiguity area in order to locate the correct cell. A method to calculate the Doppler shift probability density function within a satellite spot-beam is proposed. It is shown that depending on the satellite's velocity and position as well as the position of the centre of the spot-beam, not all Doppler shifts are equally probable to occur. Under well defined conditions, the Doppler *pdf* within the spot-beam can be approximated by a parabola-shaped function. Several searching strategies, suitable for the given prior information, are analysed. The effects on the mean frequency searching time are evaluated.

In the second part of the thesis a novel acquisition technique, based on a fast preliminary search of the ambiguity area, is described. Every cell of the ambiguity area is examined two times. The first search is a fast straight line serial search, the duration of which is a crucial parameter of the system that must be optimised. The output of the first search is then used as *a priori* information which determines the search strategy of the second and final search. The system is compared with well known active acquisition systems and results in a large improvement in the mean acquisition time. Its performance is evaluated in Gaussian and fading Rayleigh channels.

Acknowledgements

I would like to express my gratitude to the following people:

The Eugenides Foundation, Greece, and the University of Edinburgh for providing financial support.

My supervisors, Gordon Povey and Jimmy Dripps for their help and guidance throughout my Ph.D. My deepest gratitude to Gordon, who helped me out during a difficult period.

My friends and colleagues, in the signals and systems group office for creating an enjoyable and pleasant environment. Special thanks to Apostolos Georgiadis for his invaluable help in many aspects and Nick Thomas for reviewing a large part of this work and for many thought provoking discussions.

My good friends, Barbara Mitliaga and Apostolos Georgiadis for everything we lived together during the past three years.

Nomiki Karpathiou, for her restless support and for sharing our dreams and lives.

My parents Georgia and Thanasis, for their love, guidance and support for everything I ever did. They have always been an example for me.

Declaration of originality

I hereby declare that the research recorded in this thesis and the thesis itself was composed and originated entirely by myself in the Department of Electronics and Electrical Engineering at The University of Edinburgh.

George Vardoulias

Nomenclature

A	The square root of the average power of a signal
$\{a_n\}$	An $m-$sequence
B	The bandwidth of the filter
$ci(x)$	The cosine integral
$c(t)$	The PN code
$E[\cdot]$	Mean of the quantity within the brackets
E_P	Mean of the partial correlation of an m-sequence
$E(T_{acq})$	Mean acquisition time
E_y	Mean output voltage of the FPS I-D circuit
$d(t)$	Data
F_d	Doppler shift
F_{dmin}	Minimum Doppler shift
F_{dmax}	Maximum Doppler shift
$f_{pi}(v_n)$	The pdf of the output of the I-D circuit
F_s	Doppler step in Hz
$floor(x)$	The largest integer smaller than or equal to x
H	Altitude of the satellite
H_0	State where a wrong cell is tested
H_1	State where the correct cell is tested
$H_D(z)$	Gain of the detection branch of the acquisition Markov process
$H_{FA}(z)$	Gain of the false alarm branch of the acquisition Markov process
$H_M(z)$	Gain of the miss branch of the acquisition Markov process
$H_{NFA}(z)$	Gain of the non-false alarm branch of the acquisition Markov process
h	Number of false alarms which have occurred during the acquisition
$int[x]$	The integer part of x
(i,j)	Correct detection happened during the i^{th} test of the j^{th} cell
$I_N(\cdot)$	Modified Bessel function of the first kind of order N
k, k_p	Penalty time factor
L	Period of PN code

lg	Longitude
lat	Latitude
M	Partial correlation length
$m(i,j)$	Total number of cells tested during the acquisition
n	Degrees of freedom of (non-central) chi-square pdf
$n(t)$	Noise
N_o	Noise power spectral density
$P_{aa}(K,n,\tau)$	the partial autocorrelation function of length K
$P_c(j)$	The *a priori* probability of the correct cell location
P_d	Detection Probability
P_{fa}	False Alarm Probability
P_{fr}	False Ranking Probability
P_{Fo}	Out-phase false alarm probability for the AFA system
P_{Fi}	In-phase false alarm probability for the AFA system
$P_{T_a}(t)$	The pdf of the acquisition time
$\|p\|$	Absolute phase offset in chips between the received code and the local replica
q	The length of the ambiguity area or PN code in chips
$Q(\cdot)$	Marcum's function
R_e	Radius of the Earth
R_{sb}	Radius of the spot beam
s	Doppler pdf shape factor
$si(x)$	The sine integral
T_{acq}	Acquisition time
Th	Threshold
T_c	PN code chip duration
t_1, t_2	Dwell times for the double dwell acquisition system
$V_{i,j}$	Output voltage of I-D circuit
V_n	Output voltage of I-D circuit when non-synchronised
V_P	Variance of the partial correlation of an m-sequence
V_s	Output voltage of I-D circuit when synchronised
U	Velocity of the satellite
α, β, γ	The parameters of the parabola
Γ_E	Euler's constant

γ_o	SNR at the output of the correlator
$\delta\tau$	Phase cell
δf	Doppler cell
λ	Non-centrality parameter of non-central chi-square pdf
μ	Normalised mean acquisition time
ν	State number in the ECD diagram
σ_y	Standard deviation of the output voltage of the FPS I-D circuit
θ, ϕ	Geometrical angles or signal phase
τ_d	Dwell time
τ_p	Penalty time
ω_d	Doppler frequency in radians
ω_e	Angular velocity of the Earth
ω_{IF}	Intermediate radian frequency
$\lceil x \rceil \ or \ ceil(x)$	The smallest integer greater than or equal to x
$(x)_{mod\, y}$	The remainder of the division x/y

Acronyms and abbreviations

ACQ	Acquisition
AFA	Adaptive Filter Acquisition
AWGN	Additive White Gaussian Noise
BCH	Broadcast Channel
BCZ	Broken Centre Z
BPF	Band Pass Filter
CaD	Carrier Doppler
CDA	Constant Doppler Area
cdf	Cumulative Distribution Function
CDL	Constant Doppler Line
CDMA	Code Division Multiple Access
CoD	Code Doppler
CW	Continuous Wave
DD	Double Dwell
DFT	Discrete Fourier Transform
DS	Direct Sequence
ECD	Equivalent Circular Diagram
eq.	Equation
FA	False Alarm
FDD	Frequency Division Duplex
FFT	Fast Fourier Transform
FH	Frequency Hopping
FHT	Fast Hadamard Transform
FPS	Fast Preliminary Search
3G	Third Generation
I-D	Integrate & Dump
IF	Intermediate Frequency
iid	Independent Identically Distributed
ISI	Inter-Symbol Interference

LEO	Low Earth Orbit
LMS	Least Mean Square
LPF	Low Pass Filter
MAP	Maximum a Posteriori
ML	Maximum Likelihood
MSE	Mean Square Error
MUSIC	MUltiple SIgnal Classification
NUEA	Non Uniformly Expanding Alternate strategy
OVSF	Orthogonal Variable Spreading Factor
PCCPCH	Primary Common Control Physical Channel
PCN	Partial Correlation Noise
pdf	Probability Density Function
PN	Pseudo Noise
pSCH	primary SCH
psd	Power Spectral Density
RF	Radio Frequency
SBC	Spot Beam Centre
SCH	Synchronisation Channel
SDSS	Single Dwell Serial Search
SL	Straight Line
SNR	Signal to Noise Ratio
SRS	Shift Register Sequences
SS	Spread Spectrum
sSCH	secondary SCH
SSP	Sub-Satellite point
TDD	Time Division Duplex
TDMA	Time Division Multiple Access
TDSS	Two Dwell Serial Search
UEA	Uniformly Expanding Alternate strategy
UMTS	Universal Mobile Telecommunications System
VCO	Voltage Controlled Oscillator
W-UMTS	Wideband UMTS
XWIN	Expanding Window strategy

Contents

List of figures

List of tables

Chapter 1
Introduction and theoretical background

1.1 Introduction

In order to function successfully, a receiver in a digital communication system must first synchronise itself with the incoming signal. Golomb in [8], described the synchronisation problem as "not a mere engineering detail, but a fundamental communication problem as basic as detection itself !". There are many facets to this synchronisation process. The receiver must achieve carrier synchronisation by synchronising its oscillator to the radio-frequency of the carrier signal at its input. Synchronisation in both phase and frequency is needed for coherent demodulation, while only frequency synchronisation suffices for noncoherent demodulation. Once carrier synchronisation has been achieved, the receiver attempts symbol synchronisation, i.e., the receiver determines where each symbol starts and ends so that it can sample the demodulated baseband waveform at the appropriate time instants. Since the symbols are usually grouped into codewords or frames, the receiver must also achieve frame synchronisation, that is, determine where its group starts and ends [9]. The subject of this thesis, however, is an additional task that must be performed by the receiver in any Code Division Multiple Access (CDMA) system, and that is the achievement of code synchronisation whereby the receiver synchronises its locally generated pseudonoise (PN) code (also known as the signature sequence) to the PN code of the received signal. The synchronisation process in spread spectrum systems, is one of the most crucial and difficult tasks that must be performed before communication can be established. It is often considered to be composed of two parts: acquisition and tracking. Acquisition involves a search through the region of time-frequency uncertainty and determines that the locally generated and the incoming code are closely enough aligned. Tracking is the process of maintaining alignment of the two signals using some kind of feedback loop. Usually, there are two measures of performance of the acquisition procedure, namely, the mean acquisition time and the probability of successfully acquiring the code. The mean acquisition time is well suited for commercial mobile networks where time constrains are crucial.

This work is focused on the code acquisition problem and more precisely, on the use and production of any information that can make the acquisition faster, i.e. minimise the mean acquisition time. Although code acquisition is a very important aspect, there has been very limited research efforts into using and analysing any kind of *a priori* information into the acquisition procedure. Moreover, there has been virtually no effort, as far as we know, to actually produce reliable prior information, useful for the acquisition system. This gap is what motivated us to investigate this difficult but exciting field.

When prior information is given, it is important to identify which is the optimum way of using it effectively, i.e. define searching strategies that, based on the provided information, will search for, and locate the correct cell as fast as possible. In a classic paper on optimum search processes by C.Gumacos [10], it is shown that the search strategy that minimises the mean acquisition time, is the one based on the maximum *a posteriori* (MAP) method. According to the MAP method, at any instant the search is performed on the cell which is the most likely to be the correct one based not only on the *a priori* information, but also on all decisions made up to this point of the search procedure. More precisely, the cell under test is the one that maximises the *a priori* probability multiplied by the probability that all previous tests on this cell were unsuccessful. Unfortunately, the MAP method is not practical at all and has only been used in [11] in order to evaluate other strategies. Other suboptimum search strategies were defined and analysed in [11–15]. In [14] two strategies (the Z-strategy and the expanding window) are analysed theoretically using the equivalent circular diagram (ECD) method. In [11, 15] the previous two strategies and two more powerful strategies (UEA and NUEA) are analysed using the direct approach technique. Those six papers form the basis for studying the effects of the use of prior information in the acquisition procedure.

1.1.1 Thesis objectives

So far, three probability density functions, namely the uniform, Gaussian and triangular have been used as prior information for the calculation of the mean acquisition time. The uniform pdf corresponds to the case where no prior information is provided, the triangular pdf was chosen because of its simplicity and good mathematical properties while, the Gaussian because of the powerful central limit theorem and its good properties. Nevertheless, a prior pdf which is determined by the communication system constraints, has never been derived and used in the acquisition process. Thus, at first we focused our attention on providing information that de-

rives from the specifications and characteristics of the communication system. Low Earth Orbit (LEO) satellite CDMA systems were ideal. The problem in LEOs is the large Doppler ambiguity area that has to be searched fast. This problem can be overcame by providing information about which Doppler is the most probable to occur. We were able to show that depending on the satellite's velocity and position as well as the position of the spot-beam, not all Doppler shifts are equally probable to occur. The Doppler *pdf* within the spot-beam was calculated for circular and elliptical spot beams. It was found that under some geographical conditions the Doppler pdf can be approximated by a parabola-like function with the Doppler shift corresponding to the centre of the beam, being the most probable to occur.

Next, searching strategies able of using this information effectively, had to be defined and tested. Based on the work of V. Jovanovic (direct approach) [11], the mean acquisition time of a single dwell active acquisition system, for six different strategies was calculated. Some of the basic equations of the direct approach were modified in order to reduce their computational load and time. It was shown that some of the conclusions presented in [11] that were based on the Gaussian/triangular distribution were not valid in the case of a parabolic pdf. It was also shown that a reduction of up to 20% in the mean acquisition time is feasible, when suitable searching strategies are used.

The previous work is applicable to LEO satellites only, and can provide information about the frequency but not about the time uncertainty area. It is the objective of this thesis to study methods that are able to provide prior information for every communication system (terrestrial or satellite) and for both the time and frequency ambiguity area. The fast preliminary search (FPS) system is well suited for this purpose. The idea was that every cell of the ambiguity area is examined two times. The first search is a fast straight line serial search the duration of which is a crucial parameter of the system that must be optimised. The output of the first search is then used as *a priori* information, which determines the search order of the cells during the second and final search. An FPS mode can be combined with every acquisition system and can provide information about both the time and the frequency ambiguity area, in terrestrial and satellite systems. Simple equations for the mean acquisition time were derived. The system was compared with other active acquisition systems and it was shown that it outperforms all of them, in terms of the acquisition time.

1.1.2 Thesis layout

This thesis is organised in seven chapters. In the remainder of this first chapter, the basic background for spread spectrum systems and PN code synchronisation techniques, is given.

In the second chapter, the calculation of the Doppler pdf within a LEO spot beam is described. The analytical models for a flat spot beam are briefly discussed, while the full analysis is given in appendix A. The Doppler pdf for a spherical Earth, based on simulations, is given and the condition under which the Doppler pdf can be approximated by a parabola is described.

In the third chapter, the parabolic Doppler pdf that was derived in chapter 2, is used to improve the mean PN code acquisition time. Six searching strategies are presented, analysed and simulated. Conclusions are drawn.

In the fourth chapter, the FPS system is described and a theoretical analysis for the mean acquisition time based on the direct approach is given. The problem of partial correlation is addressed for $m-$sequences and Gold codes.

In chapter five, the fast preliminary search method is compared with three systems, namely, the single dwell acquisition scheme with non uniform *a priori* information, the active double dwell straight line system and an adaptive-filter based synchronisation system.

In the sixth chapter, a brief literature review of the acquisition problem in fading channels is given, and the performance of the fast preliminary search acquisition system is evaluated in a frequency selective Rayleigh fading channel, using mainly simulations.

The final chapter summarises the work presented in the main body of this thesis, evaluates the extent to which the original goal has been accomplished and shows the contribution of this thesis to the research on the code acquisition problem.

1.2 Spread Spectrum review

Spread spectrum communications grew out of research efforts during World War II to provide secure means of communication, remote control and missile guidance in hostile environments. This work remained classified, for the most part, until the 1970s. In 1977, the first special issue of the IEEE Transactions in communications on spread spectrum appeared [16], to be followed by four more special issues and numerous papers on every aspect of the spread spectrum tech-

nology. Spread spectrum modulation refers to any modulation scheme that produces a spectrum for the transmitted signal much wider than the bandwidth of the information being transmitted *independently* of the information-bearing signal. Why would such an apparently wasteful approach to modulation be used ? There are several reasons. Among them are: (1) to provide resistance to interference and jamming; (2) to provide a means for masking the transmitted signal in the background noise in order to lower the probability of intercept by an adversary; (3) to provide resistance to signal interference from multiple transmission paths; (4) to permit the access of common communication channel by more than one user; (5) to provide a means of measuring range, or distance between two points.

After many years of strict military use, it was obvious that spread spectrum systems can have a large number of useful civilian applications. Among others is the Global Positioning System (GPS-also known by its military name NAVSTAR) which makes use of 24 satellites in 12 hour orbits spaced uniformly around the earth, to provide geodesic survey, position location for civilian vehicles including navigation aids for travellers, position location for hunters and fishermen, and position location for commercial vehicles and ships. Another application of the spread spectrum (SS) techniques that is strictly civilian is cellular mobile radio. The first cellular mobile systems were narrowband and made use of frequency division multiple access for accommodating multiple users. The last years, standards for SS-based systems have been proposed and commercial mobile radio systems using CDMA techniques are already in use (IS-95) or ready to be deployed in the near furure (UMTS, CDMA2000). A related system for which spread spectrum has been proposed as an accessing modulation is satellite-land-mobile communications. A number of such systems have been proposed and are in varying stages of development. Such systems use networks of satellites to provide world-wide communications between personal users with hand-held telephones, in some cases, and telephone booth-type facilities in other cases. Generally, connections will take place through a network of multiple satellites. At least one of these proposed systems will use spread spectrum modulation for accessing communications satellites as relays. Low Earth Orbit satellites are such an example and we will refer to them later in detail. Another developing area in which spread spectrum is expected to play a significant role is the Personal Communications Service (PCS) and Universal Personal Telecommunication (UPT) service systems. The concept behind PCS and UPT is that a person's telephone number will not be assigned to a location but rather to their person. More specifically, PCS is defined as a set of capabilities that allows some combination of terminal mobility, personal mobility and service profile management, while UPT is a service that

provides personal mobility, service profile management and involves the network capability of identifying uniquely a UPT user by means of a UPT number [17]. In what follows a more detailed analysis of spread spectrum systems and techniques is presented.

1.2.1 The transmitter

Roughly speaking a spread spectrum signal is generated by modulating a data signal onto a wideband carrier so that the resultant transmitted signal has bandwidth which is much larger than the data signal bandwidth and which is relatively insensitive to the data signal. A block diagram of the transmitter is shown in figure 1.1. In the notation used here, *u* indicates that the quantity involved should be viewed as being random in some way. Double lines in the diagram indicate in-phase and quadrature channel signals, with the in-phase channel carrying the real part of the indicated complex signal, and the quadrature channel carrying the imaginary part. Thus the transmitted signal $s(u,t)$ is viewed as the real part of the product of three complex random signals:

$$s(u,t) = Re[d(u,t)c(u,t)e^{j(\omega_o t+\phi(u))}] \tag{1.1}$$

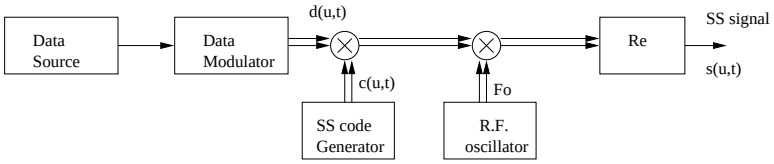

Figure 1.1: *A spread spectrum transmitter. [1]*

The expression for the SS transmitted signal $s(u,t)$ would be the same as for non-SS modulation schemes if it were not for the extra factor $c(u,t)$ which we will refer to as the *PseudoNoise code* or simply the *PN code*. By far the two most widely used SS modulation formats are the following:

- **Direct Sequence with chip time** T_c

  In direct sequence systems each data bit is encoded with the use of a spreading code that has bandwidth many times larger than that of the information. Each PN code bit is called a chip. The PN code must have a number of properties to which we will refer later. The

PN code can be expressed as:

$$c(t) = \sum_{n=1}^{N} a_n p(t - (n-1)T_c) \tag{1.2}$$

where:

$$a_n = \pm 1,\ p(t) = \begin{cases} 1 & : \quad 0 \leq t \leq T_c \\ 0 & : \quad otherwise \end{cases}$$

and N is the length or period of the PN code. The value of N depends on the communication system and can vary between hundreds and thousands of chips. Some typical values for UMTS (where N is variable) are: $N = 32, 64, 128, 256$ chips.

- **Frequency Hopping with hop time** T_c

  In frequency hopping (FH) systems, the carrier frequency of the transmitter changes (hops) in accordance with the PN code sequence. The order of the frequencies selected by the transmitter is dictated by the code sequence. The PN code is now given by:

$$c(t) = \sum_{n=1}^{N} e^{j(\omega_n t + \phi_n(u))} p(t - (n-1)T_c) \tag{1.3}$$

  where $\phi_n(u)$ is a sequence of independent random phase variables, uniform on $(-\pi, \pi)$.

The sequence a_n in the direct sequence (DS) case, or the frequency sequence ω_n in the FH case, must be agreed upon in advance by the transmitter and the receiver, and in fact have a status similar to that of a key in a cryptographic system. That is, with knowledge of the appropriate sequence, demodulation is possible and without knowledge of that sequence, demodulation is very difficult. From a cryptographic view-point, it would be nice to make the PN code purely random with no mathematical structure. However, since all systems have a finite memory constraint, all practical PN codes have some periodic structure. It is a common practise for the DS-SS systems to use one period of the spreading sequence for every bit of data.

Apart from DS and FH spread spectrum systems there are other modulation schemes, namely the *Time Hopping* as well as some *Hybrid SS systems*.

- **Time Hopping**

  In time hopping systems the period and duty cycle of a pulsed RF carrier are varied in a

pseudorandom manner under the control of a coded sequence:

$$c(t) = \sum_{n=1}^{N} p\left(t - \left(n + \frac{a_n}{M_T}\right) T_s\right) \tag{1.4}$$

Assuming that the pulse waveform $p(t)$ has duration at most T_s/M_T, time has been segmented into T_s s intervals, with each interval containing a single pulse pseudorandomly located at one of M_T locations within the interval.

- **Hybrid modulations**

  Each of the above techniques possesses certain advantages and disadvantages, depending on the system design objectives. Potentially, a blend of modulation techniques may provide better performance at the cost of some complexity. Some of the most common hybrid systems are: Direct Sequence - Frequency Hopping, Direct Sequence - Time Hopping, Frequency Hopping - Time Hopping, Direct Sequence - Frequency Hopping - Time Hopping.

1.2.2 The receiver

Neglecting interference and receiver noise, the receiver ideally is presented with a waveform $r(u,t)$ from which the data modulation $d(u,t)$ must be extracted. We assume that:

$$r(u,t) = Re[d(u,t-\tau(u))c(u,t-\tau(u))e^{j((\omega_o+\omega_d)t+\theta(u))}] \tag{1.5}$$

i.e the channel inserts a random delay and Doppler shift. This simple model is sufficient to illustrate the demodulation difficulties which the receiver encounters. A mathematical block

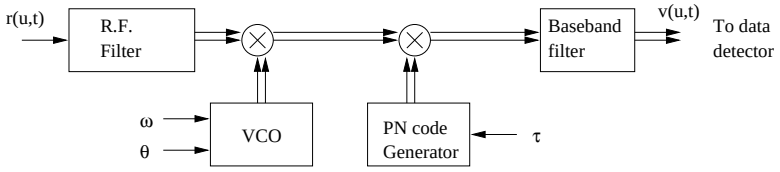

Figure 1.2: *A spread spectrum receiver. [1]*

diagram of the receiver is shown in figure 1.2. The indicated mixing operations are the receiver's attempt to first reduce the received signal to baseband and then strip the PN code from the data signal. The baseband filter can be considered to be the basic data detection filter (e.g., a matched filter in the digital signal case), possessing a bandwidth comparable to the bandwidth

of the data modulation. Assuming that the RF filter passes $r(u,t)$ without distortion, the output of the baseband filter is:

$$v(u,t) = \int_{-\infty}^{\infty} 2h(t-\alpha)r(u,\alpha)c_r^*(u,\alpha-\hat{\tau})e^{-j((\omega_o+\hat{\omega}_d)\alpha+\hat{\theta})}d\alpha \tag{1.6}$$

where $h(t)$ is the impulse response of the baseband filter, $c_r(u,t)$ is the receiver generated replica of the transmitter's PN code and $(\cdot)^*$ denotes conjugation. Assuming that second harmonics of the carrier frequency are eliminated and ideal mixing takes place, by using equation (1.5) in (1.6) we obtain:

$$v(u,t) = \int_{-\infty}^{\infty} h(t-\alpha)d(u,\alpha-\tau(u))c(u,\alpha-\tau(u))c_r^*(u,\alpha-\hat{\tau})e^{j((\omega_d(u)-\hat{\omega}_d)\alpha+\theta(u)-\hat{\theta})}d\alpha \tag{1.7}$$

The values $\hat{\omega}_d, \hat{\theta}, \hat{\tau}$ are provided by the acquisition system and the tracking loop in an attempt to align the receiver VCO and PN code generator with the corresponding received signal. When the receiver is perfectly locked and the receiver PN code is an exact replica of that transmitted, the output of the baseband filter is given by:

$$v(u,t) = \int_{-\infty}^{\infty} h(t-\alpha)d(u,\alpha-\hat{\tau})d\alpha \tag{1.8}$$

In an SS system, the signal energy in any portion of the RF spectrum is dominated by the noise energy. This fact makes it extremely difficult to first lock up the RF carrier tracking loop which supplies $\hat{\omega}_d$ and possibly $\hat{\theta}$ in the receiver, even using sophisticated loops. It seems that PN code synchronisation must be established first to concentrate the received energy in a narrow band and allow suppressed carrier tracking to be established. Many aspects of the synchronisation procedure will be discussed in detail in section 1.3.

1.2.3 The advantages of spectrum spreading

Spread spectrum systems have a number of features that make them valuable for telecommunications. Perhaps the primary motivation for utilising spread spectrum systems is that they are highly insensitive to interference (noise, intentional or unintentional jamming) and multipath distortion. A typical sequence of power spectral densities for the processing of a SS signal and a narrowband interference is shown in figure 3. The key operation is obviously the mixing pro-

cess with the PN code, which compresses the desired signal into the bandwidth of the baseband filter and simultaneously spreads the interference power. In figure 1.3, B_{bb} is the baseband

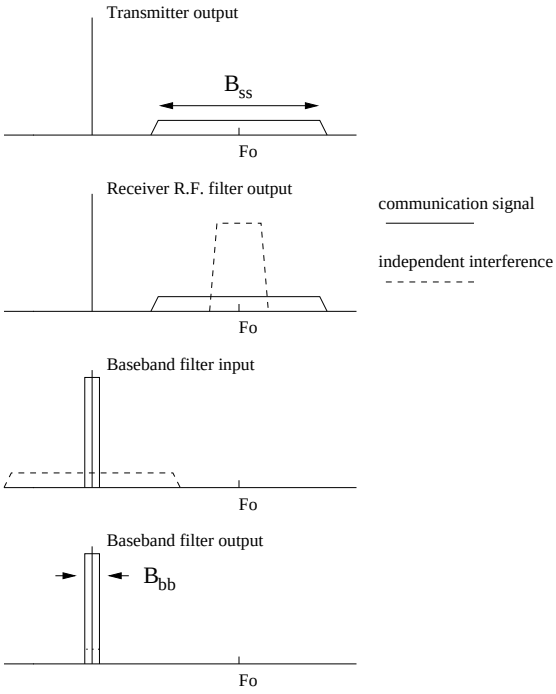

Figure 1.3: *Simplified interference rejection principle. [1]*

bandwidth and B_{ss} the bandwidth of the PN code, i.e., the SS bandwidth of the system. A very important parameter of the system is the *Processing Gain* which is defined as:

$$Processing\ Gain = \frac{B_{ss}}{B_{bb}} \tag{1.9}$$

This definition of the processing gain depends on both the modulation and coding technique, but it is used widely to characterise the SS systems. Another more fundamental definition depends on the *data rate* R_b in bits per s:

$$Processing\ Gain = \frac{B_{ss}}{R_b} \tag{1.10}$$

The latter definition may not agree with the first one but as a general comment we could say that the higher the processing gain is, the more insensitive to jamming and noise the system becomes. The processing gain of practical SS systems can be as high as 30 dB. One byproduct of SS system design with high processing gain is the *inherent nonobservability of the transmitted signal*. Suppose for example that an SS system with a 30 dB processing gain is operating with a 10 dB SNR at the output of the baseband filter. This implies that the SNR in the RF

portion of the receiver is -20 dB. Another receiver, with an identical antenna and RF section but not containing the PN code multiplier, would have an extremely difficult time determining the presence of the RF signal at -20 dB SNR. Even if it was possible, the listener could not demodulate the data without first knowing the PN code. The main advantages of spread spectrum communication systems are outlined below:

- **Jam resistance** is what made SS systems important for military purposes at first place. The anti-jam ability results from the correlation process used in spread spectrum systems and cancels out to a certain degree, any kind of uncorrelated jamming or interfering signals with a ratio depending on the processing gain of the system.
- **Low probability of intercept** i.e. it is difficult for an unintended listener to detect the signal. The signal detection problem is complicated for a surveillance receiver in two ways: (1) a larger frequency band must be monitored, and (2) the power density of the signal to be detected is lowered in the spectrum-spreading process.
- **Independent interference rejection and multiple access operation** The ability of a SS system to reject independent interference is the basis for the multiple access capability of SS systems, so called because several SS systems can operate in the same frequency band, each rejecting the interference produced by the others by a factor depending on the processing gain of the system. The asynchronous form of spectrum sharing is called *code division multiple access (CDMA)*.
- **Privacy** is obtained by using a different PN code for every user in a multiple access environment. The message can be demodulated successfully only if the receiver has knowledge of the transmitted pseudonoise code. It can easily be proven that in order to keep the data safe from unintended listeners, the data clock must be divided down from the PN clock so that possible phase change times in the data modulation line up with phase change times in the PN code modulation, so that no unscheduled phase shifts occur [1].

Spread spectrum implementation of communication systems has of course certain disadvantages, such as more complex and expensive hardware, large bandwidth requirements and the *Near-Far problem* which is an important consideration in DS/SS systems. If there is more than one active user, the transmitted power of the non-intended users is suppressed by a factor dependent on the correlation between the code of the desired user and the code of the non-intended

users. However, when a non-intended user is closer to the receiver than the desired user, it is possible that the interference caused by the non-intended user (however suppressed) has more power than the desired user. The Near-Far problem can be solved by using interference cancellers that cancel the effect of the strong unknown PN code. Another way to deal with this problem is by careful power control of mobile transmitters. The near-far problem is one of the most important issues and a very difficult problem for commercial SS systems such as the UMTS.

1.3 Principles and problems of PN code acquisition

One of the most crucial functions in any DS/SS system is the despreading of the received PN code. This is accomplished by multiplying the incoming signal by a local replica of the PN code. To achieve a proper despreading the local and received PN codes must be perfectly aligned, i.e. synchronised. The process of synchronising the two codes is accomplished in two stages:

- PN code acquisition: It is the initial coarse alignment of the two codes (typically less than a fraction -usually $1/2$- of a chip),
- PN tracking: It is the process of bringing and maintaining the two codes in fine synchronisation after the PN acquisition has been accomplished. In this thesis we focus our attention, only on the acquisition problem.

In what follows the basic concepts of PN code acquisition are presented and a classification of the receivers is performed. If the received signal is subject to high Doppler shifts, the acquisition problem becomes complicated and more sophisticated techniques are required in order to achieve fast and reliable communication. Section 1.3 presents the problems arising from extreme Doppler shifts while the basic techniques for compensating those effects are described in section 1.3.1.

1.3.1 PN acquisition: the basic concepts

PN codes are usually generated using a shift register whose contents during each time interval is some linear or nonlinear combination of the contents of the register during the preceding

time interval. For the spread spectrum system to operate efficiently, the PN code is selected to have certain desirable properties. For example, the phase of the received spreading code $c(t - T_d)$ must be initially determined and then tracked by the receiver. These functions are facilitated by choosing $c(t)$ to have a two-valued autocorrelation function as exhibited by the maximal-length sequences to be considered later. It is also desirable to employ a PN code having a very wide bandwidth. This implies that electronically simple PN code generators which can operate at very high speeds should be considered. When the SS system is used for multiple access, sets of codes $c(t)_1, c(t)_2 ... c(t)_m$ must be found which have good cross-correlation properties. When jamming resistance is a concern, PN codes must have extremely long periods and are difficult for the jammer to generate. The ideal spreading code would be an infinite sequence of equally likely random binary digits. Unfortunately, the use of an infinite random sequence implies infinite storage in both the transmitter and receiver. This is clearly not possible, so that periodic PN codes are always employed. The most widely used PN codes are the *maximal-length sequences* (m-sequences). M-sequences are a special case of Shift-Register Sequences (SRS) which are generated by shift registers as in figure 1.4

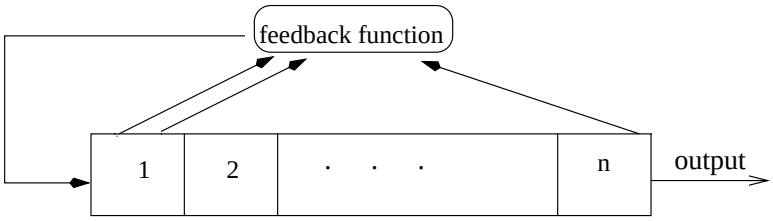

Figure 1.4: *General scheme for the production of SRS [2,3].*

The feedback function can be linear of the form $F = \sum_{i=1}^{n} c_i x_i$ where $c_i = 0$ or 1, x_i is the content of the i^{th} cell and the sum is modulo 2. Shift-register sequences having the maximum possible period ($N = 2^n - 1$) for an n-stage shift register are called m-sequences and have a number of useful properties for spread-spectrum systems. Some of them are given below [2]:

- **Property I** A maximal-length sequence contains one more one than zero. The number of ones in the sequence is $\frac{1}{2}(N + 1)$.
- **Property II** The modulo-2 sum of an m-sequence and any phase shift of the same sequence is another phase of the same m-sequence (shift and add property).
- **Property III** If a window of width r is slid along the sequence for N shifts, each r-tuple except the all zero r-tuple will appear exactly once.

- **Property IV** The most important for the PN code acquisition is that the periodic auto-correlation function $\theta_b(k) = \sum_{i=1}^{N} a_n a_{n+k}$ is two-valued and is given by:

$$\theta_b(k) = \begin{cases} 1.0 & : \quad k = lN \\ -\frac{1}{N} & : \quad k \neq lN \end{cases} \tag{1.11}$$

  where l is any integer and N is the sequence period [4].

According to equation 1.11, if long PN codes are used, the correlation between the received code and a local generated reference will be very small, unless the two codes are perfectly aligned. The calculation of the correlation of the local and received PN codes (figure 1.5) and the comparison with a pre-defined threshold is the basic technique that many DS/SS receivers use in order to detect the synchronisation condition. Unfortunately maximal-length sequences

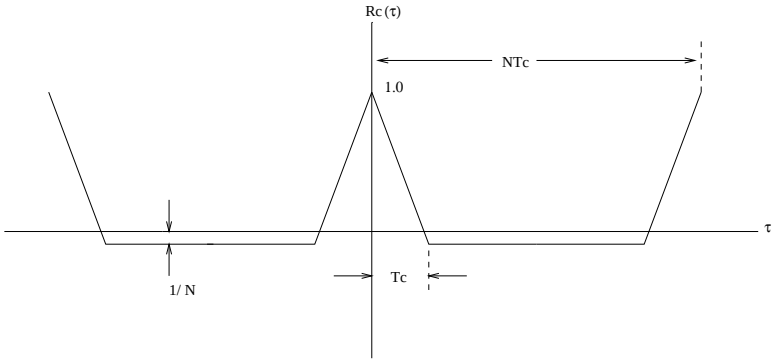

Figure 1.5: *Autocorrelation function of an m-sequence with chip duration T_c and period NT_c. [4]*

are not secure, i.e., if a jammer or intercepter can receive a relatively noise-free copy of the transmitted signal, the spreading code feedback connections and initial phase can be determined in a straightforward manner. The number of symbols that must be received without error is $2m$ where m is the number of stages of the shift register generator and $2m$ is much shorter than the period $N = 2^m - 1$ of the m-sequence. The assumption that $2m$ symbols be received without error can only be made in special circumstances so that the security of m-sequences may in fact be slightly better than theory implies.

Another family of spreading codes that is widely used is the *Gold codes*. The Gold codes were invented in 1967 specifically for multiple-access applications of spread spectrum. A goal of the spread spectrum system designer for a multiple-access system is to find a set of spreading codes such that as many users as possible can use a band of frequencies with as little mutual

interference as possible. The specific amount of interference from a user employing a different spreading code is related to the cross-correlation between the two spreading codes. Relatively large sets of Gold codes exist which have well controlled cross-correlation properties. The Gold code sets have a cross-correlation spectrum which is three-valued. The cross correlation $\theta_{b\grave{b}}(k) = \sum_{i=1}^{N} a_n \grave{a}_{n+k}$ spectrum of pairs of m-sequences can be three-valued, four-valued, or possibly many-valued. Certain special pairs of m-sequences whose cross-correlation spectrum is three-valued, where those three values are:

$$\theta_{b\grave{b}}(k) = \begin{cases} -\frac{1}{N}t(n) \\ -\frac{1}{N} \\ \frac{1}{N}[t(n)-2] \end{cases} \tag{1.12}$$

where:

$$t(n) = \begin{cases} 1 + 2^{0.5(n+1)} & for\ n\ odd \\ 1 + 2^{0.5(n+2)} & for\ n\ even \end{cases} \tag{1.13}$$

where the code period $N = 2^n - 1$, are called *preferred pairs* of m-sequences. Gold codes are families of codes which are constructed by a modulo-2 addition of specific relative phases of a preferred pair of m-sequences [5]. Gold codes are used widely in real systems such as the Tracking and Data Relay Satellite System (TDRSS-NASA) and the UMTS. Another important family of PN codes is the Kasami sequences which have optimal cross-correlation values touching the Welch lower bound [5],pg 326. Details on Kasami sequences can be found in [5]. Finally we should refer to the orthogonal codes which have zero cross-correlation. They may seem to be attractive to replace PN codes which have non-zero cross-correlations but on the other hand, the cross-correlation value is zero only when there is no offset between the codes. In fact, they have large cross-correlation values with different offsets, much larger than PN codes. The autocorrelation properties are usually not good either. The Welsh codes are an example of orthogonal codes which are generated by applying the Hadamard transform upon 0 repeatedly.

1.3.2 Basic acquisition techniques, crucial parameters and performance measures.

Let us suppose that the transmitted signal is given by:

$$s(t) = \sqrt{2S}d(t)c(t)\cos\omega_c t \tag{1.14}$$

In equation 1.14, the parameters S and ω_c stand for the waveform's average power and carrier frequency respectively, $c(t)$ is the ± 1 PN code with chip duration T_c and $d(t)$ is a binary data sequence (which might or might not be present during the acquisition mode). The received waveform is, then, given by:

$$r(t) = \sqrt{2S}d(t)c(t+\zeta T_c)\cos\left[(\omega_c+\omega_D)t+\phi\right] + n(t) \tag{1.15}$$

where $n(t)$ is Additive White Gaussian Noise, ω_D denotes the frequency offset due to the Doppler effect, ζT_c is the PN code delay with respect to an arbitrary time reference and ϕ the carrier phase offset. According to equation 1.15 the synchroniser's task is to provide the receiver with reliable estimations $\hat{\zeta}$, $\hat{\omega}_D$ and $\hat{\phi}$, of the corresponding unknown quantities so that despreading and demodulation can follow [18]. Usually the receiver assumes that there are certain bounds for both the phase and frequency offsets (denoted by ΔT and Δf respectively) which are subdivided into smaller areas $\delta T \times \delta f$. Each of the pairs $(\delta T, \delta f)$ is evaluated by attempting to despread the received signal using the central phase and frequency of the $(\delta T, \delta f)$ region. An energy detector at the despreader output measures the signal plus noise energy in a narrow bandwidth at a known frequency. If the phase and frequency of the local generated code are correct, the received signal will be despreaded, translated to the central frequency of the bandpass filter, and the energy detector will detect the presence of signal. Figure 1.6 is a block diagram of the main functions, previously described.

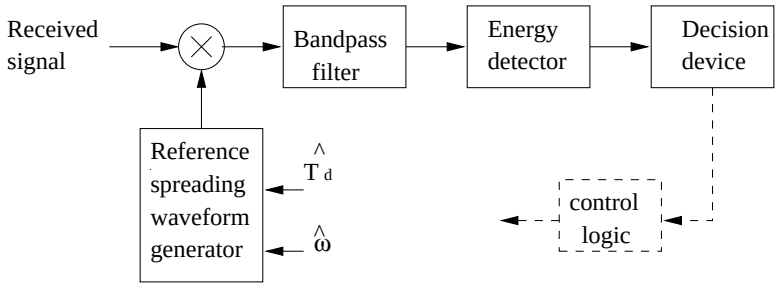

Figure 1.6: *Simplified block-diagram of a synchroniser. [4]*

Crucial parameters and performance measures: The most important parameter of interest is probably the *mean acquisition time* T_{acq} and its statistics. The mean acquisition time must be as short as possible, as communication can be accomplished only after synchronisation has been established. The time that the decision device spends examining each one of the possible uncertainty subregions $(\delta T, \delta f)$ is known as the *dwell time* τ_d. Two additional parameters are also associated with the detector performance. The *detection probability* P_d is the probability that the detector correctly indicates synchronisation when the local and the received codes are properly aligned. The *false alarm probability* P_{fa} is the probability that the detector will falsely indicate synchronisation when the two codes are actually misaligned. When a false alarm does occur it is assumed that it can be recognised and thus resuming the search for the proper cell after some time, known as *penalty time* T_p. The penalty time in some systems is random, but for simplicity reasons it is usually modelled with fixed time, multiple of the dwell time, i.e. $T_p = k\tau_d$. The detection and false alarm probabilities strongly depend on the *threshold* choice. If the threshold is too high then the P_{fa} will be low enough but at the same time the P_d is also reduced. On the other hand, a low threshold will lead to high P_d and high P_{fa}. In spread spectrum systems, usually, a Constant False Alarm Rate (CFAR) criterion is adopted according to which the threshold is set so as to maintain a fixed false alarm probability. It can be easily shown [5] that for an active implementation of the acquisition system, similar to that in figure 1.7, the set of equations that determine the threshold for a given false alarm probability is:

$$\begin{cases} P_d &= Q\left(\frac{Q^{-1}(P_{fa})-\gamma_o\sqrt{B\tau_d}}{\sqrt{1+2\gamma_o}}\right) \\ Th &= B\tau_d + \sqrt{B\tau_d}\cdot Q^{-1}(P_{fa}) \end{cases} \tag{1.16}$$

where $Q(\cdot)$ is the Marcum's function, B is the bandwidth of the bandpass filter in figure 1.6, τ_d the dwell time and γ_o is the SNR at the output of the correlator (i.e before the energy detector in figure 1.6). For a matched filter implementation of the acquisition system, the threshold Th for a given P_{fa} [19] can be set using:

$$P_{fa} = e^{-\frac{Th^2}{2\sigma^2}} \tag{1.17}$$

where σ^2 is the variance of the AWGN. We must notice that, although we will not discuss it in detail, the CFAR algorithms is a very important issue for the PN code acquisition systems. For a detailed analysis of some CFAR algorithms, see [20–22], while an adaptive scheme suitable for fading channels is described in [23]. The T_{acq} also depends on the choice of the uncertainty

regions $(\Delta T, \Delta f)$ and subregions $(\delta T, \delta f)$, as well as *the search strategy*, i.e. the procedure adopted by the receiver in its search through the uncertainty region, the choice of which is an important aspect and is well documented in the references [4, 5, 11].

Decision strategy. The decision whether the system has accomplished synchronisation or not, involves procedures that can be further categorised as follows:

- Decision rate: Correlators can be divided into *active* and *passive*. In the case of active correlators, the received PN waveform is multiplied by the local reference and, after square-law envelope detection to remove the unknown carrier phase, an integrate-and-dump device is used to make an acquisition decision by comparison with a threshold (figure 1.7). This type of correlation is characterised by the fact that the local PN generator is running continuously, and hence, a completely new set of τ_d/T_c chips of the received signal is used for each successive threshold test. There is a basic limitation in the search speed, since the local PN reference can be updated only at τ_d-s intervals. If the position update is $1/M$ chips then the search rate in chips/s (for the single dwell serial search) is:

$$R_{AC} = \frac{1}{\tau_d M} \tag{1.18}$$

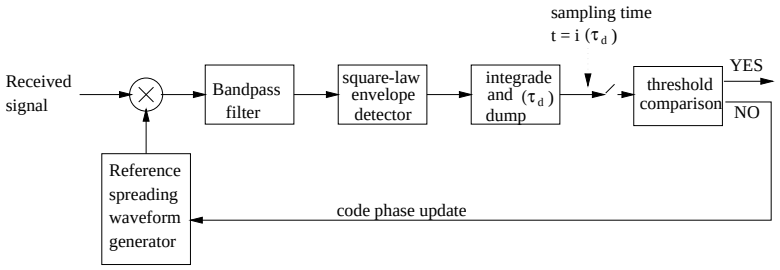

Figure 1.7: *Simplified block-diagram of an active serial search synchroniser. [5]*

A passive or matched filter correlator (figure 1.8), on the other hand can provide fast acquisition, as the search rate is highly increased compared to the active correlators. An N-chip segment of a PN waveform can be represented by the expression:

$$\sum_{n=1}^{N} c_n p(t - (n-1)T_c) \tag{1.19}$$

where:

$$c_n = \pm 1,\ p(t) = \begin{cases} 1 & : \quad 0 \leq t \leq T_c \\ 0 & : \quad otherwise \end{cases} \tag{1.20}$$

Using equation 1.19, the Fourier transform of the impulse response $h(t)$ of the matched filter is given by:

$$H(\omega) = P^*(\omega) \sum_{n=1}^{N} c_n e^{-j\omega(N-n+1)T_c} \tag{1.21}$$

where $P^*(\omega)$ is the complex conjugate of the Fourier transform of $p(t)$. Ideally the MF gives no correlation with the received code until the identical segment in the incoming code matches perfectly with the impulse response of the filter, at which moment maximum correlation occurs. A filter matched to a PN code can be implemented as an analogue taped delay line or as a digital shift register [3]. If M is the sampling rate of the waveform, the search rate (in chips/s) is now given by:

$$R_{MF} = \frac{1}{T_c} \tag{1.22}$$

which is $\frac{\tau_d}{T_c} M$ times faster then the active correlator. On the other hand, the presence of data modulation and frequency offsets can significantly deteriorate the performance of a matched filter synchronisation system. Extensive analysis of the matched filter implementation can be found in references [2, 5, 24–30]

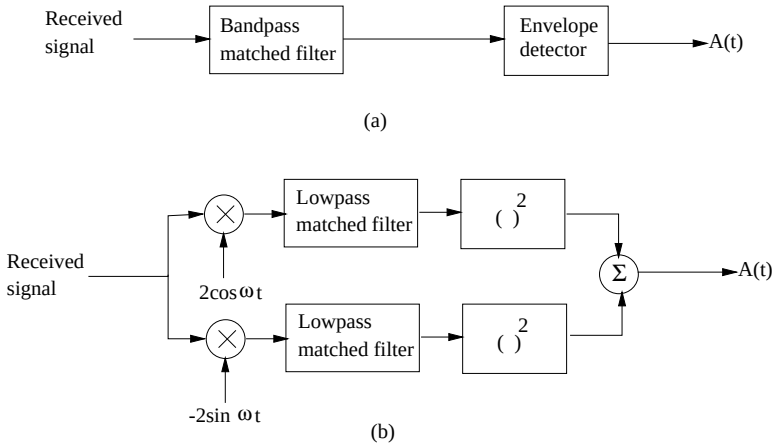

Figure 1.8: *Matched filter implementations: (a) bandpass, (b) lowpass equivalent. [4]*

- Integration time type: The observation time of the detector can either be *fixed*, or *variable*. For the category of fixed dwell time there is a further subdivision into *single dwell* and *multiple dwell* detectors. The single dwell detector will actively correlate the received signal with the local replica of the PN code and then spend a well defined time duration τ_d (the dwell time) in order to decide whether the system is synchronised or not. It is important to notice that every phase of the local PN code is examined for the same time, even though only one of them is the correct one. The statistical properties of this method are well studied [4, 5, 31, 32]. Multiple dwell detectors (figure 1.9) are based on the idea of discarding the false cell as fast as possible while not letting the P_{fa} become too large due to this fast rejection. Every cell undergoes n successive tests, each one having duration of τ_{di}, such as:

  $$\tau_{d1} \leq \tau_{d2} \leq ... \leq \tau_{dn}$$

  As soon as one of the tests fails, the detector declares out of synchronisation state and updates the phase of the local reference. If one cell succeeds in all tests, the detector declares in-synchronisation state and proceeds to the code tracking mode. A detailed analysis of multiple dwell detectors can be found in [4, 5, 31]. The multiple dwell time system uses discrete steps to increase the dwell time of each test. Another possibility is to allow the integration time to be continuous and replace the multiple threshold tests by a continuous test of a single dismissal threshold. This is a case of a variable dwell time system, known as *sequential detector* and the underlying idea is to minimise the mean time to dismiss a false cell. Thus, since all the cells, except one, are false, sequential detection can reduce the mean acquisition time. Further details about sequential detection can be found in [4, 5, 33], while a comparative evaluation of the previous methods can be found in [27]

- Search strategies: There are two straightforward ways of looking into the uncertainty area in order to locate the correct cell. The *serial* search i.e., going through every possible cell serially is the simplest method. Assuming ideal conditions ($P_d = 1$ and $P_{fa} = 0$) the worst case acquisition time will be $T_{acq} = N\tau_d$, where N is the total cell number and τ_d the dwell time. An obvious improvement to the previous method is to search all cells at the same time. This is the *full-parallel* search and the acquisition time will be $T_{acq} = \tau_d$. The main disadvantage of the serial search is that for large number of cells (as in the

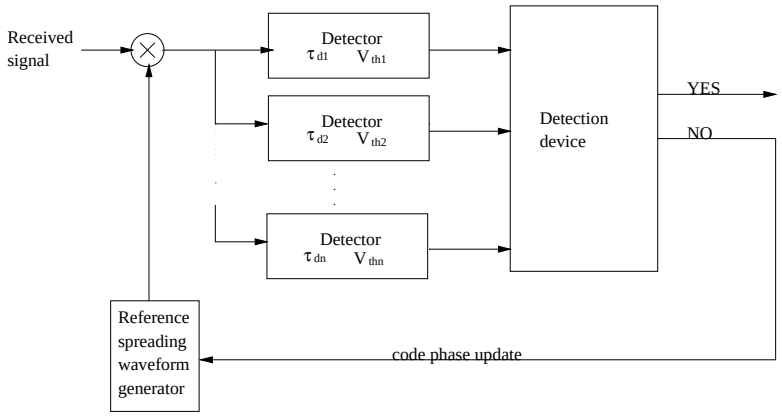

Figure 1.9: *Simplified block-diagram of a multiple dwell synchroniser [5].*

case of two-dimension search due to frequency offsets) the acquisition time can be very large. On the other hand, the full-parallel search of a two-dimension area leads to non-practical hardware complexity. A good compromise between the two previous methods is the *serial-parallel* search. For a total number of N cells to be searched, a block of $M : M \leq N$ cells is searched in parallel. If no synchronisation occurs the search phase is updated by M cells, until synchronisation occurs. The acquisition time (ideal conditions) is:

$$T_{acq} = \frac{N}{M}\tau_d \tag{1.23}$$

which is better than the serial search and the hardware complexity is lower compared to the full-parallel case. Apart from those three main techniques there are numerous special cases depending on the acquisition criterion (maximum a posteriori, maximum likelihood) and whether there is an *a priori* information about the position of the correct cell in the uncertainty area. Extensive analysis can be found: *serial* [11, 14, 31] , *parallel* [4, 5, 34] , *serial-parallel* [19, 35] , *general on acquisition techniques* [20, 21, 36–38]. In the next chapter an *a priori* probability density function of the position of the correct cell for a LEO satellite spot beam will be derived and certain search strategies suitable for this pdf will be analysed and simulated.

1.4 Doppler Effects

In order to fully describe the effects of Doppler, equation 1.15 must be modified into:

$$r(t) = \sqrt{2S}d(t)c(\frac{t}{1-\zeta'} + \zeta T_c)\cos\left[(\omega_c + \omega_D)t + \phi\right] + n(t) \tag{1.24}$$

The parameter ζ' is the received code-frequency offset (expanded or compressed PN pulse) and ω_D is the carrier-frequency offset. The rest of the symbols are defined as in equation 1.15. The sampled, baseband model of the received signal (assuming no data) can be written as:

$$r(i) = e^{j\phi}e^{-j2\pi\frac{f_c U_r}{c}iT_s}\sum_{k=0}^{L-1} c_k[(1-\frac{U_r}{c})iT_s + \tau] + n(i) \tag{1.25}$$

where U_r is the projection of the velocity of the transmitter on the line connecting the transmitter and the receiver, c is speed of light, $\frac{f_c U_r}{c}$ is the carrier-frequency offset, τ the unknown PN code phase, T_s is the sampling time ($T_s = T_c/2$) and L is the length in chips of the PN code. Equations 1.24 and 1.25 show that there are two major effects, namely:

- Carrier-frequency offset (CaD)
- Code-frequency offset (CoD)

If the CaD is small enough we can usually neglect CoD (this may not be the case in LEO satellites where both Doppler effects, are not only large but also time-varying). The main problems caused by Doppler are:

- Long-term decorrelation between the received and local generated PN code
- Prohibitively large mean acquisition time
- Decrease of the detection probability P_d
- Unpredictable search rate

It can be shown [19] that for a matched filter implementation and code length M, the normalised frequency response is given by:

$$G_D(f_D) = \frac{1}{M^2}\frac{\sin^2(\pi f_D T_c M)}{\sin^2(\pi f_D T_c)} \tag{1.26}$$

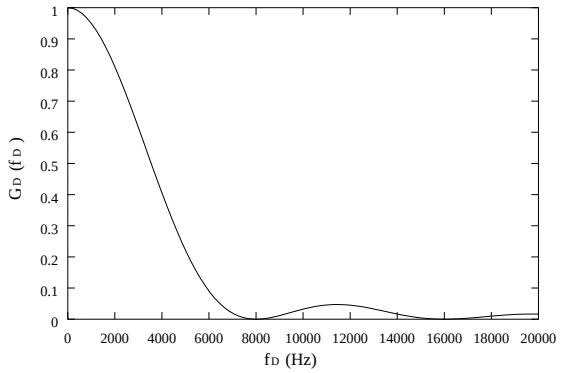

Figure 1.10: *Normalised frequency response of MF in Doppler environment.*

We can easily see from figure 1.10, which is drawn for $MT_c = 125 \cdot 10^{-3}$ s, that acquisition is impossible unless Doppler is compensated. Generally it has been shown [28] that loss of coherence between the local and received carrier frequencies over the correlation integration period (τ_i) leads to a loss given by:

$$Loss = -20\log_{10}[\frac{\sin(\pi f_D \tau_i)}{\pi f_D \tau_i}] \tag{1.27}$$

Equation 1.27 implies that there is a maximum useful length of the coherent correlation block.

Due to the CoD even if the reference and received waveforms are initially coincident (zero timing-offset), the relative time offsets will grow linearly with time, according to [39]:

$$Timeoffset \propto (N_i + i)T_s\frac{\hat{U}_{r,k} - U_r}{c} \tag{1.28}$$

where $\hat{U}_{r,k}$ is the candidate Doppler velocity and N_i the time progress in samples. Therefore when high Doppler is present the CoD causes code chip slipping during the correlation, which leads to decorrelation, resulting in reduced detection probability. Another point is that in the two-dimensional search, described in the previous section, the time offset is now time-varying and not a constant parameter. The CoD also affects the average search rate. An extreme case is when the code phase shift caused by CoD over a single dwell time is equal to the step size of the search, resulting into zero search rate. It has been shown [40] that the mean search update (μ) in chips caused by CoD is:

$$\mu = \frac{\Delta T_c}{T_c} + \tau_D \Delta f_c + k\tau_D \Delta f_c P_{fa} \tag{1.29}$$

The mean acquisition time is given by:

$$\bar{T}_{acq} = \frac{(2 - P_d)(1 + kP_{fa})}{2P_d} \frac{N\tau_D}{\frac{\Delta T_c}{T_c} + \tau_D \Delta f_c + k\tau_D \Delta f_c P_{fa}} \tag{1.30}$$

where N is the number of chips to be searched, $\frac{\Delta T_c}{T_c}$ the step size of search in fractions of a chip, Δf_c the code Doppler in chips, $\tau_D \Delta f_c$ the PN code phase shift due to CoD during dwell time, $k\tau_D \Delta f_c$ the code phase shift during hit verification. The mean acquisition time if no Doppler is present is given for comparison:

$$\bar{T}_{acq} = \frac{(2 - P_d)(1 + \kappa P_{fa})}{2P_d} \frac{N\tau_D}{\frac{\Delta T_c}{T_c}} \tag{1.31}$$

Δf_c can be negative or positive leading to an increased/decreased acquisition time. We must note that equations 1.30, 1.31 are valid under the assumption that the detection probability P_d is constant, which, as previously mentioned, is not usually the case.

In the last paragraphs of this section, the main points of all the anti-Doppler methods that have been retrieved from bibliography will be presented, highlighting the basic ideas of each technique. A very general mathematical concept on which many of the known anti-Doppler techniques are based is the *Maximum-Likelihood* (ML) criterion. According to ML criterion a search area is defined (usually two dimensional) and a statistical function depending on the correlation between the received and local generated PN codes, is calculated for every cell of the uncertainty area, following some searching strategy (ideally full parallel search). The cell that maximises the statistical function is the correct one. Referring to equation 1.24, the ML estimates of ζ, ζ' and ω_D are those who simultaneously maximise the:

$$L(\zeta, \zeta', \omega_D) = \left| \int_{T_1}^{T_2} r_o(t) c(\frac{t}{1 - \zeta'} - \zeta T_0) e^{-j\omega_D t} dt \right|^2 \tag{1.32}$$

To implement the ML criterion, the Approximate ML estimator (AMLE) has been proposed [41, 42] which approximates the operation of a two-dimensional ML estimator using a discrete correlator for delay and an FFT for frequency estimation. The all-digital implementation of the correlation will be based on the so called 'Fast Convolution' which is a fast way to calculate the correlation (which can be calculated as a convolution) between two signals, using FFT techniques, based on the fact that a convolution in the time domain is a multiplication in the frequency domain.

As mentioned before, due to carrier and code Doppler and also due to data modulation (if any) there is a maximum useful length of coherent correlation. A common way to combat the effects of decorrelation is the *coherent/incoherent correlation* method. According to this method the overall correlation is done in two parts: the first one is a linear, coherent correlation performed on relatively short code segments (short enough to consider the Doppler shifts constant over this interval) and the second one is the incoherent correlation which is the sum of the squares of the linear correlation results which is not affected by phase rotations. The final two parts correlations are used for the ML-based decision. The number of incoherent summations is limited by the fact that the squaring of the noise terms degrades the performance. Extensive analysis on the coherent/incoherent correlation can be found in [24, 43].

Matched filters are extensively used in anti-Doppler techniques resulting in improved acquisition times. In [26] four rapid code acquisition algorithms using PN matched filters have been reported. Those algorithms use the coherent/incoherent correlation method, described earlier. Two of them are fixed dwell algorithms [parallel (PL-FDD) and parallel-serial (PS-FDD)], while the other two are based on sequential detection [parallel (PL-SD) and parallel-serial (PS-SD)]. All four of them use a certain search strategy to go through the uncertainty area. They all involve the calculation of coherent partial correlations for each cell or block of cells (sections) and then an incoherent summation to calculate a final statistical quantity, upon which a decision is based.

Sequential detection in the presence of data modulation and Doppler shift has been studied in [33]. The a) ideal log-likelihood function, b) quantised log-likelihood function and c) biased square law sequential detectors were studied for a 1 kHz residual carrier Doppler frequency offset, 100 chips/s code Doppler offset, code length $L = 127$ chips and chip rate $R_c = 100$ kchips/s. It was found that high code Doppler shifts are tolerated in the absence of data modulation and residual carrier Doppler. A serious degradation of mean acquisition time was observed when data modulation and residual carrier Doppler were present.

In [39] a joint acquisition of both the time delay and Doppler velocity was attempted. A *two-dwell system*, using a short duration correlation to acquire the timing information, with a subsequent longer correlation to acquire the Doppler velocity is proposed. The joint acquisition process is modelled by a finite state Markov chain, and the performance of the system is characterised by the mean and variance of the acquisition time, which are calculated with a technique different from the well-known equivalent circular diagram [14]. A different analytical tech-

nique for evaluating mean and variance of the acquisition time, is presented. This system is not suitable for multiple-access scenarios, since the two-dwell correlator structure is highly sensitive to interference.

A *DFT technique* for measurement and correction of the carrier Doppler shift in a QPSK received signal has been presented in [44]. There are two proposed systems: The first one utilises a DFT of the input signal and estimates the Doppler shift, by the corresponding shifts of the raised cosine envelope of the DFT values, while the second system makes use of two correlators to evaluate the Doppler shift simpler and faster. A reduction in the residual Doppler shift from 5 kHz to less than about 100 Hz can be achieved in less than 3 s.

A different approach to PN acquisition, suitable for CDMA LEOS systems, has been presented in [45]. This approach is based on transforming the two-dimensional code Doppler and delay uncertainty area (D, t) into a new uncertainty region (T_c, t), where T_c is the period of the correlation pulses at the output of a sliding correlator. The basic idea is that, for each specific code Doppler D_i the interval between two correlation pulses during synchronisation, has a different value $T_{c,i}$, so by using serial or parallel search through a T_c uncertainty area we can locate the correct cell.

A different acquisition technique in high Doppler environment has been analysed in [46] according to which an FFT technique is used to estimate the Doppler offset of a *CW pilot carrier* signal which is located at the edge of the spread spectrum signal where the first null occurs. This CW signal is detected by the receiver, which estimates its frequency and hence the carrier offset. The method allows a Doppler shift compensation to within 250 Hz (with an initial Doppler shift range of $-40.1 ... 39.3$ kHz) and by using serial search method, single correlator matched to the PN code and a good urban channel model gives mean acquisition time ranging between 0.1 and 0.7 s. This method has the disadvantage of using power (CW pilot carrier) for non-data transmission.

A fast acquisition system can be derived by combining the serial-parallel architecture, described in an earlier section, with an *FFT technique* which scans all possible Doppler frequency in one dwell time by correlating the incoming signal with a set of phasors rotating at frequencies covering the range of possible Doppler shifted carrier frequencies [19, 35, 47]. The system utilises N complex correlators of length x such that $Nx = m$, where m is the length of the PN code. The output of the N correlators are fed into a N point FFT processor, the output

of which depends on the frequency difference between the local oscillator and the received signal (i.e for zero frequency difference -that is zero Doppler shift- the maximum output of the FFT is obtained from the first bin of the FFT corresponding to a zero Hz frequency offset). A maximum signal selector after the FFT processor is used to locate the correct Doppler shift.

1.5 The acquisition problem in the third generation (3G) systems

Over the past decade a significant, nearly global, effort has been made to upgrade and unify (as much as possible) the existing mobile networks. The new system, known as Universal Mobile Telecommunications System or UMTS, is a complicated mixture of proposals, standards and specifications. Many aspects of UMTS are still ambiguous or even unknown, as these lines are written. What is definitely known and well established, is that UMTS is a spread spectrum based communication system and as such, synchronisation is an important task. In what follows, we will, briefly, describe the initial synchronisation procedure in the frequency division duplex-UMTS system based on the guidelines that can be found in the 3GPP documents. The documents are publicly available at the 3GPP website: http://www.3gpp.org . Certain details and terminology of UMTS are considered to be known.

Before describing the synchronisation procedure, it is useful to define the channels and codes that are involved. The synchronisation procedure uses two channels, the synchronisation channel (SCH) and the primary common control physical channel (primary CCPCH) as depicted in figure 1.11. The SCH consists of two sub-channels: the primary SCH (pSCH) and the secondary SCH (sSCH) which are code multiplexed. The pSCH consists of a 256 chips long Gold code, the primary synchronisation code, which is transmitted at the beginning of every slot and it is the same for all the cells within the system. The pSCH is used for slot synchronisation. The sSCH consists of a repeatedly transmitted sequence of 15 codes, which are called secondary codeword. The sSCH is related to the downlink scrambling code identification. The scrambling codes are divided into 64 code groups with 8 codes in each group ($64 \cdot 8 = 512$). They are based on the Gold codes and they are assigned to each cell (each base station has its own scrambling code) at the initial deployment. They are one frame long (40960 chips=10 ms). The secondary synchronisation codes are derived from a (15,3) Reed-Solomon code over a 16-ary alphabet (made of 16 possible secondary synchronisation codes) and each codeword corresponds to a particular group of scrambling codes. As a result, the sSCH is used for frame synchronisation and code group identification. A detailed description of the channels and codes can be found

in [6, 48]. During the initial cell search the mobile station searches for the base station to which

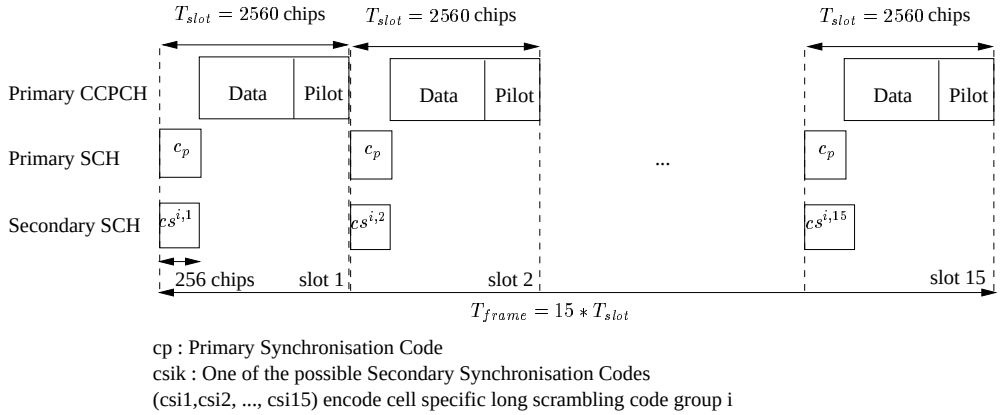

Figure 1.11: *Synchronisation and primary common control physical channel [6]*

it has the lowest path loss. It then determines the downlink scrambling code and frame synchronisation of that base station. This is accomplished in three steps:

step 1: slot synchronisation

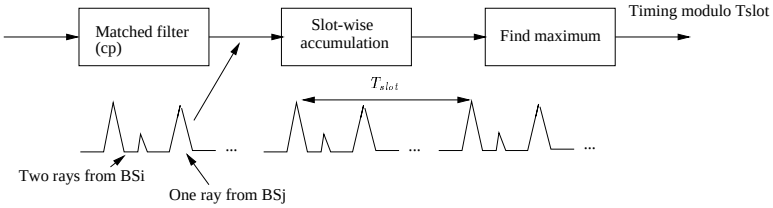

Figure 1.12: *Slot synchronisation using matched filter to the c_p [6]*

During the first step of the initial cell search the mobile uses the pSCH to acquire slot synchronisation to the strongest base station. This can be done using a matched filter (or any similar device) matched to the primary synchronisation code c_p which is common to all base stations (cells) as depicted in figure 1.12. The output of the matched filter will have peaks for every ray of each base station within range of the mobile. The position of the strongest peak gives the timing of the strongest base station modulo the slot length. Non coherent accumulation can be used to improve the reliability of the decision. The number of accumulated slots is a parameter that must be optimised as shown in [48].

step 2: frame synchronisation and code group identification

During the second step, the mobile station uses the sSCH to acquire frame synchronisation and identify the code group of the base station found in the first step. This is done by correlating the received signal at the positions of the secondary code with all possible secondary synchronisation codes and identifying the maximum correlation value. Since the cyclic shifts of the

sequences are unique the code group as well as the frame synchronisation is determined [6, 48].

step 3: scrambling code identification

During this last step of the initial cell-search procedure, the mobile station determines the exact scrambling code used by the found base station. At this point, the primary CCPCH is used and the scrambling code is identified through symbol-by-symbol correlation over the primary CCPCH with all codes of the code group identified in the second step. In order to reduce the probability of wrong/false acquisition, due to channel effects, the correlations have to be performed over a number of symbols. This third stage requires a large amount of computational power and all the relative parameters must be optimised in order to achieve small acquisition times.

Details of the optimisation analysis for all 3 stages can be found in [49], a discussion on the differences among the various code planning configurations (scrambling code allocation) in terms of various synchronisation performance parameters can be found in [50], details on the effects of the mobile station's crystal oscillator drifts as well as other practical acquisition issues for UMTS can be found in [51] and finally a more detailed description of all three initial cell search stages can be found in [6, 48].

There is a large number of papers describing PN code acquisition methods and techniques suited for DS/CDMA third generation mobile networks. We will describe and use some of these techniques during this thesis in order to compare and evaluate our results. At this point, a short reference to interesting or simply non-conventional techniques will be given. A synchronisation system based on adaptive filtering techniques is described in [52]. The LMS algorithm is used to minimise the Mean Square Error (MSE) between the filter output, and a desired response, which is chosen as the locally generated PN sequence. If convergence is detected, the delay offset is estimated from the tap number at which the tap-weight vector is peaked. We will refer to this system in a later chapter. Another adaptive technique based on the Hebb rule is described in [53]. In [54], an idea is introduced according to which, an auxiliary signal is used, as opposed to the PN signal itself, for correlation with the incoming signal. The cross-correlation function of the auxiliary and the PN signal has a triangle shape that covers the entire period of the PN signal. The method gives good performance compared to serial search active techniques. The performance of a matched filter acquisition system, with a median filter as the aiding device to cancel CW jamming in the AWGN channel is investigated in [55]. Near-far robust acquisition techniques, are described in [56, 57]. They are subspace-based, joint time-delay and frequency-shift estimation techniques where, MUSIC-type algorithms are analysed and used for code

acquisition. The use of a sequential probability ratio test for the code acquisition in chips synchronous DS/SS systems is considered in [58]. The out-of-phase sequence is modelled as a random sequence, rather than a zero sequence model. It is shown that the random sequence assumption is more accurate, (under certain conditions) than the usual zero sequence model. An interesting idea, is examined in [59] according to which, space diversity techniques are introduced to the code acquisition of a DS/SS signal. In [60] a very interesting problem, that is usually totally ignored, is addressed. The impact of the chips waveform shaping in the acquisition procedure, is investigated. Most papers assume a square pulse shape for the PN code, while in this paper five different pulse shapes are examined. For further reading on spread spectrum communications and general aspects of code acquisition, refer to [36, 61–72].

1.6 An overview of LEO satellites CDMA systems

LEO satellites will probably play a significant role in world wireless communications of the near future. LEOs are either elliptical or (more usual) circular orbits at a height of less than 2,000 km above the surface of the earth. The orbit period at these altitudes varies between ninety minutes and two hours. The radius of the footprint of a communications satellite in LEO varies from 3000 to 4000 km. The maximum time during which a satellite in LEO orbit is above the local horizon for an observer on the earth is up to 20 minutes. A global communications system using this type of orbit, requires a large number of satellites, in a number of different, inclined, orbits. When a satellite serving a particular user moves below the local horizon, it needs to be able to hand over the service to a succeeding one in the same or adjacent orbit. Further, the coverage area is subdivided among a large number of individual spot beams, rather than spread across a single broad beam. This permits the reuse of frequency channels among non-interfering beams. It also increases the gain at the transmitting antenna, thereby increasing the power received at the small hand-held terminals. But these benefits come at the cost of greater complexity in the satellites. Due to the relatively large movement of a satellite in LEO with respect to an observer on the earth, satellite systems using this type of orbit need to be able to cope with large Doppler shifts. Satellites in LEO are also affected by atmospheric drag which causes the orbit to gradually deteriorate.

The communication channel is usually modelled as a Rician fading process. The exact channel model depends on various parameters like the orbit type, atmospheric effects, terrain and elevation angle, [73–78]. From the code acquisition point of view, the main difficulty, that does not

Features	**Globalstar**	**Iridium**	**Teledesic**
Service types	voice, data, fax, paging, position location, short message service,	voice, data, fax, paging, messaging position location	voice, data, fax, voice, data, fax, paging, video
Voice (kbps)	adaptive 2.4/ 4.8/ 9.6	2.4/ 4.8	16
Data (kbps)	7.2 sustained throughput	2.4	16-2048
Modulation	QPSK	QPSK	–
Satellite lifetime - years	7.5	5	10

Table 1.1: *Services and communication-related features*

Orbits and geometry	**Globalstar**	**Iridium**	**Teledesic**
Altitude (km)	1410	780	695-705
Number of satellites	48 active 8 in-orbit spares	66 active 6 in-orbit spares	840 active up to 84 in-orbit spares
Inclination - degrees	52	86.4	98.16
Satellite visibility - min.	16.4	11.1	3.5
Minimum mobile terminal elevation angle	10	8.2	40
Min. mobile link one way propagation delay - ms	4.63	2.60	2.32
Max. mobile link one way propagation delay - ms	11.5	8.22	3.40

Table 1.2: *Orbital and geometrical features*

exist in terrestrial systems, is the large Doppler frequency [35, 45, 46, 74, 79]. Most of the time, carrier Doppler is several times higher than the bit rate so that cross-correlation function of the input signal and a local code would be significantly degraded. More details were given in an earlier section of this chapter, while in the next chapter a method of providing information for the Doppler pdf is described.

Currently there are three major commercial LEO satellites projects: Globalstar, Iridium and Teledesic. The following tables summarise the basic features of those three commercial projects. The terms **L-Band** is 0.5 to 1.5 GHz, **C-Band** is 4 to 8 GHz and **Ka-Band** is 18 to 31 GHz. All tables as well as the following two figures showing the constellations and the spot-beam patterns of two major commercial LEO projects have been retrieved from Lloyd Wood's homepage: http://www.ee.surrey.ac.uk/Personal/L.Wood/ [7] (all figures created using the SaVi software). Extensive analysis and reports on both technical and commercial subjects concerning LEO satellites can be found in [7, 80–89]. For further reading on satellite communications and digital signal processing, refer to [9, 90–96] [97–100] [101–107]

Beam and re-use characteristics	**Globalstar**	**Iridium**	**Teledesic**
Multiple access method	CDMA-FDMA FDD	TDMA-FDMA TDD	TDMA-SDMA FDMA
Beams per satellite	16	48	64 beams(supercells), 576 cells
Beam diameter - km	2254,average	600,minimum	2.9 (cell diameter)
Footprint diameter - km	5850	4700	1412
Reuse factor	768	180	2222
Satellite antenna	fixed, moving cells	fixed, moving cells	steerable, earth-fixed cells

Table 1.3: *Beam and reuse characteristics*

RF characteristics	**Globalstar**	**Iridium**	**Teledesic**
Mobile downlink frequencies - MHz	2483.5-2500.0 (S-band)	1616.0-1626.5 (L-Band)	Ka-Band
Mobile uplink frequencies - MHz	1610.0-1626.5 (L-band)	1616.0-1626.5 (L-Band)	Ka-Band
Feeder uplink frequencies - GHz	5.091-5.250 (C-band)	27.5-30.0 (Ka-Band)	Ka-Band
Feeder downlink frequencies - GHz	6.875-7.055 (C-band)	18.8-20.2 (Ka-Band)	Ka-Band
Inter-satellite link frequencies - GHz	N/A	22.55-23.550	60
Handover	yes	yes	yes
Link (fade) margins (dB)	11-16 dB equivalent margin	16 dB voice, 35 dB paging	–
Satellite output power - W	1000	1400	–

Table 1.4: *Frequencies and other RF characteristics*

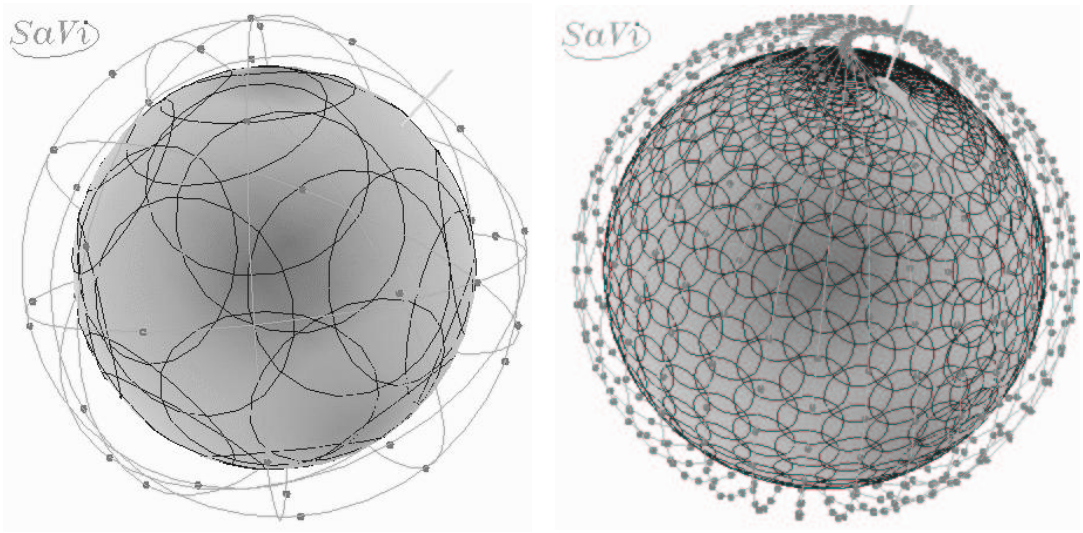

(a) *Globalstar satellites and spot-beams.*

(b) *Teledesic satellites and spot-beams.*

Figure 1.13: *Orbital representation of Globalstar and Teledesic (figures reprinted with permission from [7]).*

Chapter 2
Doppler shift Probability Density Function calculation

Initial acquisition of the PN code phase is generally the most difficult operation to be performed in any spread spectrum system. The mean acquisition time can be significantly improved if we provide the searching mechanism with some *a priori* information about the position of the correct cell in the uncertainty region. Using this information and a suitable searching strategy one can usually optimise the search and improve the statistics of the acquisition time.

In this chapter a method to calculate the Doppler shift probability density function (*pdf*) within a satellite spot-beam is presented. It is shown that depending on the satellite's velocity and position as well as the position of the spot-beam, not all Doppler shifts are equally probable to occur. The Doppler pdf within the spot-beam is a parabola-like function with the Doppler shift corresponding to the centre of the beam, being the most probable to occur.

2.1 The flat spot beam assumption

LEO satellites have large velocities due to the low altitude of the corresponding orbits. Assuming a circular orbit the velocity U is given by the formula:

$$U = \sqrt{\frac{MG}{d}} \tag{2.1}$$

where d is the distance between the satellite and the centre of the earth and the product $MG = 3.986 \cdot 10^{14}$ m^{3}s^{-2}. From equation 2.1 and assuming a maximum altitude of 2000 km, LEO satellites' velocities can be greater than 6500 m/s. Thus, for a carrier frequency of $F_c = 2.2$ GHz the Doppler shift ambiguity can be as large as ± 50 kHz and the time to locate the correct Doppler shift can be quite large. In order to minimise the search time, we try to calculate the *probability density function (pdf) of the Doppler shift within a satellite spot beam*. The basic assumption made, in order to produce a simple and usable model for the density function, is

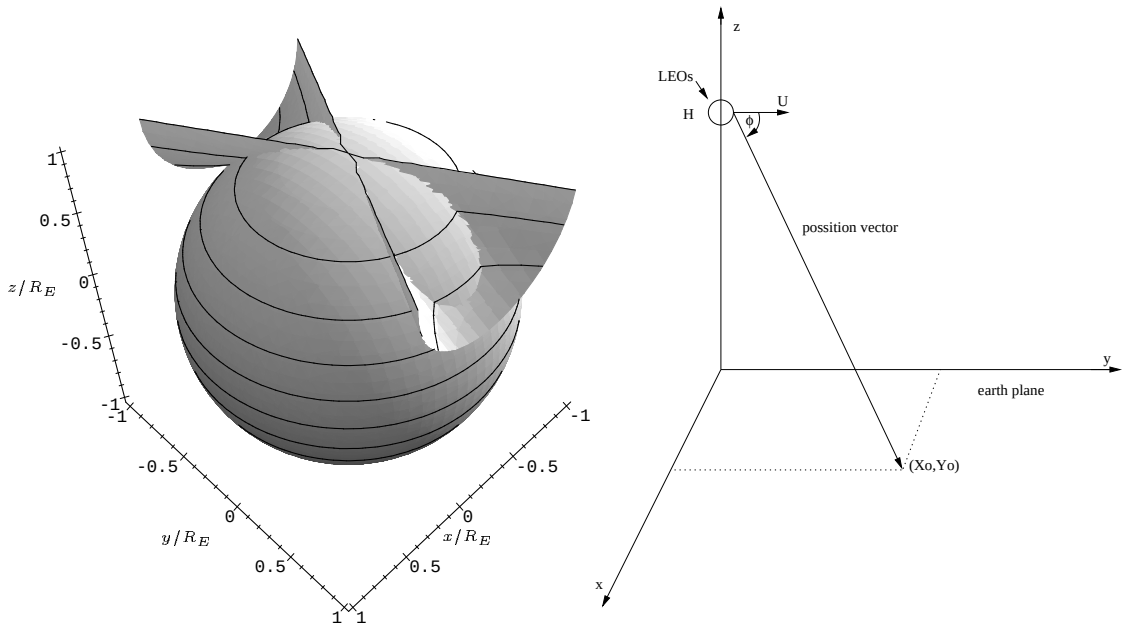

(a) *A constant Doppler cone (with axis of revolution the velocity of the satellite) and the intersection with the earth.*

(b) *Simplified geometry (flat earth) for Doppler calculation*

Figure 2.1: *Basic geometrical models for the calculation of the Doppler pdf.*

that of a flat spot beam area. The validity of this assumption for LEO systems will be discussed in the next section. We define a rectangular coordinate system (figure 2.1(b)) where the y-axis is parallel to satellite's velocity. The satellite is at $(0, 0, H)$ and (x_o, y_o) is a point on the earth which we assume to be the $z = 0$ plane [88]. The Doppler frequency at (x_o, y_o) is given by:

$$F_d = \frac{F_c U \cos(\phi)}{c} \tag{2.2}$$

where F_d is the Doppler frequency offset, F_c the carrier frequency, ϕ the angle between the velocity U and the position vector and c the speed of light. It is easy to see from equation 2.2 that all the points that belong to a conic surface with axis of revolution the line $z = H$ of the $x = 0$ plane, vertex at $(0, 0, H)$ and cone semi-angle θ, have the same Doppler shift [88] (figure 2.1(a)) which can be calculated by the equation 2.2 for $\phi = \theta$. Thus the intersection of this cone with the $z = 0$ plane (representing the surface of the earth), corresponds to constant Doppler lines (CDL) on earth (figure 2.2). It can be shown that the CDLs, corresponding to the

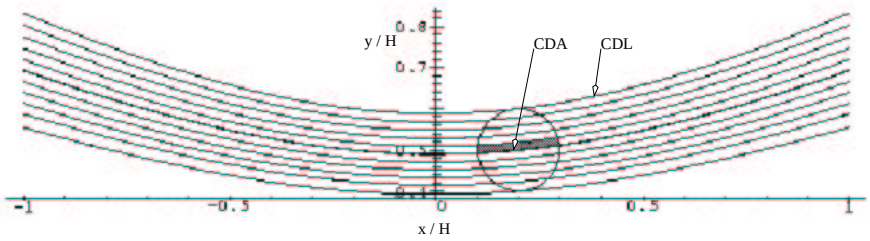

Figure 2.2: *CDLs and the corresponding CDAs. The satellite is at (0,0,750) km, the velocity U=7425 m/s, the spot beam radius is 75 km and the centre of the beam is at (150,375) km. All distances are normalised to H=1. The cone semi-angle θ varies between $\theta_{min} = 0.859$ rad and $\theta_{max} = 1.197$ rad.*

flat earth geometry previously described, are hyperbolas given by the equation:

$$x^2 + H^2 = y^2 \tan^2(\theta) \tag{2.3}$$

where θ is the cone semi-angle and H the altitude of the satellite. We assume a circular spot beam (although the same analysis applies to an elliptical beam) the centre of which is at (x_o, y_o) and that the receiver can tolerate a small Doppler shift (F_s), which is taken to be ± 250 Hz [46] for the simulations that have been performed. Thus, we can assume that all the mobile receivers which happen to be between two successive CDLs face approximately the same Doppler shift. As a result, two successive CDLs corresponding to an F_s Doppler frequency difference, define a constant Doppler area (CDA) in the spot beam as illustrated in figure 2.2. The number of CDAs defines the number of the Doppler bins to be searched. It is obvious from figure 2.2 that some CDAs are larger than others leading in a greater probability for a mobile user to be in this area and thereby greater probability for the corresponding Doppler shift to occur. The number of Doppler bins is a function of the spot beam's centre position and the Doppler step (F_s) and can be calculated by the simple formula:

$$q = \frac{F_{dmax} - F_{dmin}}{F_s} \tag{2.4}$$

where F_{dmax}, F_{dmin} are the maximum and the minimum Doppler shifts that a mobile user will have to handle in the spot beam. Those two frequencies can be calculated using equation 2.2 by substituting ϕ with θ_{min} and θ_{max} respectively. A detailed mathematical analysis of the CDL model can be found in appendix A. We must note that another assumption was made at this point. It was assumed that all mobile users are uniformly distributed within the spot beam. The

uniform distribution of the users is often used in terrestrial systems. In satellite systems, though, this assumption may not be as accurate as in the terrestrial networks. This is particularly true for spot beams with large sea-area or spot beams that include areas of very different population density. Nevertheless, it is necessary in order to get a first idea of the Doppler distribution within the spot beam and it will be used throughout this work.

The probability of each Doppler cell is calculated as a fraction of the area between the two CDLs defining the cell (figure 2.2) and the total spot beam area. The pdf is extracted by the probability curve by normalising it, so that the total area below the pdf curve is 1. Three mathematical models for the Doppler pdf have been developed, based on area calculations. In all models the hyperbolas have been replaced by straight lines (their tangents) in order to simplify the area calculations. Each model was more accurate than the previous one and the goal was to obtain a simple analytical formula for the Doppler pdf in order to use it for the calculation of the PN code acquisition time statistics. However, the area models are complicated. As a result a fourth model, that of a parabola, is being proposed. All the mathematical details of the 4 models are presented in the appendix A.

- **Model 1**: The tangents to the hyperbolas are all parallel to the x-axis. This assumption is accurate only if the spot beam centre is close to the $x = 0$ line ($x < 0.2H$).
- **Model 2**: The tangents to the hyperbolas are all parallel to each other, but form a certain angle with the x-axis. The angle is calculated (see appendix A) and used in the pdf calculations. This assumption is accurate enough for the greatest part of the x-y plane, but not when the spot beam centre is far away from the $(0, 0)$ point ($x > 0.6H$).
- **Model 3 (area model)**: The tangents to the hyperbolas are not parallel to each other any more. The angle between them is calculated and used in the pdf calculations. It is very accurate and we will refer to it as the area model.
- **Model 4 (the parabola)**: A simple analytical formula (that of a parabola) is used to fit the Doppler pdf. The parabola is not as accurate as the area model, but it is very simple and will later enable the calculation of the acquisition time statistics. This would be very difficult by using the area model because the final equation is too complicated to be used in the mean acquisition time calculations.

Figure 2.3 presents the theoretical Doppler pdf for the area model in comparison with the exper-

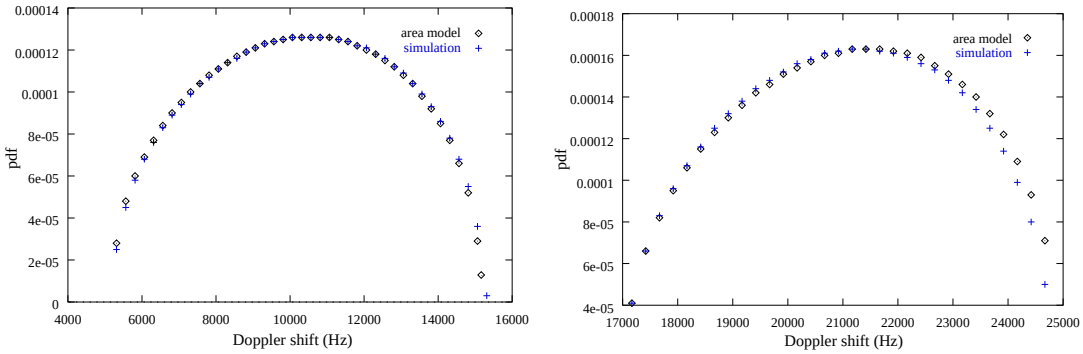

(a) *Doppler pdf results for (xo,yo)=(150,150) km.* **(b)** *Doppler pdf results for (xo,yo)=(350,350) km.*

Figure 2.3: *Doppler pdf for various spot beam centres*

imental one, generated by simulations using the geometry of figure 2.1(b). In the simulations the spot beam is replaced by a N_{tot} points grid of uniform density. The Doppler shift is calculated at each one of the grid points. If N_i points have Doppler frequencies corresponding to the i bin, then the probability of this bin is $P_i = N_i/N_{tot}$. The satellite's altitude is 750 km (which is the altitude of the *Iridium* constellation), while the spot beam radius is 75 km which is smaller than the Iridium spot beam (600 km) but almost the size of a *Teledesic* supercell (square 160 km on each size). As we can see in the figures, the area model is very accurate. The results for models 1 and 2 are not given here as they are similar to the area model, only not as accurate. It is obvious from figure 2.3(b) that the area model becomes less accurate for spot beam centres away from the sub-satellite point $(0, 0)$. This is due to the fact that the hyperbolas are not very well approximated by their tangents anymore. All simulations, under the flat earth assumption, resulted into almost symmetrical pdfs, like those in figure 2.3. Thus, it is reasonable to fit the actual pdf with a simple, symmetrical function such as the parabola. The result is depicted by the solid line in figure 2.4, where the parabola $y = \frac{(x-\alpha)^2}{4\gamma} + \beta$ fits the simulation pdf. The parabola is calculated using the Marquardt-Levenberg non-linear least squares algorithm [98]. In all cases, a parabola that fits the actual pdf accurately enough can be calculated. Thus, the parabola can be used as *a priori* information in the calculations of the mean acquisition time.

In all the previous simulations we assumed a flat circular spot beam. Nevertheless, elliptical spot beams are a better approximation of the real spot beam patterns. In order to investigate if the parabola-shaped Doppler pdf is valid for elliptical spot beams we repeat the previous simulations for the elliptical pattern. It has been found that, in all cases, the Doppler pdf can be

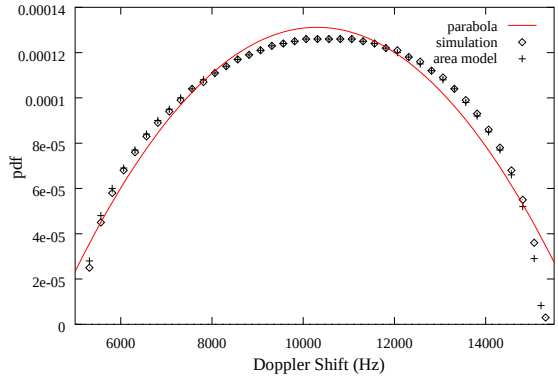

Figure 2.4: *The three Doppler pdf models. The satellite is at (0,0,750) km, the spot beam radius is 75 km and the centre of the beam is at (150,150) km.*

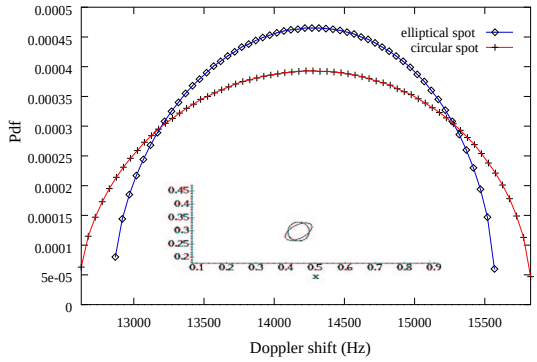

(a) *Doppler pdf results for (xo,yo)=(332,223) km,* $F_s = 250$ *Hz.*

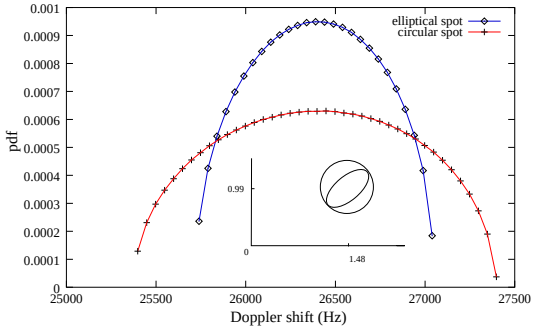

(b) *Doppler pdf results for (xo,yo)=(1110,742) km,* $F_s = 50$ *Hz.*

Figure 2.5: *Doppler pdf for elliptical and circular spot beam patterns (*$H = 750$ *km).*

modeled as a parabola-shaped function. It is worth noticing that for a given spot beam centre, in the case of an elliptical pattern beam a parabola-shaped function usually fits the actual pdf much better than in the case of a circular beam. Figure 2.5 depicts the Doppler pdf for two random spot beam centres. For each centre an elliptical and a circular spot beam have been simulated. It is obvious that the pdf for the elliptical pattern can still be approximated by a parabola-shaped function which is, of course, different form the parabola of the corresponding circular spot beam. The number of Doppler bins, F_{dmax} and F_{dmin} are also different between the two patterns, as a result of the different geometry. The geometrical figures below the pdf curves in figures 2.5(a) and 2.5(b) depict the spot beam patterns that were used in the simulations. The distances are normalised to the orbital altitude $H = 750$ km.

2.2 The validity of the flat spot beam assumption.

The basic assumption that we used so far, is that of a flat spot beam area. We did that in order to simplify the calculations and thus gain a better insight of the problem and be able to evaluate our results. Moreover, LEO satellites have relatively small footprints, due to their low altitude, and furthermore large reuse factors (see table 1.3) which means that the footprint is subdivided in a large number of sub-spot beams. The area of those spot beams seem to be small enough to allow us to consider them as being flat. Nevertheless, it is important to be able to evaluate the error introduced by the flat spot beam assumption. In what follows, we will present the results of our simulations, performed taking into account the actual spheroid shape of the surface of the earth.

In the simulations we used a perfect sphere of radius $R_e = 6480$ km the centre of which is at $(x, y, z) = (0, 0, 0)$ (referring to figure 2.1(b)). We assumed that the satellite is at $(x_s, y_s, z_s) = (R_e + H, 0, 0)$, which corresponds to $(lg_{ssp} = 0, lat_{ssp} = 0)$ degrees, where lg_{ssp} and lat_{ssp} are the longitude and latitude of the sub-satellite point respectively and H is the orbital altitude. The velocity of the satellite at $(lg_{ssp} = 0, lat_{ssp} = 0)$ degrees is taken to be $\vec{u} = u \cdot \vec{y}$. For our simulations the surface of the earth was replaced by a grid of points which are located at the intersection of parallel and meridian planes, all taken with uniform angular distance. By doing so, the grid density increases toward the poles (see [73]) but in our simulations this did not cause any inaccuracies, as we simulated spot beams located far away from the poles. Furthermore, the area of the spot beams is small enough to allow a constant grid density. Details of all the relative calculations for a non flat spot beam can be found in appendix B. Figure 2.6 depicts the Doppler shift for a random spot beam centre for a non-flat spot beam. We found out that in general, when spherical earth is considered the CDLs can still be approximated by hyperbolas (figure 2.7) but the resulting Doppler pdf is not a symmetrical function and can not be approximated by a parabola-shaped function. However, for some positions of the spot beam centres the Doppler pdf is almost symmetrical and the parabolic approximation of the pdf is still valid. We found out, that the resulting pdf can be approximated by a parabola if the difference between the spot beam latitude and the sub-satellite point latitude is large compared to the corresponding longitude difference. Thus, we defined the fraction:

$$s = \frac{|lat_{ssp} - lat_{sbc}|}{|lg_{ssp} - lg_{sbc}|} \tag{2.5}$$

where, lg_{ssp} and lat_{ssp} are the longitude and latitude of the sub-satellite point respectively

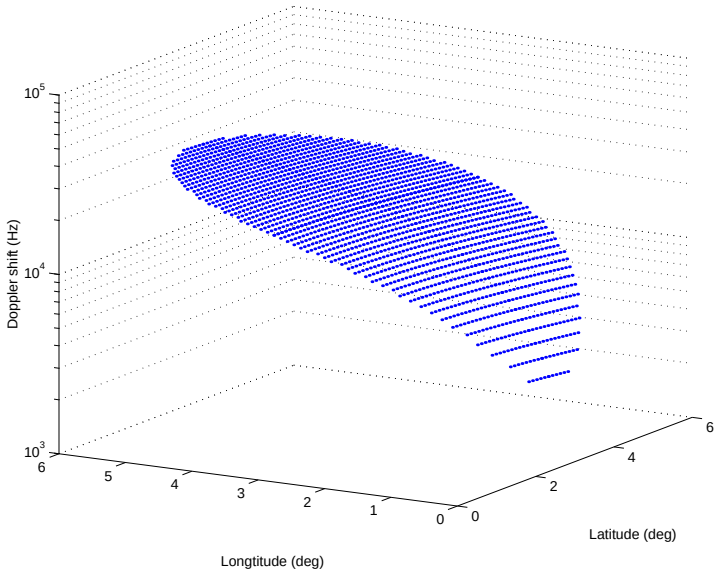

Figure 2.6: *The Doppler shifts for a spot beam when a spherical earth has been considered. The centre is at* $(lg_{sbc}, lat_{sbc}) = (3, 3)$*degrees, the orbital altitude is* $H = 780$ *km and the spot beam radius is* $R_{sb} = 300$ *km.*

while, lg_{sbc} and lat_{sbc} are the same quantities for the spot beam centre. After a large number of simulations, we concluded that an empirical rule in order to decide whether the Doppler pdf can be approximated by a parabola or not, is:

$$Doppler\ pdf = \begin{cases} parabola & : \quad if\ s > 3 \\ non\ symmetrical & : \quad if\ s < 3 \end{cases} \tag{2.6}$$

Figures 2.8 and 2.9 present various Doppler pdfs for a spherical earth and a sub-satellite point at $(lg_{ssp} = 0, lat_{ssp} = 0)$ degrees. The orbital altitude is $H = 780$ km and the spot beam radius is $R_{sb} = 300$ km (which are, approximately, the *Iridium* constellation's characteristics). In figure 2.8 the spot beam centre position result into $s > 3$ and the pdf can be approximated by a parabola. In figure 2.9 the coordinates of the spot beam centre result into $s < 3$ and the corresponding pdfs are not symmetrical. In figure 2.9(b) the spot beam centre is "behind" the satellite $(lg_{sbc} = -2, lat_{sbc} = -2)$ degrees and the negative frequencies denote the fact that the satellite is moving away from the mobile user. It is also interesting to notice that in the case of a non-flat spot beam the most probable Doppler shifts are towards the largest (in the absolute sense) frequencies.

The percentage of the spot beam for which $s > 3$, in which case the Doppler pdf can be approximated by a parabola, depends on the geographical characteristics of the area that the

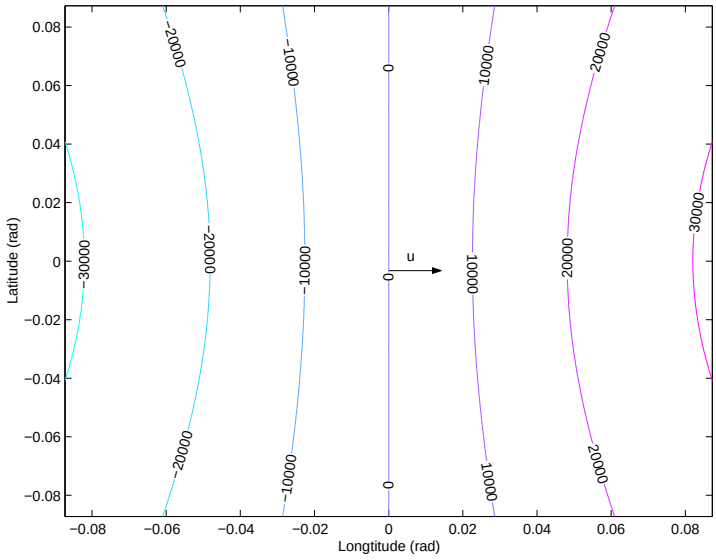

Figure 2.7: *The Doppler CDLs when a spherical earth is considered. The satellite is at* $(lg_{sbc}, lat_{sbc}) = (0, 0)$ *rad, the orbital altitude is* $H = 780$ *km. The arrow indicates the velocity of the satellite.*

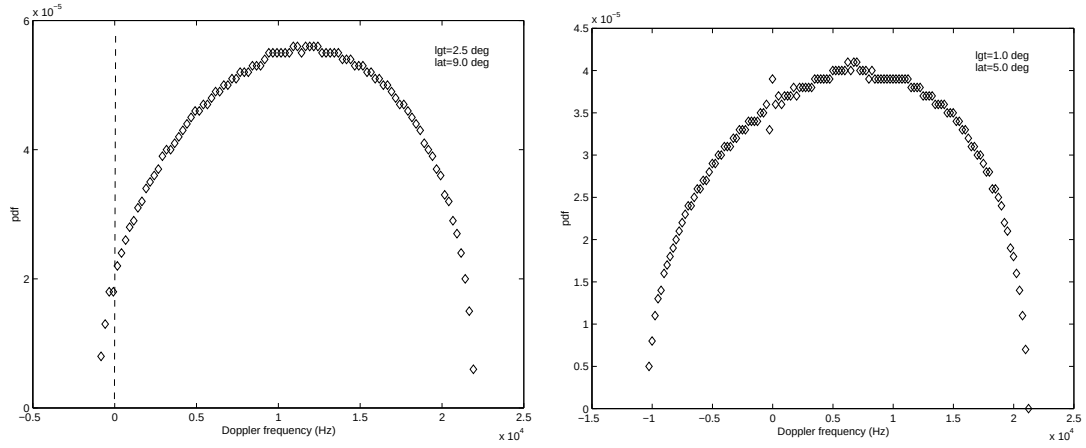

(a) *Doppler pdf for* $s = 3.6$

(b) *Doppler pdf for* $s = 5$

Figure 2.8: *The Doppler pdf for two different spot beam centres such as* $s > 3$*. A spherical earth has been considered. The orbital altitude is* $H = 780$ *km and the spot beam radius is* $R_{sb} = 300$ *km.*

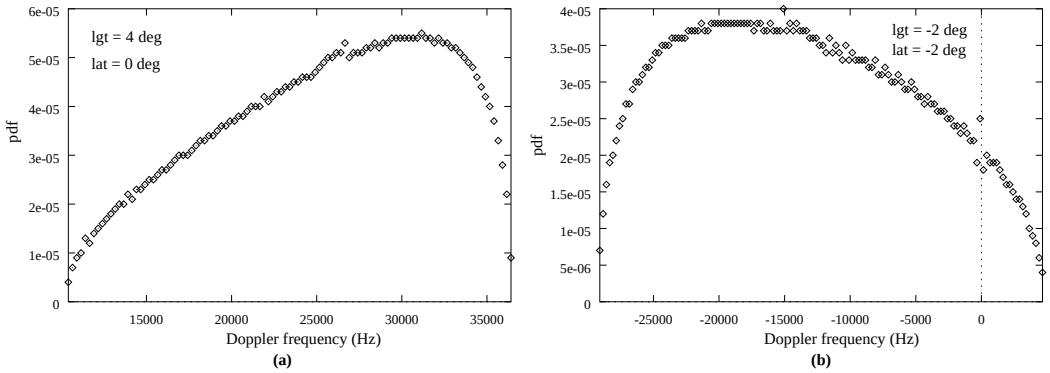

Figure 2.9: *The Doppler pdf for two different spot beam centres such as $s < 3$ ($s = 0$ for (a) and $s = 1$ for (b)). A spherical earth has been considered. The orbital altitude is $H = 780$ km and the spot beam radius is $R_{sb} = 300$ km.*

spot beam covers and the distribution of the users in this area. In fact, it is more appropriate to calculate the percentage of the users for which $s > 3$. This depends on the particular coverage characteristics of each satellite network. The percentage p_{area} of the spot beam area for which $s > 3$ is approximately $p_{area} < 20\%$ when a uniform distribution of users is assumed.

2.3 General remarks

We have to notice that all the previous results are based on ideal geometrical assumptions that do not apply on a real LEO satellite system. Besides, if a LEO operator decides to use any kind of information (Doppler pdf or any other) it would certainly base this information on real measured data and not just theoretical calculations. The author spent a considerable amount of time trying to obtain real satellite data but LEO systems are new commercial systems and of course this kind of information is either unavailable or confidential. Thus, the purpose of this work is not to provide accurate models for the Doppler pdf but to provide a reasonably accurate framework which will allow us to investigate the implications of the Doppler shifts in the synchronisation procedure and estimate the improvement, in terms of the mean acquisition time, that the use of a relative *a priori* information would offer.

Despite the simple model we used to calculate the Doppler frequencies (as presented in Appendix B.2), we must note that the results are accurate as long as we ignore the influence of the rotation of the earth on the velocity of the satellite. Our results concerning the calculation of the Doppler shift, were verified by the results presented in [86]. In [86] an accurate, analytical model is derived to calculate the observed Doppler shift for a given terminal location

and a maximum elevation angle. Although they look different, after careful examination, one can verify that equation B.7 is identical with equation 5 of [86]. Equation B.7 was derived using vector analysis and the Doppler shift is given as a function of the mobile's coordinates (x_m, y_m, z_m) relative to the earth centred fixed system. On the other hand, in [86] equation 5 was derived using trigonometric formulas for spherical triangles and the final Doppler shift is given as a function of the maximum elevation angle θ_{max} and the angle $\psi(t) - \psi(t_o)$, between the sub-satellite point N (at the time when the Doppler is calculated) and the sub-satellite point M when the satellite is at maximum elevation. In appendix B, equation 5 of [86] is reproduced and the equivalence of the two methods is proven. The only difference in our calculations is that the velocity of the satellite is calculated using equation 2.1 while in [86] the velocity is given by:

$$|U_F| \approx |U| - (R_e + H)\omega_e \cos i \tag{2.7}$$

where U can be calculated from equation 2.1, $\omega_e = 2\pi/86164.2\ \text{s}^{-1}$ is the angular velocity of the rotation of the Earth (see [108,109]), R_e is the radius of the earth, H the orbital altitude and i is the orbital inclination. For $H = 750$ km, $R_e = 6480$ km and $i = 0^o$ (worst case) the error in the velocity of the satellite introduced by the rotation of the earth is 7.64%. Thus we expect a proportional error in the Doppler shift calculation but the basic form of the resulting Doppler pdf (parabolic and non-symmetrical) will not change at all.

Finally, a very important aspect is that of the Doppler rate, i.e., the first time derivative of the Doppler shift at a given point. It is an important parameter, as it determines for how long a given pdf can be considered to be constant (time-invariant). In [74], a table of global ranges of parameters values for satellite-to-ground part parameters (at 2.2 GHz) is given. The Doppler rate range is $[-198... - 13]$ Hz/s. That means, that for a Doppler-cell size of $F_s = 250$ Hz the pdf can be considered to be time-invariant for over 1 s. As the mean acquisition time is usually expected to be shorter than 1 s, we can assume that the pdf is time-invariant and we will use this assumption for the rest of this work. If the Doppler rate is much larger than the Doppler cell, than the mobile will have to update this information and redefine its searching strategy (see next chapter). This would cause the mean acquisition time to increase and result in more complicated protocols between the satellite and mobile user.
In the next chapter, we will analyse the PN code acquisition procedure, using *the parabolic Doppler pdf*.

Chapter 3

Analysis and simulations of Searching Strategies for a parabolic *a priori* Doppler Probability Density Function in a DS/SS LEO system

In this chapter, the parabolic Doppler pdf that was derived in chapter 2 is used to improve the mean PN code acquisition time. Six searching strategies are presented, analysed and simulated using this pdf as an *a priori* information. The results are compared with the standard straight line search without any *a priori* information. The overall analysis shows that the use of the Doppler pdf combined with an appropriate search strategy can reduce the mean acquisition time significantly. The basic theoretical tools used to analyse the searching strategies and derive the mean acquisition time are presented in the first part of this chapter. Analysis and simulations of six searching strategies, namely

- The straight line with a uniform *a priori* Doppler pdf.
- The straight line with a parabolic *a priori* Doppler pdf.
- The broken centre $\mathcal{Z}$ with a parabolic *a priori* Doppler pdf.
- The expanding window with a parabolic *a priori* Doppler pdf.
- The uniformly expanding alternate (UEA) with a parabolic *a priori* Doppler pdf
- The non-uniformly expanding alternate (NUEA) with a parabolic *a priori* Doppler pdf

are presented in the second and third part, while the acquisition time pdf for every strategy, the mean acquisition time and a general discussion are given in the final section of this chapter.
Important notice: The prior information concerns the location of the frequency cell only. The time cell acquisition is not considered at all. We can consider the acquisition time to be a sum of

two terms, the first one due to the search through the time ambiguity area, and the second due to the search through the frequency ambiguity area. The purpose of this chapter is to calculate the second term and evaluate the improvement that a suitable searching strategy would introduce. We assume a straight line search through the time uncertainty area while the aforementioned strategies are applied in the frequency cell search. Thus, *the term "mean acquisition time" in this chapter, refers to the mean acquisition time of the frequency cell only*, i.e. a one dimensional ambiguity area (Doppler only) is considered for all our calculations.

3.1 General theory

As mentioned in chapter 1, communication in spread spectrum systems is impossible unless the received spreading waveform and receiver-generated replica of the spreading waveform are initially synchronised in both phase and frequency. Phase/frequency synchronisation is difficult because typical spreading waveform periods are long and bandwidths are large. Thus uncertainty in the estimated propagation delay $\hat{T}_d$ translates into a large number of symbols of code phase uncertainty. Oscillator instabilities and Doppler frequency shifts result in frequency uncertainties which must also be resolved. It is obvious that the synchroniser must perform a two-dimensional search (figure 3.1) in the $(\Delta T, \Delta F)$ area. In many cases this process must be accomplished at very low SNRs, as quickly as possible, using the minimum amount of hardware. A widely used technique for initial synchronisation, is to search serially through

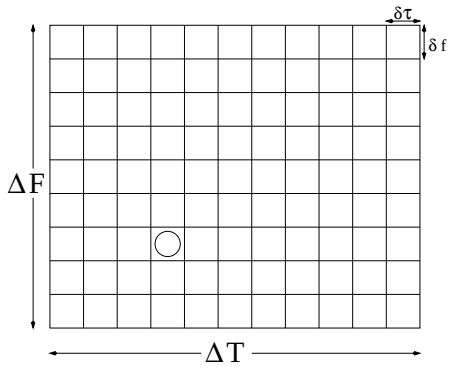

Figure 3.1: *The 2-dimensional ambiguity area*

all potential code phases and frequencies until the correct phase and frequency are identified. Each reference phase/frequency is evaluated by attempting to despread the received signal. if the estimated code phase or frequency is incorrect, the received signal will not be despread, and the reference waveform will be stepped to a new phase/frequency for evaluation. This technique

is called *serial search* and is a widespread synchronisation technique for the SS systems. All the searching strategies which will be discussed are serial search strategies. The mean acquisition time calculation requires as inputs the probability of detection, P_d, when the correct cell is being evaluated, and the probability of false alarm, P_{fa}, when an incorrect cell is being evaluated (for more details on P_d and P_{fa} see chapter 1) and the probability P_c for every cell to be the correct one (i.e. the *a priori* information for the phase/frequency cell). The number of code phases and frequencies that must be evaluated to obtain initial synchronisation is proportional to propagation delay uncertainty expressed in spreading code chips and the relative dynamics of the transmitter and receiver. Since the code chip duration is inversely proportional to the chip rate, synchronisation time is also directly proportional to the clock rate used for the spreading code generators. In what follows, we will refer only to DS/SS systems.

3.1.1 Acquisition time calculation techniques

Calculating the statistics of the PN code acquisition time can be a difficult mathematical problem. Analytical solutions and closed formulas for the mean and variance of the acquisition time can only be derived for simple cases (like the single dwell DS/SS system) and under specific assumptions which are not always close to reality (Gaussian channel, a number of approximations to the pdf of the integrator output, symmetrical *a priori* pdf). In what follows three general analytical methods are presented, (a) the *Markov chain (flow graph)* acquisition model, by Holmes and Chen [40] (b) the *Unified Approach* by Polydoros [14, 28, 31] and (c) the *direct approach*, by Jovanovic [11].

3.1.1.1 The flow graph technique

Flow graph techniques seem to have been used for the first time in spread spectrum context by Holmes and Chen in [40]. The flow graph approach is largely based on the properties of the well known signal flow graphs [110, 111] and the Markov chain theory. This was probably the first work in which a general method was used to obtain the mean and variance of the acquisition time for a single dwell DS/SS system. The acquisition process is described as a Markov chain. The Markov chain nature of the acquisition procedure is a result of the way that the output of the receiver is processed using integrate and dump methods. If the output of the noncoherent correlator receiver is greater than a predetermined value or threshold, then a "hit" is declared. If the hit corresponds to a real hit, (i.e. the correct code phase has been determined) then the

system has been synchronised and the search comes to an end. If the hit is a false alarm, there is the time loss of the verification time and then the search continues. If the output is lower than the threshold level than the search proceeds in the next cell. The most important results of this approach, which was suitable mainly for the analyses of the straight line search with a uniform *a priori* distribution were as follows:

- mean and variance of the acquisition time for the single and double dwell (immediate rejection) systems, by Holmes and Chen [40].
- pdf of the acquisition time for the single dwell system, by DiCarlo and Weber [32].
- mean and variance for the immediate rejection system with an arbitrary number of dwells, by DiCarlo and Weber [112].

That was the first general effort to model efficiently the acquisition procedure and gave good results for simple acquisition systems. However, it does not allow the analysis of more complicated systems. The following methods are more complicated but able to provide results for more sophisticated acquisition systems.

3.1.1.2 The Unified Approach (or equivalent circular state diagram)

Holmes and Chen suggested the use of the flow graph technique in the serial-dwell acquisition problem, since the underlying process of the serial search with fixed dwell times is of the aforementioned Markovian nature. However, the flow graph developed, is complicated and does not easily lend itself to generalisations. The Unified Approach provides a transform-domain framework which is formulated in a general manner that allows for significant freedom in the receiver modelling (active or passive systems, arbitrary verification logic schemes and arbitrary prior distributions). The basis of the Unified Approach is, once more, the signal flow graphs properties [110, 111]. In what follows we give the basic points of the theory which is presented in detail in [14, 28, 31] by A.Polydoros (the next paragraph is based on the original papers and therefore included in quotation marks).

"...If $|p|$ is the absolute phase offset in chips between the received code and the local replica, in what follows, H_1 denotes the hypothesis that $|p| < 1$, i.e. the codes are synchronised and H_0 denotes the alternative hypothesis where $|p| \geq 1$. The system has $\nu + 2$ states of which, $\nu - 1$ correspond to the cells belonging to hypothesis H_0, while one state corresponds to the

collective state H_1. These ν stages are indexed in a circular arrangement, with the i^{th} state ($i = 1, 2, ..., \nu - 1$) corresponding to the i^{th} cell position to the right of H_1. A segment of that circle, including the states numbered $\nu - 1$, ν, 1 and 2 is shown in figure 3.2. The two

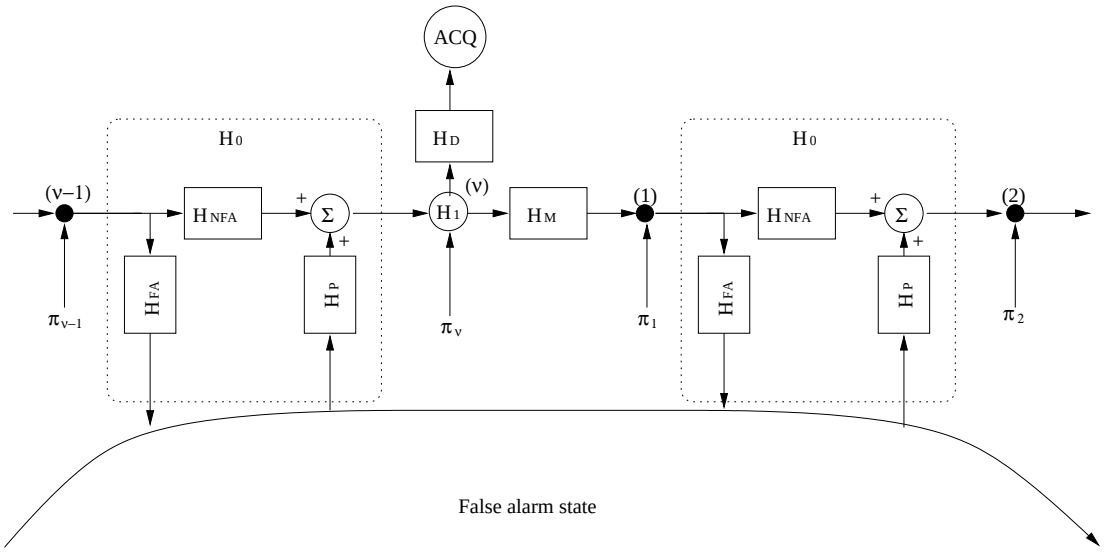

Figure 3.2: *A portion of the flow graph diagram of serial search acquisition with an arbitrary a priori distribution (π_i) and various gains*

remaining states are the correct acquisition (ACQ) and false alarm (FA) states. Entry into the search process can occur at any one of the ν states, according to some *a priori* distribution ($\pi_j, j = 1, 2..., \nu$). Total uncertainty corresponds to a uniform distribution ($\pi_j = 1/\nu;\ j = 1, 2..., \nu$). Let $p_{ij}(n)$ indicate the probability that the Markov process will move from state i to state j in n steps and let z indicate the unit-delay operator. If the unit delay specifically corresponds to τ s, z is replaced by z^τ in the following. It has been shown that the state transition diagram can be mapped to its equivalent flow graph if each transition branch from i to j in the Markovian diagram is assigned a gain equal to $p_{ij}z$, where $p_{ij} \stackrel{\text{def}}{=} p_{ij}(1)$ is the one step transition probability and z represents the unit delay associated with that transition. The *generating function* is defined as:

$$P_{ij} \stackrel{\text{def}}{=} \sum_{n=0}^{\infty} p_{ij}(n)\, z^n \tag{3.1}$$

The generating function represents the transfer function from node i to node j on the flow graph and it is useful as it contains statistical information about the Markovian process. The generating function of a system can be derived using Mason's formula [110, 111]. In figure 3.2

$H_D(z)$ is the gain of the branch leading from node H_1 (ν^{th} node) to the code ACQ; $H_M(z)$ is the gain of the branch connecting H_1 with node 1 while $H_0(z)$ is the gain of the branch connecting any other two successive nodes $(i, i+1); i = 1, ..., \nu - 1$. Furthermore, the process can move between any two successive nodes $(i, i+1)$ with $i \neq \nu$ either without false alarm [in which case the gain is $H_{NFA}(z)$] or by first reaching the FA state [branch gain $H_{FA}(z)$], then pass from FA to node $i+1$ [branch gain $H_P(z)$] so that $H_0(z) = H_{NFA}(z) + H_{FA}(z)H_P(z)$. It has been shown in [31] that the generating function $P_{ACQ} \stackrel{\text{def}}{=} \sum_{n=0}^{\infty} p_{ACQ}(n) z^n$ of figure 3.2 is:

$$P_{ACQ}(z) = \frac{H_D(z)}{1 - H_M(z) H_0^{\nu-1}(z)} \sum_{i=1}^{\nu} \pi_i H_0^{\nu-i}(z) \tag{3.2}$$

Using equation 3.2 we can easily calculate the mean acquisition time with:

$$E[T_{acq}] = \left[\frac{dP_{ACQ}(z)}{dz} \right]_{z=1} \tag{3.3}$$

Equations 3.2 and 3.3 are very general and can provide good statistical description of the acquisition process as long as the branch gains are calculated and the *a priori* distribution π_i is determined."

Our initial attempt to calculate the mean acquisition time, using various searching strategies and the parabolic *a priori* distribution was based on this method. The first strategy we tried was the *Broken/Centre Z search*. For this strategy, the search is initiated at the centre of the code phase uncertainty region and proceeds following the arrows in the manner shown in figure 3.3, i.e. it reverses direction every time the boundaries are reached. At this point the same cells are not searched twice in a row but instead, when one of the two boundaries is reached, the local code is quickly rewound to the centre and the search continues to the opposite direction. Another similar *Z-type* search, the *Continuous/Centre Z search*, does not rewind the code but goes again through the same cells on the way back to the centre. Clearly, for prior distributions which are peaked around the centre (as the parabolic we use), the Broken/Centre Z search is expected to give better acquisition performance compared with the Continuous/Centre Z search. Using the same notation as in figure 3.2 and the same indexes for the all the nodes, the parabolic *a priori*

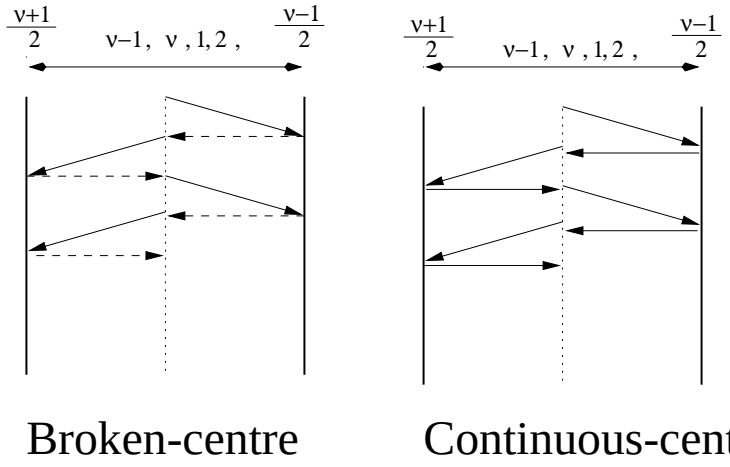

Figure 3.3: *Broken and Continuous/Centre Z search*

pdf for the Doppler shifts can be written as:

$$\pi_j = \begin{cases} \beta + \frac{(\alpha + j \cdot F_{step})^2}{4\gamma} & for\, j = 1, 2, ..., \frac{\nu-1}{2} \\ \beta & for\, j = \nu \\ \pi_{\nu-j} & for\, j = \frac{\nu+1}{2}, ..., \nu - 1 \end{cases} \tag{3.4}$$

where α, β and γ are the parameters of the parabola as defined in chapter 2. In order to correctly interpret equation 3.4 we must note that since the search is always initiated at the centre, π_j is the probability that the central (entrance) cell is not the ν^{th} (H_1) but the j^{th}; in other words, π_j stands for the probability that H_1 is actually $\nu - j$ positions to the right (if $j \geq (\nu + 1)/2$) or j positions to the left (if $j \leq (\nu - 1)/2$). It has been shown in [14] that the generating function for the Broken/Centre *Z* search, for an arbitrary prior distribution π_j is:

$$\begin{aligned} P_{ACQ}(z) &= H_D(z) \frac{\sum_{j=1}^{(\nu-1)/2} \left[\pi_{\nu-j} + \pi_j z^{T_r/\tau_d} H_0^{(\nu+1)/2}(z)\right] H_0^j(z)}{1 - z^{2T_r/\tau_d} H_M(z) H_0^{\nu}(z)} \\ &\quad + H_D(z) \frac{\pi_\nu}{1 - z^{T_r/\tau_d} H_M(z) H_0^{(\nu-1)/2}(z)} \end{aligned} \tag{3.5}$$

where T_r is the time required to rewind the code and τ_d is the dwell time. We replaced equation 3.4 in 3.5 in order to calculate the generating function for the Broken/centre *Z* with a parabolic *a priori* and then the mean acquisition time using equation 3.3. The gains we used for the calculations where:

- $H_M = (1 - P_d) z^{\tau_d}$ gain for missed verification of detection.

- $H_0 = (1 - P_{fa})z^{\tau_d} + P_{fa}z^{(k+1)\tau_d}$ total gain for not being at the right cell
- $H_D = P_d z^{\tau_d}$ gain for verification of detection

Finally, the generating function was derived, however problems arose in calculating the mean acquisition time. The reason for this was that in order to calculate the mean acquisition time using equation 3.3, the derivative of the P_{ACQ} at $z = 1$ had to be calculated. Throughout the complex calculations the term $(z - 1)$ appeared in the denominators of several fractions. When the L'Hospital rules were applied to these limits, one of them led to an infinite term in the mean acquisition time. Apart from this, it became obvious that the calculations were far too complicated and time consuming. As more advanced searching strategies were described by more complicated circular diagrams and generating functions, there was no choice other than to look for a simpler, general method that would not make use of state diagrams, but instead would utilise direct mathematical methods to calculate the pdf and moments of the acquisition time.

3.1.1.3 The direct approach

In this section, the *direct approach* to obtain statistics of the code acquisition time for serial-search spread spectrum receivers will be presented. In respect to the flow graph and the equivalent circular state diagrams, the main difference comes from the fact that the search strategy is characterised algebraically, and not by using any kind of state graphs. The method also makes use of the generating function concept, combining combinatorial arguments with the transform-domain methods. The *direct approach* is presented in detail in [11, 15] while an earlier similar work by H.Meyr and G.Polzer can be found in [113]. In what follows the basic ideas will be given, and all the equations used to simulate the searching strategies will be analysed in detail (the next paragraph is based on the original paper and therefore included in quotation marks).

"..Assuming that there are q possible cells in the uncertainty region, with only one correct cell, the acquisition problem can be regarded as the problem of finding the correct one with the aid of a synchronisation detector characterised by its probability of correct detection P_d and false alarm P_{fa}. During the search, we thus have three possible outcomes of the tests and three (generally random) times associated with them: T_r which is the time required for the rejection of the incorrect cell (including the eventual "penalty" time τ_p introduced by the verification logic in the case of the false alarm) T_m which is the time required for the false dismissal of the

correct cell and T_d which is the time required for the correct detection. The functional $m(i,j)$ is defined as the total number of cells tested during the acquisition under the assumption that the correct location is in the cell marked with $''j''$ and that the correct detection happened during the i^{th} test of the j^{th} cell. This functional is determined by the searching strategy and must be calculated for each one separately, as will be shown later. With the functional $m(i,j)$ thus defined, we next note that the acquisition time conditioned on events i and j is a sum of the times required for $m(i,j)-i$ tests of the incorrect cells, $i-1$ tests of the correct cell that ended unsuccessfully and the last (successful) test. Using combinatorial arguments and properties of the generating function one can show that the pdf of the acquisition time is given by ([11]):

$$\begin{aligned} P_{T_a}(t) &= \sum_{i=1}^{\infty} P_d(1-P_d)^{i-1} \sum_{j=1}^{q} P_c(j) \sum_{h=0}^{m(i,j)-i} \begin{pmatrix} m(i,j)-i \\ h \end{pmatrix} \\ &\quad \cdot P_{fa}^h (1-P_{fa})^{m(i,j)-i-h} \delta(t - m(i,j)\tau_d - h\tau_p) \end{aligned} \tag{3.6}$$

where the parameter h accounts for the number of false alarms which have occurred during the acquisition and $P_c(j)$ represents the *a priori* probability of the correct cell location. Using equation 3.6, we can calculate the probability that the acquisition occurred after searching $m(i,j)$ cells (at the $m(i,j)$ acquisition occurred) during which $i-1$ times the search failed to detect the correct cell (and the i^{th} finally did) which is located at the j^{th} cell (out of q that the uncertainty area contains) and during the search procedure h false alarms occurred. The Dirac function is used to show that decisions about whether the code is synchronised or not, are made only at specific time points. It is convenient to rewrite equation 3.6 in the equivalent form ([11]):

$$\begin{aligned} P_{T_a}(t) &= \sum_{m=1}^{\infty} P_d(1-P_d)^{i(m)-1} P_c[j(m)] \sum_{h=0}^{m-i(m)} \begin{pmatrix} m-i(m) \\ h \end{pmatrix} \\ &\quad \cdot P_{fa}^h (1-P_{fa})^{m-i(m)-h} \delta(t - m\tau_d - h\tau_p) \end{aligned} \tag{3.7}$$

where the new functionals $j(m)$ and $i(m)$ are introduced, showing that in the m^{th} step of the search, the cell marked with $''j''$ is tested for the i^{th} time. Again $j(m)$ and $i(m)$ are determined by the searching strategy. It should be noted at this point that it is $j(m)$ that completely determines the search procedure so that $i(m)$ can always be evaluated when $j(m)$ is given, although this dependence may be implicit. If we are interested in the explicit solution $P_{T_a}(t)$ for any given t then equations 3.6 and 3.7 will not give a closed-form result (equation 3.7 for

instance represents a series of Dirac's impulses for various i, j and h, and one has to find out which are to be taken into account for any particular t). The situation is simpler if the quotient τ_p/τ_d is an irrational number, in which case no two Dirac's pulses can be overlapping. In that case, $P_{T_a}(t) = 0$ for all $t \neq \alpha\tau_d + b\tau_p$ where α and b are integers such that $\alpha - i(\alpha) \geq b$ (this last condition comes from the fact that the number of false alarms (b) cannot exceed the total number of incorrect cells tested ($\alpha - i(\alpha)$)). In this case equation 3.7 becomes:

$$P_{T_a}(t) = \begin{cases} P_d(1-P_d)^{i(\alpha)-1} P_c[j(\alpha)] \begin{pmatrix} \alpha - i(\alpha) \\ b \end{pmatrix} P_{fa}^b (1-P_{fa})^{\alpha - i(\alpha) - b} & , t = \alpha\tau_d + b\tau_p \\ 0 & , otherwise \end{cases} \tag{3.8}$$

Unfortunately, the penalty time τ_p is always modelled as an integer multiple of the dwell time τ_d, i.e. $\tau_p = k\tau_d$. As a result some of the impulses will be overlapping for every t which is an integer multiple of the dwell time τ_d. In order to extract the terms in equation 3.7 which should be summed for some particular $t = n\tau_d$ (at this point it is helpful to normalise all times to τ_d and work with discrete pdf $P_{T_a}(n)$), we have $\alpha = n - bk$ and need to sum all terms for which b satisfies:

$$n - bk - i(n - bk) \geq b \tag{3.9}$$

and thus $P_{T_a}(n)$ becomes:

$$\begin{aligned} P_{T_a}(n) \quad = \quad & \sum_{b=0}^{b_{max}} P_d(1-P_d)^{i(n-bk)-1} P_c[j(n-bk)] \begin{pmatrix} n - bk - i(n-bk) \\ b \end{pmatrix} \\ & \cdot P_{fa}^b (1-P_{fa})^{n-bk-i(n-bk)-b} \end{aligned} \tag{3.10}$$

where b_{max} is the maximum b which satisfies equation 3.9. Equation 3.10 represents the most general solution for the pdf of any single dwell acquisition system, with arbitrary search strategy and arbitrary *a priori* distribution."

A very convenient alternative for the numerical calculation of the array $P_{T_a}(1), P_{T_a}(2), ..., P_{T_a}(n_{max})$

starts directly from the discrete version of equation 3.7:

$$P_{T_a}(n) = \sum_{m=1}^{\infty} P_d(1-P_d)^{i(m)-1} P_c[j(m)] \sum_{h=0}^{m-i(m)} \begin{pmatrix} m-i(m) \\ h \end{pmatrix} \cdot P_{fa}^{h}(1-P_{fa})^{m-i(m)-h}\delta(n-m-hk) \tag{3.11}$$

In what follows, equation 3.11 is used to calculate the pdf of the acquisition time for different searching strategies. In all cases the first summation was calculated for an appropriate m_{max}. Finally the mean acquisition time can easily be calculated as:

$$E(T_a) = \sum_{m=1}^{\infty} P_d(1-P_d)^{i(m)-1} P_c[j(m)] \cdot ([m-i(m)]E(T_r) + [i(m)-1]E(T_m) + E(T_d)) \tag{3.12}$$

where $E(T_r)$, $E(T_m)$, $E(T_d)$ are the expected values of T_r which is the time required for the rejection of the incorrect cell, T_m which is the time required for the false dismissal of the correct cell and T_d which is the time required for the correct detection, respectively. In the special case of a single dwell acquisition system we have:

$$\begin{aligned} E(T_m) &= E(T_d) = \tau_d \\ E(T_r) &= \tau_d + P_{fa}\tau_p \end{aligned} \tag{3.13}$$

3.2 Analysis of searching strategies

Equation 3.11 is the general acquisition time pdf solution which will be used for some of the searching strategies. The distinctive characteristic of every strategy are the functionals $j(m)$ and $i(m)$ which have to be calculated. The two functionals show that the correct position is the j^{th} cell and was detected at the m^{th} overall step. The detector had to look i times at the correct cell. In what follows the *a priori* probabilities $P_c[j(m)]$ and the functionals $j(m)$ and $i(m)$ are presented for each strategy. All the analysis presented in the rest of this chapter, concerns a single dwell acquisition system like the one in figure 1.7.

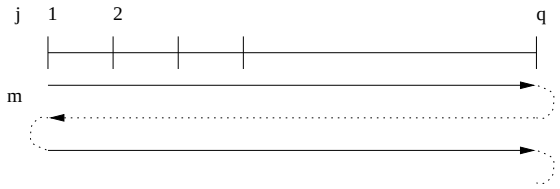

Figure 3.4: *The straight line search through the q Doppler bins*

3.2.1 Strategy 1: Straight line with a uniform *a priori* Doppler pdf

Straight line search is the simplest method to go through the uncertainty area, simply examining one cell after another until the correct one is detected, as depicted in figure 3.4. In appendix A the number of Doppler bins N_D (or q) that have to be searched are calculated for every position of the spot beam centre (equation A.9). A uniform *a priori* means that all Doppler bins are equiprobable and thus:

$$P_c[j(m)] = \frac{1}{N_D} \tag{3.14}$$

The functionals $j(m)$ and $i(m)$ for the straight line search are easily found to be:

$$j(m) = (m)_{mod\, q} \tag{3.15}$$

$$i(m) = int\left[\frac{m-1}{q}\right] + 1 \tag{3.16}$$

where $(M)_{mod\, N}$ is the remainder of the division M/N, and $int[x]$ denotes the integer part of x. The straight line search with a uniform *a priori* Doppler pdf will be used to compare it with the straight line search with a parabolic Doppler pdf in order to see if the *a priori* information itself can improve the mean acquisition time without utilising any advanced searching strategy.

3.2.2 Strategy 2: Straight line with a parabolic *a priori* Doppler pdf

The straight line search is now utilised but this time using the parabolic *a priori* Doppler pdf (figure 3.5(a)). The functionals $j(m)$ and $i(m)$ are given by equations 3.15 and 3.16 since the strategy is the same, only the prior distribution has changed. Using the same notation as in appendix A it is convenient to write the parabolic distribution as:

$$P_{dp}(j) = \frac{(F_{dmin} + j \cdot F_{step} - \alpha)^2}{4\gamma} + \beta \tag{3.17}$$

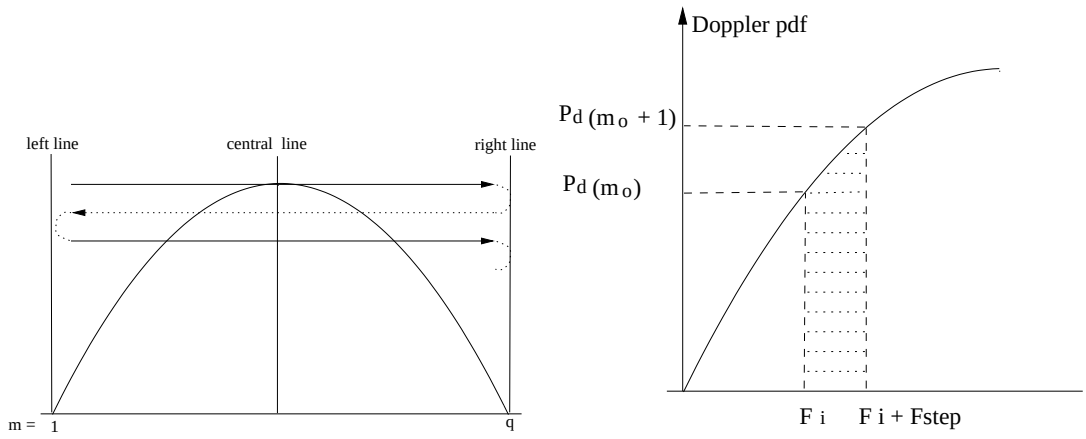

(a) *The straight line search with parabolic a priori* **(b)** *From Doppler pdf to Doppler probability*

Figure 3.5: *The straight line search with parabolic a priori pdf (a) and the calculation of probabilities from the pdf (b)*

where j takes the values $j = 0, 1, 2, ..., (q-1)$, q is the number of Doppler bins, F_{dmin} is the minimum Doppler frequency shift (see equation A.7) and F_{step} is the frequency step. We must note at this point, that $P_{dp}(j)$ describes the Doppler pdf and is not the actual probability $P_c[j(m)]$ for each Doppler cell to occur. In order to calculate the probability $P_c[j(m)]$ we are using figure 3.5(b). From the definition of pdf we take that the probability for a certain Doppler frequency F_i to occur, equals the shaded area which can be approximated by a trapezoid, given that $F_{step} \ll F_i$. Thus we obtain:

$$P_c[j(m)] = \frac{P_{dp}(j) + P_{dp}(j+1)}{2} \cdot F_{step} \tag{3.18}$$

We will use this strategy in order to evaluate the improvement that more sophisticated searching strategies offer.

3.2.3 Strategy 3: Broken/Centre *Z* with a parabolic *a priori* Doppler pdf

When non-straight line searching strategies are employed it is not always possible to derive closed form formulae describing the procedure for every (j, i, m), for the functionals $j(m)$, $i(m)$ and the prior distribution. Instead, various cases had to be examined, depending on the total number m of the cells that had been examined before the correct one was detected. The

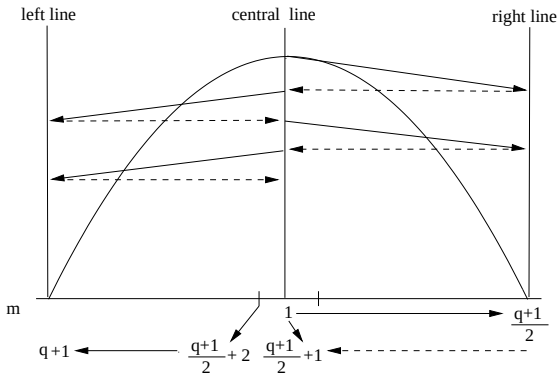

Figure 3.6: *The Broken/Centre Z with a parabolic a priori*

algorithm to calculate $P_{dp}(m)$ (and afterwards $P_c[j(m)]$ using equation 3.18) for odd values of the number of Doppler bins q is as follows:

$$P_{dp}(m) = \begin{cases} \beta + \frac{[(m-1)F_{step}]^2}{4\gamma} & if\ m \leq \frac{q+1}{2} \\ \beta + \frac{[(m-\frac{q+1}{2}-1)F_{step}]^2}{4\gamma} & if\ m \leq (q+1) \\ \beta + \frac{[(\hat{m}-1)F_{step}]^2}{4\gamma} & if\ m > (q+1)\ and\ int[\frac{m}{\frac{q+1}{2}}] = even\ (right\ area) \\ \beta + \frac{[(\check{m}-\frac{q+1}{2}-1)F_{step}]^2}{4\gamma} & if\ m > (q+1)\ and\ int[\frac{m}{\frac{q+1}{2}}] = odd\ (left\ area) \\ \beta & if\ (m-1)_{mod(\frac{q+1}{2})} = 0\ and\ m \neq 1\ (cental\ line) \end{cases} \tag{3.19}$$

where $\hat{m} = m_{mod(\frac{q+1}{2})}$, $\check{m} = \frac{q-1}{2} + m_{mod(\frac{q+1}{2})}$, $(M)_{mod\,N}$ is the remainder of the division M/N, and $int[x]$ denotes the integer part of x. In order to calculate i we used the following:

$$i(m) = \begin{cases} int[m/(q+1)] & if\ m_{mod(q+1)} = 0\ (left\ line) \\ \frac{2(m-1)}{q+1} + 1 & if\ (m-1)_{mod(\frac{q+1}{2})} = 0\ (central\ line) \\ int[m/(q+1)] + 1 & otherwise \end{cases} \tag{3.20}$$

We must make clear at this point, that the search starts (i.e. $m = 1$) from the most probable cell to occur (i.e. the maximum of the parabola which is marked by the central line in figure 3.6), continues until the right minimum of the parabola ($m = (q+1)/2$), then returns to the maximum ($m = \frac{q+1}{2} + 1$), continues until the left minimum ($m = q + 1$) has been reached and after that point the whole procedure is repeated until a "hit" has been declared. We can easily see that all the steps which examine points belonging to the central line are numbered as $m = (i-1)\frac{q+1}{2} + 1$ from which we derive the $i(m)$ for the central line shown in equation 3.20.

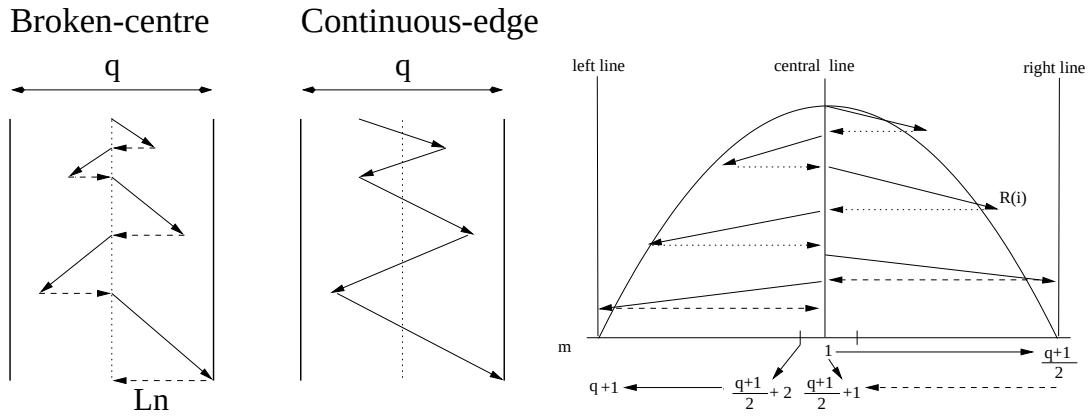

(a) *Various forms of the expanding window strategy* **(b)** *The Broken/Centre expanding window strategy*

Figure 3.7: *The expanding window strategy*

Extension of the theory for even number of Doppler bins is straightforward.

3.2.4 Strategy 4: Expanding Window with a parabolic *a priori* Doppler pdf

Various forms of expanding window search strategies exist. They all have the common feature that starting from some cell with high *a priori* probability, tests are performed until a cell at the distance L_1 from the centre is reached; if the correct cell has not been detected, a new search within a radius $L_2 > L_1$ is initiated, etc. Figure 3.7(a) presents characteristic forms of the expanding window search. There are four forms, namely the "centre expanding window" where the starting cell is the central one, the "edge expanding window" where the starting cell is a non-central, the "broken expanding window" where rewind of the code to the starting point is performed after reaching the edge of the window and the "continuous expanding window" where no rewind is performed and the same cells are searched on the way back. Apart from [11] an interesting study of the expanding window strategy by A.Weinberg can be found in [13] while in [14] the same strategy is examined using the Unified Approach. It is obvious that for centrally peaked prior distributions the *Broken/Centre expanding window* will be the optimum choice among all the expanding windows strategies. This is going to be the one that we will further analyse. We must also note that the following mathematical analysis is different from that presented in [11, 13, 14].

We define the minimum radius by the formula:

$$R_{min} = floor\left(\frac{q}{N}\right) \tag{3.21}$$

where the $floor(x)$ function rounds the value specified in the x argument down to the largest integer not greater than the x argument, and N is an arbitrary integer ($N \geq 2$) which determines the minimum radius and finally the number of sweeps through the uncertainty area (the smaller the radius, the larger is the possible number of sweeps). If the correct cell has not been detected when the $(l-1)^{th}$ sweep is completed, then the next searching radius would be set at:

$$R = floor\left(l \cdot \frac{q}{N}\right) \tag{3.22}$$

From equation 3.22 we can see that the window will not be uniformly expanding in general (unless when $q_{modN} = 0$). As we can see from figure 3.7(b), after a certain point the Broken/Centre expanding window strategy reduces to the corresponding *Z* search (the numeration of m is the same as in Broken/Centre *Z*). The searching strategy is an expanding window one, as long as $q\frac{l}{N} \leq \frac{q+1}{2}$. From this relation, we can calculate after how many sweeps the expanding window strategy reduces to the *Z* search:

$$l_{max} = ceil\left(\frac{q+1}{q}\frac{N}{2}\right) \tag{3.23}$$

where the function $ceil(x)$ rounds the value specified in the x argument up to the next largest integer. Finally, we can calculate the exact step number m_{max} in which the transition from expanding window to *Z* search happens, using:

$$m_{max} = 2 \sum_{j=1}^{ceil\left(\frac{(q+1)N}{2q}\right)} floor\left(j\frac{q}{N}\right)$$

The quantity $2 \cdot floor\left(j\frac{q}{N}\right)$ in the previous loop is the actual number of steps taken within the j^{th} sweep. Thus the quantity $\sum_{j=1}^{l} 2 \cdot floor\left(j\frac{q}{N}\right)$ is the total number of steps m, at the end of the l^{th} sweep. Finally we define $K(l) = 2\sum_{j=1}^{l-1}[floor\left(j\frac{q}{N}\right)] + floor(l\frac{q}{N})$. We have now

defined all the necessary quantities in order to describe the algorithm used to calculate $P_{dp}(m)$:

$$P_{dp}(m) = \begin{cases} \beta + \frac{[(m-1)F_{step}]^2}{4\gamma} & if\ m \leq floor(\frac{q}{N}) \\ \beta + \frac{[(m_1 - \frac{q+1}{2} - 1)F_{step}]^2}{4\gamma} & if\ floor(\frac{q}{N}) \leq m \leq floor(2\frac{q}{N}) \\ \beta + \frac{[(m_2 - 1)F_{step}]^2}{4\gamma} & if\ m \leq K(l) \qquad l = 2,3,...,l_{max}-1 \\ \beta + \frac{[(m_3 - \frac{q+1}{2} - 1)F_{step}]^2}{4\gamma} & if\ m \leq K(l) + floor(l\frac{q}{N}) \qquad l = 2,3,...,l_{max}-1 \\ if\ m \geq m_{max} & replace\ m := m - m_{max} \qquad follow\ eq.3.19 \end{cases} \tag{3.24}$$

where:

- $m_1 = \frac{q+1}{2} + m - floor(\frac{q}{N})$
- $m_2 = m - K(l) + floor(l\frac{q}{N})$
- $m_3 = \frac{q+1}{2} + m - K(l)$

It was not possible to derive a closed form formula for the $i(m)$ and all the necessary values in order to proceed with the acquisition time pdf and mean acquisition time calculations were derived using computer simulations.

3.3 Alternate search strategies

In this section the so called "alternate search strategies" will be described. Two strategies, namely, the uniformly expanding alternate (UEA) and the non uniformly expanding alternate (NUEA) will be further analysed. The basic idea behind those strategies is to examine the cells following the order of the decreasing *a priori* probability. It was shown in [11], that for triangular and Gaussian prior pdfs, the NUEA strategy results into acquisition times which are near the optimum values given by using the MAP method (chapter 1). We must note that in what follows we have assumed that the code rewinding time is negligible in comparison to the mean time required for the rejection of the incorrect cell $E(T_r)$. Finally, as in the expanding window strategy, we developed a different analysis of the two alternate strategies than the one by V. M. Jovanovic in [11].

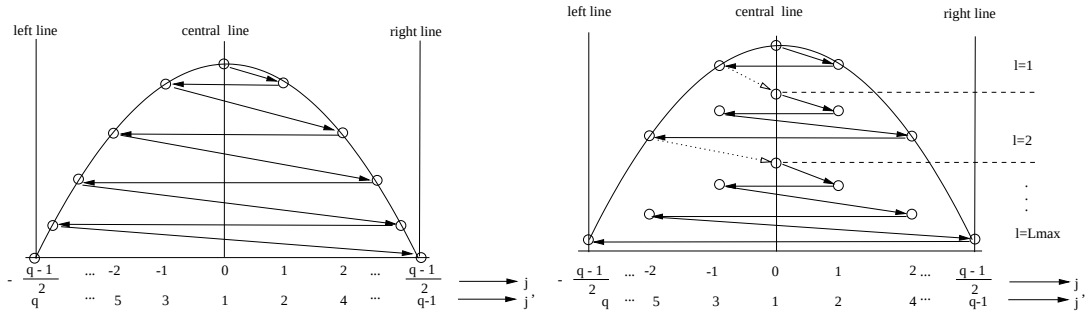

(a) *The UEA strategy* **(b)** *The NUEA strategy*

Figure 3.8: *The two alternate strategies with a parabolic a priori pdf*

3.3.1 The uniformly expanding alternate strategy

The cells are tested following the order of the decreasing *a priori* probability until the cell with the lowest *a priori* probability is reached. If the correct cell is not detected during the first iteration the procedure is repeated (see figure 3.8(a)). In order to calculate the pdf and the mean value of the acquisition time for the UEA strategy we will use the functional $m(i,j)$ which is the total number of cells tested during the acquisition under the assumption that the correct location is in the cell marked with $''j''$ and that the correct detection happened during the i^{th} test of the j^{th} cell(see section 3.1.1.3). The pdf can be calculated from the discrete version of equation 3.6 which can be written as:

$$\begin{aligned} P_{T_a}(n) &= \sum_{i=1}^{\infty} P_d(1-P_d)^{i-1} \sum_{j=-\frac{q-1}{2}}^{\frac{q-1}{2}} P_c(j) \sum_{h=0}^{m(i,j)-i} \begin{pmatrix} m(i,j)-i \\ h \end{pmatrix} \\ &\quad \cdot P_{fa}^{h}(1-P_{fa})^{m(i,j)-i-h}\delta(n-m(i,j)-hk) \end{aligned} \tag{3.25}$$

Equation 3.25 is given in [11] but we modified it before using it for our simulations. The term $\sum_{h=0}^{m(i,j)-i} \begin{pmatrix} m(i,j)-i \\ h \end{pmatrix}$ was replaced by $\sum_{h=0}^{\varepsilon} \begin{pmatrix} \varepsilon \\ h \end{pmatrix}$, where $\varepsilon = min[m(i,j)-i, n]$ which denotes the minimum between $m(i,j)-i$ and n. The reason is that the number of false alarms (i.e. $m(i,j)-i$) can not exceed n (see equation 3.11 for the definition of n). This change, reduces significantly the simulation time for both alternate strategies. The numeration of j shown in figure 3.8(a) is used as it leads to simpler formulas and calculations. The formula

to calculate $P_{dp}(j)$ (once again for odd values of the number of Doppler bins q) in this case is:

$$P_{dp}(j) = \beta + \frac{(j \cdot F_{step})^2}{4\gamma} \tag{3.26}$$

where $j = -\frac{q-1}{2}, ..., \frac{q-1}{2}$ as in figure 3.8(a). The actual *a priori* probability $P_c(j)$ (by combining formulas 3.18 and 3.26) is given by:

$$P_c(j) = \begin{cases} \frac{F_{step}}{2}\left(2\beta + \frac{[(j-1)F_{step}]^2}{4\gamma} + \frac{[jF_{step}]^2}{4\gamma}\right) & if\ j > 0 \\ \frac{F_{step}}{2}\left(2\beta + \frac{[jF_{step}]^2}{4\gamma} + \frac{[(j+1)F_{step}]^2}{4\gamma}\right) & if\ j < 0 \\ \frac{F_{step}}{2}\beta & if\ j = 0 \end{cases} \tag{3.27}$$

It is easy to see that the functional $m(i,j)$ is given by:

$$m(i,j) = (i-1)q + j' \tag{3.28}$$

where j' is defined by (see also figure 3.8(a)):

$$j' = \begin{cases} 1 & if\ j = 0 \\ 2j & if\ j > 0 \\ -2j+1 & if\ j < 0 \end{cases} \tag{3.29}$$

Finally the mean acquisition time can be calculated using a modified version of equation 3.12. This equation provides the mean acquisition time as a function of the $m(i,j)$ functional and can be considered self-explanatory:

$$\begin{aligned} E(T_a) \quad = \quad & \sum_{i=1}^{\infty} P_d(1-P_d)^{i-1} \sum_{j=-\frac{q-1}{2}}^{\frac{q-1}{2}} P_c(j) \\ & \cdot \left([m(i,j)-i]E(T_r) + [i-1]E(T_m) + E(T_d)\right) \end{aligned} \tag{3.30}$$

where $E(T_r)$, $E(T_m)$, $E(T_d)$ are the expected values of T_r which is the time required for the rejection of the incorrect cell, T_m which is the time required for the false dismissal of the correct cell and T_d which is the time required for the correct detection, respectively (see also section 3.1.1.3, equation 3.13).

3.3.2 The non uniformly expanding alternate strategy

The cells are tested following the order of decreasing *a priori* probability within a predetermined window. If the correct cell is not detected, the window is expanded until the cell with the lowest probability is reached. After that point, NUEA reduces to the corresponding UEA strategy (see figure 3.8(b)). We notice that while the UEA strategy is similar to the broken-centre family, the NUEA strategy is more similar to the expanding window family. Thus we will use a similar method in order to analyse this strategy but this time the functional $m(i,j)$ will be used as it makes the calculation of the acquisition time statistics easier. Similar to the expanding window search strategy, we define the minimum radius by the formula:

$$R_{min} = floor\left(\frac{q}{N}\right) \tag{3.31}$$

where the $floor(x)$ function rounds the value specified in the x argument down to the largest integer not greater than the x argument, and N is an arbitrary integer ($N \geq 2$) which determines the minimum radius and finally the number of sweeps through the uncertainty area (the smaller the radius, the larger is the possible number of sweeps). If the correct cell has not been detected when the $(l-1)^{th}$ sweep is completed, then the next searching radius would be set at:

$$R = floor\left(l \cdot \frac{q}{N}\right) \tag{3.32}$$

From equation 3.32 we can see that the window will not be uniformly expanding in general (unless when $q_{mod(N)} = 0$). After a certain point, the NUEA strategy reduces to the corresponding UEA strategy (exactly like the expanding window strategy reduces to the corresponding *Z* search). Using the same numeration of $m(i,j)$ as in the UEA strategy (see figure 3.8(b)), we can see that the searching strategy is a NUEA one (that is, it has not been reduced to the corresponding UEA strategy), as long as $floor(q\frac{l}{N}) \leq \frac{q-1}{2}$. Using this relation and a simple computer loop we can calculate the number of sweeps L_{last}, at which the NUEA strategy reduces to the UEA, as the largest integer for which $floor(q\frac{l}{N}) \leq \frac{q-1}{2}$. In order to be able to calculate the functional $m(i,j)$ we need a function which shows in which round l of the NUEA strategy the cell j ($j = -\frac{q-1}{2}, ..., \frac{q-1}{2}$) is being tested for the first time. This function ($RIF(i,j)$) can be calculated for every (i,j) (given the radii $R(l)$) with the following

algorithm:

$$RIF(i,j) = \begin{cases} l & ,j \geq 1 \; and \\ & R(l-1) < j < R(l) \\ l & ,j \leq -1 \; and \\ & R(l-1) - 1 < |j| < R(l) - 1 \\ 1 & ,j = 0 \end{cases} \tag{3.33}$$

in which l represents the current iteration within the NUEA search procedure ($l < L_{last}$), $R(l)$ is the corresponding radius and $R(0) = 0$. Finally, we define the quantity max_i such as (for a given j):

$$if \begin{cases} i \leq max_i \mapsto & the\ search\ is\ still\ an\ NUEA\ one \\ i > max_i \mapsto & the\ search\ is\ reduced\ to\ the\ corresponding\ UEA \end{cases} \tag{3.34}$$

The quantity max_i can be calculated by the formula:

$$max_i = \begin{cases} 0 & for\ j = -\frac{q-1}{2} \\ L_{last} - RIF(i,j) + 1 & for\ every\ other\ j \end{cases} \tag{3.35}$$

We now have all the necessary parameters in order to calculate the functional $m(i,j)$. We notice that the quantity $\sum_{l=1}^{l_0} 2 \cdot floor\left(l\frac{q}{N}\right)$ represents the total number of cells that have been examined at the end of the l_0 sweep. It is not difficult to see that $m(i,j)$ is given by:

$$m(i,j) = \begin{cases} \sum_{l=1}^{lim} 2 \cdot floor\left(l\frac{q}{N}\right) + j' & if\ i \leq max_i \\ \sum_{l=1}^{L_{last}} 2 \cdot floor\left(l\frac{q}{N}\right) + (i - max_i - 1)q + j' & if\ i > max_i \end{cases} \tag{3.36}$$

where:

$$lim = \begin{cases} maximum(RIF(i,j), i) & if\ i > 1\ and\ RIF(i,j) > 1 \\ maximum(RIF(i,j), i) - 1 & for\ every\ other\ i\ and\ RIF(i,j) \end{cases} \tag{3.37}$$

and j' is defined by equation 3.29. Using the same numeration of j and j' as in the UEA case, all the equations for the *a priori* Doppler probability remain valid (see equations 3.25, 3.26, 3.27, 3.30), using of course the $m(i,j)$ given by the equation 3.36.

3.4 Results and commentary

All our simulations were carried out for orbital altitude $H = 750$ km, circular spot beam of radius $R = 75$ km and centre $(x_o, y_o) = (150, 150)$ km. The carrier frequency is assumed to be $F_c = 2.2$ GHz, the maximum and minimum Doppler shifts are $F_{dmax} = 15372.4$ Hz and $F_{dmin} = 5313.8$ Hz respectively and the Doppler step is $F_{step} = 250$ Hz. Under those conditions and using equation A.9 we calculated the number of Doppler bins $q = 41$. The parabola which fits the Doppler pdf has been calculated using the *Marquardt-Levenberg* nonlinear least squares fit algorithm [98] and it is given by the equation $y = 0.000131184 + \frac{(x-10301.9)^2}{4\cdot(-6.50614\cdot 10^{10})}$. Similar to [11], we define the normalised mean acquisition time by the equation:

$$\mu = \frac{E(T_a)}{qE(T_r)} = \frac{E(T_a)}{q(\tau_d + P_{fa}\tau_p)} \tag{3.38}$$

We will use μ to compare the different searching strategies, as it does not depend on the number of Doppler bins, penalty time and probability of false alarm P_{fa}. As a reference point, notice that for the single dwell system with uniform *a priori* information [40] and $P_d = 1$, $P_{fa} = 0$, the normalised mean acquisition time is $\mu = 0.5$. The penalty time we used is $\tau_p = 20\tau_d$ i.e. $k = 20$. For our simulations we used a simple CFAR criterium described in [5], page 783 (see also chapter 1 of this Thesis, equation 1.16) according to which if we maintain a constant false alarm probability P_{fa}, the probability of detection as a function of the SNR and the P_{fa} is:

$$P_d = Q\left(\frac{Q^{-1}(P_{fa}) - \gamma_o\sqrt{B\tau_d}}{\sqrt{1+2\gamma_o}}\right) \tag{3.39}$$

where $Q(\cdot)$ is the Marcum's function, B is the bandwidth of the bandpass filter in figure 1.6, τ_d the dwell time and γ_o is the SNR at the output of the correlator. Finally, the time is given as $t = n\tau_d$, i.e. as a multiple of the dwell time (see also equation 3.11).

Figure 3.9 is the pdf of the acquisition time for the straight line search with uniform and parabolic *a priori* information for two different (P_d, P_{fa}). Both pdfs were calculated using equation 3.11. The pdf of the uniform *a priori* case is in agreement with that presented in [11]. It is interesting to notice in figure 3.9(a) that the pdf retains the form of the *a priori* information for a time length equal to the number of bins that are examined. The main energy of the pdf is concentrated in the same time length, which indicates that it is very probable that acquisition will occur during the first round. Under bad conditions though (low P_d and high P_{fa}-figure 3.9(b)), both pdfs are deformed and the energy of the pdf is spread towards larger times as a

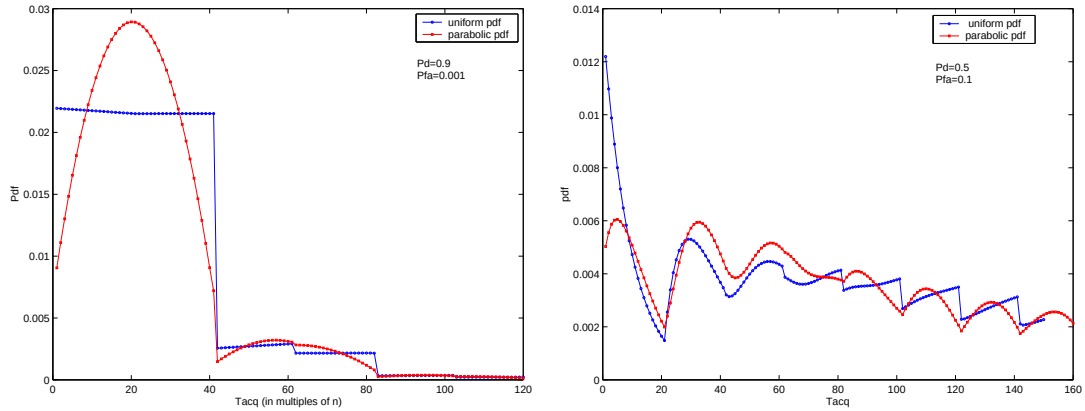

(a) *Pdf for the case* (P_d, P_{fa})=$(0.9, 0.001)$. **(b)** *Pdf for the case* (P_d, P_{fa})=$(0.5, 0.1)$.

Figure 3.9: *The pdf of the acquisition time for the straight line strategy*

large number of false alarms will probably occur. Figure 3.10 depicts the normalised mean acquisition time μ for the two cases as calculated using equation 3.12. Figure 3.10(a) depicts μ for relatively large SNRs while figure 3.10(b) is the image for a larger range of SNRs. As it was expected, the two cases (uniform and parabolic) are almost identical. The conclusion is that a straight line search does not take any advantage of the given *a priori* information and thus more advanced searching strategies must be employed. A last comment on figure 3.10; what might seem strange is that $P_{fa} = 0.1$ results into smaller μ than the $P_{fa} = 0.001$ case. However, this is justified as higher $P_{fa} = 0.1$ results into much higher P_d (see chapter 1). Thus if the penalty time is not too high a result like the one in figure 3.10(b) is expected.

The results for the Broken-centre Z (BCZ) strategy in comparison with straight line (SL) search with a parabolic pdf are depicted in figures 3.11 and 3.12. In figure 3.11 we compare the pdfs of the two strategies. We can see that the BCZ pdf has a larger portion of its area towards the small acquisition times. This is valid for all P_{fa}. This is a first indication that BCZ works better under the given *a priori* pdf compared with the SL strategy. Figure 3.12 presents the normalised mean acquisition time μ as a function of the SNR for two different P_{fa}. For very low SNRs (SNR< -12 dB) BCZ does not perform any better than the simple SL. We would like to point out, once more, that the SNR is not the one of the received signal SNR$_r$. It is calculated at the output of the correlator and it is $SNR_r + Processing\ Gain$. Thus, for CDMA systems with large processing gains, it is unlikely that SNR< -12 dB. On the other hand, for SNR> -12 dB

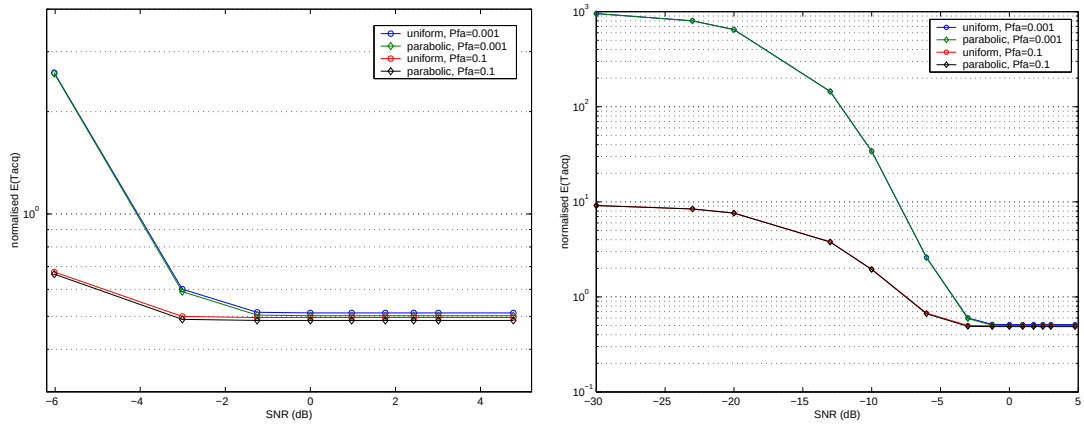

(a) *The normalised mean T_{acq} for $SNR > -6$ dB*

(b) *The normalised mean T_{acq} for $-30dB < SNR < 5dB$*

Figure 3.10: *The normalised mean acquisition time as a function of the SNR for the straight line strategy*

BCZ performs better in terms of μ. The improvement is more significant for larger P_{fa}. This is due to the fact that BCZ will probably have to deal with less false cells as it examines first the most probable. This, in average, results into fewer false alarms for the BCZ strategy even for high P_{fa}.

In the expanding window searching strategy (XWIN) analysis, we saw that one of the basic parameters is N which defines the length of the window for each round by the equation $R = floor\left(l \cdot \frac{q}{N}\right)$. The smaller the N is, the larger is the searching window and the less rounds would take place before XWIN reduces to the corresponding BCZ strategy. The performance of the XWIN strategy in terms of the acquisition time greatly depends on the parameter N. In general, there is an optimum value N_{opt} which depends on the false alarm probability and the detection probability. In [2, 11, 14] the same optimisation problem is discussed. An analytical approach to this problem is very difficult and not practical at all. Thus, all our results concerning the optimisation of N are based on simulations. Figure 3.13 depicts the pdf under the same conditions but for two different N. It is clear that the statistical characteristics of the acquisition time, greatly depends on N. The pdf for $N = 2$ has a larger part of its energy towards the small times, compared to the $N = 6$ case. Thus, we expect the $N = 2$ case to give lower mean acquisition time, under the given conditions. Figure 3.14 depicts the normalised mean acquisition time μ for various N and for $P_{fa} = 0.001$ as a function of the SNR. It becomes

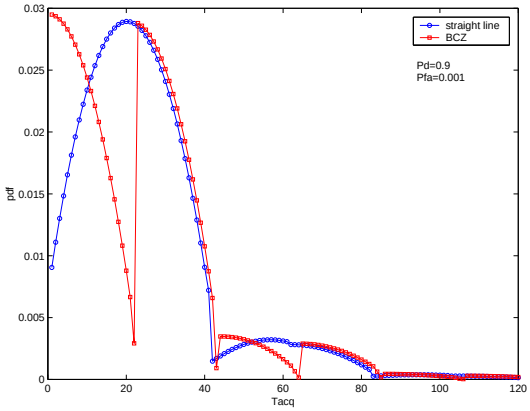

(a) *Pdf for the case* (P_d, P_{fa})=$(0.9, 0.001)$.

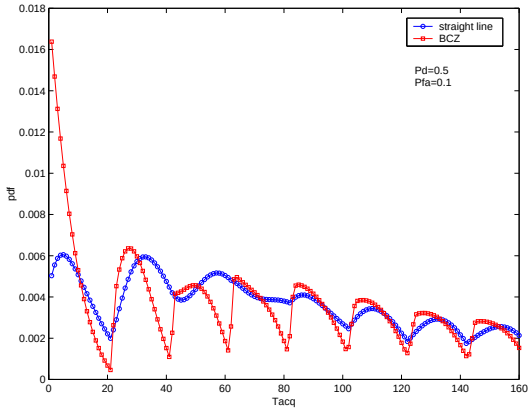

(b) *Pdf for the case* (P_d, P_{fa})=$(0.5, 0.1)$.

Figure 3.11: *Typical pdfs for the BCZ strategy*

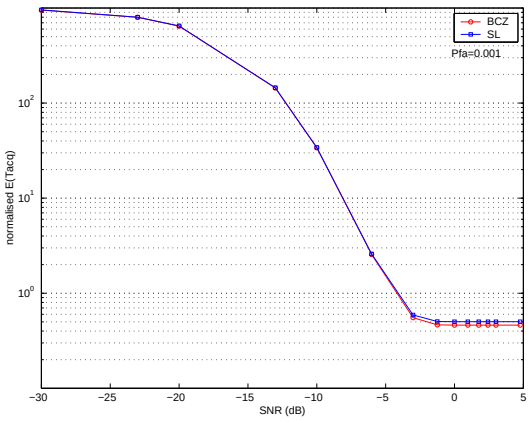

(a) μ *for the SL and BCZ strategies,* $P_{fa} = 0.001$

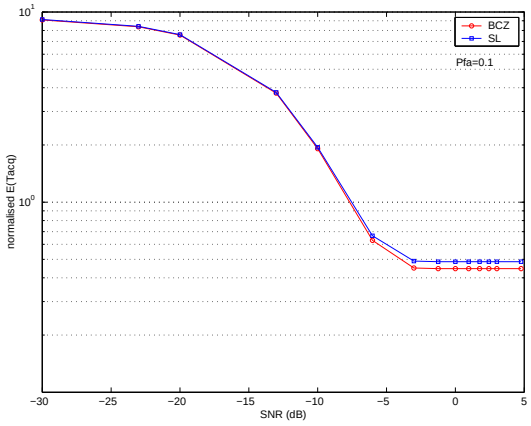

(b) μ *for the SL and BCZ strategies,* $P_{fa} = 0.1$

Figure 3.12: *A comparison between the SL and BCZ strategies*

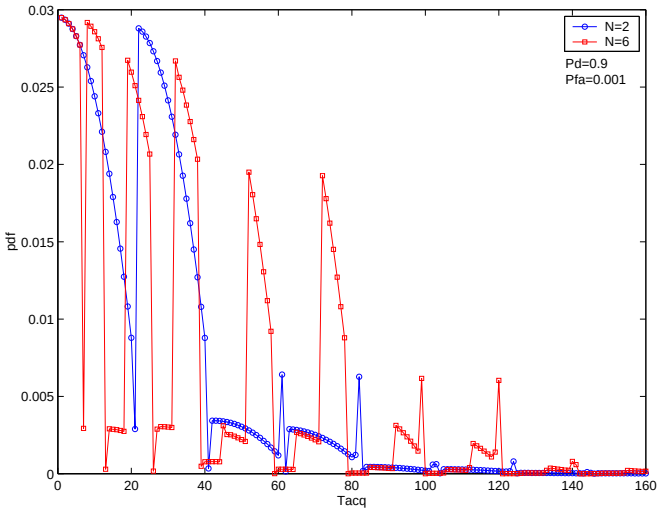

Figure 3.13: *The pdf for the XWIN strategy and two different N.*

clear, that depending on the SNR, the parameter N must be carefully chosen in order to take full advantage of the strategy. We can also notice that, for SNR> -5 dB, $N = 2$ results into lower μ while, for lower SNRs larger Ns are required (figure 3.14(b)). Figure 3.15 presents μ as a function of N for various detection probabilities. From figure 3.15(a) we can see that, for detection probabilities $P_d > 0.5$ the optimum value is $N_{opt} = 2$, while for $P_d < 0.5$ larger values must be used in order to optimise the performance of the XWIN strategy. Clearly, N_{opt} increases as P_d (or equivalently the SNR in figure 3.14) decreases; this is because, as the reliability of the individual cell tests decreases, one has to rely more on the prior information and thus, spend more time around the peak (more windows-larger N). These general conclusions are in agreement with the results presented in [11, 14]. Using the two diagrams of figure 3.16 we can compare the three non-alternate strategies, namely, the straight line (SL), broken-centre Z (BCZ) and expanding window (XWIN). Figure 3.16(a) presents μ as a function of the SNR while figure 3.16(b) presents μ as a function of the detection probability P_d. Notice, that P_d is determined by the SNR and P_{fa} using equation 3.39. In that sense, figures 3.16(a) and 3.16(b) are equivalent. A general conclusion is that, for the parabolic *a priori* information the XWIN strategy does not offer a significant improvement over the simpler BCZ. On the contrary, for SNR> -3 dB (which corresponds to $P_d > 0.9$ for $P_{fa} = 0.001$), BCZ results into marginally better acquisition times, as we can see from figure 3.16(a). For $P_d < 0.9$ (figure 3.16(b)) the XWIN offers a small advantage over the BCZ strategy. For the XWIN we always use the optimum N_{opt} according to table 3.1. Finally, it should be noticed that in the analysis of the BCZ and XWIN strategies, we neglected the time to "rewind" the code, i.e. assumed that this time is

P_d	**0.5-0.9**	**0.4, 0.45**	**0.3, 0.35**	**0.25**	**0.2**	**0.15**	**0.1**
XWIN N_{opt}	2	3	4	5	8	10	14

Table 3.1: *The optimum N for the XWIN and various detection probabilities*

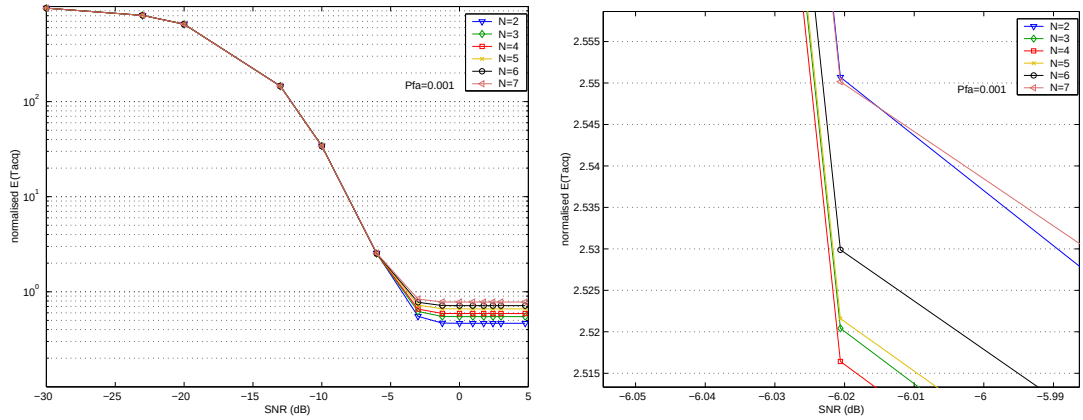

(a) *The normalised mean acquisition time for the XWIN strategy and various N.*

(b) *A detail of the previous diagram for $SNR \approx -6$ dB*

Figure 3.14: *The normalised mean acquisition time for the XWIN versus SNR for various N. The change of N_{opt} with SNR is obvious.*

small in comparison to the dwell time.

Figure 3.17(a) depicts the pdf of the uniform expanding alternate (UEA) strategy in comparison with that of the BCZ strategy, while, figure 3.17(b) depicts the cumulative density function (cdf) of the two strategies. The cdf is calculated by integrating the pdf and it allows an easier comparison of the strategies than the pdf. For every (P_d, P_{fa}), the cdf of the UEA strategy rises towards unity faster than the cdf of the BCZ strategy. Thus, we expect UEA to perform better than the BCZ. Indeed, as we can see in figure 3.18, UEA results into lower mean acquisition times for every SNR and P_{fa}. For the same reasons that were previously explained, the improvement becomes more significant for larger false alarm probabilities and larger SNRs (i.e. larger detection probabilities). The triangular signs, in both figures 3.18, named as *General Direct Approach Equation*, depict the normalised mean acquisition time for the UEA strategy and an arbitrary *a priori* distribution [11], given by:

$$\mu_n = \frac{1}{P_d} + \frac{2}{q}\sum_{j=0}^{\frac{q-1}{2}} 2j\,P_c(j) - 1 \tag{3.40}$$

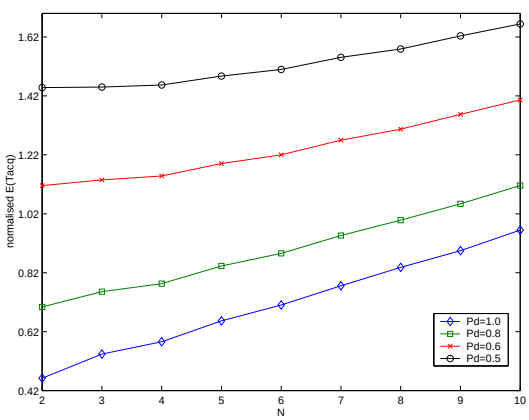

(a) *The normalised mean acquisition time versus the parameter N for $P_d > 0.5$*

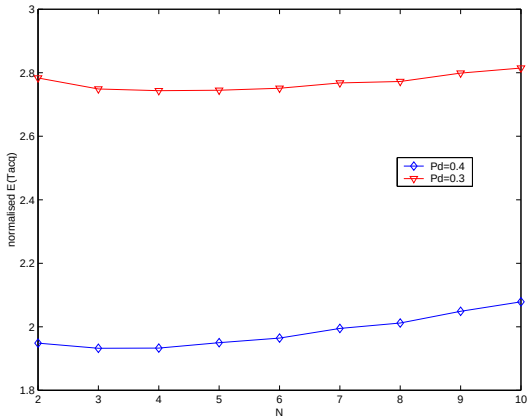

(b) *The normalised mean acquisition time versus the parameter N for $P_d < 0.5$*

Figure 3.15: *Optimising the parameter N for the XWIN strategy.*

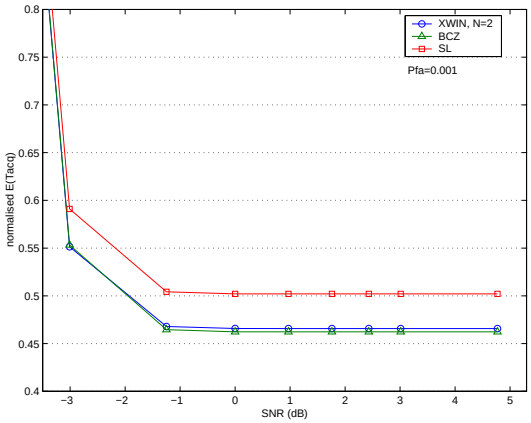

(a) *The normalised mean acquisition time versus the SNR for the SL, BCZ, XWIN strategies.*

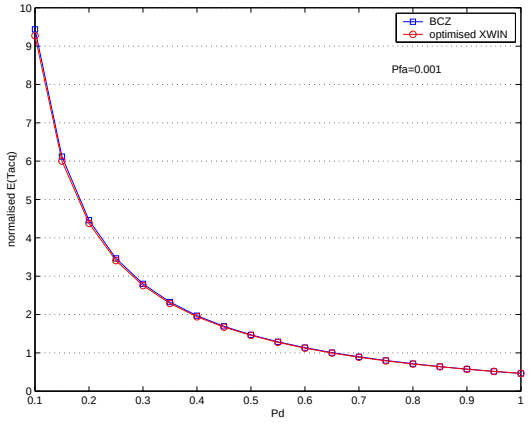

(b) *The normalised mean acquisition time versus the P_d for the BCZ and the optimised XWIN.*

Figure 3.16: *A comparison between the non-alternate strategies:SL,BCZ,XWIN.*

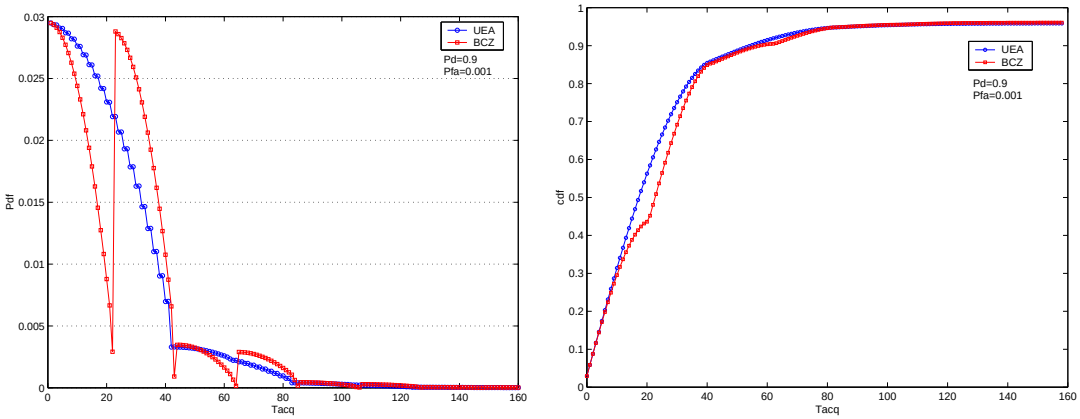

(a) *The pdf of the UEA and BCZ strategies.*

(b) *The cdf of the UEA and BCZ strategies.*

Figure 3.17: *A comparison of the pdf and cdf of the UEA and BCZ strategy.*

where, for the case of a parabolic *a priori*, the $P_c(j)$ is given by equation 3.27. We used this equation to check the correctness of our work. We found out that the results from equation 3.40 are in excellent agreement with our results. The maximum difference is 4% for SNR< -25 dB, while for most SNRs it is less than 1%.

The last strategy that we examined is the NUEA strategy. Similar to the expanding window, NUEA needs to be optimised. The optimisation parameter is the quantity N, defined by equations 3.31 and 3.32. As in the XWIN case, N determines the number of the sweeps of the uncertainty area, before NUEA degenerates to the corresponding UEA. The analytical optimisation of N is a very complex task; thus, the optimum value N_{opt} will be numerically defined, as we did for the XWIN case. Figure 3.19 depicts the pdf (for $N = 2, 3$) and cdf (for $N = 2, 3, 4$) of the NUEA strategy. It is obvious that its performance depends heavily on the choice of the parameter N. The normalised mean acquisition time as a function of the SNR for two different values of N is depicted in figure 3.20 (solid lines). Similar to the XWIN strategy, for large SNRs $N_{opt} = 2$ while for lower SNRs, N_{opt} is larger. In the same figure, labelled as *General theory* (no line), we present the normalised mean acquisition time as predicted by the general equation of the *Direct approach* [11]. The equation for the NUEA and an arbitrary *a priori*

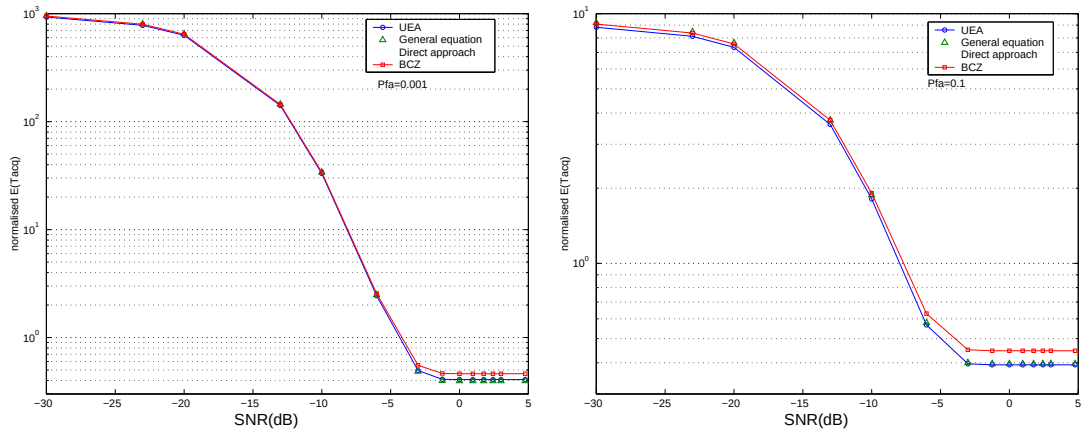

(a) $P_{fa} = 0.001$ **(b)** $P_{fa} = 0.1$

Figure 3.18: *The normalised mean acquisition time versus the SNR for the BCZ and UEA strategies.*

information is:

$$\begin{aligned}\mu_n &= \frac{2}{q}\sum_{j=0}^{\frac{q-1}{2}} 2jP_c(j) + \frac{2}{q}\sum_{k=0}^{L_{last}-1}\sum_{i=1}^{L_{last}-k} P_d(1-P_d)^{i-1}SP_kSL_{k+i-1} \\ &+ \sum_{k=0}^{L_{last}-1}(1-P_d)^{L_{last}-k}SP_k\left[\frac{2}{q}SL_{N-1}+\frac{1}{P_d}\right] \end{aligned} \tag{3.41}$$

where, $SL_k = \sum_{l=0}^{k} R_l$, $SL_0 = 0$, R_l is the searching radius given by equation 3.32, $SP_k = \sum_{j=R_k+1}^{R_{k+1}} 2P_c(j)$ and $P_c(j)$ is given by equation 3.27. We remind that the parameter L_{last} is defined as the number of sweeps at which the NUEA reduces to the corresponding UEA. It is interesting to notice that, although we used a different approach than this in [11] in order to calculate the searching radius and functional $m(i,j)$, our results are in very good agreement with equation 3.41 which is a slightly modified version of the original, presented in [11]. The normalised mean acquisition time as a function of the parameter N for various detection probabilities, is shown in figure 3.21. Table 3.2 summarises the results for the N_{opt}. We can see that they are quite different from the XWIN strategy, although in both cases, N_{opt} becomes larger as the detection probability drops, for a reason that was explained before. Finally, the performance in terms of the normalised mean acquisition time is depicted in figure 3.22. For low false alarm probabilities (figure 3.22(a)) the two alternate strategies have only minor differences; UEA be-

P_d	**0.5-0.9**	**0.35-0.45**	**0.25-0.3**	**0.2**	$<$ **0.15**
NUEA N_{opt}	2	3	5	14	> 20

Table 3.2: *The optimum N for the NUEA and various detection probabilities*

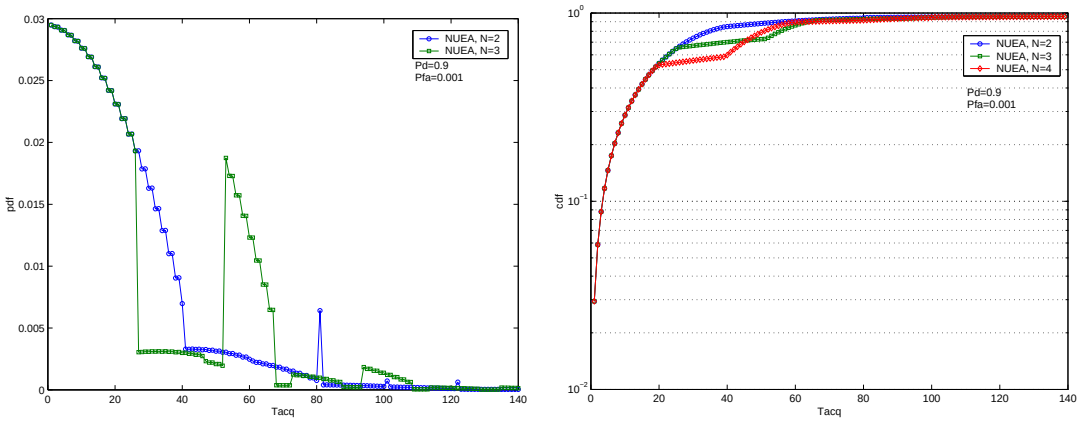

(a) *The pdf for the NUEA and various N*

(b) *The cdf for the NUEA and various N*

Figure 3.19: *A comparison of the pdf and cdf of the NUEA strategy and various N.*

haves marginally better for SNR> -4 dB while NUEA gives a very small advantage for very low SNRs. The situation is similar for high false alarm probabilities. The difference is that, for low SNRs, the NUEA strategy performs much better than the UEA. Both alternate strategies, clearly outperform the non-alternate strategies.

3.4.1 Conclusions

It is important to see what is the overall advantage in the mean acquisition time when the synchronisation system uses an *a priori* information and a suitable searching strategy. Figure 3.23 depicts the $\%$ improvement in the normalised mean acquisition time that the NUEA offers over the simple straight line (SL) (figure 3.23(a)) and the more advanced BCZ strategy (figure 3.23(b)). The basic points that became clear so far and that they are highlighted once more by figure 3.23 are:

- The improvement in the mean acquisition time for all strategies is more significant for low false alarm probabilities and high SNRs (or, equivalently, high detection probabilities). The reason is that a good searching strategy will have to deal with less false cells before

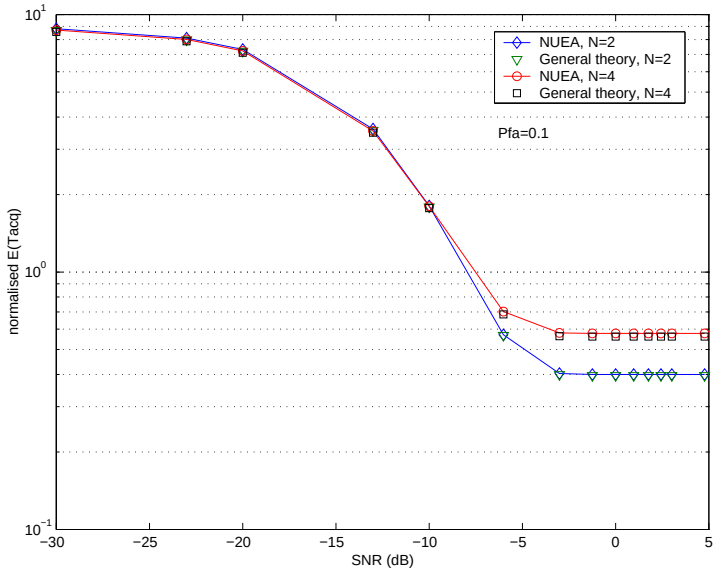

Figure 3.20: *The effects of the parameter N in the mean acquisition time.*

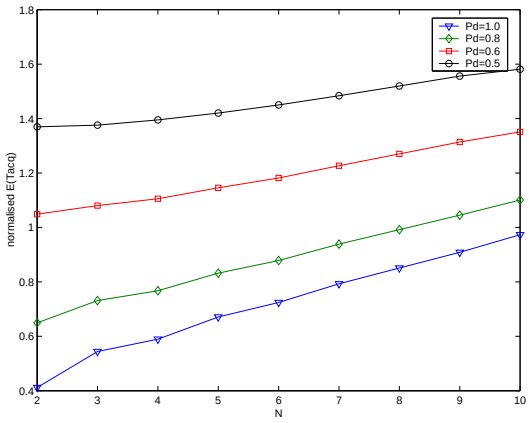

(a) *The normalised mean acquisition time versus the parameter N for $P_d > 0.5$*

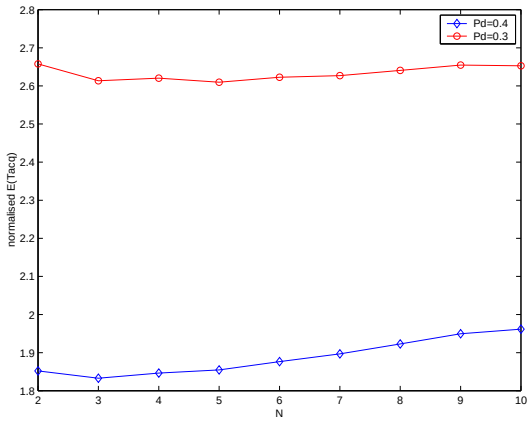

(b) *The normalised mean acquisition time versus the parameter N for $P_d < 0.5$*

Figure 3.21: *Optimising the parameter N for the NUEA strategy $(P_{fa} = 0.01)$.*

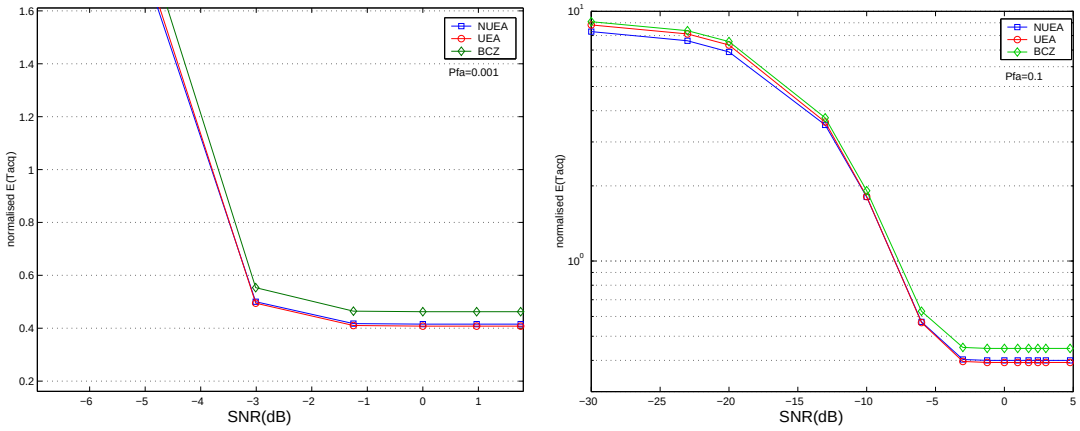

(a) *The normalised mean acquisition time versus the SNR for the BCZ, UEA, NUEA strategies*

(b) *The normalised mean acquisition time versus the SNR for the BCZ, UEA, NUEA strategies*

Figure 3.22: *A comparison between the BCZ and the two alternate strategies. NUEA is optimised*

testing the correct one and thus, given a high P_d, the number of false alarms will be reduced even if the P_{fa} is high.

- For the parabolic *a priori* pdf the expanding-window family (XWIN and NUEA) does not offer great improvement over the Z-family (BCZ and UEA). On the contrary, for high SNRs the simpler Z-family performs slightly better. In [11], where the triangular and Gaussian pdfs are examined, BCZ and XWIN are almost equivalent but NUEA always outperforms the UEA. This is a significant difference with our case where NUEA is not always better than the UEA strategy.

- The alternate strategies outperform all the conventional non-alternate strategies under all conditions. As we can see from figure 3.23, NUEA offers an improvement of between $2-18\%$ compared to the SL method, and to $2-11\%$ compared to the BCZ strategy. Once more we have to notice that the time required to "rewind" the code in all strategies is neglected. According to [11], this is a valid assumption for all spread spectrum systems which rely on simple codes like those from linear-feedback shift registers. In the case of more sophisticated code generators, this may not be true and the benefit of all strategies compared to the SL becomes smaller.

- All the searching strategies that were presented in this chapter are suitable for centrally

peaked prior distributions. In chapter 2 though, it became clear that the parabola-shaped Doppler pdf is valid for only a part of the total spot beam. For the rest of the area the pdf is edge-peaked (figure 2.9) and thus different strategies must be employed. Those strategies will examine first the cells closer to the peak of the distribution and then will move towards the other end. Some searching strategies suitable for edge-peaked distributions are described in [11], although there are better strategies that can be studied and tested. In general, it is expected that the improvement in the acquisition time will be less significant than that of the symmetrical pdf. This is due to the fact that, the searching is not initiated from the most probable cell (as in the symmetrical case) but from the edge which is closer to the peak, i.e. the searching is initiated from the less probable cell which is closer to the most probable (unless the distribution has its maximum to the edge). Thus, in the case of non symmetrical prior pdfs the only strategies that are expected to give any advantage over the simple straight line search is the UEA/NUEA type of strategies, where the search follows the exact ranking of the cells according to the prior pdf. The theoretical analysis of these strategies is bound to be a very complicated task which, in any case, is unlikely to provide deep insight to the optimum searching problem. Thus, it is our belief that simulations are the best way of evaluating strategies for non-symmetrical prior distributions like those in chapter 2.

- A general conclusion is that the use of any prior information is not always a straightforward procedure. The searching strategies must be well planned and evaluated. In the literature, the pdfs which are usually analysed are the uniform, Gaussian and triangular distributions. It seems, though, that some of the general results which were based on those distributions are not valid in every case. Furthermore, in order to take full advantage of the prior information, complicated searching strategies must be employed. The complexity is getting larger for non-symmetrical distributions and at the same time the improvement in the mean acquisition time is getting less valuable. This implies that prior information is not used optimally by just defining suitable searching strategies. In the next chapter, a novel way of obtaining and using the *a priori* information is presented.

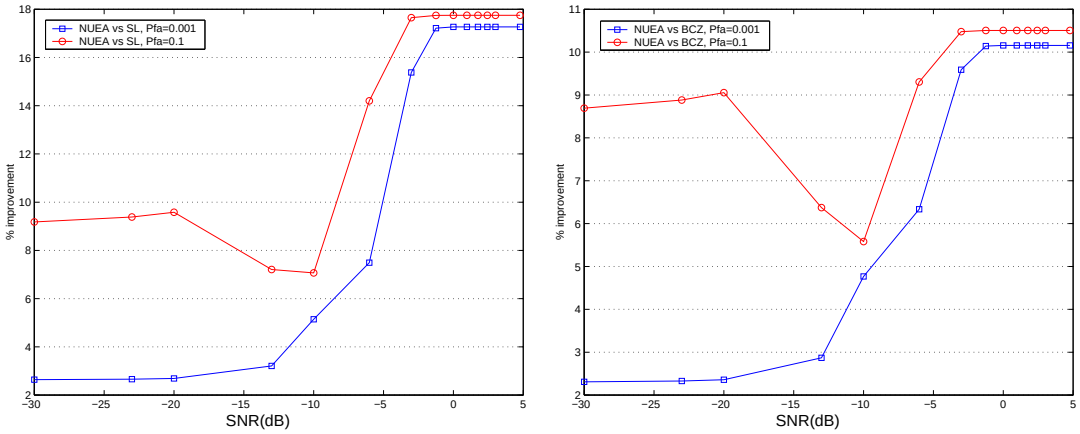

(a) *Improvement (%) in μ of the optimised NUEA over the straight line (SL) strategy*

(b) *Improvement (%) in μ of the optimised NUEA over the BCZ strategy*

Figure 3.23: *% improvement in μ offered by the NUEA strategy.*

Chapter 4
The Fast Preliminary Search (FPS) system: theoretical analysis for a DS/SS system

In this chapter, a novel PN code acquisition system is described and analysed. Every cell of the 1 or 2 dimensional ambiguity area is examined two times using a single dwell time acquisition system. The first search is a fast straight line serial search -the fast preliminary search (FPS)- the duration τ_{d1} of which is a crucial parameter of the system that must be optimised. The output of the first search is then used as *a priori* information, which determines the search order of the second and final search. The dwell time τ_{d1} of the first search is a fraction of τ_{d2} i.e. $\tau_{d1} = \alpha \cdot \tau_{d2}$ with $\alpha < 1$. The probability of false ranking P_{fr} is defined as a measure of the reliability of the *a priori* information provided by the fast preliminary search. The mean acquisition time $E(T_{acq})$ of the system is found using the direct approach. It is shown that by optimising τ_{d1} the mean acquisition time can be significantly improved.

In [12] an interesting problem is described. The scenario involves a lost satellite in a region of the sky and the searching procedure is very similar to the searching procedures that a synchronisation system usually employs. The difference is that in this problem, the energy detector was actually replaced by a radar beam. The method that E.C.Posner describes in [12], involves a preliminary search of the ambiguity area (the sky). The purpose of this search is to obtain a ranking of the various portions of the sky, so that the final search can examine the more likely regions of the sky first. It was shown that a preliminary search can reduce the expected search time. It is this idea that we actually used, in order to improve the mean acquisition time of the synchronisation procedure, but the analysis we will present here is totally different from that in [12].

The basic idea behind the FPS system (figure 4.1) is to provide reliable *a priori* information about the location of the correct cell in order to improve the acquisition time. The motivation for this work is that although, the idea described in chapter 2 about obtaining reliable *a priori*

information is valuable, the method of geometrically calculating the Doppler pdf has many problems: 1) extra information (the position of the mobile user and the coordinates of the subsatellite point and spot beam centre) is essential, 2) the Doppler pdf is time varying and as the satellite moves fast it must be updated in order to be usable, 3) a lot of extra calculations are involved, 4) finally, this method can only provide information about the Doppler ambiguity area. The FPS system is designed so that it overcomes these problems. More specifically, the FPS system:

- Provides reliable information about both time and frequency.
- Uses no extra location information in order to provide *a priori* information.
- Can be used with any CDMA mobile radio system, satellite or terrestrial.
- Can be used with any of the well known commercial synchronisation systems.
- Uses no extra hardware.

This chapter is organised as follows: 1) The basic idea and crucial parameters are described in detail. The false ranking probability, P_{fr}, is defined and calculated theoretically. 2) An approximation for the P_{fr} is presented and evaluated. 3) The optimisation procedure of the fast dwell time, τ_{d1}, is described. 4) The mean and variance of the acquisition time are derived for a single dwell active DS/SS system. 5) Finally, the performance of the system is briefly discussed. A more detailed presentation of its performance and comparison with other systems is given in the next chapter.

4.1 The basic concepts and parameters.

As described in chapter 1, in a direct sequence spread spectrum (DS/SS) communication system the transmitted signal can be modelled as:

$$s(t) = \sqrt{2}Ad(t)c(t)\cos\omega_c t \tag{4.1}$$

In equation 4.1, the parameters A^2 and ω_c represent the waveform's average power and carrier frequency respectively, $c(t)$ is the ± 1 PN code with chip duration T_c and $d(t)$ is a binary data sequence (which might or might not be present during the acquisition mode). The received

waveform is, then, given by:

$$r(t) = \sqrt{2}Ad(t)c(t - \zeta T_c)\cos\left[(\omega_c + \omega_D)t + \phi\right] + n(t) \tag{4.2}$$

where $n(t)$ is Additive White Gaussian Noise, ω_D denotes the frequency offset due to the Doppler effect, ζT_c is the PN code delay with respect to an arbitrary time reference and ϕ the carrier phase offset. According to equation 4.2 the synchroniser's task is to provide the receiver with reliable estimations $\hat{\zeta}$, $\hat{\omega}_D$ and $\hat{\phi}$, of the corresponding unknown quantities so that despreading and demodulation will be successful [18]. Usually the receiver assumes that there are certain bounds for both the phase (time) and frequency offsets (denoted by ΔT and ΔF respectively) which are subdivided into smaller areas $\delta\tau \times \delta f$. It is obvious that the synchroniser must perform a two-dimensional search in the $(\Delta T, \Delta F)$ area as previously described in chapter 3. The basic parameters that usually describe a DS/SS synchroniser are: the probability of correct detection, P_d, i.e. the probability that the detector correctly indicates synchronisation when the local and the received codes are properly aligned, the probability of false alarm, P_{fa}, i.e. the probability that the detector will falsely indicate synchronisation when the two codes are actually misaligned, the *dwell time*, τ_d, i.e. the time that the decision device spends examining each one of the possible uncertainty subregions $(\delta\tau, \delta f)$, and the *penalty time*, τ_p, i.e. the time in order to recognise that a false alarm occurred and resume the search. The functions and

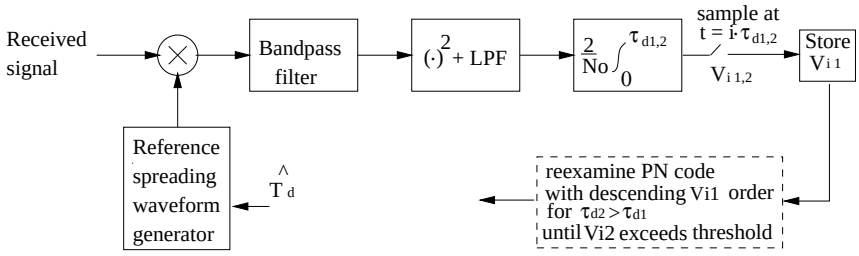

Figure 4.1: *The FPS system:each cell i is examined twice, using the same hardware.*

characteristics of the FPS system are:

- Each cell (marked with i in figure 4.1) is examined for a short time τ_{d1}, using the single dwell serial acquisition system.
- For a noiseless procedure the correct cell would give the maximum output V_{i1} (figure 4.1).
- The cells are ranked according to the I-D circuit output V_{i1} and then re-examined (final

search), following a descending V_{i1} order for a larger period τ_{d2} until a predetermined threshold is exceeded, i.e. by using again the same single dwell serial acquisition system.

- The critical parameters for the first (fast) search are: *SNR*, the short dwell time τ_{d1}, the bandwidth B of the filter and the probability of false ranking P_{fr}, i.e. the probability that the output V_{i1} of a wrong cell will be larger from that of the correct cell.
- The critical parameters for the second search are: the probability of detection P_d, the probability of false alarm P_{fa}, the threshold T_h and the dwell time τ_{d2}.

Figure 4.2 is a flowchart which depicts the basic functions of the FPS system. We assume that the fast search and ranking procedure are performed in parallel, i.e. as one cell is being examined, the cells that were tested before that cell are sorted and ranked using an appropriate sorting algorithm. Thus, we can assume that the ranking procedure does not contribute to the mean acquisition time of the FPS system.

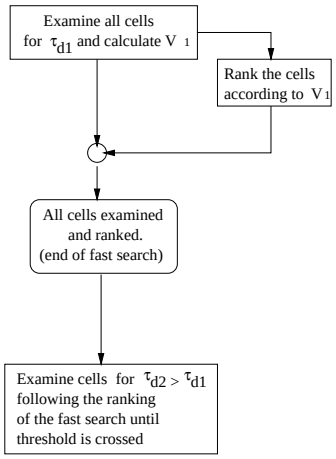

Figure 4.2: *A flowchart of the FPS sysyem*

The following analysis concerns the fast search part of the FPS system, and it was carried out assuming a one-dimensional ambiguity area, i.e. the PN code delay. In this case, equation 4.2, assuming no data during the acquisition mode, can be written as:

$$r(t) = \sqrt{2}Ac(t - \zeta T_c)\cos\left[\omega_c t + \phi_r\right] + n(t) \tag{4.3}$$

while the local reference is given by:

$$l(t) = c(t - \gamma T_c)\cos\left[(\omega_c + \omega_{IF})t + \phi_l\right] \tag{4.4}$$

The situation of interest is shown in figure 4.1. The input to the intermediate frequency (IF) bandpass filter (the bandwidth of which is B, centred around ω_{IF}) is taken from the output of the despreading mixer. When the reference waveform phase is correct, the received signal will be despread and it will appear at the filter output, as a carrier, corrupted by white Gaussian noise. If the reference is not correct we assume that only AWGN is present at the output of the filter. The AWGN has a two-sided power spectral density N_{o1} over the frequency range $|f - f_{IF}| < B/2$. The squaring device is combined with a low pass filter which eliminates the double-frequency terms that result from the squaring operation. An Integrate-and-Dump (I-D) circuit follows, where the lowpass squared output is integrated for τ_{d1} s and, finally, the output of this operation V_{i1} is stored in order to be used in the final search.

It has been shown (for a detailed analysis see [4]-chapter 5 and [114]) that when the reference waveform is not correct, (we will refer to this as H_0 case), the output V_n of the I-D circuit follows the chi-square pdf:

$$f_{p0}(v_n) = \begin{cases} \frac{1}{2^{n/2}\Gamma(n/2)} v_n^{(n/2)-1} exp(-\frac{v_n}{2}) & , V_n \geq 0 \\ 0 & , V_n < 0 \end{cases} \tag{4.5}$$

where $n = 2B\tau_{d1}$ is the degrees of freedom of the pdf (n is also the mean value of the chi-square pdf, and the variance is $2n$ [115]). When the phase of the reference waveform is the correct one, (we will refer to this as H_1 case, which we assume to be unique), the output V_s of the I-D circuit follows the non-central chi-square pdf ([4, 114]):

$$f_{p1}(v_s) = \begin{cases} \frac{1}{2}\left(\frac{v_s}{\lambda}\right)^{(n-2)/4} exp\left(-\frac{v_s}{2} - \frac{\lambda}{2}\right) I_{\frac{n}{2}-1}(\sqrt{v_s\lambda}) & , V_s \geq 0 \\ 0 & , V_s < 0 \end{cases} \tag{4.6}$$

where $n = 2B\tau_{d1}$, $\lambda = 2B\tau_{d1}\frac{(A/2)^2}{N_{o1}B} = n\gamma_o$ is the non-centrality parameter (the mean value of the non-central chi-square is $n + \lambda$ and the variance is $2(n + 2\lambda)$ [115]), γ_o is the SNR at the output of the bandpass filter and $I_N(\cdot)$ is the modified Bessel function of the first kind of order N. In the case where the search is being advanced in non-integer steps of a chip (1/4 or 1/2), A must be replaced by:

$$\hat{A} = \begin{cases} A\left(1 - \frac{|\tau|}{T_c}\right) & , |\tau| \leq T_c \\ 0 & , |\tau| > T_c \end{cases} \tag{4.7}$$

where $|\tau| = |\zeta - \gamma|T_c$ and T_c is the PN code chip duration. We must note at this point that the previous definition of the γ_o is simplified, as it does not take into account the effects of the partial correlation, the filter and the reduction in the noise spectral density caused by the PN despreading. Details about how the γ_o must be modified due to those factors can be found in [5] (part 4, chap.1), [2], [28], [116]. In this work however, we will use the simplified definition of the SNR, as it will allow us to evaluate the FPS system more easily. In any case, the exact definition of the SNR will not alter the results and conclusions about the FPS system.

In order to calculate the probability of false ranking we define the random variable Y as:

$$Y = V_n - V_s \tag{4.8}$$

where the random variables V_n and V_s are defined in equations 4.5 and 4.6. The pdf of Y is given ([97]-chap.6) by:

$$f_{pY}(y) = \int_{-\infty}^{+\infty} f_{p0}(y + v_s) f_{p1}(v_s) dv_s \tag{4.9}$$

Combining equations 4.5, 4.6, 4.9 will finally result into:

$$f_{pY}(y) = \frac{1}{2} \frac{e^{-y/2} e^{-\lambda/2}}{\lambda^{(n-2)/4} 2^{n/2} \Gamma(n/2)} \cdot \int_0^{+\infty} v_s^{\frac{n-2}{4}} (y + v_s)^{\frac{n}{2}-1} e^{-v_s} I_{\frac{n}{2}-1}(\sqrt{v_s \lambda}) dv_s \tag{4.10}$$

The probability of false ranking P_{fr} is defined as the probability $\mathbf{P}$ that the output v_n of a wrong cell will be larger from the output of the correct cell v_s:

$$P_{fr} = \mathbf{P}(Y > 0) = \int_0^{+\infty} f_{pY}(y) dy \tag{4.11}$$

From equations 4.10 and 4.11 the probability of false ranking is:

$$P_{fr} = \frac{1}{2} \frac{e^{-\lambda/2}}{\lambda^{(n-2)/4} 2^{n/2} \Gamma(n/2)} \cdot \int_0^{+\infty} e^{-\frac{y}{2}} \int_0^{+\infty} v_s^{\frac{n-2}{4}} (y + v_s)^{\frac{n}{2}-1} e^{-v_s} I_{\frac{n}{2}-1}(\sqrt{v_s \lambda}) dv_s dy \tag{4.12}$$

Equation 4.12 is the exact analytical formula for the probability of false ranking but it is complicated and requires a lot of computational power and time in order to give accurate numerical values. In the next section we present a method to approximate equation 4.12 with the simple Marcum's function.

4.2 The Gaussian approximation

In order to provide a simpler expression for the numerical computation of the probability of false ranking we will approximate the probability density at the output of the integrator by a Gaussian pdf for both the H_0 and the H_1 cases. Due to the central limit theorem, the approximation will be improved as the time-bandwidth product $B\tau_{d1}$ increases. The density functions that must be evaluated are:

$$\begin{array}{ll} \tilde{f}_{p0}(v_n) = \frac{1}{\sigma_n\sqrt{2\pi}} exp\left(-\frac{(v_n-E_n)^2}{2\sigma_n^2}\right) & , H_0\, case \\ \tilde{f}_{p1}(v_s) = \frac{1}{\sigma_s\sqrt{2\pi}} exp\left(-\frac{(v_s-E_s)^2}{2\sigma_s^2}\right) & , H_1\, case \end{array} \tag{4.13}$$

where $E_{n,s}$, $\sigma^2_{n,s}$ are the mean value and the variance, respectively, for the two cases that need to be calculated. In what follows we will only give the basic points of the computations. A detailed mathematical analysis can be found in [4, 114] while, some comments can also be found in appendix C.

For the H_0 case, the input to the integrator (after squaring and retaining only the baseband components) can be modelled as:

$$w(t) = n_I^2 + n_Q^2 \tag{4.14}$$

where n_I and n_Q are baseband Gaussian noise processes with power spectral densities $N_o/2$ over the frequency range $|f| < B/2$. It can be shown that:

$$E_n = E\left[\frac{2}{N_o}\int_0^{\tau_{d1}} w(t)dt\right] = 2B\tau_{d1} \tag{4.15}$$

where $E[\cdot]$ represents the mean value of the quantity within the brackets. We can see that E_n is the same as the mean value of the chi-square pdf (see equation 4.5). The variance at the output of the integrator ([4, 97]) is given by:

$$\sigma_n^2 = \frac{8\tau_{d1}}{N_o^2}\int_0^{\tau_{d1}} \left(1 - \frac{x}{\tau_{d1}}\right)\left[R_w(x) - E^2(w(t))\right] dx \tag{4.16}$$

where $w(t)$ is the integrator (baseband) input and $R_w(x)$ the autocorrelation function of $w(t)$. It can be shown ([4]) that $R_w(\tau) = 4R_n(\tau)^2 + 4\sigma^4_{nlp}$, where $\sigma_{nlp} = \sqrt{N_oB/2}$ is the standard deviation of n_I and n_Q and $R_n(\tau) = \frac{N_oB}{2}sinc(B\tau)$ is the autocorrelation function of the same

quantities. After some algebra, the variance σ_n^2 is:

$$\sigma_n^2 = 4nB \int_0^{\tau_{d1}} \left(1 - \frac{x}{\tau_{d1}}\right) sinc^2(Bx)dx \tag{4.17}$$

where $n = 2B\tau_{d1}$ as in equation 4.6. It is interesting to notice that:

$$\lim_{B\tau_{d1}\to\infty} \sigma_n^2 = 2n$$

i.e. for large time-bandwidth products both the variance and the mean value of the Gaussian approximation of the H_0 case equal that of the exact chi-square pdf, as expected due to the central limit theorem.

For the H_1 case, the input $s(t)$ to the square-law detector is the bandpass component of the $r(t)l(t)$ product:

$$s(t) = \frac{\sqrt{2}}{2} A \cos\phi \cos\omega_{IF} - \frac{\sqrt{2}}{2} A \sin\phi \sin\omega_{IF} \tag{4.18}$$

The integrator input is the baseband components of $w(t) = [s(t) + n(t)]^2$ and the mean value of the integrator output is:

$$E_s = E\left[\frac{2}{N_o}\int_0^{\tau_{d1}} w(t)dt\right] = 2B\tau_{d1}\left(1 + \frac{P}{N_o B}\right) \tag{4.19}$$

where $P = A^2/4$ is the signal power at the output of the bandpass filter. It is convenient to write equation 4.19 in the equivalent form: $E_s = 2B\tau_{d1}(1 + \gamma_o) = n + \lambda$. Once more we notice that the mean value of the approximate Gaussian is the same as the mean value of the exact non-central chi-square pdf. The variance σ_s^2 is given again by equation 4.16 where $E(w(t)) = P + N_o B$, $R_w(\tau) = (P + 2\sigma_n^2)^2 + 4PR_n(\tau) + 4R_n(\tau)^2$ and σ_{nlp}, $R_n(\tau)$ as defined for the H_0 case. The final expression for the variance is:

$$\sigma_s^2 = 4nB\gamma_o \int_0^{\tau_{d1}} \left(1 - \frac{x}{\tau_{d1}}\right) \left[2sinc(Bx) + (\gamma_o)^{-1} sinc^2(Bx)\right] dx \tag{4.20}$$

For large time-bandwidth products we have:

$$\lim_{B\tau_{d1}\to\infty} \sigma_s^2 = 2n(1 + 2\gamma_o)$$

Similar to the H_0 case, for large time-bandwidth products both the variance and the mean value

of the Gaussian approximation of the H_1 case equal that of the exact non-central chi-square pdf.

As the pdfs of both random variables V_n and V_s have been approximated by the Gaussian pdf, the new random variable $Y = V_n - V_s$ can also be approximated by a Gaussian pdf, the mean value of which is $E_y = E_n - E_s = -2B\tau_{d1}\gamma_o$ and the variance is $\sigma_y^2 = \sigma_n^2 + \sigma_s^2$ which can be written as:

$$\sigma_y^2 = 8Bn \left[\int_0^{\tau_{d1}} \left(1 - \frac{x}{\tau_{d1}}\right) sinc^2(Bx)dx + \gamma_o \int_0^{\tau_{d1}} \left(1 - \frac{x}{\tau_{d1}}\right) sinc(Bx)dx \right] \quad (4.21)$$

which after some algebrical manipulations (see appendix C) becomes:

$$\sigma_y^2 = \frac{8}{\pi^2} \left[2\gamma_o \cos(\frac{n}{2}\pi) + \cos(n\pi) + n\pi Si(n\pi) + \gamma_o n\pi Si(\frac{n}{2}\pi) + Ci(n\pi) - ln(n\pi) - 2\gamma_o - 1 - \Gamma_E \right] \quad (4.22)$$

where $n = 2B\tau_{d1}$, $\Gamma_E = 0.5772156649$ is the Euler's constant and the functions $Si(x)$ and $Ci(x)$ are related to the sine and cosine integrals $si(x)$ and $ci(x)$ by the integrals ([117]-page xxxv):

$$\begin{aligned} Si(x) &= \int_0^x \frac{\sin t}{t} dt = si(x) + \pi/2 \\ Ci(x) &= \Gamma_E + lnx + \int_0^x \frac{\cos t - 1}{t} dt \end{aligned}$$

The probability of false ranking is:

$$P_{fr} = \mathbf{P}(Y > 0) = \int_0^{+\infty} \frac{1}{\sigma_y\sqrt{2\pi}} exp\left(-\frac{(y - E_y)^2}{2\sigma_y^2}\right) dy = Q\left(-\frac{E_y}{\sigma_y}\right) \quad (4.23)$$

where $Q(\cdot)$ denotes the Marcum's function. Equation 4.23 is the Gaussian approximation for the probability of false ranking. The Marcum's Q-function can be easily evaluated as a polynomial expansion ([115] and appendix C) while the overall computational time is very short compared to that of equation 4.12. Simulations for various time-bandwidth products $B\tau_{d1}$ have been carried out in order to evaluate the accuracy of the approximation. For $2 < B\tau_{d1} < 8$, the approximate result is within 5% of the exact result, while for $B\tau_{d1} > 8$ the two results are almost identical. Figure 4.3 depicts the probability of false ranking as a function of the γ_o for both the exact case and the Gaussian approximation. We must note that the maximum value of P_{fr} is $P_{frMAX} = 0.5$, as it is a binary decision taken for every cell individually. By inserting σ_y

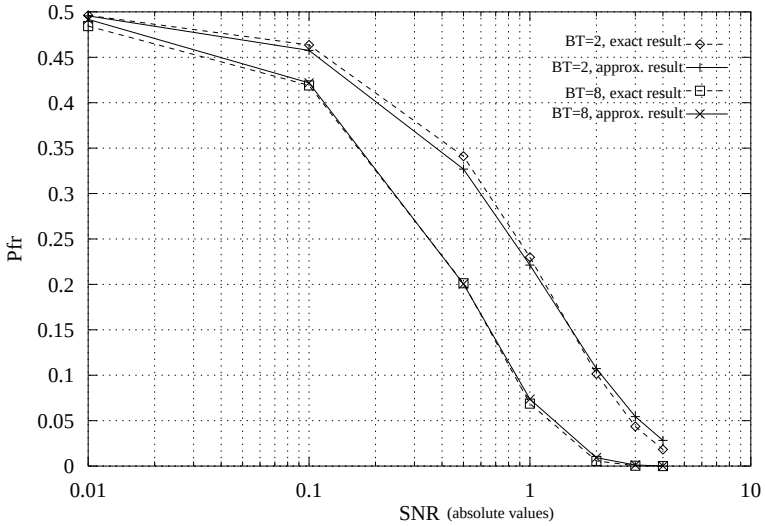

Figure 4.3: *The P_{fr} as a function of γ_o for the exact case and the Gaussian approximation.*

and E_y into equation 4.23 we can plot figure 4.4, which depicts the probability of false ranking as a function of the τ_{d1} for various SNRs and time-bandwidth product $B\tau_{d1} = 102.4$. The τ_{d1} is given as a fraction of the second dwell time τ_{d2} which is set to be $\tau_{d2} = 1$. Figures 4.4(a) and 4.4(b) present the same results but using different scales (linear and logarithmic respectively). Thus, it is possible to see how P_{fr} depends on the τ_{d1} even for high SNRs for which, the false ranking probability is very small. As was expected, P_{fr} tends to be reduced as $\tau_{d1} \rightarrow 1 \cdot \tau_{d2}$. We will use this fact later in order to optimise the mean acquisition time with respect to the fast dwell time τ_{d1} for a given SNR. It is also interesting to notice that P_{fr} is less sensitive at very low SNRs. Figure 4.5, depicts the same function but for a smaller time-bandwidth product $B\tau_{d1} = 12.4$. The difference with the previous case (figure 4.4) is that the curves are not as steep, i.e. the improvement in the false ranking probability as $\tau_{d1} \rightarrow 1 \cdot \tau_{d2}$ is much larger for large time-bandwidth products.

4.3 Calculation of the mean acquisition time

The *direct approach* [11] was used in order to calculate the mean acquisition time. It was shown in [11] that the mean acquisition time $E(T_{acq})$ is given by the equation:

$$\begin{aligned} E(T_{acq}) &= \sum_{i=1}^{\infty} P_d(1-P_d)^{i-1} \sum_{j=1}^{q} P_c(j) \\ &\quad \cdot ([m(i,j)-i]E(T_r) + [i-1]E(T_m) + E(T_d)) \end{aligned} \tag{4.24}$$

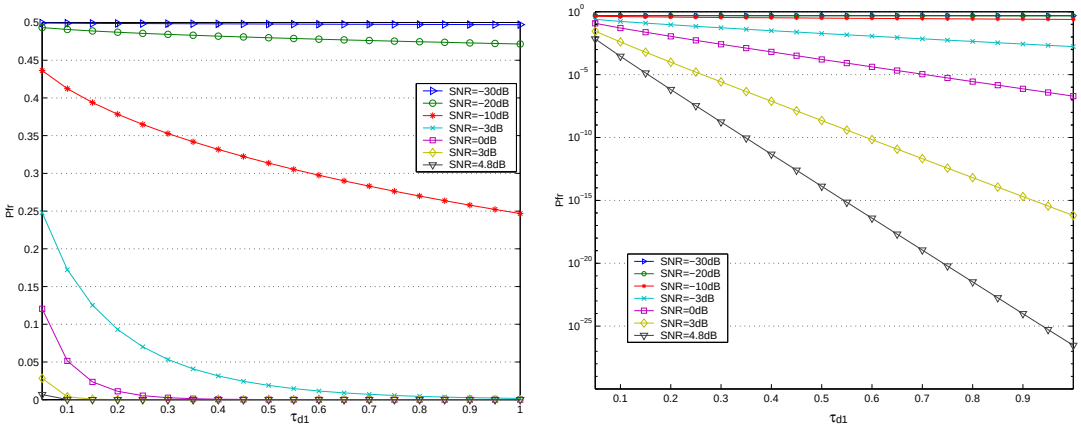

(a) *The P_{fr} as a function of τ_{d1} (linear scale)*

(b) *The P_{fr} as a function of τ_{d1} (logarithmic scale)*

Figure 4.4: *The P_{fr} as a function of the fast dwell time τ_{d1} for $q = 200$, $k = 20$ and $B\tau_{d1} = 102.4$)*

Equation 4.24 provides the mean acquisition time assuming that there are q possible cells in the uncertainty region, there is only one correct cell, the probability of correct detection is P_d, and the probability of false alarm is P_{fa}. The functional $m(i,j)$ is defined as the total number of cells tested during the acquisition under the assumption that the correct location is in the cell marked with $''j''$ and that the correct detection happened during the i^{th} test of the j^{th} cell. $P_c(j)$ represents the *a priori* probability of the correct cell location, i.e. the probability that the j^{th} cell is actually the correct one. During the search, there are three possible outcomes of the tests and three (generally random) times associated with them: T_r which is the time required for the rejection of the incorrect cell (including penalty time τ_p in the case of false alarm), T_m which is the time required for the false dismissal of the correct cell and T_d which is the time required for the correct detection. In equation 4.24 $E(T_r)$, $E(T_m)$, $E(T_d)$ are the expected values of the corresponding times.

The FPS system is a combination of two procedures: the fast search mode, the duration T_1 of which is constant $(T_1 = q\tau_{d1})$ and the final search mode which is a simple, single dwell acquisition system. If $E(T_2)$ is the mean acquisition time for this final search, the overall mean acquisition time for the FPS system is simply:

$$E(T_{acq}) = q\tau_{d1} + E(T_2) \tag{4.25}$$

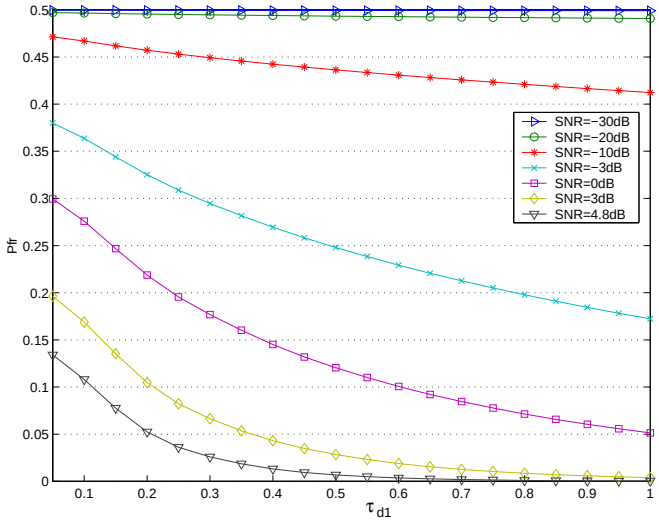

Figure 4.5: *The P_{fr} as a function of the fast dwell time τ_{d1} for $q = 200$, $k = 20$ and $B\tau_{d1} = 12.4$)*

The term $E(T_2)$ can be calculated using equation 4.24. The *a priori* probability $P_c(j)$ of the correct cell location for this case must be replaced by the probability that the correct cell will be tested after $j-1$ wrong cells have been tested before it. This would have been the result of $j-1$ wrong decisions and $q-1-(j-1) = q-j$ correct decisions, during the fast search procedure. Thus, $P_c(j)$ is the probability that the event "wrong decision" occurs exactly $j-1$ times in $q-1$ independent trials:

$$P_c(j) = \begin{pmatrix} q-1 \\ j-1 \end{pmatrix} P_{fr}^{j-1}(1-P_{fr})^{q-j} \tag{4.26}$$

where P_{fr} is the probability of false ranking. With the functional $m(i,j)$ and also i,j thus defined, it is straightforward to see that:

$$m(i,j) = (i-1)q + j \tag{4.27}$$

It is proven in [11] that:

$$\begin{aligned} E(T_m) &= E(T_d) = \tau_{d2} \\ E(T_r) &= \tau_{d2} + P_{fa}\tau_p \end{aligned} \tag{4.28}$$

By inserting equations 4.25, 4.26, 4.27, 4.28 into equation 4.24 and after some algebrical ma-

nipulations which can be found in Appendix C, we have:

$$E(T_{acq}) = q\tau_{d1} + \frac{\tau_{d2}}{P_d} + \tau_{d2}(1 + kP_{fa}) \left[1 + (q-1)P_{fr} + \frac{q(1-P_d) - 1}{P_d}\right] \tag{4.29}$$

In order to calculate the variance of the acquisition time we used the equation [11] (see also appendix C):

$$Var(T_{acq}) = [F_2(P_d) - F_1^2(P_d)] \cdot (\tau_{d2} + P_{fa}\tau_p)^2 \tag{4.30}$$

where:

$$F_1(P_d) = \sum_{i=1}^{\infty} P_d(1-P_d)^{i-1} \sum_{j=1}^{q} P_c(j) m(i,j) \tag{4.31}$$

and:

$$F_2(P_d) = \sum_{i=1}^{\infty} P_d(1-P_d)^{i-1} \sum_{j=1}^{q} P_c(j) m(i,j)^2 \tag{4.32}$$

After substituting equation 4.26 in 4.31 and 4.32 we find:

$$\begin{aligned} F_2(P_d) - F_1^2(P_d) &= P_d + (q-1)P_d P_{fr}[3 + (q-2)P_{fr}] - \left(\frac{q(1-P_d)}{P_d}\right)^2 \\ &\quad -[1-(q-1)P_{fr}]^2 + q^2 P_d \sum_{i=1}^{\infty} (i-1)^2 (1-P_d)^{i-1} \end{aligned} \tag{4.33}$$

The variance can be calculated by inserting equation 4.33 into 4.30. Figure 4.6 is a typical example of the mean and variance of the acquisition time as a function of the false ranking probability P_{fr} for a given probability of false alarm and detection. Simulations have been carried out in order to test the accuracy of equation 4.29 and the results are shown in figure 4.7 for various combinations of $(P_d, P_{fa}, P_{fr}, \tau_{d1})$. We notice that the theoretical and experimental mean acquisition times are in very good agreement. The error is less than 1%.

We saw before (figure 4.4), that P_{fr} decreases as $\tau_{d1} \rightarrow 1 \cdot \tau_{d2}$. On the other hand, it is obvious from equation 4.29 that large τ_{d1} will probably result into large $E(T_{acq})$. By inserting equation 4.23 into equation 4.29 we can express $E(T_{acq})$ as a function of τ_{d1} and γ_o. Figure 4.8 depicts the results for various SNRs. It is obvious, that for most γ_o there is an optimum τ_{d1opt} that minimises the $E(T_{acq})$. Nevertheless, for very low and very high SNRs, it seems that there is

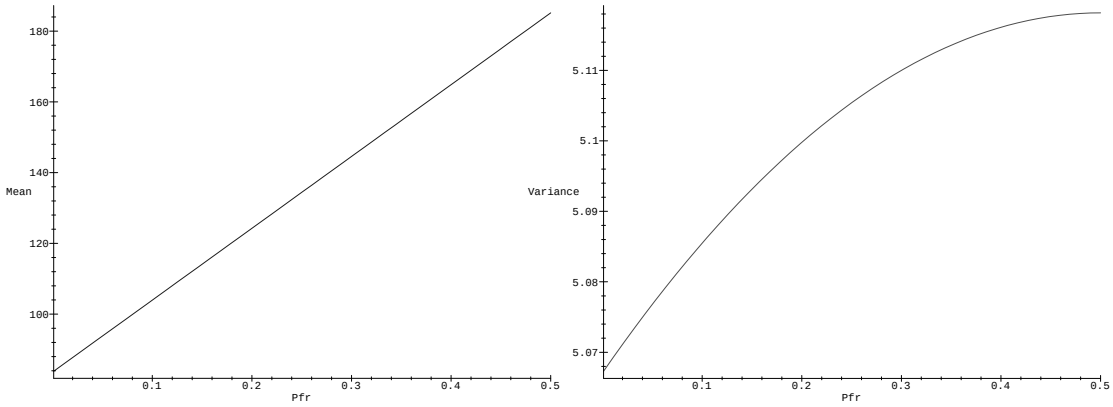

(a) *The mean acquisition time* **(b)** *and the corresponding variance*

Figure 4.6: *The mean and variance of the acquisition time as multiples of the* τ_{d2} *(*$q = 200, P_d = 0.9, P_{fa} = 0.001$*).*

not an optimum τ_{d1}. That is due to the fact (see the previous section) that P_{fr} is almost constant for the extreme SNRs. The optimum τ_{d1opt} is the root of $\frac{d[E(T_{acq})]}{d\tau_{d1}} = 0$ for which the second derivative is negative. The first derivative is given by the equation:

$$\frac{d[E(T_{acq})]}{d\tau_{d1}} = q - \frac{\sqrt{\pi}}{4}(q-1)(1+kP_{fa})B\gamma_o\tau_{d2}F_1 e^{(-1/8)\gamma_o^2\tau_{d1}/F_2} \tag{4.34}$$

where:

$$\begin{aligned}
F_1 &= F_{1a}/F_{1b} \\
F_{1a} &= -1 + cos(n\pi) + n\pi Si(n\pi) - 2ln(n\pi) + 2Ci(n\pi) - 2\Gamma_E + \gamma_o\pi n Si(\pi n/2) \\
&\quad +4\gamma_o cos(\pi n/2) - 4\gamma_o \\
F_{1b} &= -1 + cos(n\pi) + n\pi Si(n\pi) - ln(n\pi) + Ci(n\pi) - \Gamma_E + \gamma_o\pi n Si(\pi n/2) \\
&\quad +2\gamma_o cos(\pi n/2) - 2\gamma_o \\
F_2 &= 0.5\frac{-1 + cos(n\pi) + n\pi Si(2\pi B\tau_{d1})}{\pi^2 B^2\tau_{d1}} - 0.5\frac{ln(\pi n/2) - Ci(n\pi)}{\pi^2 B^2\tau_{d1}} - 0.5\frac{\Gamma_E + \ln(2)}{\pi^2 B^2\tau_{d1}} \\
&\quad +\frac{\gamma_o Si(\pi n/2)}{\pi B} + \gamma_o\frac{cos(\pi n/2)}{\pi^2 B^2\tau_{d1}} - \frac{\gamma_o}{\pi^2 B^2\tau_{d1}}
\end{aligned}$$

The optimum τ_{d1} can be calculated by solving numerically the $\frac{d[E(T_{acq})]}{d\tau_{d1}} = 0$. Equation 4.34 is complicated but the numerical solution is very fast and accurate.

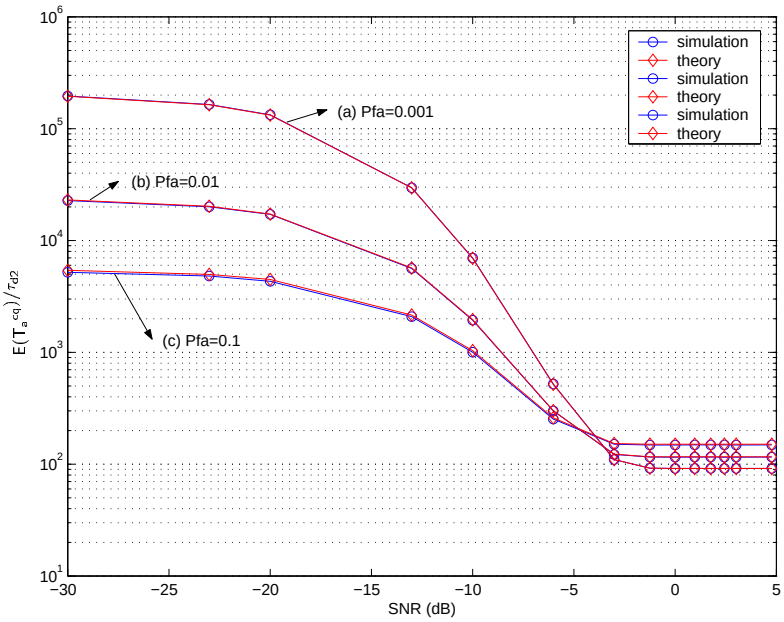

Figure 4.7: *A comparison between the theoretical and experimental mean acquisition time of the FPS system. The mean acquisition time and* τ_{d1} *are given as multiples of* $\tau_{d2} = 1$ *while,* $q = 200$, $k = 20$ *and (a)* $\tau_{d1} = 0.2$, *(b)* $\tau_{d1} = 0.1$, *(c)* $\tau_{d1} = 0.45$

4.4 Performance indications

In this section, we will present a comparison between the single dwell serial search acquisition system combined with a fast preliminary search mode, and the simple single dwell serial search (SDSS) acquisition system. We will compare the two systems in terms of the resulting mean acquisition time. This will allow us to determine under what conditions the utilisation of a fast preliminary search mode can improve the mean acquisition time of the system. It will also give an indication of the improvement that the FPS system can offer. The mean acquisition time for the SDSS system with no *a priori* knowledge of the location of the correct cell [5] is:

$$E(T_{acq})_{sd} = \tau_{d2}\frac{2 + (2 - P_d)(q-1)(1 + kP_{fa})}{2P_d} \tag{4.35}$$

while for the FPS system we will use equation 4.29. The mean acquisition time is given as a function of the SNR and the probability of false alarm P_{fa} for both systems. The probability of detection for the SDSS and the second search of the FPS system, assuming a CFAR criterion, is now given by:

$$P_d = Q\left(\frac{Q^{-1}(P_{fa}) - \gamma_o\sqrt{B\tau_{d2}}}{\sqrt{1 + 2\gamma_o}}\right) \tag{4.36}$$

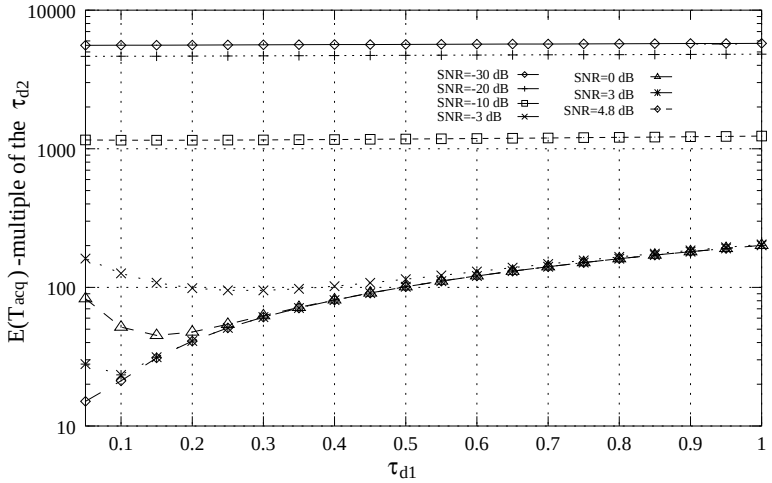

Figure 4.8: $E(T_{acq})$ *versus* τ_{d1} *for various* $SNRs$, $P_{fa} = 0.1$, $q = 200$, $k = 20$, $B = 100$ *kHz. All times are given as multiples of* $\tau_{d2} = 1$.

while P_{fr} for the fast search of the FPS system is calculated using equation 4.23. The two systems were compared under various conditions and the general conclusion is that, in most cases, FPS outperforms the conventional SDSS system. The crucial parameter that determines the performance of the FPS system for a given SNR and P_{fa} is the fast dwell time τ_{d1}. Figure 4.9a presents the τ_{d1opt} as a function of the SNR for various P_{fa}. What might seem as a paradox is that for the combination of low SNR and low P_{fa}, τ_{d1opt} is very short. This shows, though, that for those conditions it is preferable to switch to the final search as soon as possible as, in order to get reliable information from the fast search (low P_{fr}), we should spend a long time examining each cell, which will, in any case, increase the $E(T_{acq})$. Nevertheless, in spread spectrum systems with high processing gains it is probably unlikely to encounter the combination of very low SNR and low P_{fa} (note that the SNR is calculated at the output of the correlator of figure 4.1). For a given SNR and P_{fa} there is a maximum τ_{d1} (denoted by τ_{d1max}) such that for every $\tau_{d1} \leq \tau_{d1max}$, the mean acquisition time of the FPS system is better than that of the SDSS system. The maximum τ_{d1} can be easily calculated by equating 4.35 and 4.29 and solving for τ_{d1}. Figure 4.9b depicts the results for various P_{fa}. For P_{fa} up to 10^{-3} the τ_{d1max} as a function of the SNR is practically independent of the P_{fa} and in order to get an improved acquisition time from the FPS system we must keep $\tau_{d1} < 0.4\tau_{d2}$ for the SNRs of practical interest. For higher P_{fa}, the acceptable range of values of τ_{d1} for which FPS outperforms the SDSS is very large as can been seen from figure 4.9b and we can even have $\tau_{d1} > \tau_{d2}$ for very large P_{fa}. The two systems are compared in terms of the resulting mean acquisition time in figure 4.10. The FPS performs better for the SNRs of practical interest. The difference is more

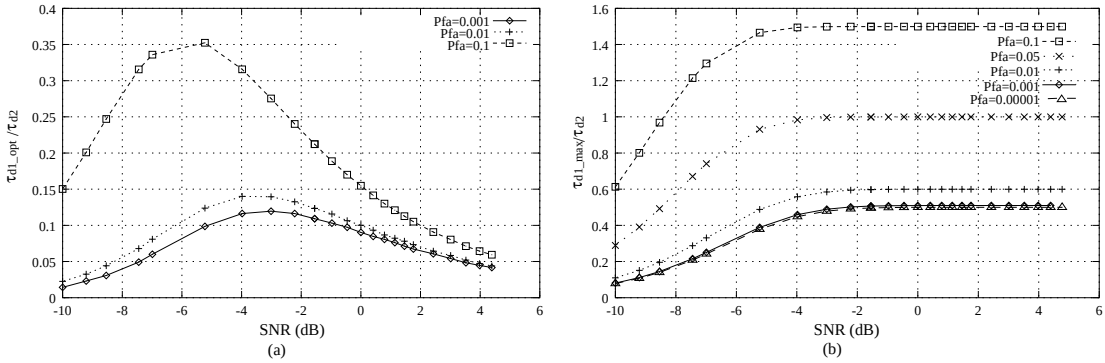

Figure 4.9: *τ_{d1opt}/τ_{d2} and τ_{d1max}/τ_{d2} as a function of the SNR and different P_{fa} ($q = 2046$, $k = 20$, $B = 100$ kHz).*

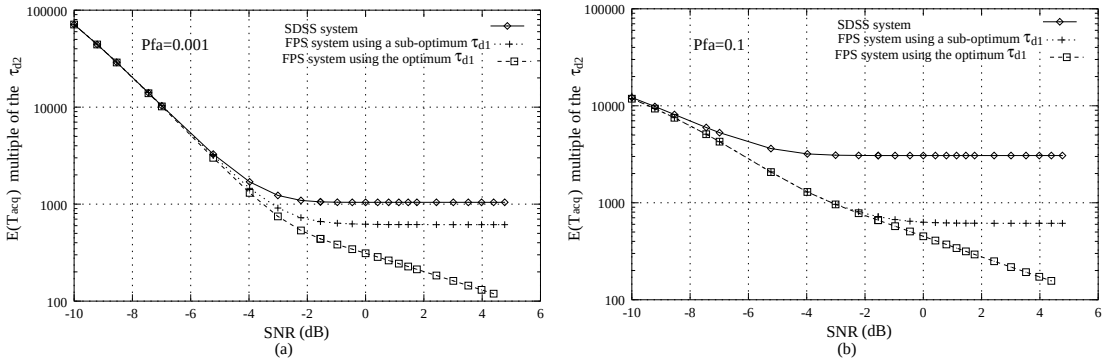

Figure 4.10: *$E(T_{acq})$ as a function of the SNR and two different P_{fa}. The sub-optimum time used is $\tau_{d1} = 0.3\tau_{d2}$ and $q = 2046$, $k = 20$, $B = 100$ kHz)*

significant for high P_{fa} and the reason is that the FPS system will have to recover from less false alarm situations, due to the fact that the fast search provides information, which allow the correct cell to be examined early enough in the final search, and thus the mean number of false alarms is reduced significantly.

It is clear from figures 4.9 and 4.10 that it is not necessary to use the optimum τ_{d1} in order to get better acquisition time, from the FPS system compared to the SDSS system. On the other hand, figure 4.10 shows that we get impressive improvements by using the τ_{d1opt} compared to what we get by using a sub-optimum τ_{d1}. Nevertheless, the use of τ_{d1opt} is restricted by two factors. The first is that τ_{d1opt} does not always exist (see section 4 and also notice in figure 4.10 that for the last value of the SNR the $E(T_{acq})$ is not calculated for the τ_{d1opt} case). The second factor is that the Gaussian approximation and thus all the previous results are valid for $B\tau_{d1} > 2$. For smaller product equation 4.12 must be used for the calculation of the P_{fr} and thus all the

results will be significantly different. There is another, more fundamental, limitation on the fast dwell time imposed by the effects of the partial correlation. More details on this constrain will be given in the next section.

The FPS system seems to be a very good compromise between the passive (matched filter) and the active straight line synchronisation schemes. It combines the hardware simplicity and robustness under bad conditions (low SNR, data modulation, Doppler) of the active schemes but it improves significantly their performance in terms of the mean acquisition time. The proposed FPS system is the simplest version. We did not consider any kind of verification modes or multiple dwell systems following the second search. The good results that we obtain, from the combination of the fast preliminary search of the ambiguity area with the simple single dwell system, allow us to be optimistic that a fast preliminary search mode could be included to any of the well known acquisition systems and result in better performance.

4.5 Limitations of the work

In the calculation of the false ranking probability, the usual assumption of perfect autocorrelation properties was made. It was assumed, that when the system is synchronised, the output of the correlator in figure 4.1 would be $(1 + AWGN)$ while in the non-synchronised case the output would be just the $AWGN$. This is a very usual assumption in the literature which is used in order to simplify the calculations of the detection/false alarm probabilities. In the FPS case however, this assumption must be examined carefully as the correlation length can be very short. Let us assume an $m-$sequence $\{a_n\}$ of period N. If we define the partial autocorrelation function for a period M, $M \leq N$ as:

$$P_{aa}(M, n, \tau) = \frac{1}{M} \sum_{j=0}^{M-1} a_{n+j+\tau} a_{n+j}^{*} \tag{4.37}$$

then, by using the theory of [118], [5],pg.291 and the identity $var(\alpha X) = \alpha^2 var(X)$, (where X is a random variable, α a constant and var the variance), it can be shown that the mean E_P and variance V_P of the time-average of $P_{aa}(M, n, \tau)$ are:

$$E_P = \begin{cases} 1, & \tau = 0 mod N \\ -\frac{1}{N}, & \tau \neq 0 mod N \end{cases} \tag{4.38}$$

$$V_P = \begin{cases} 0, & \tau = 0 mod N \\ \frac{1}{M}\left(1 - \frac{M-1}{N}\right) - \frac{1}{N^2}, & \tau \neq 0 mod N \end{cases} \tag{4.39}$$

respectively, for $M \leq N$ and $0 mod N$ depicts the multiples of the code period N. We must note that equations 4.38 and 4.39 are valid for chip offsets τ which are integer multiples of the chip duration T_c.

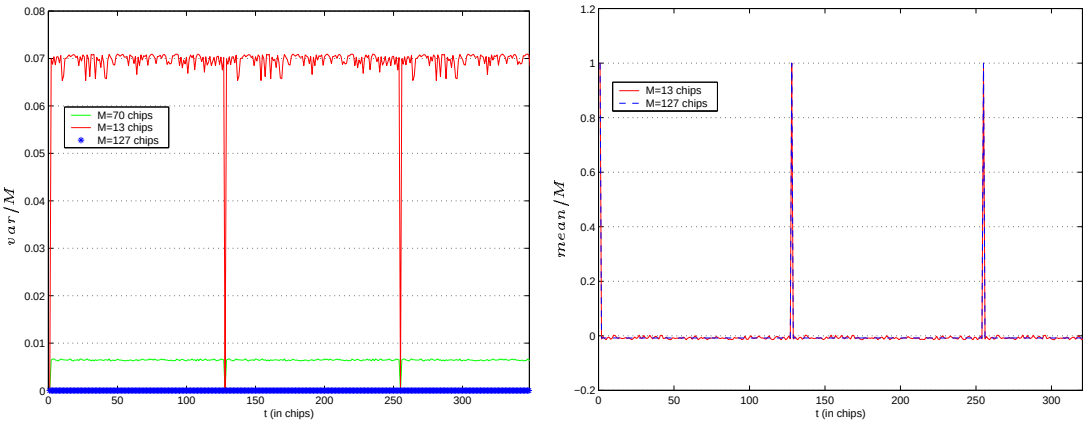

(a) *The autocorrelation variance*

(b) *The autocorrelation mean*

Figure 4.11: *The normalised mean and variance of the autocorrelation as a function of the relative time offset in integer chips for different integration lengths M and code length of 127 chips.*

Equations 4.38 and 4.39 were verified with simulations. Figure 4.11 depicts the variance and mean of the partial autocorrelation of an m-sequence of $N = 127$ chips for $M_1 = 13$ chips, $M_2 = 70$ chips and $M_3 = 127$ chips (full correlation). The variances according to equation 4.39 are $V_{P1} = 0.07$, $V_{P2} = 0.0065$ and $V_{P3} = 0$ respectively, which are in total agreement with the simulation results of figure 4.11(a). Similarly, the simulated and theoretical means are in excellent agreement.

It is obvious now, that if the dwell time is very short compared to the code period, then in the H_0 case we can not assume that the output of the bandpass filter in figure 4.1 is only AWGN. An extra term of self noise due to the partial correlation must be added. It has been shown in [5, 116] that the random variable $C = P_{aa}(M, n, \tau)$ can be regarded as Gaussian. In short, for $M \ll N$, C behaves like a binomial distribution and the additional constraint $M \gg 1$

causes the binomial distribution to behave like a Gaussian one. Thus, in order to take the effect of partial correlation into account, we can consider it as an extra Gaussian term that should be added to the thermal noise. The variance of the partial correlation noise (PCN) is given by equation 4.39 and it is depicted as a function of the lengths M and N in figure 4.12.

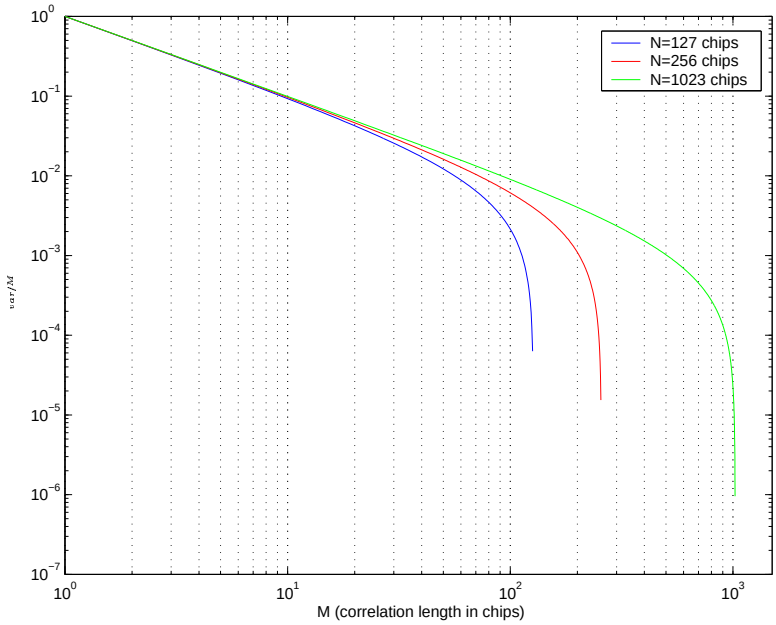

Figure 4.12: *The autocorrelation normalised variance (or equivalently the PCN power) as a function of M for various N.*

Figure 4.12 shows that even for short codes ($N = 127$) the variance of the PCN is ≈ 10 dB below the signal energy (i.e. the normalised autocorrelation mean) for partial autocorrelation lengths M as low as $M = 10$ chips. Thus, the PCN is well below the expected AWGN for all practical SNRs and M. As a result, we can approximate the output of the bandpass filter in the H_0 state with AWGN even for very small M as long as the SNR< 5 dB. Referring to figure 4.10, the effect of the PCN is that, after a certain SNR point it will dominate over the AWGN and the mean acquisition time (in the optimum τ_{d1} case) will stop decreasing and will be stabilised.

We must note however that, the previous results are valid for m-sequence PN codes only, for which equation 4.39 is valid. Figure 4.13 depicts the normalised variance of the autocorrelation as a function of the relative time offset for a Gold code of 127 chips length. It is obvious that the variance for small correlation length is not as good as for the simple $m-$sequences, but once more the differences with the theory will be significant only for the combination of large SNRs

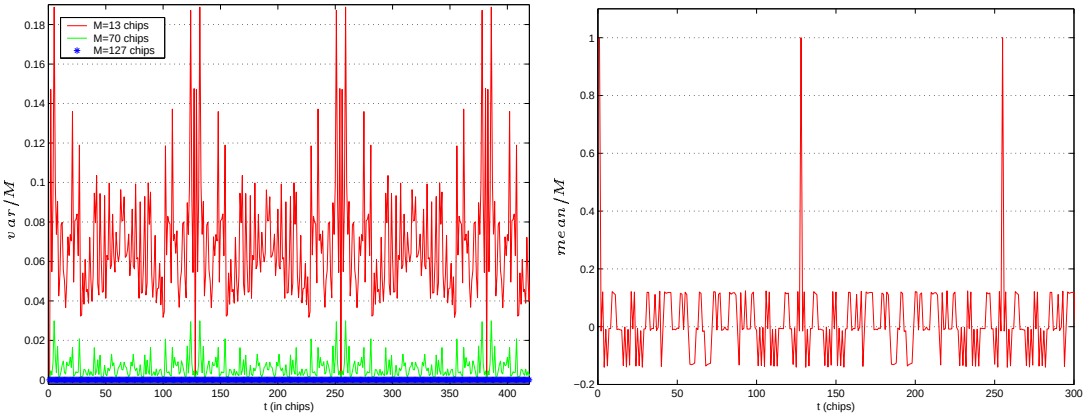

(a) *The autocorrelation variance*

(b) *The autocorrelation mean*

Figure 4.13: *The normalised mean and variance of the autocorrelation as a function of the relative time offset in integer chips for different integration lengths M for a Gold code with length 127 chips.*

and very short correlation lengths. The problem of partial correlation can be serious when the Walsh codes are used. The Walsh codes are orthogonal codes with good cross-correlation properties (when synchronised). Their autocorrelation properties though, are not good at all and furthermore they depend on the specific code. In general, the FPS system will have a poor performance when handling Walsh codes.

To summarise, the partial autocorrelation effects were studied and it is shown that for the $m-$sequences and Gold PN codes, the partial correlation can be ignored in the analysis of the FPS system, for all SNRs and fast dwell times of practical interest. In the next chapter, the performance of the FPS system is compared with that of more advanced acquisition systems.

Chapter 5
The Fast Preliminary Search (FPS) system: a comparative evaluation

In this chapter, the fast preliminary search method, which was introduced and analysed in chapter 4, is compared in terms of the resulting mean acquisition time with three synchronisation systems, namely:

- the single dwell acquisition scheme, in the case where a non uniform *a priori* information is provided and advanced searching strategies are utilised.
- the active double dwell straight line system.
- an adaptive filter based synchronisation system.

All the results support the view that a fast preliminary search mode can improve significantly the mean acquisition time of the system.

5.1 The FPS system versus the single dwell scheme with a known *a priori* distribution

In this section we compare the FPS system with the single, fixed dwell system (SD), assuming a one dimensional (time only) ambiguity area and using the parabola-shaped function, that was described earlier in chapters 2 and 3, as *a priori* information. We must notice at this point that we will use the parabola-shaped pdf as a time *a priori* information. In chapter 2, we derived this pdf, under certain geometrical assumptions, as the Doppler pdf within a LEO satellite spot-beam. In this section though, we will use it as a time information. This does not affect the results for the mean acquisition time and all the results of chapter 3, concerning the various searching strategies are valid. For the comparison we will use the two alternate strategies (NUEA and UEA) which always give the lower mean acquisition time for centrally peaked *a*

priori pdfs. The UEA and NUEA strategies are described in detail in chapter 3, where results are given for a parabolic *a priori* pdf and in [11] where results are given for a triangular and Gaussian *a priori* pdf of the (one dimensional) ambiguity area. The basic idea behind UEA and NUEA is to examine the cells following the order of the decreasing *a priori* probability. For the triangular and Gaussian *a priori* pdfs, NUEA performs better than UEA, although for large probabilities of detection ($P_d > 0.8$) the two strategies perform similarly. For the parabolic Doppler pdf, it was shown in chapter 3, that UEA performs slightly better than NUEA for $P_d > 0.5$ while for low P_d NUEA performs marginally better than UEA. The differences, though, are so small that we can consider the two strategies to be equivalent concerning the mean acquisition time performance. It was also shown in chapter 3 that by using NUEA or UEA, given a parabolic pdf, the mean acquisition time can be reduced by up to 18% compared to the straight line search (i.e. examining one cell after another without any particular order) of the ambiguity area. Motivated by those results, we compare the FPS system with the SD acquisition scheme that utilises the alternate strategies. The mean acquisition time is given as a function of the SNR (denoted by γ_o) and the probability of false alarm P_{fa} for both systems. For the FPS system we use equation 4.29 while for the SD/alternate we use the theory presented in chapter 3, i.e. equation 3.40 for the UEA strategy and equation 3.41 for the NUEA strategy. The probability of detection for the SD and the second search of the FPS system is given by equation 4.36 (assuming a CFAR criterion), while P_{fr} for the fast search of the FPS system is calculated using equation 4.23. For the FPS system a sub-optimum fast dwell time τ_{d1} was used for all the simulations and was set to be $\tau_{d1} = 0.3\tau_{d2}$, where τ_{d2} is the dwell time for both the SD system and the second search of the FPS system. Finally, the penalty time is $\tau_p = 20\tau_d$ for both systems and for the FPS system we used $B\tau_{d1} = 100$. Figures 5.1, 5.2 and 5.3(a) present the normalised mean acquisition time $E(T_{acq})/\tau_{d2}$ as a function of the SNR, for the SD/NUEA, SD/UEA, straight line/SD and FPS systems. For very low SNRs, as in figures 5.1(a) and 5.2(a), (which is unlikely to occur in spread spectrum systems with high processing gains-note that the SNR is the one at the output of the bandpass filter of figure 4.1), the two alternate strategies perform marginally better than the FPS and straight line SD. In fact, FPS is the poorest of all strategies. The reason for this poor performance is that for very low SNRs the $P_{fr} \to 0.5$ (as can be seen in figures 5.3(b), 4.4 and 4.5). A probability of false ranking near 50% indicates that the provided information is effectively random and thus, no improvement is expected. In fact, under these conditions we expect a larger acquisition time compared even to the straight line SD system due to the extra dwell time τ_{d1} that the FPS uses. On the other

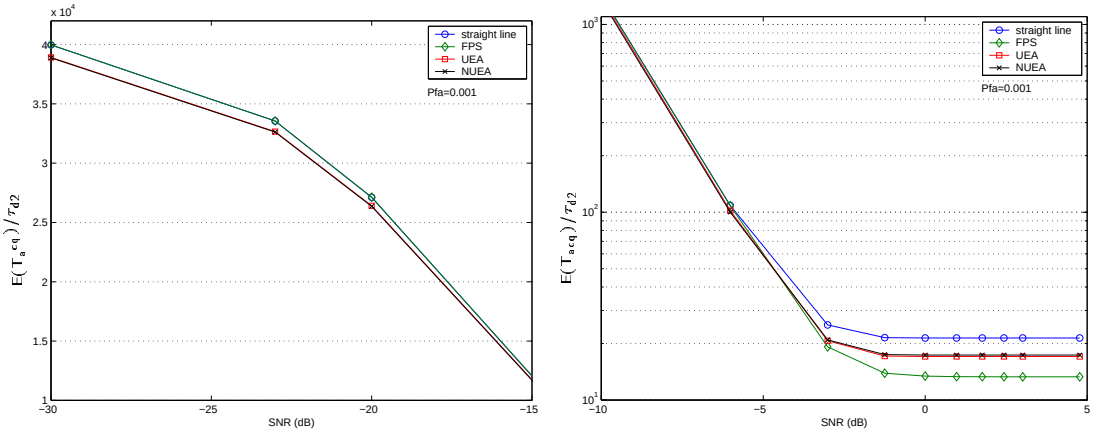

(a) $E(T_{acq})/\tau_{d2}$ *as a function of the SNR for* $SNR < -15$ *dB.*

(b) $E(T_{acq})/\tau_{d2}$ *as a function of the SNR for* $SNR > -10$ *dB.*

Figure 5.1: $E(T_{acq})$ *as a function of the SNR and* $P_{fa} = 10^{-3}$

hand, for the SNRs of practical interest (figures 5.1(b) and 5.2(b)), the FPS strategy clearly outperforms all the single dwell systems (straight line, UEA and NUEA). The reason is that for these SNRs the false ranking probability is low. Thus, the information according to which the second search is performed, is very reliable and results in a very good performance. Figure 5.3(a) is a comparison between the SD/UEA and the FPS scheme for all SNRs and various false alarm probabilities. We can see that the performance of the FPS is further improved for larger P_{fa} and this indicates that the FPS system has to recover from a small number of false alarm situations compared to any SD system. This is due to the fact, that the correct cell will be examined soon and if the probability of detection is high enough the number of false alarms is reduced dramatically, since the mean number of false cells that are actually examined is very small.

5.2 The FPS system versus the double dwell time scheme.

The multiple dwell serial search system is a generalisation of the single dwell serial PN acquisition system. As discussed in the first chapter, the scheme falls into the class of fixed dwell time synchronisation schemes in the sense that the variation in integration time is achieved by allowing the examination interval to consist of a series of fixed short dwell periods (each longer than

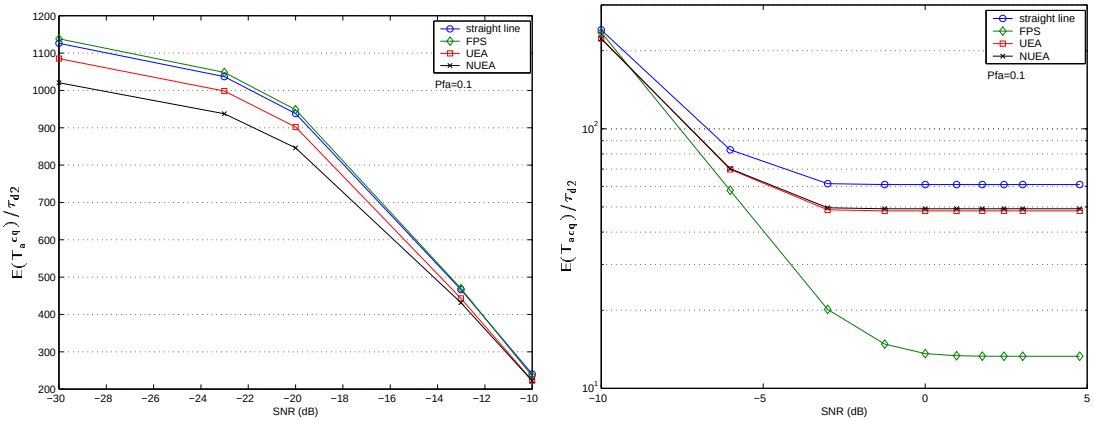

(a) $E(T_{acq})/\tau_{d2}$ *as a function of the SNR for* $SNR < -10$ *dB.*

(b) $E(T_{acq})/\tau_{d2}$ *as a function of the SNR for* $SNR > -10$ *dB.*

Figure 5.2: $E(T_{acq})$ *as a function of the SNR and* $P_{fa} = 10^{-1}$

its predecessor) with a decision being made after each. More details can be found in chapter 1, while an extensive analysis can be found in [5, 40, 112]. The most important multiple dwell search system is the two dwell serial search system (TDSS), which we will also use in order to compare it with the FPS system. The calculation of the mean acquisition time $E(T_{acq})_N$ for the general N-dwell system, can be found in [112] and for $q \gg 1$ is given by:

$$E(T_{acq})_N \approx q\frac{(2-P_D)}{2P_D}\sum_{j=1}^{N}\left[t_j\prod_{i=1}^{j-1}P_{fai} + P_{FA}\tau_p\delta_{jN}\right] \tag{5.1}$$

where t_j is the dwell time of each of the N dwells, P_{fai} and P_{di} the corresponding false alarm and detection probabilities, $P_{FA} = \prod_{i=1}^{N} P_{fai}$, $P_D = \prod_{i=1}^{N} P_{di}$, τ_p the penalty time and δ_{jN} the well known Kronecker delta function. For the double dwell (DD) system ($N = 2$), equation 5.1 becomes:

$$E(T_{acq})_2 = q\frac{(2-P_{d1}P_{d2})}{2P_{d1}P_{d2}}[t_1 + t_2P_{fa1} + P_{fa1}P_{fa2}\tau_p] \tag{5.2}$$

Equation 5.2 is the same as the one presented in page 782 of [40], in which the penalty time has been set equal to $\tau_p = kt_2$. In order to compare the two systems we will use the following parameters:

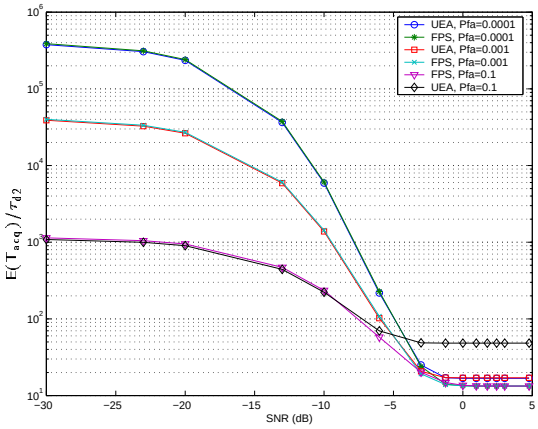

(a) *$E(T_{acq})/\tau_{d2}$ as a function of the SNR and three different P_{fa}.The FPS and SD/UEA are compared.*

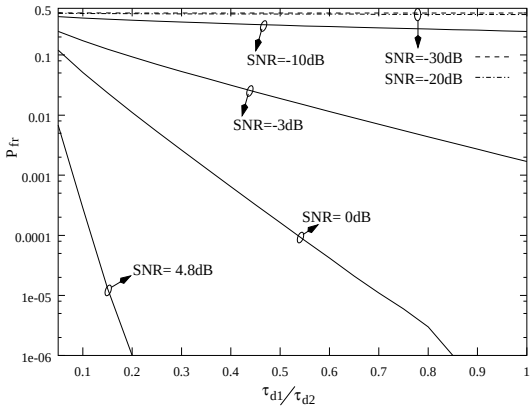

(b) *The P_{fr} as a function of the fast dwell time τ_{d1} ($P_{fa} = 0.01$).*

Figure 5.3: *Comparison of the mean acquisition time and the P_{fr} as a function of the fast dwell time*

- $P_{fa1} = P_{fa2} = P_{fa}$, where P_{fa} is the false alarm probability for the FPS system and P_{fa1}, P_{fa2} are the false alarm probabilities for the first and second dwell of the double dwell system. The corresponding detection probabilities are calculated using equation 4.36.

- $t_1 = \tau_{d1}$ and $t_2 = \tau_{d2}$ where, τ_{di} denotes the dwell times for the FPS system and t_i the dwell time for the double dwell system. The choice of the dwell times is a reasonable one for two reasons: (i) since the dwell times of the two systems are the same, we can decide, according to their relative performance, which one makes the best use of the available time resources and (ii) both systems perform better when the first dwell time is much shorter than the second one.

The results of this comparison are summarised in figures 5.4 and 5.5. Figure 5.4(a) depicts the role of the false alarm probabilities. In general, for low false alarm probabilities ($P_{fa} < 10^{-2}$), the FPS system outperforms the double dwell for very low SNRs, while for large SNRs (SNR> -5 dB) their performance is similar (that is, for a non-optimised fast dwell time τ_{d1} and t_1). For large false alarm probabilities FPS performs better for SNR> -3 dB, while for lower SNRs the double dwell system results into lower mean acquisition time. The significance of the dwell times is depicted in figure 5.4(b). It has been proven in chapter 4 that the fast

dwell time for the FPS system can be optimised. An optimisation for the double dwell system is also possible but, as far as we know, it has not been explicitly and analytically presented in the literature. Accordingly, the performance of the two systems, greatly depends on the correct choice of the fast/first dwell time. Nevertheless, the optimisation ability of the FPS system is much larger, i.e. the improvement in the mean acquisition time by optimising the fast/first dwell time is much larger in the FPS system. This is obvious in figure 5.5 where the $\mu = E(T_{acq})/\tau_{d2}$ is given as a function of the SNR and fast/first dwell time. An optimum τ_{d1} or t_1 exist for both systems (for which the mean acquisition time is minimised), but the minimum achieved by the FPS system is better than that of the double dwell system. This is the reason for which we observe a large improvement in the performance of the FPS system compared to the double dwell system for $\tau_{d1} = 0.1\tau_{d2}$ of figure 5.4(b). In this figure, the fast dwell time τ_{d1} is very close to the optimum value and, as a result the performance is rapidly improved. Figure 5.6 depicts the role of the parameter k, which determines the length of the

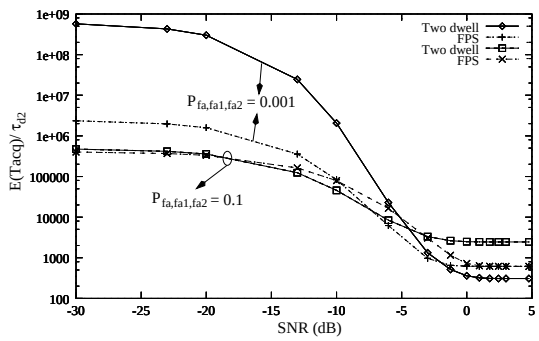

(a) *$E(T_{acq})/\tau_{d2}$ as a function of the SNR for two different sets of false alarm probabilities ($\tau_{d1} = 0.3\tau_{d2}$) and k=200.*

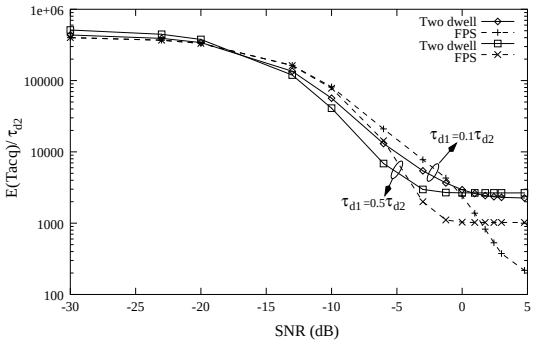

(b) *$E(T_{acq})/\tau_{d2}$ as a function of the SNR for two different sets of dwell times (P_{fa}=0.1) and k=200.*

Figure 5.4: *$E(T_{acq})/\tau_{d2}$ as a function of the SNR under various conditions*

penalty time ($\tau_p = k\tau_{d2}$). A combination of a large k and large false alarm probability P_{fa} means that a large part of the required acquisition time is due to false alarm situations. This is the case in figure 5.6(a) for $k = 200$ and $P_{fa} = 0.1$. The FPS system outperforms the DD system for high SNRs (i.e. high detection probabilities) while for lower values DD results into better acquisition times. A very interesting point in figures 5.6 (which is also noticeable in 5.4) is that *for non-optimum τ_{d1} the mean acquisition time of the FPS system finally converges to a value which only depends on the τ_{d1} and is independent of the false alarm parameters (P_{fa} and*

k). This indicates that the FPS system is very robust against false alarms. Given a good SNR, i.e. SNR> -5 dB at the output of the correlator (figure 4.1), which is feasible for SS systems with good processing gain, the mean acquisition time is almost free of the significant penalty time part. The reason, as explained before, is that if the SNR is high enough the false ranking probability is very small. As a result, the correct cell will be one of the first to be tested during the final search and thus a very small number of wrong cells will be examined. Summarising

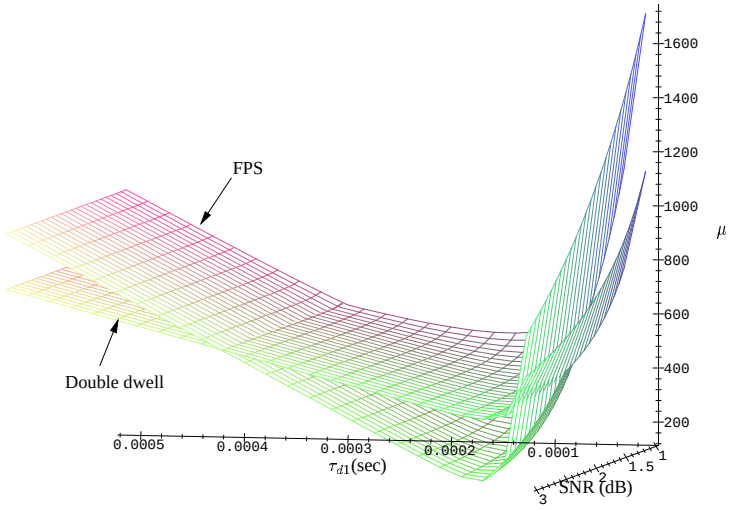

Figure 5.5: *The $\mu = E(T_{acq})/\tau_{d2}$ for the FPS and double dwell system ($P_{fa1} = P_{fa2} = P_{fa} = 0.01$).*

the previous results, we could say that the main differences between the FPS and DD systems can be stated as follows:

- The FPS system allows a large degree of optimisation by controlling the fast dwell time τ_{d1}.
- The DD system performs better than the single dwell because it allows incorrect cells to be quickly discarded. The FPS system moves one step forward by not allowing incorrect cells to be examined, which in turn can result in shorter acquisition times if the τ_{d1} is correctly chosen.

5.3 The FPS system versus the adaptive filter acquisition system.

The class of PN code acquisition system that use adaptive filter techniques was discussed in chapter 1. It became clear, that the performance of the adaptive filter acquisition schemes is

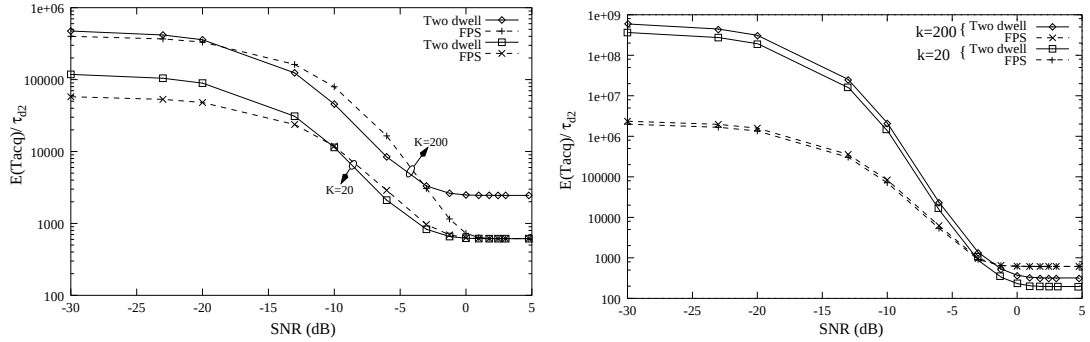

(a) $P_{fa} = 0.1$, $\tau_{d1} = 0.3\tau_{d2}$

(b) $P_{fa} = 0.001$, $\tau_{d1} = 0.3\tau_{d2}$, *same vales for* k *as before.*

Figure 5.6: $E(T_{acq})/\tau_{d2}$ *as a function of the SNR for two different penalty times (different* k*).*

similar to that of the matched filter approach. The FPS system can be classified as an active serial search system. As such, it is not expected to result into acquisition times which are better than the passive matched/adaptive filter approach. It is clear that under certain conditions passive acquisition systems perform better, in terms of the mean acquisition time, than the active systems, for the simple reason that passive systems are designed to test several code phases at a time, while active systems test only one. Nevertheless, active systems have other advantages such as, simple and cheap hardware implementation and better usage of the processing gain of the system. The purpose of this comparison is to evaluate the FPS system against the adaptive filter acquisition (AFA) system which, although promising and powerful, have not received considerable attention in the literature. The AFA system of interest uses the LMS algorithm in order to evaluate the optimum tap weights. The mean acquisition time for the AFA system is derived in [52] and is given by:

$$E(T_{acq}) = \frac{T_c}{P_D}\left((k_a + k_d)\left[1 + (q_a + 1)\frac{2 - P_D}{2}\right] + k_p\left[P_{Fi} + (q_a - 1)P_{Fo}\frac{2 - P_D}{2}\right]\right) \tag{5.3}$$

where T_c is the chips duration, $k_a T_c$ the time required for the tap coefficients to converge to their optimum values, $k_d T_c$ is a decision period about the mean square error (MSE) convergence, $k_p T_c$ is the false alarm penalty time and is modelled as $k_p = q_a(k_a + k_d)$, P_D is the detection probability, P_{Fo} is the out-phase false alarm probability and P_{Fi} is the in-phase false alarm probability [52]. Finally, q_a is the length of the uncertainty area which is given by $q_a = \lceil L/M \rceil$

where, L is the length of the PN code, M the number of the taps of the filter and $\lceil x \rceil$ is the smallest integer greater than or equal to x. Figures 5.7 and 5.8 are based on equations 5.3 and

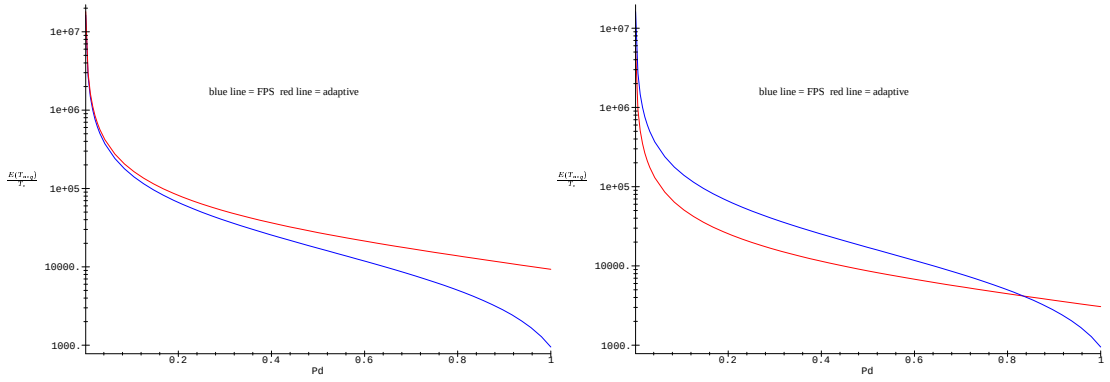

(a) $M = 4$ **(b)** $M = 16$

Figure 5.7: *$E(T_{acq})/T_c$ as a function of the detection probability P_d for $P_{Fa} = P_{Fao} = 0.0001$, $P_{Fai} = 0.00001$, $P_{Fr} = 0.001$, $\tau_{d1} = 0.05\tau_{d2}$*

4.29 for the acquisition times of the AFA and FPS systems respectively, and we used $k_d = 30$, $k_a = 500$, $k_p = q_a(k_a + k_d)$, code length $L = 127$ chips, filter length $M = 16$ (unless, when a different value is given). For the FPS system, the second dwell time is $\tau_{d2} = LT_c$, and the false alarm constant is $k = kp/L$ in order for the two systems to have the same penalty time (the penalty time for the FPS system is $\tau_p = k\tau_{d2}$ while for the AFA is $\tau_p = k_pT_c$). Figure 5.7 presents a comparison of the FPS and AFA for very low false alarm and false ranking probabilities ($P_{Fa} = P_{Fao} = 0.0001$, $P_{Fai} = 0.00001$, $P_{Fr} = 0.001$). This is the only case for which the mean acquisition time of the FPS system is comparable with that of the AFA system. For very short filter length ($M = 4$), the FPS acquisition time is better than that of the AFA system. This highlights a significant characteristic of the FPS system, that under relatively good SNR conditions, it allows a large degree of optimisation which results in very low mean acquisition times. For more realistic conditions, the results are presented in figure 5.8. All the false alarm probabilities that were used are given in the figures. The results are the same for any combination of false alarm probabilities. As was expected, the AFA system outperforms the FPS system for the reason that was explained before. The difference in their performance is more significant for the combination of low detection probabilities and high false alarm probabilities (figure 5.8(b)). It is shown in [52, 119], that the performance of the AFA system in terms of the mean acquisition time, is similar to that of the matched filter

acquisition systems. Thus, we expect that, a comparison of the FPS system with the matched filter system will produce results similar to those of the AFA/FPS comparison. We must note

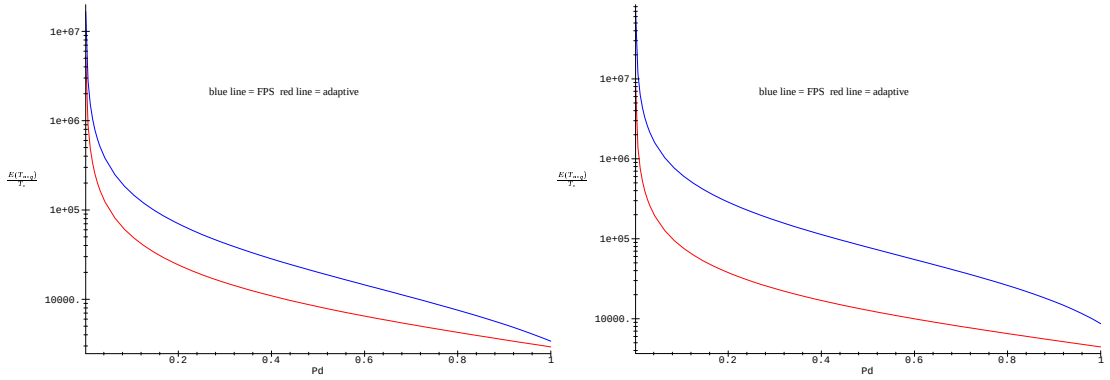

(a) $P_{Fa} = P_{Fao} = 0.001$, $P_{Fai} = 0.0001$, $P_{Fr} = 0.1$, $\tau_{d1} = 0.1\tau_{d2}$

(b) $P_{Fa} = P_{Fao} = 0.1$, $P_{Fai} = 0.01$, $P_{Fr} = 0.1$, $\tau_{d1} = 0.1\tau_{d2}$

Figure 5.8: *$E(T_{acq})/T_c$ as a function of the detection probability P_d under various conditions*

that, the performance of the AFA system depends on a significant number of parameters that must be suitably chosen in order to minimise the mean acquisition time. Thus, the filter length M, the LMS step size μ_s, the averaging window S and the threshold Th are crucial for the good performance of the system.

5.4 Concluding discussion

In the last two chapters a novel PN code acquisition system was studied. The Fast Preliminary Search (FPS) system is an active acquisition system, which provides reliable *a priori* information about the location of the correct cell in the ambiguity area. This is accomplished by utilising a fast preliminary search of the ambiguity area, the results of which are used to accelerate the second and final search. The performance of the system in terms of the mean acquisition system was studied thoroughly. Both theoretical and experimental (simulations) results were given and they were in excellent agreement. The system was compared with a number of well known acquisition systems and it was found that, in most cases, it performs better than the typical active acquisition schemes. Its good performance is mainly attributed to two factors:

- The system greatly reduces the probability of the examination of false cells and thus, the number of false alarms is significantly reduced.
- The system allows a large degree of optimisation by correctly choosing the fast dwell time τ_{d1}.

We must also notice that the configuration of the FPS system that was analysed in chapters 4 and 5 is a worst case study of the system. It is obvious that, if the second stage (the final search) is performed by a matched filter device, the mean acquisition time would be better. In the next chapter, the performance of the FPS system in a fading channel is examined.

Chapter 6
The Fast Preliminary Search (FPS) system: performance in a fading channel

In this chapter, the performance of the fast preliminary search acquisition system is evaluated in a frequency selective Rayleigh fading channel. Using simulations, the effects of the channel in the probability of false ranking P_{fr} and the mean acquisition time are evaluated. The chapter starts with a discussion on the acquisition problem in fading channels. In section 2, simulation results are presented concerning the false ranking and detection probability in fading channels. Finally, a comparison of the mean acquisition time of the FPS system in AWGN and fading channels is presented.

6.1 Acquisition over fading channels: an overview

The theoretical analysis of the acquisition problem over fading channels and the calculation of the relative crucial parameters (i.e. detection and false alarm probabilities, mean and variance of the acquisition time) is an exciting but very demanding task. Despite the fact that over the last 15 years, the problem has attracted a considerable amount of research efforts, the fundamental issue of setting a general theoretical framework for the analysis of the acquisition system over fading channels remains unsolved. The main difficulty that must be overcome is the *influence that the fading correlation has on the search through the uncertainty region* [120]. As discussed in chapter 3, there are basically two general frameworks that allow the analysis of any acquisition system, namely, the equivalent circular state diagram technique, introduced by Polydoros and Weber in [31] and the direct approach introduced by Jovanovic in [11]. Both techniques, which are described in detail in chapter 3, are based on the assumption that there is no memory to the channel, i.e. the examination of each cell of the uncertainty area is statistically independent from the examination of any other cell. This allowed for the acquisition procedure to be described by a Markov chain which gave useful and accurate results in Gaussian channels. The

problem is, that in a fading channel this fundamental assumption is no longer valid, at least not in the general case of any fading channel. This effectively means that the Markovian description of the acquisition procedure is not valid and thus both the circular state diagram and the direct approach are not valid in the general case of a fading channel.

Nevertheless, in practice both methods can be used under specific assumptions. There has been a significant number of publications in which the circular state diagram has been used in order to calculate the mean acquisition time in fading channels. In [30, 121–124] the authors examine the performance of a matched filter based acquisition system in Ricean and Rayleigh fading channels. The mean acquisition time is derived using the circular state diagram and then a number of probabilities (detection, false alarm, missing probabilities) are calculated using the fading channel statistical properties. The papers [121–123] by Sourur and Gupta, are considered to be important contribution in the field of acquisition over fading channels. In [121] the case of a frequency non-selective Rayleigh channel is examined. The treatment in terms of the circular state diagram is the same as for the simple non-fading Gaussian channel. Only the calculation of the various probabilities takes into account the fading statistics. In [123] a Rician channel is examined; both frequency non-selective and frequency selective channels are considered. The main difference compared to the Rayleigh case is that the authors distinguish between different H_0 cells in the case of a Rician frequency selective channel; there are the H_{no} cells for which the intersymbol interference (ISI) can be ignored and the H_{oq} cells for which ISI is taken into account. Nevertheless, the circular state diagram is the same and the mean acquisition time is calculated as in a non-fading channel with modified detection, false alarm and missing probabilities to account for the fading channel effects. In [122] the same authors examine the same system as in [121, 123] but using a serial acquisition method, while in [121, 123] the analysis concerned a parallel system. In [123] the H_0 cells were divided into two groups only for the frequency selective case, in [122] the authors distinguish between different H_0 cells even in the case of a Rician frequency non-selective channel. In this case, there is only one H_{oq} cell, which is actually a correct cell and does not belong to the dominant specular component while the rest of the H_0 cells are taken to be i.i.d. For the frequency selective channel, the H_0 cells are divided as in [123]. A common assumption to all three [121–123] is that the H_1 cell is unique. We should notice that there is no direct comparison between the theoretical and experimental results in [121–123]. On the other hand, the work of Sourur and Gupta has been cited regularly in later literature. In [30], for example, the authors evaluate an acquisition system in fading channels using the framework of Sourur and Gupta.

It seems that even for relatively high Doppler to PN code frequency ratio ($f_D/f_{PN} = 10^{-3}$), the theoretical and experimental results are in acceptable agreement. In [124] a similar but simpler approach is presented; the H_0 cells are all equivalent and the equivalent circular state diagram is applied as in the simple Gaussian case. The detection and false alarm probabilities are determined for the Ricean fading channel. Unfortunately, there is no comparison between the theoretical and experimental work. It is the personal opinion of the author, based on results that will be presented later in this chapter, that, at least in slowly fading channels, the direct approach and the equivalent circular diagram can be applied to the calculation of the mean acquisition time as long as all the relative probabilities are modified to account for the effects of the fading channel.

A different approach is presented in [125]. According to this, the influence of random amplitude of the received signal is included in the analysis by averaging the detection probability of the correct cell over the distribution of the amplitude given that the amplitude follows a certain distribution (Rice or Rayleigh). The results presented in this paper concern the pdf and cdf of the acquisition time. There is no comparison between simulations and theory. On the other hand, it is suggested in [126, 127], that using the mean acquisition time equation for an AWGN channel and substituting the average value of P_d in the equation, is not exactly correct because the mean acquisition time is not linearly but inversely dependent on P_d. The philosophy used in this paper is the same as when deriving the bit error probability in fading channels. It is assumed that during each acquisition, the channel is static having fixed P_{di} and that the acquisition time $T_{MA} = T_{MA}(P_{di})$ is conditional, i.e. $T_{MA} = T_{MA}(P_{di}|A_i)$ where A_i is the amplitude of the signal distributed according to $p(A_i)$. Thus, the mean acquisition time is calculated by averaging as:

$$T_{MA} = \int_0^\infty T_{MA}(P_{di}|A_i)p(A_i)dA_i \tag{6.1}$$

This approach can be valid only if the channel is fading slowly compared to the acquisition time. If the fading is fast enough leading to approximately the same P_d in each acquisition, the averaging should be performed over conditional P_d as stated in [126]. The comparison between theory and simulations presented in [126] concerns only the static channel case. For the more realistic time-varying channels, only simulation results are presented.

In [128] Wilson used Gilbert's two-state Markov chain model to study the effect of correlated fading on the performance of parallel acquisition of frequency hopped signals. The two

states represent the good (unfaded) condition and the bad (faded) condition respectively. This model has the ability to generate burst errors, but it has limitations in representing real channels. A similar approach is presented in [129] where the time varying channel is modelled as a finite-state Markov chain. Each state represents a specified stationary channel model; they can be frequency selective or frequency non-selective, fast or slow fading, Rayleigh or Rician fading channel. In order to calculate the acquisition time statistics, the moment generating function $H_{acq}(z)$ for the acquisition time is used (see chapter 3) and the processes $H_D(z), H_M(z), H_0(z)$ are evaluated as functions of the Markov model transition probabilities. Theory and simulations seem to be in good agreement but on the other hand, there are very few results given and thus, a thorough evaluation of the proposed model is not possible.

The application of adaptive techniques in the code acquisition procedure was discussed earlier in chapter 5. Adaptive techniques are powerful and result in low mean acquisition times. Their performance in fading channels is investigated in [130, 131] using simulations. It is shown that the degradation of their performance in fading channels is significantly smaller than that suffered by matched filters based systems. The application of maximum likelihood techniques in the acquisition procedure in the presence of multipath, Doppler shift and data modulation is investigated in [132]. A MUSIC-based estimator of the propagation delays of the transmitted signals in a DS-CDMA system and the effects of the fading channel and the near-far problem in the acquisition procedure is studied in [57]. Interesting results are also presented in [133–138] where various aspects of the acquisition procedure (threshold setting, tracking loop, spreading sequences optimisation) under fading channel and multiple access interference are discussed.

6.2 Performance of the FPS system over fading channels

After an extensive search of the relative literature it became clear that the theoretical analysis of any acquisition system in non AWGN channels is still problematic. Thus, the evaluation of the performance of the FPS system in fading channels, is based only on simulations. In what follows, results concerning the effects of the fading channel on the probability of false ranking P_{fr}, detection probability P_d and the mean acquisition time are presented. For our simulations we used a frequency selective two-path Rayleigh channel with various power losses per path.

channel	Power loss, path 1	Power loss, path 2	Tap weight 1	Tap weight 2
P1	3 dB	3 dB	0.707	0.707
P2	5 dB	1.65 dB	0.5621	0.82698
P3	9 dB	0.58 dB	0.35481	0.9349

Table 6.1: *Power losses for each path and tap weights for the simulated 2-paths channel models.*

For a Rayleigh channel, the distribution $p(A_i)$ of the amplitude A_i of the signal is:

$$p(A_i) = \frac{2A_i}{\Omega} e^{-\frac{A_i^2}{2\Omega}} \tag{6.2}$$

where $\Omega = E[A_i^2]$ [94]. We will not give any more details on the general aspects of fading channels as it is a well known subject for which extensive literature can be found. Of particular interest for spread spectrum applications we found the following references [4, 5, 139–141]. Table 6.1 describes the three different channels P_1, P_2, P_3 that we used. Channel P_1 is one with equal power at each path, while the power distribution per path is unequal for channels P_2 and P_3. The simulations covered both the slow and the fast fading case for each one of the three channels. In order to simulate a fast fading channel we used $f_{max}/f_{PN} = 10^{-2}$, while for the slow fading case we used $f_{max}/f_{PN} = 5 \cdot 10^{-4}$ where, f_{PN} is the PN code frequency and f_{max} the maximum Doppler frequency. We also assumed a classic (Jakes) Doppler psd [142] given by:

$$S_D(f) = \begin{cases} \frac{2\sigma_o^2}{\pi f_{max}\sqrt{1-(f/f_{max})^2}} & ,|f| \leq f_{max} \\ 0 & ,|f| > f_{max} \end{cases} \tag{6.3}$$

where $2\sigma_o^2$ is the variance of the zero-mean complex Gaussian noise procedure that is used to produce the Rayleigh distributed signal amplitude. The simulation of the Rayleigh channel was achieved by using the method of the finite sum of weighted sinusoids as described in [142] because it allows the complete control of the parameters of the channel. A PN code $m-$sequence of length $q = 127$ chips was used.

Figure 6.1 depicts the false ranking probability as a function of the SNR in all three P_1, P_2, P_3 channels for both slow and fast fading. The Gaussian case is also given for comparison. As expected, the false ranking probability is getting larger compared to the Gaussian channel case. Similar to the Gaussian case, P_{fr} is getting lower as the fast dwell time τ_{d1} increases, as can be seen by comparing figures 6.1(a) and 6.1(b). The crucial parameter of the channel, that

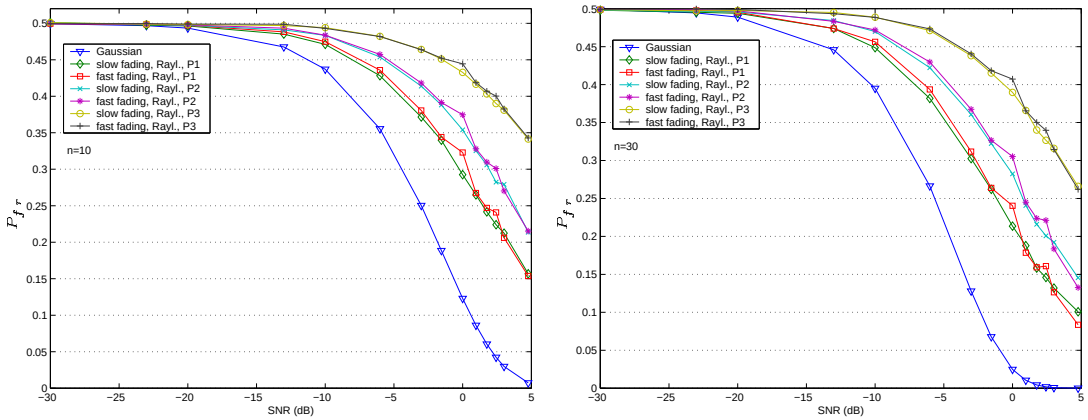

(a) $\tau_{d1} = 0.1\tau_{d2}$ **(b)** $\tau_{d1} = 0.25\tau_{d2}$

Figure 6.1: *The false ranking probability as a function of the SNR for a Gaussian channel and three fading (fast and slow) Rayleigh channels with different path losses and dwell times.*

determines the effects on the false ranking probability is the channel coherence time T_{co}. We can distinguish three different cases of interest

- $q\tau_{d1} \ll T_{co}$: Very slow fading, the channel is effectively constant throughout the preliminary search.
- $\tau_{d1} \gg T_{co}$: Very fast fading, the channel will change several times during a single fast test of one cell.
- $q\tau_{d1} \approx T_{co}$: Normally fast/slow fading, the channel may be constant during a single fast cell test but will change during the total length of the preliminary search.

It is essential for the correct ranking of the cells, that the channel power is constant for the period $T_r = q\tau_{d1}$ where the variables, according to which the cells are ranked, are obtained. Given this, we can see that the first two extreme cases will result in almost equivalent results in terms of the false ranking probability. The reason is that in both cases the mean channel power is almost the same for all cells. This is obvious for the very slow fading, but it is also valid for the very fast fading as all cells are subject to deep fades and thus, the effects of the channel are more or less the same for every cell. On the other hand, the third case is probably the worst as the channel may be different as different cells are tested. This is particularly harmful for the

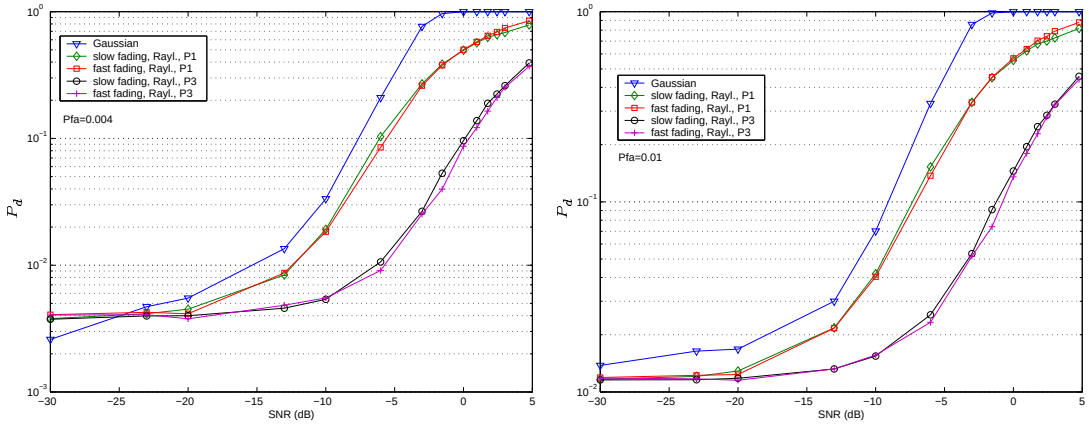

(a) $P_{fa} = 0.004$ **(b)** $P_{fa} = 0.01$

Figure 6.2: *The detection probability as a function of the SNR for a Gaussian channel and two fading Rayleigh channels (P_1 and P_3) with different path losses.*

ranking procedure where a constant power level is very important. In this case, the average false ranking probability will be the same for both slow and fast fading channels. Using the simple formula $T_{co} = 0.5/f_{max}$, [141], the values of f_{max}/f_{PN} and $q = 127$ that we used for our simulations, it is easy to verify that our results belong to the third case. This is the reason for which, in figures 6.1(a) and 6.1(b) (a result of averaging over many hundreds of code periods) the P_{fr} is the almost the same for slow and fast fading channels. It is interesting to notice that channel P_1 (equal power per path) results in the best performance in terms of the false ranking probability. The reason is the advantage of the selection diversity, which is obtained in a fading channel. Both paths have enough power to provide reliable information for the cell ranking procedure.

Figure 6.2 depicts the effects of the fading channel in the detection probability of the final search. A simple CFAR criterion was used to provide a constant false alarm probability. The threshold was constant and set according to equation 1.16, for both the Gaussian and the fading case. A numerical fine tuning was necessary in the case of fading channels in order to keep the false alarm close to the desirable value. Nevertheless, the difference, in terms of the false alarm rate, between the fading and Gaussian channels is not significant. Thus, by using a more suitable adaptive threshold setting [23] one can justify the assumption presented in [120] according to which, if the test variable is normalised to achieve CFAR, then fading does not

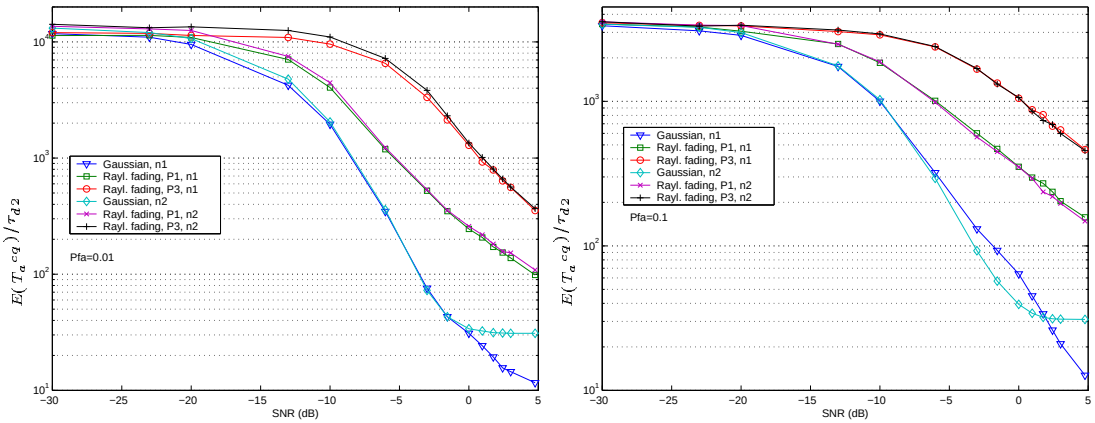

(a) $P_{fa} = 0.01$, *n1 corresponds to* $\tau_{d1} = 0.1\tau_{d2}$ *and n2 to* $\tau_{d1} = 0.25\tau_{d2}$

(b) $P_{fa} = 0.1$

Figure 6.3: *The mean acquisition time normalised to the second dwell time* τ_{d2} *as a function of the SNR for a Gaussian channel and two fading Rayleigh channels (*P_1 *and* P_3*) with different path losses.*

affect H_0-sector testing. A significant reduction in the detection probability, as expected, is caused by the fading channel. Similarly to the false ranking probability, the P_1 channel, with equal distributed power among its paths, gives the best performance compared with channel P_3

The results for the mean acquisition time, for two different false alarm probabilities and two different fast dwell times, are depicted in figure 6.3. The mean acquisition time is normalised to the second dwell time τ_{d2}. One of the two fast dwell times (depicted in the figures as n_1 case) is chosen to be $\tau_{d1} = 0.1\tau_{d2}$ which, for most cases, is close to the exact optimal fast dwell time. This is the deep blue line in figures 6.3(a) and 6.3(b) for which we get the lowest mean acquisition time. As expected, fading channels result into increased acquisition times, as a result of the increased false ranking probability and the decreased detection probability. Note that in both diagrams, for fading channels, there seems to be no difference in the resulting mean acquisition time for the two different fast dwell times (cases n_1 and n_2). Those results indicate that the fast dwell time cannot be effectively optimised if the channel is fading. Although, more simulations are necessary in order to verify this conclusion, all our efforts gave results similar to that in figure 6.3. This is an important result for the FPS system, because as stated in chapter 5, the large optimisation capability was one of the major advantages of this system.

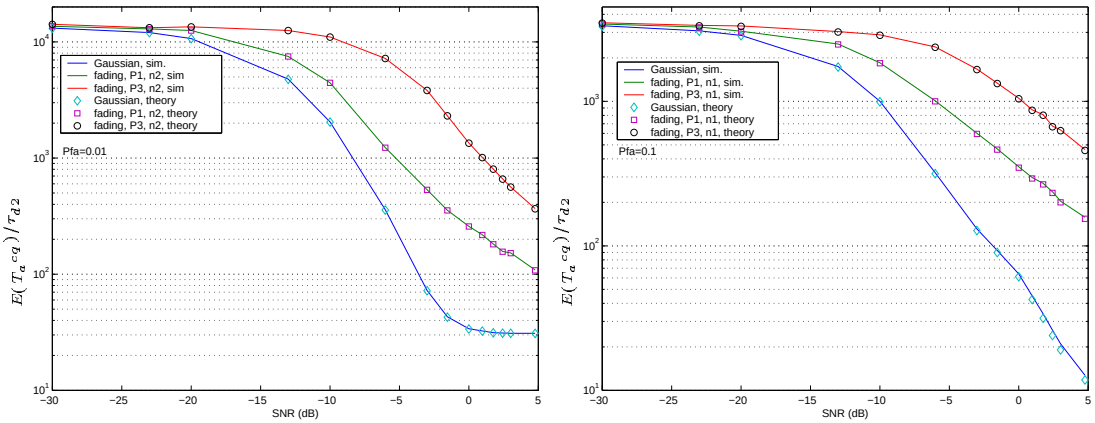

(a) $P_{fa} = 0.01$ **(b)** $P_{fa} = 0.1$

Figure 6.4: *Comparison of the theoretical and simulated mean acquisition time for a Gaussian channel and two fading Rayleigh channels (P_1 and P_3) with different path losses.*

Figure 6.4 depicts a comparison between the simulated and the theoretical mean acquisition time. The latter is calculated using equation 4.29 where the false ranking and detection probabilities are given by simulations. Theory and simulations are in excellent agreement. Figure 6.4 is obtained by applying the *direct approach* to the FPS system. The results of figure 6.4 indicate that, as long as, all the necessary probabilities take into account the fading characteristics of the channels, then equation 4.29 is valid. In the first section of this chapter, we saw that this is the most widely used technique for calculating the mean acquisition time in fading channels. Although, strictly speaking, this method is not correct, it seems to give accurate results for the FPS system and for most cases that are described in the literature.

6.3 Conclusions

In this chapter, the performance of the FPS acquisition system in a Rayleigh fading channel was studied. An overview of the most important work on the acquisition problem in fading channels was presented. It was shown that the accurate and generic mathematical description of a PN code acquisition system in fading channels is still an open problem. The most common approach to the calculation of the mean acquisition time in non-Gaussian channels is to use the corresponding equations for the Gaussian case and modify the probabilities of detection and false alarm. For the FPS system we used the results of chapter four for the mean acquisition

time, while the probabilities of false alarm and false ranking were calculated using simulations. This approach gave a very good agreement between theory and simulations. More specifically, we simulated slow and fast fading conditions for a two-path channel with three different path power loss profiles. It was shown that the channel with equal power loss per path gives the best performance in terms of the mean acquisition time. The mean acquisition time and the detection and false ranking probability in comparison with the Gaussian channel are significantly degraded. Another difference with the Gaussian case is that in a fading environment the fast dwell time can not be effectively optimised.

The following chapter concludes this thesis, summarises the purpose and motivation of this research effort and outline the novelties that were proposed.

Chapter 7
Summary, conclusions and future work

The purpose of this work, as defined in the introduction of the thesis, is to study techniques able to provide reliable *a priori* information which will be used in the PN code acquisition procedure of a DS-CDMA system. The final goal is to improve the performance of the acquisition system in terms of the mean acquisition time, i.e. acquire the PN code as fast as possible. This final chapter summarises the work presented in the main body of this thesis, evaluates the extent to which the original goal has been accomplished and shows clearly our contribution to the research on the code acquisition problem.

7.1 Summary of the results

The idea of providing prior information is very well suited to systems that include features which are, at least to a certain extent, deterministic. Low Earth Orbit (LEO) satellite communications systems is a typical example. The position of the satellite can be determined accurately. Thus, the uncertainty in time and frequency that the synchronisation system must overcome, is due to the uncertainty of the position of the mobile and of course due to the channel statistical nature. The time uncertainty is a sum of the propagation delay uncertainty and the time offset introduced by the channel (which is usually modelled as a Rician fading channel). Unfortunately, the overall time offset is a random variable. Thus, it is not possible to provide any kind of reliable information about the time ambiguity area. On the other hand, the Doppler frequency is more deterministic and reliable information can be provided. We focused our attention to the Doppler shift caused by the movement of the satellite which is very large compared to the Doppler spread of the channel. A simple and accurate model to calculate the Doppler frequency at any point on the earth, given the position of the satellite, was developed. Assuming a uniform distribution of mobile terminals within the satellite spot beam, *we calculated the probability density function of the Doppler shift within the spot beam*. It was shown

that under certain conditions the Doppler pdf can be approximated by a parabola-shaped function, while in the general case the Doppler pdf is a non-symmetrical function. The calculation of the Doppler pdf in a satellite spot beam is, to the best of our knowledge, presented for the first time in the open literature.

The idea behind the calculation of the Doppler pdf was to use it as *a priori* information for the code acquisition procedure. This is done in chapter 3 using the parabolic Doppler pdf. It was noted before that in the general case, the Doppler pdf is non-symmetrical. Nevertheless, we used the parabolic pdf although it is only valid for a limited area of the total satellite footprint. This was done due to the simplicity of the parabola-shaped function which allowed us to analyse mathematically and compare six different searching strategies of the ambiguity area and derive equations for the mean acquisition time. All the calculations were based on the *direct approach* although the equivalent circular diagram (ECD) is more popular in the literature. In the case of a parabolic pdf though, the complexity of the ECD became prohibitively large. On the contrary, the direct approach gave relatively simple and tractable equations for every searching strategy. A minor change in the original acquisition time pdf equation (see equation 3.25) was proposed in order to reduce the computational time. Six different searching strategies were compared in terms of the resulting pdf, cdf and mean value of the acquisition time. All the results were verified using both simulations and the general equations that were presented in [11]. It was found that some of the conclusions reached by Jovanovic in [11] concerning the UEA and NUEA strategies were not valid for the given *a priori* pdf. Finally, it was shown that by using suitable searching strategies for the given prior information the mean acquisition time can be reduced up to 20% compared to the straight line search method where no prior information is provided.

Chapters 2 and 3 gave a good insight not only to the advantages of providing prior information, but also to the price that has to be paid in order to obtain it, namely a large amount of computational effort. The method described in chapter 2 requires "external data", i.e. the position of the satellite and the centre of the spot beam, that must become known to the receiver. Moreover, if the acquisition is slow compared to the Doppler rate of change, new geographical information has to be provided to the receiver. Furthermore, in order to use efficiently the *a priori* information, suitable searching strategies must be employed, the analysis and optimisation of which is not a trivial task. Finally, the method described in chapter 2 is applicable only to the frequency ambiguity area of satellite systems. The fast preliminary search (FPS) system, described in

chapter 4, overcomes all these problems. It performs a fast search of the ambiguity area and then uses the results of the first search as *a priori* information that determines the order that the cells are examined during the second and final search. The FPS system provides information using only its own resources, i.e. no external information is necessary. It can be used for both the time and frequency uncertainty area of any CDMA system, satellite or terrestrial. Simple and accurate analytical expressions for the mean and variance of the acquisition time are derived using the direct approach. The results are verified by simulations. Its performance depends basically on the fast dwell time τ_{d1}. As this is the only parameter that must be optimised, the FPS system seems to be a very simple, effective and reliable synchronisation system.

The performance of the FPS system in a Gaussian channel and a comparison with other systems are examined in detail in chapter 5. It was found that the FPS system outperforms most of the well known acquisition systems which use active correlation techniques. Its good performance is attributed to the large reduction of the mean number of false alarms and to the role of the fast dwell time τ_{d1}, the optimisation of which, results into very low mean acquisition time. The performance of the FPS system in various types of Rayleigh fading channels was studied in chapter 6. It was shown that the mean acquisition time depends on the relative duration of the fast dwell time and the coherence time of the channel, and that, optimisation in terms of the fast dwell time is not as easy as in the Gaussian case. Equation 4.29 was used to calculate the mean acquisition time, with all the relative probabilities determined by simulations. The results were in very good agreement with the simulated acquisition time.
The *proposal and study of the fast preliminary search system* is presented, to the best of our knowledge, for the first time in the open literature and it is what we consider to be the second novelty of this thesis.

7.2 Future work

The work concerning the FPS system, which is done and presented so far, sets the basis for a complete understanding of how a preliminary search mode can improve the acquisition procedure. The original theoretical analysis, presented in chapter 4, although compact and relatively simple consumed a great lot of our, limited, time resources. On the other hand, every possible effort was made to ensure the reliability of all the theoretical and experimental results. In what follows, we present certain points that we consider to be of great interest and worthy of extra research effort.

The FPS system as presented in the previous chapters, is comprised of two stages both of which use active correlators. This is probably a worst case study (at least for Gaussian channels) of the FPS system. It is clear that the performance of the system will be much better if one of the two or even both stages are implemented using matched filter devices. One possible implementation is depicted in figure 7.1. The fast search stage is identical to that in figure 4.1, i.e. an active acquisition system with short dwell time. The cells, which are ranked according to the first search, are subsequently examined using a typical matched filter acquisition system. The matched filter FPS (MF-FPS) system is bound to result into lower mean acquisition time

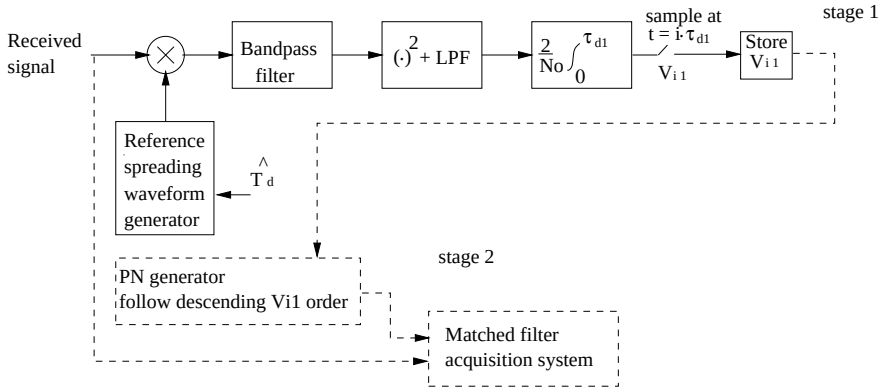

Figure 7.1: *A matched filter implementation of the FPS system.*

than the original proposed FPS system. The reason is that the final search system is replaced by a passive system which, by definition, gives lower acquisition times. The calculation of the statistics of the acquisition time of the MF-FPS system is simple. The false ranking probability, P_{fr}, can be calculated using equation 4.23, while the mean time calculation requires a few changes due to the replacement of the active system with a matched filter. This would be rather trivial as the matched filter implementation of acquisition systems has been studied extensively. An interesting task would be to evaluate mathematically the performance of the system, when codes other than the m-sequences are used.

A more demanding task would be the theoretical analysis of the FPS system in fading channels. Some results based on simulations were given in chapter 6. A comparison with other systems would be useful in order to fully evaluate the capabilities of the FPS system. The MF-FPS can also be simulated in fading channels. The optimisation of the fast dwell time and of the length of the matched filter as a function of the channel parameters will be an interesting problem.
Our opinion is that the most important goal of the code acquisition research in the following years should be the development of an accurate theoretical model of the acquisition procedure

in fading channels and multiuser environment.

Appendix A
The CDA method and derivation of Doppler pdf

A.1 Derivation of basic CDA equations

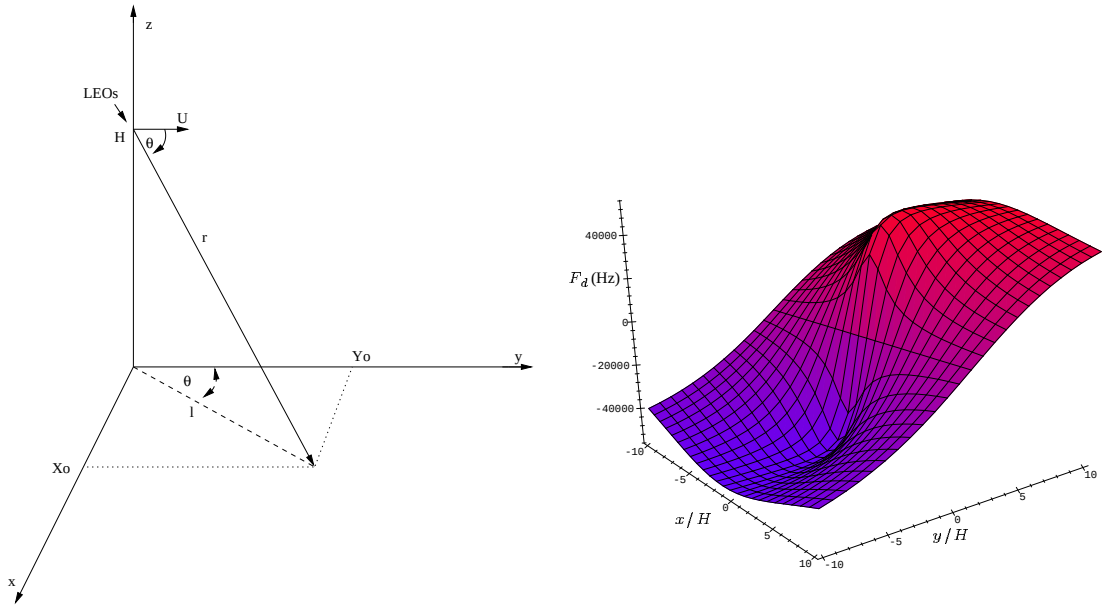

(a) *Definition of the vectors*

(b) *Typical Doppler shifts for the previous flat spot beam geometry (orbital altitude $H = 780km$).*

Figure A.1: *The flat spot beam geometry and the corresponding doppler shifts*

Position vector: $\vec{r} = x_o \cdot \hat{x} + y_o \cdot \hat{y} + H \cdot \hat{z}$

Length of position vector $\vec{r}$: $\mid r \mid = \sqrt{x_o^2 + y_o^2 + H^2}$

The velocity vector is $\vec{u} = u \cdot \hat{y}$

We can now calculate the dot product $\vec{r} \cdot \vec{u}$:

$$\vec{r} \cdot \vec{u} = \mid r \mid \cdot \mid u \mid \cdot cos\theta \Rightarrow \cos\theta = \frac{y_o}{\sqrt{x_o^2 + y_o^2 + H^2}} \tag{A.1}$$

From equation 2.2 we can see that all the position vectors $\vec{r}$ that have the same angle θ with the velocity $\vec{u}$ correspond to points on the $z = 0$ plane which have the same Doppler shift. Thus in order to have constant angle θ (figure A.1) we must have $\cos(\theta) = K$ where K is a constant number. From equation A.1 we have:

$$\frac{y_o}{\sqrt{x_o^2 + y_o^2 + H^2}} = K \tag{A.2}$$

Utilising simple mathematics we can easily derive from equation A.2 the following expression which describes the constant Doppler lines:

$$x^2 + H^2 = y^2 \tan^2(\theta) \tag{A.3}$$

Equation A.3 corresponds to hyperbolas like those in figure 2.2. The intersection point with the y-axis is the $(0, \frac{H}{\tan\theta})$. From equation A.3 we can calculate the cone semi-angle corresponding to each point of the $z = 0$ plane. There are three points of great importance:

- spot beam centre:

$$(x_o, y_o) \rightarrow \tan\theta_o = \pm\frac{\sqrt{x_o^2 + H^2}}{y_o} \tag{A.4}$$

- spot beam's higher point:

$$(x_o, y_o + R) \rightarrow \tan\theta_H = \pm\frac{\sqrt{x_o^2 + H^2}}{y_o + R} \tag{A.5}$$

- spot beam's lower point:

$$(x_o, y_o - R) \rightarrow \tan\theta_L = \pm\frac{\sqrt{x_o^2 + H^2}}{y_o - R} \tag{A.6}$$

By taking all the cones with angles between θ_H and θ_L ($\theta_L > \theta_H$) we can find all the corresponding hyperbolas, thus covering the whole spot beam area with CDLs as in figure 2.2. It is also necessary to calculate the minimum and maximum expected Doppler shift within the spot

beam. This can be done either analytically (by minimising/maximising equation A.1) or using simulations. We used the second way in order to avoid unnecessary mathematical complexity:

- minimum Doppler frequency:

$$F_{dmin} = \frac{F_c U \cos(\theta_{min})}{c} \tag{A.7}$$

- maximum Doppler frequency:

$$F_{dmax} = \frac{F_c U \cos(\theta_{max})}{c} \tag{A.8}$$

where θ_{min} and θ_{max} are the semi-cone angles corresponding to the F_{dmin} and F_{dmax} respectivelly. Finally we can easily calculate the number of Doppler bins of the Doppler uncertainty area (given the frequency step F_{step} as described earlier):

$$N_D = \frac{F_{dmax} - F_{dmin}}{F_{step}} \tag{A.9}$$

and the cone angle step corresponding to the frequency step F_{step} by:

$$\Delta\theta_s = \frac{\theta_L - \theta_H}{N_D} \tag{A.10}$$

A.2 Derivation of Doppler pdf: Stage 1

In figure A.3(a) the main assumptions that have been made in order to calculate the Doppler pdf are illustrated. Hyperbolas are taken as straight lines parallel to the x-axis. Δy is taken small enough to allow as to calculate ΔS as a rectangular area. Figure A.3(b) is on the $x = 0$ plane where we can use the cone semi-angle as a normal plane angle:

$$\left.\begin{array}{l} y_1 = \frac{H}{\tan\theta_1} \\ y_2 = \frac{H}{\tan\theta_2} \end{array}\right\} \Rightarrow \Delta y = y_2 - y_1 = \frac{H}{\tan\theta_2} - \frac{H}{\tan\theta_1} \tag{A.11}$$

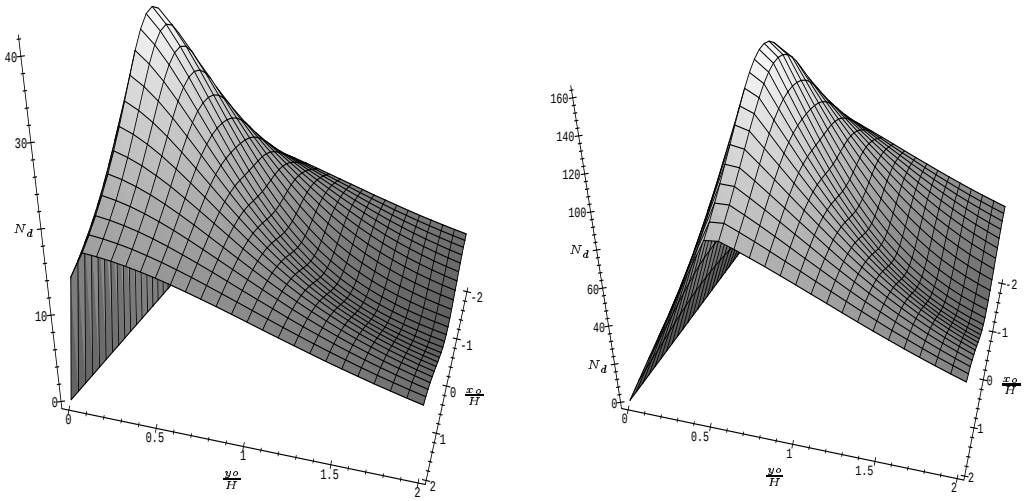

a b

Figure A.2: *(a) number of Doppler bins for $H = 730$ km and spot beam radius $R = 0.1H$, for various spot beam centres (b) number of Doppler bins for $H = 700$ km and spot beam radius $R = 0.6H$, for various spot beam centres. All coordinates (x_o, y_o) are normalised to H*

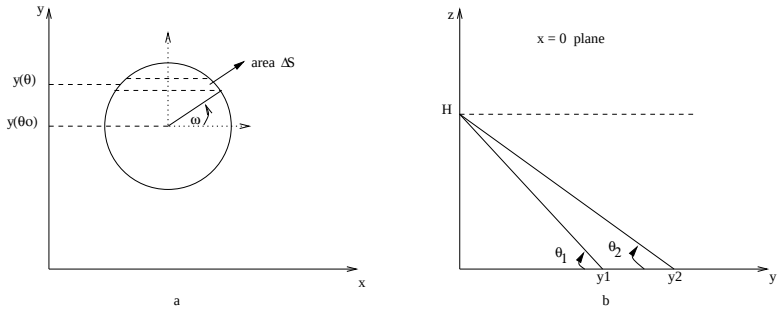

Figure A.3: *a:Figure used for the calculation of the area ΔS b:Figure used for the calculation of Δy*

From figure A.3 using equation A.11 we obtain:

$$\cos\omega = \sqrt{1-\sin\omega^2} = \sqrt{1-\left(\frac{y-y_o}{R}\right)^2} = \sqrt{1-\frac{H^2}{R^2}\left(\frac{1}{\tan\theta}-\frac{1}{\tan\theta_o}\right)^2} \qquad \text{(A.12)}$$

where R is the spot beam radius and θ_o given by equation A.4. The cone angle step $\Delta\theta_s$ (equation A.10) is very small. Thus we need to calculate the Δy for a very small change of the cone semi angle $\Delta\theta_s = \theta_1 - \theta_2$:

$$\tan\Delta\theta_s = \frac{\tan\theta_1 - \tan\theta_2}{1+\tan\theta_1\tan\theta_2}$$

Using equation A.11 and the fact that for very small $\Delta\theta_s \Rightarrow y_1 \simeq y_2$ we obtain:

$$\Delta y = H\left(1 + \frac{1}{\tan^2\theta}\right)\tan\Delta\theta_s \tag{A.13}$$

Equation A.13 gives Δy as a function of a small change of the cone angle $\Delta\theta_s$ and the cone angle θ corresponding to the position y. It is now easy to calculate the area $\Delta S = 2R\cos\omega\Delta y$ and the probability of a Doppler shift F_D (given by $F_D = \frac{F_c U cos\theta}{c}$), by:

$$P(F_D) = \frac{\Delta S}{\pi R^2}$$

A.3 Derivation of Doppler pdf: Stage 2

At this point we assume that the tangents to the hyperbolas are all parallel to each other but form a certain angle with the X-axis. For the calculations we will refer to figure A.4.

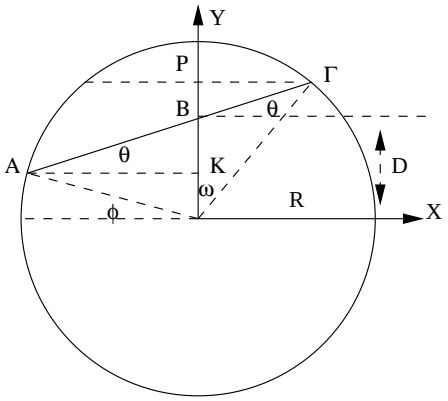

Figure A.4: *Basic geometry for stage 2*

$$\sin\theta = \frac{BK}{AB} \tag{A.14}$$

$$\cos\phi = \frac{AK}{R} \tag{A.15}$$

$$AK = \sqrt{AB^2 - BK^2} \tag{A.16}$$

$$D = OK + KB = R\sin\phi + AB\sin\theta \tag{A.17}$$

Using equations A.15 and A.16 we get:

$$\cos\phi = \frac{AB}{R}\cos\theta \tag{A.18}$$

Finally, using equations A.17 and A.18 we have:

$$AB = D\sin\theta + \sqrt{R^2 - D^2\cos^2\theta} \tag{A.19}$$

Using the same method we can easily prove that:

$$B\Gamma = \sqrt{R^2 - D^2\cos^2\theta} - D\sin\theta \tag{A.20}$$

Thus adding equations A.19 and A.20 we finally take:

$$A\Gamma = 2\sqrt{R^2 - D^2\cos^2\theta} \tag{A.21}$$

Based on figure A.5 we can now give the algorithm used to calculate the Doppler pdf. The

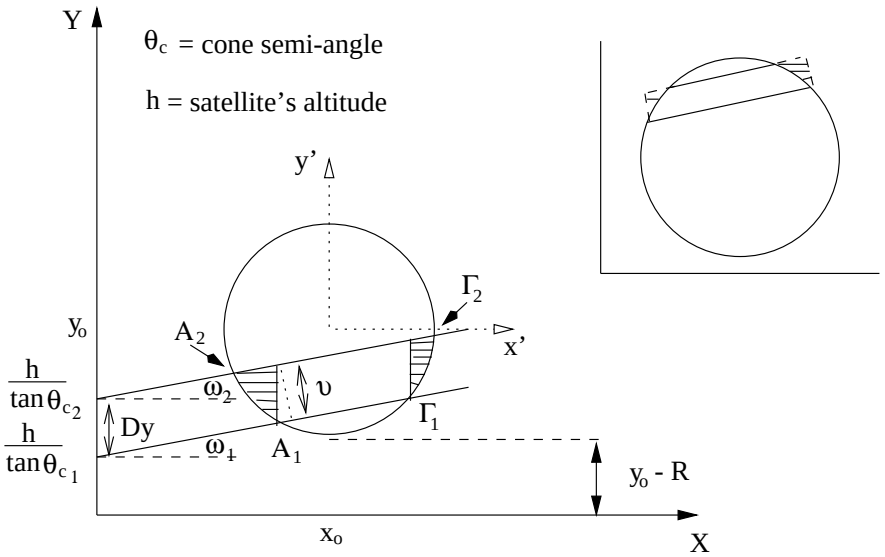

Figure A.5: *pdf computational algorithm for stage 2*

parameter Dy in figure A.5 is the same quantity as Δy of equation A.13 and if ω is the mean value $\omega = \frac{\omega_1+\omega 2}{2}$ of the angles ω_1, ω_2 then taking into account that $\omega_1 \approx \omega_2$ we can use the relation $\upsilon = Dy \cdot \cos\omega$, where υ is the distance between the lines $A_1\Gamma_1$ and $A_2\Gamma_2$. The

intersections of the tangents with the $\acute{y}$ axis are the points:

$$(x, y)_{intersection} = (x_o, y_o - R + i \cdot Dy) \tag{A.22}$$

where i is the number of constant Doppler line ($i = 0$, corresponds to the Doppler line of minimum Doppler, i.e. to the semi-cone angle θ_L). For an arbitrary couple of constant Doppler lines we have:

$$\omega_1 = \arctan\left(\frac{y_o - R + i \cdot Dy - \frac{h}{\tan\theta_{c1}}}{x_o}\right)$$

$$\omega_2 = \arctan\left(\frac{y_o - R + (i+1) \cdot Dy - \frac{h}{\tan\theta_{c2}}}{x_o}\right)$$

where $\theta_{c1} = \theta_L - i \cdot \Delta\theta_s$ and $\theta_{c2} = \theta_L - (i+1) \cdot \Delta\theta_s$, where $\Delta\theta_s$ is given by equation A.10. By using equation A.21 for $\theta = \omega_1$ and $\theta = \omega_2$ (this θ is different from the cone-semi angles θ_c) we can calculate $|A_1\Gamma_1| = l_1$ and $|A_2\Gamma_2| = l_2$ (R is the spot-beam radius and $D = y_o - R + i \cdot Dy$). We now use the assumption that the constant Doppler lines are parallel to each other, to calculate the area between the two lines as the area of the trapezoid $A_1\Gamma_1 A_2\Gamma_2$ the height of which is v. Thus the probability, as in stage 1, is given by:

$$P(F_D) = \frac{\Delta S}{\pi R^2} = \frac{(l_1 + l_2)\, Dy \cos\omega}{4\pi R^2} \tag{A.23}$$

As we can see from figure A.5, for the spot beam area which is below the centre (x_o, y_o), which corresponds to lower Doppler frequencies, the calculated probability is actually lower than the real one because of the shaded area which is not taken into account. On the contrary for the spot beam area which is over the centre (x_o, y_o), which corresponds to higher Doppler frequencies, the calculated probability is actually higher than the real one (see top right corner of figure A.5).

A.4 Derivation of Doppler pdf: Stage 3

This is the final analytical stage of the Doppler pdf calculations. The tangents to the hyperbolas are not parallel to each other any more and an effort has been made to reduce the effects of the shaded areas. They are assumed to be triangular and the corresponding areas are added or subtracted (depending on the position of the lines) before the pdf is calculated. The area

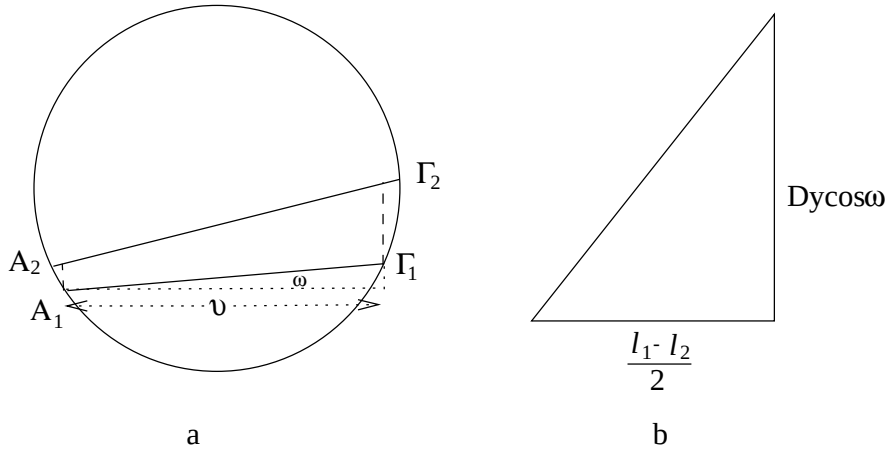

Figure A.6: *a:Geometry for stage 3 b:geometry to calculate the shaded area*

between the two lines is now calculated as a trapezoid but this time we assume that A_1A_2 and $\Gamma_1\Gamma_2$ are parallel to each other and that the height of the trapezoid is $v = A\Gamma\cos\omega$, where $A\Gamma$ is the mean value of $A_1\Gamma_1$ and $A_2\Gamma_2$. Using $A_1A_2 \approx \Gamma_1\Gamma_2 \approx Dy\cos\omega$ we have that $\Delta S = \frac{A_1A_2+\Gamma_1\Gamma_2}{2} \cdot \frac{A_1\Gamma_1+A_2\Gamma_2}{2}\cos\omega$. Using the previous formulas we take:

$$\Delta S = \frac{l_1 + l_2}{2} Dy\cos^2\omega \tag{A.24}$$

To calculate the overall shaded area we assume that for every couple of constant Doppler lines, two triangles exist, each one having the dimensions shown in figure A.6, i.e. we assume that the length difference of the two lines is equally distributed between the two shaded areas. Thus the two areas added together are:

$$\Delta S_{trg} = \pm\frac{|l_1 - l_2|}{2} Dy\cos^2\omega \tag{A.25}$$

The $\pm$ shows that the area ΔS_{trg} can be added or subtracted to ΔS depending on the position of the lines compared with the spot beam centre. Finally to calculate the Doppler pdf we use:

$$P(F_D) = \frac{\Delta S}{\pi R^2}$$

where ΔS is now given by:

$$\Delta S = \frac{l_1 + l_2}{2} Dy\cos^2\omega \pm \frac{|l_1 - l_2|}{2} Dy\cos^2\omega \tag{A.26}$$

A.5 The Doppler pdf as a parabola: Stage 4

The need to have a simple formula that describes the Doppler pdf within a LEO spot-beam, derives from the complicated mathematics which are involved in the calculations of the mean acquisition time. We figured out that the actual Doppler pdf is best fitted by the parabola:

$$y = \frac{(x-\alpha)^2}{4\gamma} + \beta \tag{A.27}$$

We can see from figure A.7 that:

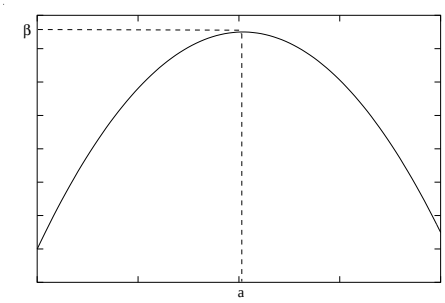

Figure A.7: *The parabola*

- the parameter α can be calculated as the most probable Doppler frequency.
- the parameter β can be calculated as the maximum value of the Doppler pdf
- The last parameter c can be calculated from equation A.27 by using α, β, one Doppler frequency as x and the corresponding pdf value as y. We can easily see that for every couple (Doppler frequency, pdf value) a different γ is calculated. Since the choice of γ determines how accurate the fitting is, we can use various methods in order to optimise the choice of this parameter. Using mainly low and high frequencies seems to produce more accurate parabolas.

Another way to calculate the parabola is using a non-linear fitting algorithm. This method is more complicated than the one we described before, but it produses the most accurate parabolas as it uses all the data for the calculation of all the parameters α, β, γ. For our results, we used the Marquardt-Levemnberg non-linear least squares algorithm.

Mathematical bibliography used: [143–147]

Appendix B
Elliptical pattern and non-flat spot beam:the equations used in the simulations.

B.1 Geometry for the elliptical spot beam

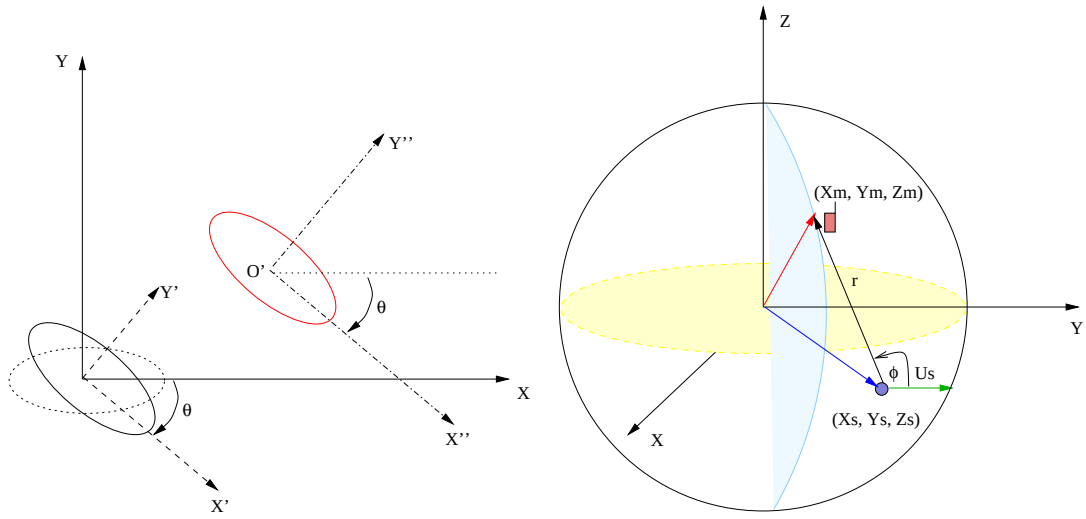

(a) *The geometry for an elliptical flat spot beam*

(b) *The geometry for a non-flat spot beam*

Figure B.1: *The geometry for an elliptical spot beam and a non-flat spot beam*

The general equation of the red ellipse (figure B.1(a)) in the (X, Y) system is:

$$Ax^2 + Bxy + Cy^2 + Dx + Ey + F = 0 \tag{B.1}$$

where $cot(2\theta) = \frac{A-C}{B}$. The same ellipse in the (X', Y') system can be written as:

$$A'x'^2 + C'y'^2 + D'x' + E'y' + F' = 0 \tag{B.2}$$

where $A' = A\cos^2\theta + C\sin^2\theta + B\cos\theta\sin\theta$, $C' = A\sin^2\theta + C\cos^2\theta - B\cos\theta\sin\theta$, $D' = D\cos\theta + E\sin\theta$, $E' = E\cos\theta - D\sin\theta$ and $F' = F$. The centre of the ellipse relative to the (X', Y') system is $O' = (\frac{-D'}{2A'}, \frac{-E'}{2C'})$. By defining $F'' = \frac{D'^2}{4A'} + \frac{E'^2}{4C'} - F'$, the ellipse relative to the (X'', Y'') system is given by the simple formula:

$$\frac{x''^2}{\frac{F''}{A'}} + \frac{y''^2}{\frac{F''}{C'}} = 1 \tag{B.3}$$

Finally, the relations between the three different systems are:

$$\begin{aligned} x &= x'\cos\theta - y'\sin\theta \\ y &= x'\sin\theta + y'\cos\theta \\ x' &= x'' + a \\ y' &= y'' + b \end{aligned} \tag{B.4}$$

where (a, b) is the centre of the ellipse (and the centre of the (X'', Y'') system) relative to the (X', Y') system. All the previous equations are used in the elliptical spot beam simulations in order to describe the ellipse mathematically, assuming a flat spot beam geometry.

B.2 Geometry for the non-flat spot beam

Referring to figure B.1(b), (x_m, y_m, z_m) is the position of the mobile user on the earth, (x_s, y_s, z_s) is the position of the satellite and $u_s = u_x \cdot \hat{x} + u_y \cdot \hat{y} + u_z \cdot \hat{z}$ is the velocity of the satellite with respect to the (X, Y, Z) system, the centre of which is the centre of the earth. In order to

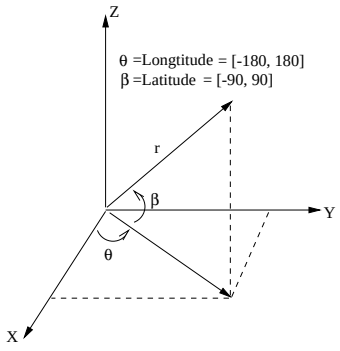

Figure B.2: *The spherical coordinate system.*

transform the coordinates of figure B.2 into Cartesian coordinates we used:

$$\begin{aligned} x &= r\cos\theta\cos\beta \\ y &= r\sin\theta\cos\beta \\ z &= r\sin\beta \end{aligned} \tag{B.5}$$

where $\beta = [-90^o, 90^o]$ is the latitude (South to North) and $\theta = [-180^o, 180^o]$ is the longitude (West to East).

The Doppler calculation is as follows (referring to figure B.1(b)):

$$F_d = \frac{F_c u_s \cos(\phi)}{c} = \frac{F_c u_s}{c}\frac{\vec{r}\vec{u_s}}{|r||u_s|} = \frac{F_c}{c}\frac{\vec{r}\vec{u_s}}{|r|} \tag{B.6}$$

where $|\cdot|$ denotes the length of the corresponding vector and ϕ is the angle between the vectors $\vec{r}$ and $\vec{u_s}$. From equation B.6 we derive:

$$F_d = \frac{F_c}{c}\frac{(x_m - x_s)u_{sx} + (y_m - y_s)u_{ys} + (z_m - z_s)u_{zs}}{\sqrt{(x_m - x_s)^2 + (y_m - y_s)^2 + (z_m - z_s)^2}} \tag{B.7}$$

By combining equations B.7 and B.5 we can calculate the Doppler at any point on earth. For our simulations we assumed that the satellite is at $(\theta, \beta) = (0^o, 0^o)$ and the inclination of the orbit is 0^o which means that $\vec{u_s} = u_{ys}\hat{y}$. For this case equation B.7 can be simplified:

$$F_d = \frac{F_c U}{c}\frac{y_m}{\sqrt{(R_e + H - x_m)^2 + y_m^2 + z_m^2}} \tag{B.8}$$

where $U = u_{ys}$.

In [86] an accurate, analytical model is derived to calculate the observed Doppler shift for a given terminal location and a maximum elevation angle (see also chapter 2). Equation 5 of [86] is reproduced here:

$$F_{d2} = \frac{-F_c}{c}\frac{R_e(R_e + H)\sin(\psi(t) - \psi(t_o))\cos\gamma(t_o)\omega_F(t)}{\sqrt{R_e^2 + (R_e + H)^2 - 2R_e(R_e + H)\cos(\psi(t) - \psi(t_o))\cos\gamma(t_o)}} \tag{B.9}$$

where all the symbols are explained in figure B.3 in which P denotes the location of the mobile, M is the sub-satellite point at the instant t_o the terminal observes maximum elevation angle, N is the sub-satellite point at the instant t that the Doppler shift is calculated, O is the centre of the earth, S depicts the satellite and $s(t)$ is the distance between the satellite and the terminal

at the instant t. Finally, $\omega_F(t) = \omega_s - \omega_E \cos i$ where ω_s is the angular velocity of the satellite, ω_E is the angular velocity of the earth and i is the orbital inclination. Equations B.9 and B.7

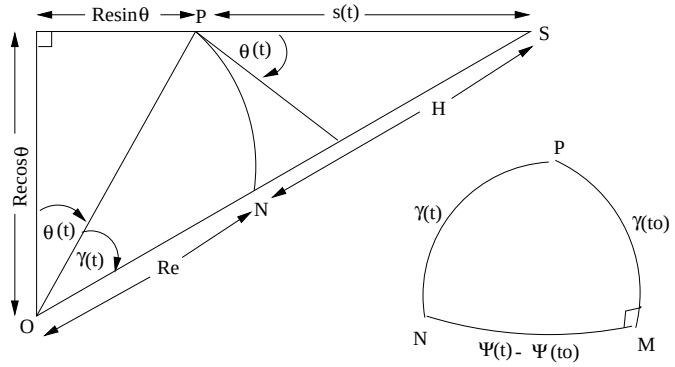

Figure B.3: *The basic satellite geometry during the visibility window, plane and spherical triangle.*

are identical. We will prove this for the special case where the satellite at the instant t is at $(\theta, \beta) = (0^o, 0^o)$ (*I*) and the inclination of the orbit is $i = 0^o$ (*II*). Note, that under the conditions *I* and *II*:

$$\begin{aligned} \psi(t) - \psi(t_o) &= \theta_m \\ \gamma(t_o) &= \beta_m \end{aligned} \tag{B.10}$$

where (θ_m, β_m) are the longitude and latitude of the mobile user. Using equation B.10, equation B.9 becomes:

$$F_{d2} = \frac{-F_c}{c} \frac{R_e \sin(\theta_m)\cos(\beta_m)(R_e + H)\omega_F(t)}{\sqrt{R_e^2 + (R_e + H)^2 - 2R_e(R_e + H)\cos(\theta_m)\cos(\beta_m)}} \tag{B.11}$$

Using equation B.5 and the fact that the linear velocity of the satellite is $|U| = (R_e + H)\omega_F(t)$ we can see that the numerators of equations B.9 and B.8 are the same. Finally, if we substitute equation B.5 in the denominator of equation B.8 and take into account that $x_m^2 + y_m^2 + z_m^2 = Re^2$ we will see that the denominators of equations B.9 and B.8 are also the same. Thus, the two methods of calculating the Doppler shift are equivalent. A generalisation for every $(\theta, \beta, i)^o$ is more laborious but straightforward and thus,will be omitted.

Appendix C
The FPS system: some mathematical details

The study of the fast preliminary seach (FPS) system requires a lot of mathematical analysis. The mathematics involved are lenghty and laborious but straightforward in the sense that only well known stochastic and probabilistic theory was used to derive all the neccesary equations. The purpose of this appendix is to clarify some points of the FPS analysis. Nevertheless, we will not present every detail of the mathematical proofs because, as stated before, most of the mathematics are straightforward and can be found in a number of books and papers that are listed in chapter 4.

C.1 Comments on the Gaussian approximation

The full analysis of the Gaussian approximation can be found in pages 241-250 of [4]. We would like to note at this point that equation (5-74), page 248 of [4] about the variance of the integrator output, has a minor mistake. The correct one is given in equation 4.16 while more details about how this equation is derived in the first place, can be found in chapter 10 of [97] (examples 10-7, 10-8, 10-12, 10-25). A slightly different (but equivalent and more complete) approach can be found in the original work [114] by H.Urkowitz.

Equation 4.14 can be derived if we represent the noise output of the bandpass filter of figure 4.1 by $n(t) = \sqrt{2}n_I(t)\cos\omega_{IF} - \sqrt{2}n_Q(t)\sin\omega_{IF}$ where n_I and n_Q are baseband Gaussian noise processes with power spectral densities $N_o/2$ over the frequency range $|f| < B/2$. Squaring the previous equation and retaining only the baseband components of the results yields equation 4.14.

The derivation of equation 4.22 from equation 4.21 is based on the integrals:

$$\int_0^{\tau_{d1}} \left(1 - \frac{x}{\tau_{d1}}\right) sinc(Bx)dx = \frac{Si(B\tau_{d1}\pi)}{B\pi} - \frac{1}{\tau_{d1}}\left(\frac{-\cos(B\tau_{d1}\pi)}{(B\pi)^2} + \frac{1}{(B\pi)^2}\right) \qquad \text{(C.1)}$$

and

$$\int_0^{\tau_{d1}} \left(1 - \frac{x}{\tau_{d1}}\right) sinc^2(Bx)dx = \frac{1}{2}\frac{-1 + \cos(2\pi B\tau_{d1}) + 2\pi B\tau_{d1} Si(2\pi B\tau_{d1})}{\tau_{d1}(\pi B)^2} - \frac{1}{\tau_{d1}}\left(\frac{1}{2}\frac{ln(\pi B\tau_{d1}) - Ci(2\pi B\tau_{d1})}{(\pi B)^2} + \frac{1}{2}\frac{ln(2) + \Gamma_E}{(\pi B)^2}\right) \quad \text{(C.2)}$$

where all symbols are defined in chapter 4.

The polynomial expansion for the Marcum's Q-function [115] is:

$$Q(x) = \frac{0.5}{(1 + b_1 x + b_2 x^2 + b_3 x^3 + b_4 x^4)^4} \qquad [x > 0] \quad \text{(C.3)}$$

where $b_1 = 0.196853578, b_2 = 0.1151945, b_3 = 0.000343653, b_4 = 0.019527$.

For $x < 0, Q(-x) = 1 - Q(x)$.

C.2 Comments on the calculation of the mean/variance of the mean acquisition time.

The calculation of the mean and variance of the acquisition time does not present any particular mathematical difficulty. It is, simply, a problem of substituting equations 4.24, 4.26, 4.27 and 4.28 into equation 4.2 (for the mean value) and equations 4.31, 4.32 and 4.33 into equation 4.30 for the variance. We will not present all the calculations, as they do not have any particular interest. We will only give the closed-form expressions for the sums that are involved in the calculations:

$$\sum_{k=0}^{n-1}(a + kr)q^k = \frac{a - [a + (n-1)r]q^n}{1 - q} + \frac{rq(1 - q^{n-1})}{(1 - q)^2} \quad [q \neq 1, n > 1] \quad \text{(C.4)}$$

$$\sum_{k=0}^{\infty}(a + kr)q^k = \frac{a}{1 - q} + \frac{rq}{(1 - q)^2} \quad [|q| < 1] \quad \text{(C.5)}$$

$$\sum_{j=1}^{q}\begin{pmatrix} q-1 \\ j-1 \end{pmatrix} B^{j-1} = (1 + B)^{q-1} \quad \text{(C.6)}$$

$$\sum_{j=1}^{q} j \begin{pmatrix} q-1 \\ j-1 \end{pmatrix} B^{j-1} = (1+B)^{q-1} + \frac{B}{1+B}(q-1)(1+B)^{q-1} \tag{C.7}$$

The sums C.4 and C.5 are given in [117] while sums C.6, C.7 were calculated using *Maple*.

According to [11], equation 4.30 for the variance of the acquisition time is valid if:

$$q \gg 1 \tag{C.8}$$

$$F_2(P_d)E(T_r)^2 \gg F_1(P_d)Var(T_r) \tag{C.9}$$

where $E(T_r) = \tau_{d2} + P_{fa}\tau_p$ and $Var(T_r) = E(T_r^2) - E(T_r)^2 = \tau_{d2}^2(1-P_{fa}) + (\tau_{d2}+\tau_p)^2 P_{fa} - (\tau_{d2} + P_{fa}\tau_p)^2 = \tau_p^2 P_{fa}(1 - P_{fa})$. The first condition $q \gg 1$ is valid for all practical systems. The second one was checked and it was found to be valid, under all conditions. Figure C.1 is typical for the relative size of the two terms of equation C.9 (a value of $F_2(P_d)E(T_r)^2 = 0.0004801837820$ corresponds to $F_1(P_d)Var(T_r) = 0.1695318384 \cdot 10^{-7}$).

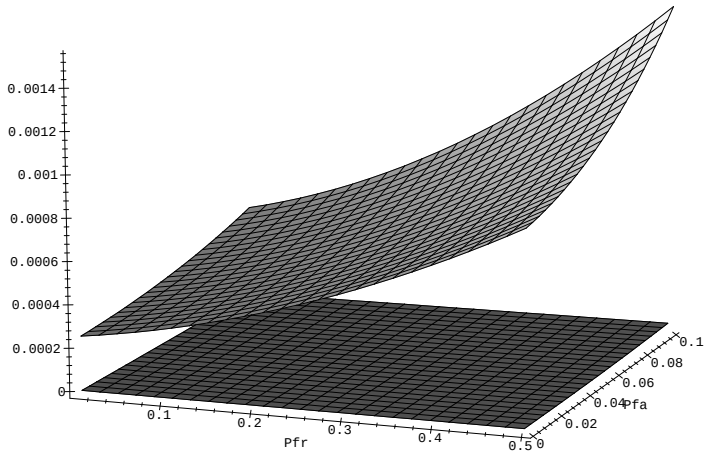

Figure C.1: *A comparison of the $F_2(P_d)E(T_r)^2$ term (top) with $F_1(P_d)Var(T_r)$ (bottom).*

Appendix D
Publications

The following two publications were achieved:

- G. A. Vardoulias, G. J. R. Povey and J. H. Dripps, “On the Doppler Probability Density Function within a Low Earth Orbit Satellite Spot Beam and its Application to the Code Acquisition Procedure”, *Proceedings of the VTC’99-Fall*, vol.5, pp. 2711-2715, Sep.1999, Amsterdam.
- G. A. Vardoulias, S. McLaughlin, J. H. Dripps and G. J. R. Povey, “A comparative evaluation of a novel PN code acquisition system using a fast preliminary search of the ambiguity area”, *Proceedings of the ISSSTA’2000*, vol.2, pp. 623-627, Sep.2000, New Jersey.

The papers follow:

On the Doppler Probability Density Function within a Low Earth Orbit Satellite Spot Beam and its Application to the Code Acquisition Procedure

George A.Vardoulias, Gordon J.R.Povey and Jimmy H.Dripps

Signals and Systems Group, Dept. of Electrical Engineering
University of Edinburgh, Edinburgh, UK
Tel: +44-(0)131-650 5655
George.Vardoulias@ee.ed.ac.uk, Gordon.Povey@ee.ed.ac.uk

Abstract— **The probability density function of the Doppler shift in a LEO satellite spot beam has been found for both a circular and elliptical shaped spot beam. The Doppler *pdf* was used as *a priori* information in order to achieve better mean acquisition time which is critical in any LEO satellite communication system. It is shown that the Doppler *pdf* can be very well approximated by a parabola-shaped function. The direct approach [1] is used for the calculation of the mean acquisition time while various searching strategies of the Doppler ambiguity area are analysed and simulated using the parabolic Doppler *pdf*. The overall analysis shows that the use of the Doppler *pdf* combined with an appropriate search strategy can reduce the mean acquisition time significantly.**

I. INTRODUCTION

Receiver synchronisation can be a major problem in a mobile radio environment where the communication channel is subject to rapid changes. This is especially true when employing low earth orbit (LEO) satellites rather than fixed terrestrial base stations. The receiver must tolerate large Doppler shifts due to the movement of the satellite over the earth's surface, as well as Doppler rate (i.e. the rate of change of the Doppler shift) and Doppler spread. As LEO satellites are visible for very short times code acquisition and synchronisation must be as fast as possible in order to maximise useful communication time.

In a direct sequence spread spectrum (DS/SS) communication system the received signal can be modelled as:

$$r(t) = \sqrt{2S}d(t)c(t+\zeta T_c)\cos\left[(\omega_c+\omega_D)t+\phi\right]+n(t) \quad (1)$$

where the parameters S and ω_c represent the waveform's average power and carrier frequency respectively, $c(t)$ is the ± 1 PN code with chip duration T_c and $d(t)$ is a binary data sequence (which might or might not be present during the acquisition mode), $n(t)$ is additive white Gaussian noise, ω_D denotes the frequency offset due to the Doppler effect, ζT_c is the PN code delay with respect to an arbitrary time reference and ϕ the carrier phase offset. According to equation 1 the synchroniser's task is to provide the receiver with reliable estimations $\hat{\zeta}$, $\hat{\omega}_D$ and $\hat{\phi}$, of the corresponding unknown quantities so that despreading and demodulation will be successful [2]. Usually the receiver assumes that there are certain bounds for both the phase and frequency offsets (denoted by ΔT and ΔF respectively) which are subdivided into smaller areas $\delta\tau \times \delta f$. The synchroniser must perform a two-dimensional search in the $(\Delta T, \Delta F)$ area. In many cases this process must be accomplished at very low SNRs, as quickly as possible, using the minimum amount of hardware.

The basic parameters that usually describe a DS/SS synchroniser are the probability of correct detection P_d i.e the probability that the detector correctly indicates synchronisation when the local and the received codes are properly aligned, the probability of false alarm P_f i.e the probability that the detector will falsely indicate synchronisation when the two codes are actually misaligned, the *dwell time* τ_d i.e the time that the decision device spends examining each one of the possible uncertainty subregions $(\delta\tau, \delta f)$ and the *penalty time* τ_p i.e the time in order to recognise that a false alarm occurred and resume the search (τ_p can be modelled as a fixed time multiple of the dwell time, $\tau_p = \kappa\tau_d$).

So far, three general analytical methods have been proposed to estimate the mean and variance of the acquisition time which are (a) the *Markov chain* acquisition model, by J.K.Holmes and C.C.Chen [3, 4] (b) the *equivalent circular state diagram* approach, by A.Polydoros [5, 6] and (c) the *direct approach*, by V.M.Jovanovic [1, 7]. We adopted the direct approach as it led to relatively simple, tractable and easy to verify results. The direct approach is presented in detail in [1].

II. Doppler shift probability density function calculation

In this section a method to calculate the Doppler shift probability density function within a satellite spot beam is presented. It is shown that depending on the satellite's velocity and position as well as the position of the spot beam, not all Doppler shifts are equally probable to occur. Under certain conditions the Doppler *pdf* within the spot beam can be modelled as a parabola-like function with the Doppler shift which corresponds to the centre of the beam being the most probable to occur.

LEO satellites have large velocities due to the low altitude of the corresponding orbits. Assuming a circular orbit, ideal conditions and a maximum altitude of 2000 km, LEO satellites' velocities can be greater than 6500 m/sec. Thus for a carrier frequency of $F_c = 2.2$ GHz the Doppler shift ambiguity can be as large as ± 50 kHz and the time to locate the correct Doppler shift can be quite large. In order to minimise the search time, we will calculate the probability density function of the Doppler shift within a satellite spot beam.

The basic assumption made, in order to produce a simple and usable model for the density function, is that of a flat spot beam area. The validity of this assumption for LEO systems will be discussed later. We define a rectangular coordinate system where the y-axis is parallel to satellite's velocity. The satellite is at $(0, 0, H)$ and (x_o, y_o) is a point on the earth which we assume to be the $z = 0$ plane. The Doppler frequency at (x_o, y_o) is given by :

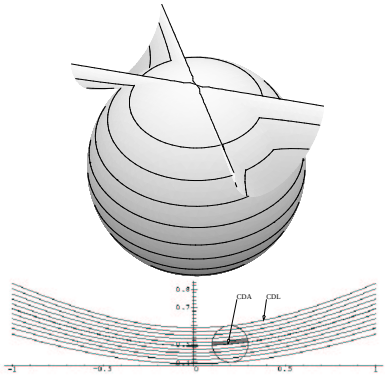

Fig. 1. A constant Doppler cone and the corresponding CDLs and CDAs for a flat earth and a circular spot beam on it.

$$F_d = \frac{F_c U \cos(\phi)}{c} \tag{2}$$

where F_d is the Doppler frequency offset, F_c is the carrier frequency, ϕ is the angle between the velocity U and the position vector and c is the speed of light. It is easy to see from equation 2 that all the points that belong to a conic surface with axis of revolution the line $z = H$ of the $x = 0$ plane, vertex at $(0, 0, H)$ and cone semi-angle θ, have the same Doppler shift [8] (figure 1) which can be calculated by equation 2 for $\phi = \theta$. Thus the intersection of this cone with the $z = 0$ plane (representing the surface of the earth), corresponds to constant Doppler lines (CDL) on the earth. It can be shown that the CDLs, corresponding to the flat earth geometry previously described, are hyperbolas given by the equation :

$$x^2 + H^2 = y^2 \tan^2(\theta) \tag{3}$$

where θ is the cone semi-angle and H the altitude of the satellite (figure 1). We assume a circular spot beam (although the same analysis applies to an elliptical beam) the centre of which is at (x_o, y_o) and that the receiver can tolerate a small Doppler shift (F_s), which is taken to be ± 250 Hz [9] for the simulations that have been performed. Thus we can assume that all the mobile receivers which happen to be between two successive CDLs face approximately the same Doppler shift. As a result, two successive CDLs corresponding to an F_s Doppler frequency difference, define a constant Doppler area (CDA) in the spot beam as illustrated in figure 1. The number of CDAs defines the number of the Doppler bins to be searched (denoted by q). It is obvious from figure 1 that some CDAs are larger than others leading in a greater probability for a mobile user to be in this area and thereby greater probability for the corresponding Doppler shift to occur. The number of Doppler bins is a function of the spot beam's centre position and the Doppler step (F_s) and can be calculated by the simple formula :

$$q = \frac{F_{dmax} - F_{dmin}}{F_s} \tag{4}$$

where F_{dmax}, F_{dmin} are the maximum and the minimum Doppler shifts that a mobile user will have to handle in the spot beam. The results are displayed in figure 2. The *pdf* depicted with a rhombic sign is given by simulations in which the spot beam has been replaced by a N_{tot} points grid of uniform density. The Doppler shift is calculated at each one of the grid points. If N_i points have Doppler frequencies corresponding to the i bin, then the probability of this bin is simply $P_i = N_i/N_{tot}$. In the *pdf* depicted with a cross sign the probability of each bin is calculated

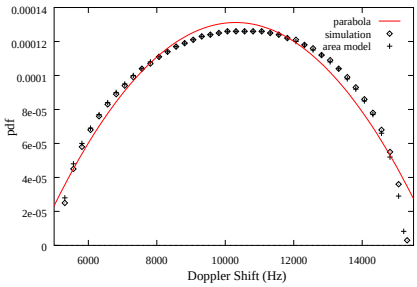

Fig. 2. The three Doppler pdf models. The satellite is at (0,0,750)Km, the spot beam radius is 75 Km and the centre of the beam is at (150,150) Km.

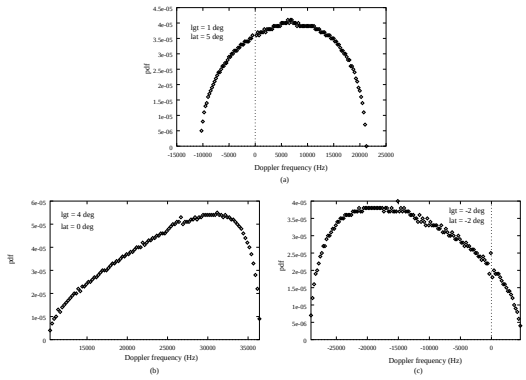

Fig. 3. The Doppler *pdf* for three different spot beam centres. A spherical earth has been considered. The orbital altitude is $H = 780$ km and the spot beam radius is $R_{sb} = 300$ km.

as a fraction of the area between the two CDLs defining the bin (figure 1) and the total spot beam area. In this model the hyperbolas have been replaced by straight lines in order to simplify the area calculations. The model is accurate but the final *pdf* equation is complicated and is not practical. Finally, the solid line shows the parabola $y = \frac{(x-\alpha)^2}{4\gamma} + \beta$ that fits the simulation *pdf*. The parabola is calculated using the Marquardt-Levemnberg non-linear least squares algorithm. The fitting is accurate enough to allow the closed form of the parabola to be used as *a priori* information in the calculations of the mean acquisition time.

In an elliptical spot beam the number of Doppler bins as well as the minimum and maximum Doppler frequencies change. Nevertheless, we have shown that the parabolic fit is still valid. Only the coefficiencies α, β, γ are different between a circular and an elliptical spot beam as a result of the different geometry.

It can be shown that the error introduced by the flat earth assumption mainly depends on $s = |lat_{ssp} - lat_{sbc}|/|lg_{ssp} - lg_{sbc}|$ where, lg_{ssp} and lat_{ssp} are the longitude and latitude of the sub-satellite point respectively while, lg_{sbc} and lat_{sbc} are the same quantities for the spot beam centre. When spherical earth must be considered (i.e. approximately when $s < 3$) the CDLs can still be approximated by hyperbolas but the most probable cell is no longer the central one. As a result, the Doppler *pdf* is not a symmetrical function and can not be approximated by a parabola-shaped function. Figure 3 presents various Doppler *pdf*s for a spherical earth and a sub-satellite point at $(lg_{ssp} = 0, lat_{ssp} = 0)$ degrees. The orbital altitude is $H = 780$ km and the spot beam radius is $R_{sb} = 300$ km (which are approximately the *Iridium* constellation's characteristics). In figure 3a the spot beam centre is at $(lg_{sbc} = 1, lat_{sbc} = 5)$ degrees (i.e. $s > 3$) and the *pdf* can be approximated by a parabola. In figures 3b,c the coordinates of the spot beam centre result into $s < 3$ and the corresponding *pdf*s are not symmetrical. In figure 3c the spot beam centre is "behind" the satellite ($lg_{sbc} = -2, lat_{sbc} = -2$ degrees) and the negative frequencies denote the fact that the satellite is moving away from the mobile user. In the following analysis we will only examine the symmetrical *pdf* case (i.e $S > 3$).

III. Analysis of the Searching Strategies

In this section, the following five searching strategies of the Doppler ambiguity area are presented:

- The straight line. The cells are examined one after another starting from the cell $m = 1$ until the cell $m = q$ and then back to the start if no detection was declared, until the correct one is detected. This strategy does not make use of any *a priori* information.
- The broken centre *Z* (BCZ). The search is initiated at the centre of the Doppler uncertainty region and it reverses direction every time the boundaries are reached. When one of the boundaries is reached, the local code is quickly rewound to the centre and the search continues to the opposite direction.
- The expanding window (X.WIN). In this strategy, tests are performed until a cell at the distance R_1 from the centre is reached; if the correct cell has not been detected, the local code is quickly rewound to the centre and a new search within the same radius R_1 but to the opposite direction is initiated. If the correct cell has not been detected at this point, a new search within a radius $R_2 > R_1$ is initiated, etc (see

figure 4).

- The uniformly expanding alternate (UEA), (figure 4).
- The non-uniformly expanding alternate (NUEA). The basic idea behind UEA and NUEA is to examine the cells following the order of the decreasing *a priori* probability. The UEA strategy is similar to the broken/centre *Z* while the NUEA is similar to the expanding window.

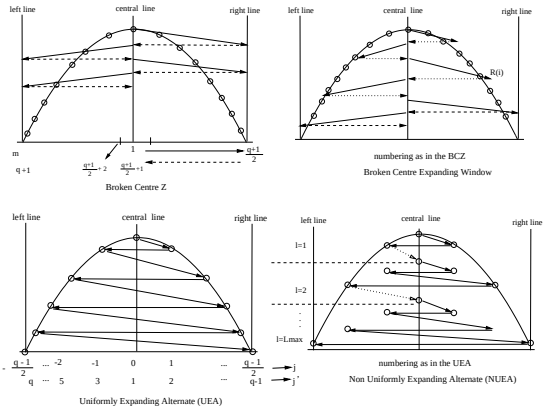

Fig. 4. The four searching strategies.

A detailed analysis can be found in [1]. The *pdf* and the mean value of the acquisition time have been calculated for each one of those strategies.

In what follows, the functional $m(i,j)$ is defined as the total number of cells tested during the acquisition under the assumption that the correct location is in the j^{th} cell and that the correct detection happened during the i^{th} test of the j^{th} cell. This functional is determined by the searching strategy and must be calculated for each one separately. It has been shown [1] that the *pdf* of the acquisition time is given by:

$$\begin{aligned} P_{T_a}(t) &= \sum_{i=1}^{\infty} P_d(1-P_d)^{i-1} \sum_{j=1}^{q} P_c(j) \\ &\cdot \sum_{h=0}^{m(i,j)-i} \left(\begin{array}{c} m(i,j)-i \\ h \end{array} \right) P_f^h \\ &\cdot (1-P_f)^{m(i,j)-i-h} \delta\big(t - m(i,j)\tau_d - h\tau_p\big) \end{aligned} \quad (5)$$

where the parameter h accounts for the number of false alarms which have occurred during the acquisition and $P_c(j)$ represents the *a priori* probability of the correct cell location.

For the two alternate strategies we used:

$$P_c(j) = \begin{cases} \frac{F_s}{2}\left(2\beta + \frac{[(j-1)F_s]^2}{4\gamma} + \frac{[jF_s]^2}{4\gamma}\right) & , j > 0 \\ \frac{F_s}{2}\left(2\beta + \frac{[jF_s]^2}{4\gamma} + \frac{[(j+1)F_s]^2}{4\gamma}\right) & , j < 0 \\ \frac{F_s}{2}\beta & , j = 0 \end{cases} \quad (6)$$

to describe the parabolic Doppler *pdf*, where $j = -\frac{q-1}{2}, ..., \frac{q-1}{2}$ as in figure 4. The $m(i,j)$ functional for the UEA is given by:

$$m(i,j) = (i-1)q + j' \quad (7)$$

where j' is defined by (see also figure 4):

$$j' = \begin{cases} 1 & , j = 0 \\ 2j & , j > 0 \\ -2j+1 & , j < 0 \end{cases} \quad (8)$$

Similar but more complicated expressions have been derived [10] for the rest of the strategies. Finally the mean acquisition time for both UEA and NUEA can be calculated [1, 10] using:

$$\begin{aligned} E(T_a) &= \sum_{i=1}^{\infty} P_d(1-P_d)^{i-1} \sum_{j=-\frac{q-1}{2}}^{\frac{q-1}{2}} P_c(j) \\ &\cdot \big([m(i,j)-i](\tau_d + P_f\tau_p) + i\tau_d\big) \end{aligned} \quad (9)$$

IV. Simulations, results and conclusions

All the simulations have been carried out assuming that the satellite's altitude is 750 Km and that the spot beam is circular with radius $R_{sb} = 75$ Km which is smaller than the Iridium spot beam (≈ 300 km) but has almost the size of a *Teledesic* supercell (square 160 Km on each size) [11–13]. The Doppler step is taken $F_s = 250$ Hz and the carrier frequency $F_c = 2.2$ GHz [9]. The number of Doppler cells for this geometry and frequencies is $q = 41$. The penalty time is $\tau_p = 20\tau_d$. Finally, the parabola which is used to fit the Doppler *pdf* is given by $y = 0.000126 - \frac{(x-10563)^2}{4 \cdot 8.911 \cdot 10^{10}}$.

It became clear that all the searching strategies perform better than the straight line search. Comparing the non-alternate strategies (BCZ and X.WIN), the expanding window performs slightly better than the Broken-*Z* strategy, while both alternate strategies (UEA and NUEA) outperform the expanding window. The UEA works slightly better for high probabilities of detection, while NUEA performance improves for very low P_d. The performance of the expanding window and the NUEA strategies depends on the choice of a parameter which determines the number of sweeps through the uncertainty area before the two strategies degenerate to the corresponding *Z* and UEA strategies respectively. In all simulations, this parameter was optimised. Figure 5 is a typical example of the acquisition time *pdf* using the parabolic Doppler *a priori* information, while figure

6 presents the normalised mean acquisition time μ versus P_f for $P_d = 0.9$ (for the single dwell straight line search strategy with $P_d = 1$ and $P_f = 0$, $\mu = 0.5$ [3]). Finally, figure 7 depicts the improvement (percentage) that the NUEA strategy offers over the straight line.

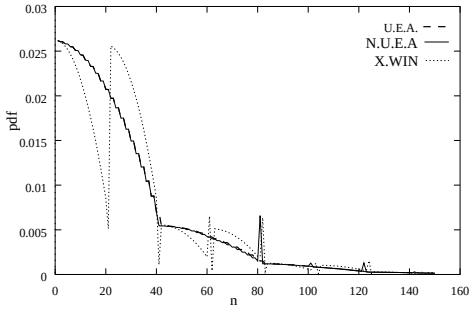

Fig. 5. The pdf for the two alternate strategies in comparison with the expanding window, $P_d = 0.8$, $P_f = 0.001$. Time is a multiple of the dwell time i.e $t = n\tau_d$

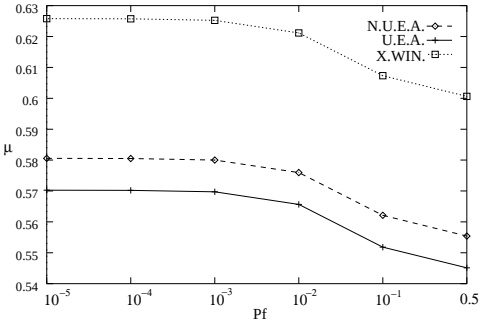

Fig. 6. The normalised mean acquisition time for the two alternate strategies in comparison with the expanding window, $P_d = 0.9$ ($\mu = E(T_{acq})/q(\tau_d + P_f\tau_p)$.

A probabilistic model to describe the distribution of the Doppler shift within a LEO spot beam was proposed. The distribution of the Doppler shift was used as *a priori* information in the PN code acquisition procedure in order to improve the mean acquisition time. Five searching strategies were analysed and simulated. It was shown that the use of certain searching strategies can improve the PN acquisition procedure in a DS/SS CDMA LEO satellite communication system.

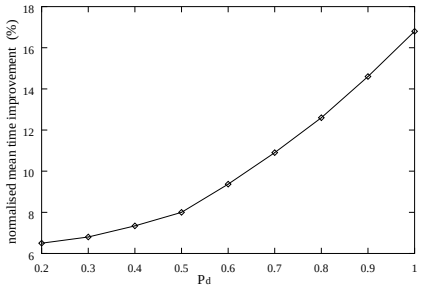

Fig. 7. Improvement of the normalised mean acquisition time for the NUEA over the straight line search.

REFERENCES

[1] V.M.Jovanovic, "Analysis of strategies for serial search spread spectrum code acquisition-direct approach," *IEEE trans.comm.*, vol. 36, pp. 1208–1220, Nov. 1988.

[2] A.Polydoros and S.Glisic, "Code synchronization:a review of principles and techniques," *IEEE ISSSTA'94*, vol. 1, pp. 115–137, 1994.

[3] J.K.Holmes and C.C.Chen, "Acquisition time performance of PN spread spectrum systems," *IEEE trans.comm.*, vol. com-25, pp. 778–784, Aug. 1977.

[4] D.M.Dicarlo and C.L.Weber, "Statistical performance of single dwell serial synchronazation systems," *IEEE trans.comm.*, vol. com-28, pp. 1382–1388, Aug. 1980.

[5] A.Polydoros and C.L.Weber, "A unified approach to serial search spread spectrum code acquisition-Part I : general theory," *IEEE trans.comm.*, vol. com-32, pp. 542–549, May 1984.

[6] A.Polydoros and M.K.Simon, "Generalized serial search code acquisition : The equivalent circular state diagram approach," *IEEE trans.comm.*, vol. com-32, pp. 1260–1268, Dec. 1984.

[7] V.M.Jovanovic, "On the distribution function of the spread spectrum code acquisition time," *IEEE Journal on selected areas in communications*, vol. 10.NO 4, pp. 760–769, May 1992.

[8] W.Zhao, R.Tafazolli, and B.G.Evans, "Positioning assisted inter-segment handover for integrated GSM-satellite mobile system," *IEE conf. satellite systems for mobile communications and navigation*, pp. 124–128, May 1996.

[9] G.J.R.Povey and J. Talvitie, "Doppler compensation and code acquisition techniques for LEO satellite mobile radio communications," *IEE conf. satellite systems for mobile communications and navigation*, pp. 16–19, May 1996.

[10] G.A.Vardoulias, G.J.R.Povey, and J.H.Dripps *submitted for publication: IEE proceedings communications*, The Doppler probability density function within a Low Earth Orbit satellite as a priori information for the PN code acquisition procedure.

[11] *http://www.ee.surrey.ac.uk/Personal/L.Wood/*, 1998.

[12] F.Vatalaro, G.E.Corazza, C.Caini, and C.Ferrarelli, "Analysis of LEO,MEO and GEO global mobile satellite systems in the presence of interference and fading," *IEEE Journal on selected areas in communications*, vol. 13, pp. 291–300, Feb. 1995.

[13] M.A.Sturza, "The Teledesic satellite system," *IEEE national telesystems conference*, pp. 123–126, 1994.

IEEE 6th Int. Sypm. on Spread-Spectrum Tech. & Appli., NJIT, New Jersey, USA, Sept. 6-8, 2000

A comparative evaluation of a novel PN code acquisition system using a fast preliminary search of the ambiguity area

George A.Vardoulias, Steven McLaughlin,
Jimmy H.Dripps and Gordon J.R.Povey
Signals and Systems Group,
Dept. of Electrical Engineering
University of Edinburgh, Edinburgh, UK
e-mail: George.Vardoulias@ee.ed.ac.uk

Abstract — **A new method for initial code acquisition in spread spectrum systems is compared in terms of the resulting mean acquisition time with the single dwell acquisition scheme in the case where a non uniform *a priori* information is provided and advanced searching strategies are utilised. The novel scheme employs a fast preliminary search of the ambiguity area. The results of the fast search are used as *a priori* information for the final search. The probability of false ranking P_{fr} is defined as a measure of the reliability of the *a priori* information provided by the fast preliminary search. A similar idea, used to perform a spatial search for a lost satellite in a region of the sky, has been described in [1]. A detailed analysis of the FPS system is presented in [2].**

I. Introduction

In a direct sequence spread spectrum (DS/SS) communication system the transmitted signal can be modelled as:

$$s(t) = \sqrt{2}Ad(t)c(t)\cos\omega_c t \qquad (1)$$

In equation 1, the parameters A^2 and ω_c represent the waveform's average power and carrier frequency respectively, $c(t)$ is the ± 1 PN code with chip duration T_c and $d(t)$ is a binary data sequence (which might or might not be present during the acquisition mode). The received waveform is, then, given by :

$$r(t) = \sqrt{2}Ad(t)c(t-\zeta T_c)\cos\left[(\omega_c+\omega_D)t+\phi\right] + n(t) \qquad (2)$$

where $n(t)$ is Additive White Gaussian Noise, ω_D denotes the frequency offset due to the Doppler effect, ζT_c is the PN code delay with respect to an arbitrary time reference and ϕ the carrier phase offset. According to equation 2 the synchroniser's task is to provide the receiver with reliable estimations $\hat{\zeta}$, $\hat{\omega}_D$ and $\hat{\phi}$, of the corresponding unknown quantities so that despreading and demodulation will be successful [3]. Usually the receiver assumes that there are certain bounds for both the phase (time) and frequency offsets (denoted by ΔT and ΔF respectively) which are subdivided into smaller areas $\delta\tau \times \delta f$. It is obvious that the synchroniser must perform a two-dimensional search in the $(\Delta T, \Delta F)$ area. In many cases this process must be accomplished at very low SNRs, as quickly as possible, using the minimum amount of hardware. The basic parameters that usually describe a DS/SS synchroniser are the probability of correct detection P_d i.e the probability that the detector correctly indicates synchronisation when the local and the received codes are properly aligned, the probability of false alarm P_{fa} i.e the probability that the detector will falsely indicate synchronisation when the two codes are actually misaligned, the *dwell time* τ_d i.e the time that the decision device spends examining each one of the possible uncertainty subregions $(\delta\tau, \delta f)$ and the *penalty time* τ_p i.e the time in order to recognise that a false alarm occurred and resume the search (τ_p can be modelled as a fixed time multiple of the dwell time, $\tau_p = k\tau_d$).

A novel PN code acquisition system that provides information about both the PN code phase and the frequency ambiguity area, for any CDMA system has been described in [2]. The system employs a fast preliminary search (FPS) of the one or two dimensional ambiguity area and uses the information obtained by the fast search in order to perform a more elaborate final search using any of the well known active or passive synchronisation systems [3,4]. The FPS system is analysed in detail in [2] where the FPS mode is combined with a simple active single, fixed dwell acquisition system. The analysis in [2] concerns a one dimensional (PN code phase) ambiguity area but can be generalised for two dimensional areas. The basic points of the FPS system analysis are given in section II. In this paper we examine the performance of the FPS system, assuming a one dimensional (time only) area, in terms of the resulting mean acquisition time. In [2], the FPS system was compared with an active single dwell (SD) system, with uniform *a priori* information and it was shown that a large improvement in the mean acquisition time is achieved. The FPS system outperforms the SD system even when prior information is provided and advanced searching strategies like the UEA or NUEA (see [6]) are employed. In this paper, the FPS system is compared with the double dwell (DD) active acquisition system. It is shown, that the FPS system is very efficient in reducing the number of false alarms and thus, improving the mean acquisition time.

This paper is organised as follows: in section II the FPS system is briefly described and the equation for the mean acquisition time is given. In section III we present the results of the comparison of the FPS scheme with the double dwell system, in terms of the mean acquisition time. Finally, in section IV we draw our conclusions.

II. The FPS system

In this section we present the basic points of the fast preliminary search system. A detailed analysis is given in [2]. Every cell of the 1 or 2 dimensional ambiguity area (marked with i in figure 1) is examined two times using an active single dwell time acquisition system. The first search is a fast straight line serial search -the fast preliminary search (FPS)- the duration τ_{d1} of which is a crucial parameter of the system. The output V_{i1} of the first search is then used as *a priori* inform-

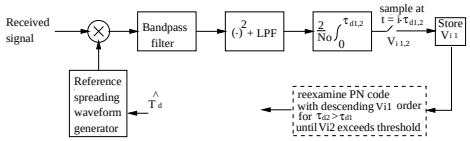

Figure 1: The FPS system :each cell i is examined twice, using the same hardware.

ation which determines the search strategy of the second and final search, i.e. the cells are ranked according to the I-D circuit output V_{i1} and then re-examined (final search), following a descending V_{i1} order for a larger period τ_{d2} until a predetermined threshold is exceeded i.e. by using again the same single dwell serial acquisition system. The dwell time τ_{d1} of the first search is a fraction of τ_{d2} i.e. $\tau_{d1} = \alpha \cdot \tau_{d2}$ with $\alpha < 1$. The critical parameters for the fast search are: SNR, the short dwell time τ_{d1}, the bandwidth B of the filter and the probability of false ranking P_{fr} i.e. the probability that the output V_{i1} of a wrong cell will be larger from that of the correct cell. The probability of false ranking P_{fr} is used as a measure of the reliability of the *a priori* information provided by the fast preliminary search. It was shown in [2] that for a given SNR γ_o which is calculated at the output of the bandpass filter, bandwidth B and fast dwell time τ_{d1}, the P_{fr} can be calculated using

$$P_{fr} = Q\left(-\frac{E_y}{\sigma_y}\right) \tag{3}$$

where $Q(\cdot)$ denotes the Marcum's function, $E_y = -2B\tau_{d1}\gamma_o$ and

$$\begin{aligned}\sigma_y^2 &= \frac{8}{\pi^2}\Big[2\gamma_o\cos(\frac{n}{2}\pi) + cos(n\pi) + n\pi Si(n\pi) + \\ &\quad \gamma_o n\pi Si(\frac{n}{2}\pi) + Ci(n\pi) - ln(n\pi) \\ &\quad -2\gamma_o - 1 - \Gamma_E\Big]\end{aligned} \tag{4}$$

where $n = 2B\tau_{d1}$, $\Gamma_E = 0.5772156649$ is the Euler's constant and the functions $Si(x)$ and $Ci(x)$ are related to the sine and cosine integrals $si(x)$ and $ci(x)$ by the integrals ([7]-page xxxv)

$$\begin{aligned}Si(x) &= \int_0^x \frac{\sin t}{t}dt = si(x) + \pi/2 \\ Ci(x) &= \Gamma_E + lnx + \int_0^x \frac{\cos t - 1}{t}dt\end{aligned}$$

We must note that the maximum value of P_{fr} is $P_{frMAX} = 0.5$, as it is a binary decision taken for every cell individually. The mean acquisition time $E(T_{acq})$ and the variance of the system is found using the direct approach [6] and it is shown [2] to be:

$$\begin{aligned}E(T_{acq}) &= q\tau_{d1} + \frac{\tau_{d2}}{P_d} + \tau_{d2}(1 + kP_{fa})[1 + \\ &\quad (q-1)P_{fr} + \frac{q(1-P_d) - 1}{P_d}\Big]\end{aligned} \tag{5}$$

$$Var(T_{acq}) = [F_2(P_d) - F_1^2(P_d)] \cdot (\tau_{d2} + P_{fa}\tau_p)^2 \tag{6}$$

where

$$\begin{aligned}[F_2(P_d) - F_1^2(P_d)] &= P_d + (q-1)P_d P_{fr}[3 + (q-2)P_{fr}] - \\ &\quad \left(\frac{q(1-P_d)}{P_d}\right)^2 - [1 - (q-1)P_{fr}]^2 + \\ &\quad q^2 P_d \sum_{i=1}^{\infty}(i-1)^2(1-P_d)^{i-1}\end{aligned} \tag{7}$$

where the penalty time is modelled as $\tau_p = k\tau_{d2}$. It is easy to see that as τ_{d1} gets larger, the P_{fr} decreases since we spend more time examining each one of the cells, thus making the decision more reliable. On the other hand it is obvious from equation 5 that large τ_{d1} will probably result into large $E(T_{acq})$. It can be shown that in most cases there is an optimum fast dwell time τ_{d1opt} for which the performance of the FPS system in terms of the mean acquisition time is greatly improved. Details on how τ_{d1opt} is calculated can be found in [2]. Figure 2 depicts a comparison between the FPS system and the simple single dwell serial search system without any *a priori* information, in terms of the mean acquisition time. The mean acquisition time of the SD was calculated according to [8]. In general, the FPS system outperforms the SD system even for suboptimal τ_{d1}. Figures 3,4 depict a comparison between the FPS system and a SD system for which a parabola-shaped pdf function $y = \frac{(x-\alpha)^2}{4\gamma} + \beta$ is used as prior information for the time ambiguity. The parabolic pdf was first derived in [5] as a Doppler shift pdf in LEO satellite spot-beams. However, it is used here as time information in order to compare the FPS system with the SD system when prior information is provided, and advanced search strategies are used. Similar results can be obtained with any other prior distribution, such as the triangular or the Gaussian. Three search strategies are considered in figures 3,4 namely, the straight line, where cells are tested one after an other without any specific order, and the two alternate strategies UEA and NUEA that were introduced by J.V.Jovanovic in [6]. The idea behind UEA and NUEA is to examine the cells following the order of the decreasing *a priori* probability and it was shown in [5] that for the parabolic pdf they can improve the mean acquisition time up to 20% compared to the straight line search. Notice, that in all previous results the SNR (denoted by γ_o) is calculated at the output of the bandpass filter of figure 1. The probability of detection for the SD and the second search of the FPS system is given ([4] pg.783) by

$$P_d = Q\left(\frac{Q^{-1}(P_{fa}) - \gamma_o\sqrt{B\tau_{d2}}}{\sqrt{1 + 2\gamma_o}}\right) \tag{8}$$

where τ_{d2} is the second dwell time of the FPS system, which equals the dwell time of the SD system. Figures 3 and 4 show that the FPS system clearly outperforms all the single dwell systems (straight line, UEA and NUEA). The improvement of the performance is more significant for high P_{fa} and the reason is that the FPS system will have to recover from less false alarm situations due to the fact that the fast search provides information which allow the correct cell to be examined early enough in the final search and thus the mean number of false alarms is reduced significantly.

III. The FPS system versus the double dwell time scheme.

The multiple dwell serial search system is a generalisation of the single dwell serial PN acquisition system. The scheme falls into the class of fixed dwell time synchronisation schemes in

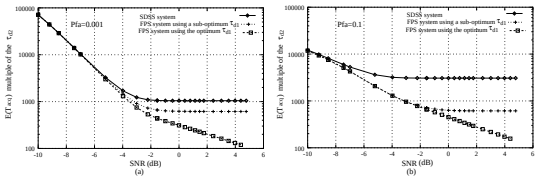

Figure 2: $E(T_{acq})$ as a function of the SNR and two different P_{fa}. The sub-optimum time used is $\tau_{d1} = 0.3\tau_{d2}$, number of cells $q = 2046$, $k = 20$, $B = 100$kHz

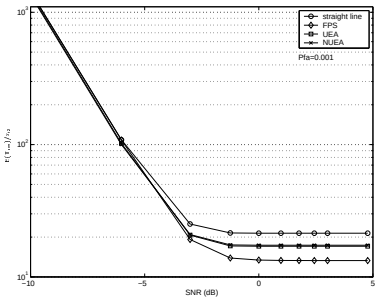

Figure 3: $E(T_{acq})/\tau_{d2}$ as a function of the SNR for a parabola-shaped pdf and various search strategies, $P_{fa} = 10^{-3}$, $\tau_{d1} = 0.3\tau_{d2}$, $k = 20$.

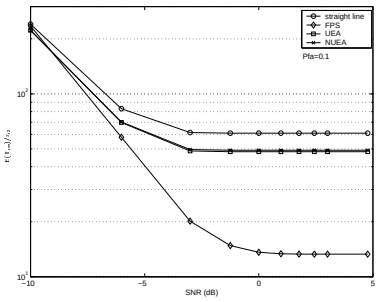

Figure 4: $E(T_{acq})/\tau_{d2}$ as a function of the SNR for a parabola-shaped pdf and various search strategies, $P_{fa} = 10^{-1}$, $\tau_{d1} = 0.3\tau_{d2}$, $k = 20$.

the sense that the variation in the integration time is achieved by allowing the examination interval to consist of a series of fixed short dwell periods (each longer than its predecessor) with a decision being made after each. An extensive analysis of the multiple dwell systems can be found in [4, 8, 9]. The most important multiple dwell search system is the double dwell serial search system (DD), which we will use in order to compare it with the FPS system. The calculation of the mean acquisition time $E(T_{acq})_N$ for the general N-dwell system, can be found in [9] and for $q \gg 1$ is given by:

$$E(T_{acq})_N \approx q\frac{(2-P_D)}{2P_D}\sum_{j=1}^{N}\left[t_j\prod_{i=1}^{j-1}P_{fai} + P_{FA}\tau_p\delta_{jN}\right] \quad (9)$$

where t_j is the dwell time of each of the N dwells, P_{fai} and P_{di} the corresponding false alarm and detection probabilities, $P_{FA} = \prod_{i=1}^{N} P_{fai}$, $P_D = \prod_{i=1}^{N} P_{di}$, τ_p the penalty time and δ_{jN} the well known Kronecker delta function. For the double dwell (DD) system ($N = 2$), equation 9 becomes:

$$E(T_{acq})_2 = q\frac{(2-P_{d1}P_{d2})}{2P_{d1}P_{d2}}[t_1 + t_2P_{fa1} + P_{fa1}P_{fa2}\tau_p] \quad (10)$$

Equation 10 is the same as the one presented in page 782 of [8], in which the penalty time has been set equal to $\tau_p = kt_2$. In order to compare the two systems we will use the following parameters:

- $P_{fa1} = P_{fa2} = P_{fa}$, where P_{fa} is the false alarm probability for the FPS system and P_{fa1}, P_{fa2} are the false alarm probabilities for the first and second dwell of the double dwell system. The corresponding detection probabilities are calculated using equation 8.
- $t_1 = \tau_{d1}$ and $t_2 = \tau_{d2}$ where, τ_{di} denotes the dwell times for the FPS system and t_i the dwell time for the double dwell system. The choice of the dwell times, is a reasonable one for two reasons: (i) since the dwell times of the two systems are the same, we can decide, according to their relative performance, which one makes the best use of the available time resources and (ii) both systems perform better when the first dwell time is much shorter than the second one.

The results of this comparison are summarised in figures 5,6 and 7. Figure 5 depicts the role of the false alarm probabilities. In general, for low false alarm probabilities ($P_{fa} < 10^{-2}$), the FPS system outperforms the double dwell for very low SNRs, while for large SNRs ($SNR > -5$dB) their performance is similar (that is, for a non-optimised fast dwell time τ_{d1} and t_1). For large false alarm probabilities FPS performs better for $SNR > -3$dB, while for lower SNRs the double dwell system results into lower mean acquisition time. The significance of the dwell times is depicted in figure 6. It is shown in [2] that the fast dwell time for the FPS system can be optimised. An optimisation for the double dwell system is also possible but, as far as we know, it has not been explicitly and analytically presented in the literature. Accordingly, the performance of the two systems, greatly depends on the correct choice of the fast/first dwell time. Nevertheless, the optimisation ability of the FPS system is much larger, i.e., the improvement in the mean acquisition time by optimising the fast dwell time of the FPS system is much larger than by optimising the first dwell time of the DD scheme. This is obvious in figure 7 where the $\mu = E(T_{acq})/\tau_{d2}$ is given as a function of the SNR and fast/first dwell time. An optimum τ_{d1} or t_1 exist for both systems (for which the mean acquisition time is minimised), but the minimum achieved by the FPS system is better than that of the double dwell system. This is the reason for which we observe a large improvement in the performance of the FPS system compared to the double dwell system for $\tau_{d1} = 0.1\tau_{d2}$ if figure 6. In this figure, the fast dwell time τ_{d1} is very close to the optimum value and, as a result the performance is rapidly improved.

Figures 8 and 9 depict the role of the parameter k, which determines the length of the penalty time ($\tau_p = k\tau_{d2}$). A combination of a large k and large false alarm probability P_{fa} means that a large part of the required acquisition time is due to false alarm situations. This is the case in figure 8 for

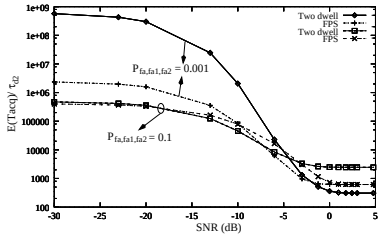

Figure 5: $E(T_{acq})/\tau_{d2}$ as a function of the SNR for two different sets of false alarm probabilities ($\tau_{d1} = 0.3\tau_{d2}$).

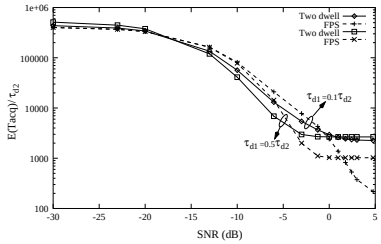

Figure 6: $E(T_{acq})/\tau_{d2}$ as a function of the SNR for two different sets of dwell times (P_{fa}=0.1).

$k = 200$ and $P_{fa} = 0.1$. The FPS system outperforms the DD system for high SNRs (i.e. high detection probabilities) while for lower values DD results into better acquisition times. A very interesting point in figures 8,9 (which is also noticeable in 5) is that *for non-optimum τ_{d1} the mean acquisition time of the FPS system finally converges to a value which only depends on the τ_{d1} and is independent of the false alarm parameters (P_{fa} and k).* This indicates that the FPS system is very robust against false alarms. Given a good SNR, i.e., $SNR > -5$dB at the output of the correlator (i.e., a large P_d), which is feasible for SS systems with good processing gain, the mean acquisition time is almost free of the significant penalty time part. The reason, as explained before, is that if the SNR is high enough the false ranking probability is very small. As a result, the correct cell will be one of the first to be tested during the final search and thus a very small number of wrong cells will ever be examined. Summarising the previous results,

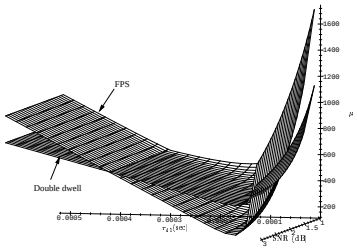

Figure 7: The $\mu = E(T_{acq})/\tau_{d2}$ for the FPS and double dwell system ($P_{fa1} = P_{fa2} = P_{fa} = 0.01$).

we could say that the main differences between the FPS and DD systems can be stated as follows:

- The FPS system allows a large degree of optimisation by controlling the fast dwell time τ_{d1}.
- The DD system performs better than the single dwell because it allows incorrect cells to be quickly discarded. The FPS system moves one step forward by not allowing incorrect cells to be examined, which in turn can result in shorter acquisition times if the τ_{d1} is correctly chosen.

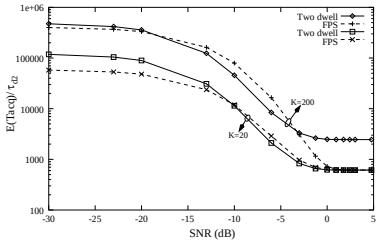

Figure 8: $E(T_{acq})/\tau_{d2}$ as a function of the SNR for two different k and $P_{fa} = 0.1$, $\tau_{d1} = 0.3\tau_{d2}$.

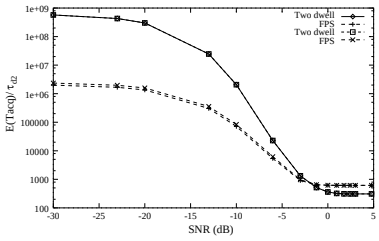

Figure 9: $E(T_{acq})/\tau_{d2}$ as a function of the SNR for two different k (same as before) and $P_{fa} = 0.001$, $\tau_{d1} = 0.3\tau_{d2}$. All symbols are the same with figure 8.

The combination of an FPS mode with a following active acquisition system, is probably a worst case study (at least for Gaussian channels) of the FPS system. The performance of the system will be much better if one of the two or even both stages are implemented using matched filters devices. One possible implementation is depicted in figure 10. The fast search stage is identical to that in figure 1 i.e., an active acquisition system with short dwell time. The cells, which are ranked according to the first search, are subsequently examined using a typical matched filter acquisition system. The matched filter FPS (MF-FPS) system is bound to result into lower mean acquisition time than the original proposed FPS system. The reason is that the final acquisition system is replaced by a passive system which, by definition, gives lower acquisition times.

IV. Conclusions

The performance in terms of the mean acquisition time of a novel PN code acquisition system, that combines a fast preliminary search of the ambiguity area with a simple fixed dwell acquisition system, was discussed. The FPS system is presented in detail in [2] where its performance is compared with

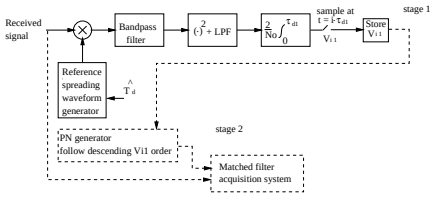

Figure 10: A matched filter implementation of the FPS system.

that of the active single dwell scheme with a uniform *a priori* pdf. It was found, that the FPS scheme outperforms all single dwell systems, even when prior information is provided and suitable search strategies are used. In this study, we considered an active double dwell system in comparison with the FPS scheme. It was shown, that if the fast dwell time is optimised, the FPS scheme will result into significantly improved mean acquisition time. The optimum use of the FPS scheme would be to replace the final active acquisition system with a matched filter. This is a subject of future research.

Acknowledgments

This work was partially supported by the Eugenides Foundation, Greece and by the University of Edinburgh under a postgraduate scholarship. The first-mentioned author would like to express his gratitude. Dr. S. McLaughlin would like to acknowledge the financial support from the Royal Academy.

References

[1] E.C.Posner, "Optimal search procedures," *IEEE transactions on information theory* , pp. 157-160, July 1963.

[2] G.A.Vardoulias and J.H.Dripps and G.J.R.Povey, "A novel PN code acquisition system using a fast preliminary search of the ambiguity area," *submitted to IEEE transactions on communications* .

[3] A.Polydoros and S.Glisic, "Code synchronization:a review of principles and techniques," *IEEE ISSSTA'94* , vol. 1, pp. 115-137, 1994.

[4] M.K.Simon and J.K.Omura and R.A.Scholtz and B.K.Levitt, "Spread spectrum communications handbook," McGraw-Hill , 2nd edition, 1994.

[5] G.A.Vardoulias and G.J.R.Poveyand J.H.Dripps, "On the Doppler Probability Density Function within a Low Earth Orbit Satellite Spot Beam and its Application to the Code Acquisition Procedure," *IEEE Vehicular Technology Conference (VTC) 1999, Fall* , vol. 5, pp. 2711–2715, Sept.1999.

[6] V.M.Jovanovic, "Analysis of strategies for serial search spread spectrum code acquisition-Direct approach," *IEEE trans.comm.*, vol. 36, pp. 1208-1220, Nov.1988.

[7] I.S.Gradshteyn and I.M.Ryzhik, 'Table of integrals, series and products'," Academic Press , 5th edition, 1994.

[8] J.K.Holmes and C.C.Chen, "Acquisition time performance of PN spread spectrum systems," *IEEE trans.comm.*, vol. com-25, pp. 778-784, Aug.1977.

[9] D.M.DiCarlo and C.L.Weber, "Multiple dwell serial search: performance and application to direct sequence code acquisition," *IEEE trans.comm.*, vol. com-31, pp. 650-659, Aug.1983.

References

[1] R. A. Scholtz, "The spread spectrum concept," *IEEE Trans. Comms.*, vol. COM-25, no.8, pp. 748–755, Aug. 1977.

[2] J. K. Holmes, *Coherent spread spectrum systems*. Krieger Publishing Company, 1st ed., 1982.

[3] S. S. Rappaport and D. M. Grieco, "Spread-spectrum signal acquisition:methods and technology," *IEEE Comms.Mag.*, vol. 22, no.6, pp. 6–21, June 1984.

[4] R. Peterson, R. Ziemer, and D. Borth, *Introduction to spread spectrum communications*. Prentice Hall, 1st ed., 1995.

[5] M. K. Simon, J. K. Omura, R. A. Scholtz, and B. K. Levitt, *Spread spectrum communications handbook*. McGraw-Hill, 2 ed., 1994.

[6] "3G TS 25.214v3.2.0 Physical layer procedures-FDD," *UMTS technical specifications*, Mar. 2000.

[7] *http://www.ee.surrey.ac.uk/Personal/L.Wood/*, 1998.

[8] S. W. Golomb, J. R. Davey, I. S. Reed, H. L. V. Trees, and J. J. Stiffler, "Synchronisation," *IEEE Trans. Comms. Systems*, vol. CS-11, no.4, pp. 481–491, Dec. 1963.

[9] S. G. Glisic and P. A. Leppanen, *Wireless communications:TDMA versus CDMA*. Kluwer Academic Publishers, 1 ed., 1997.

[10] C. Gumacos, "Analysis of an optimum sync search procedure," *IEEE Trans. Comms. Systems*, vol. CS-11, pp. 89–99, Mar. 1963.

[11] V. M. Jovanovic, "Analysis of strategies for serial search spread spectrum code acquisition-direct approach," *IEEE Trans. Comms.*, vol. COM-36, no.11, pp. 1208–1220, Nov. 1988.

[12] E. C. Posner, "Optimal search procedures," *IEEE Trans.Inform.Theory*, vol. IT-9, pp. 157–160, July 1963.

[13] A. Weinberg, "Generalized analysis for the evaluation of search strategy effects on PN acquisition performance," *IEEE Trans. Comms.*, vol. COM-31, no.1, pp. 37–49, Jan. 1983.

[14] A. Polydoros and M. K. Simon, "Generalized serial search code acquisition : The equivalent circular state diagram approach," *IEEE Trans. Comms.*, vol. COM-32, no.12, pp. 1260–1268, Dec. 1984.

[15] V. M. Jovanovic, "On the distribution function of the spread spectrum code acquisition time," *IEEE Journal on Selected Areas in Comms.*, vol. 10, no.4, pp. 760–769, May 1992.

[16] "Special issue on spread spectrum," *IEEE Trans. Comms.*, vol. COM-25, no.8, Aug. 1977.

[17] *http://www.its.bldrdoc.gov/*.

[18] A. Polydoros and S. Glisic, "Code synchronization:a review of principles and techniques," *Proceedings of the ISSSTA'94*, vol. 1, pp. 115–137, 1994.

[19] S. Spangenberg, "Receiver architectures for rapid code acquisition in spread spectrum satellite communications," *Internal report, Uni.Edinburgh*, 1998.

[20] S. G. Glisic, "Automatic decision threshold level control(ADTLC) in direct sequence spread spectrum systems based on matched filtering," *IEEE Trans. Comms.*, vol. COM-36, no.4, pp. 519–527, Apr. 1988.

[21] S. G. Glisic, "Automatic decision threshold level control in direct sequence spread spectrum systems," *IEEE Trans. Comms.*, vol. COM-39, no.2, pp. 187–192, Feb. 1991.

[22] N. Cakic, S. Glisic, and D. Krstic, "Instantaneous CFAR algorithm," *Proceedings of the GLOBECOM '90*, vol. 1, pp. 275–279, 1990.

[23] C. J. Kim, T. W. Hwang, H. J. Lee, and H. S. Lee, "Acquisition of PN code with adaptive threshold for DS/SS communications," *Electronic Letters*, vol. 33, no.16, pp. 1352–1354, July 1997.

[24] D. M. Grieco, "The application of charge-coupled-devices to spread spectrum systems," *IEEE Trans. Comms.*, vol. COM-28, no.9, pp. 1693–1705, Sep. 1980.

[25] G. L. Turin, "An introduction to digital matched filters," *Proceedings of the IEEE*, vol. 64, no.7, pp. 1092–1112, July 1976.

[26] Y. T. Su, "Rapid code acquisition algorithms employing PN matched filters," *IEEE Trans. Comms.*, vol. COM-36, no.6, pp. 724–733, June 1988.

[27] R. F. Ormondroyd, "PN code synchronisers for direct sequence spread spectrum systems-a comparative evaluation," *IEE colloquium on synchronisation techniques for radio systems*, pp. 9/1–9/7, 1995.

[28] A. Polydoros and C. L. Weber, "A unified approach to serial search spread spectrum code acquisition-Part II:a matched-filter receiver," *IEEE Trans. Comms.*, vol. COM-32, no.5, pp. 550–560, May 1984.

[29] J. R. Luecke, "Comparison of detection schemes for fast acquisition direct-sequence spread-spectrum receivers," *Proceedings of the MILCOM '89*, vol. 3, pp. 865–869, 1989.

[30] B. B. Ibrahim and A. H. Aghvami, "Direct sequence spread spectrum code acquisition in mobile fading channel using matched filter with reference filtering," *Proceedings of the GLOBECOM '93*, vol. 2, pp. 1085–1089, 1993.

[31] A. Polydoros and C. L. Weber, "A unified approach to serial search spread spectrum code acquisition-Part I : general theory," *IEEE Trans. Comms.*, vol. COM-32, no.5, pp. 542–549, May 1984.

[32] D. M. Dicarlo and C. L. Weber, "Statistical performance of single dwell serial synchronazation systems," *IEEE Trans. Comms.*, vol. COM-28, no.8, pp. 1382–1388, Aug. 1980.

[33] K. V. Ravi and R. F. Ormondroyd, "Simulation performance of a quantized log-likelihood sequential detector for PN code acquisition in the presence of data modulation and doppler-shift," *Proceedings of the MILCOM'91*, vol. 2, pp. 798–803, 1991.

[34] L. Fanucci, "Design of an ASIC for fast signal recognition and code acquisition in DS-SS-CDMA receivers," *Proceedings of the ISSSTA'96*, vol. 1, pp. 37–41, 1996.

[35] C. L. Spillard, S. Spangenberg, and G. J. R. Povey, "A serial-parallel FFT correlator for PN code acquisition from LEO," *Proceedings of the ISSSTA '98*, vol. 2, pp. 446–448, 1998.

[36] G. E. Corazza, "On the MAX/TC criterion for code acquisition and its application to DS-SSMA systems," *IEEE Trans. Comms.*, vol. COM-44, no.9, pp. 1173–1182, Sep. 1996.

[37] M. W. Thompson and S. Dianat, "Non-coherent PN code acquisition in direct sequence spread spectrum systems using a neural network," *Proceedings of the MILCOM '93*, vol. 1, pp. 30–34, 1993.

[38] S. G. Glisic, "Power density spectrum of the product of two time-displaced versions of a maximum length binary pseudonoise signal," *IEEE Trans. Comms.*, vol. COM-31, no.2, pp. 281–286, Feb. 1983.

[39] A. W. Fuxjaeger and R. A. Iltis, "Acquisition of timing and doppler-shift in a direct-sequence spread spectrum system," *IEEE Trans. Comms.*, vol. COM-42, no.10, pp. 2870–2880, Oct. 1994.

[40] J. K. Holmes and C. C. Chen, "Acquisition time performance of PN spread spectrum systems," *IEEE Trans. Comms.*, vol. COM-25, no.8, pp. 778–784, Aug. 1977.

[41] W. J. Hurd, J. I. Statman, and V. A. Vilnrotter, "High dynamic gps receiver using maximum likelihood estimation and frequency tracking," *IEEE Trans.Aerospace and Electronic Systems*, vol. AES-23, no.4, pp. 425–436, July 1987.

[42] U. Cheng, W. J. Hurd, and J. I. Statman, "Spread-spectrum code acquisition in the presence of doppler shift and data modulation," *IEEE Trans. Comms.*, vol. COM-38, no.2, pp. 241–250, Feb. 1990.

[43] L. D. Davisson and P. G. Flikkema, "Fast single-element PN acquisition for the TDRSS MA system," *IEEE Trans. Comms.*, vol. COM-36, no.11, pp. 1226–1235, Nov. 1988.

[44] A. P. Clark and A. Aftelak, "Doppler-shift correction via correlation for a received QPSK signal," *IEE Proceedings*, vol. 137, pt1, no.6, pp. 387–394, Dec. 1990.

[45] S. G. Glisic, T. Poutanec, and W. W. Wu, "New PN code acquisition schemes for LEO satellites," *Proceedings of the ISSSTA'94*, vol. 2, pp. 608–613, 1994.

[46] G. J. R. Povey and J. Talvitie, "Doppler compensation and code acquisition techniques for LEO satellite mobile radio communications," *IEE conf. satellite systems for mobile communications and navigation*, pp. 16–19, May 1996.

[47] R. A. Stirling-Gallacher, A. P. Hulbert, and G. J. R. Povey, "A fast acquisition technique for a direct sequence spread spectrum signal in the presence of a large doppler shift," *Proceedings of the ISSSTA'96*, vol. 1, pp. 156–160, 1996.

[48] S. Kourtis, "Investigation of the mobile terminal optimum operating point in UMTS-FDD synchronisation procedure," *Proceedings of the PIMRC 2000*, vol. 1, pp. 348–352, 2000.

[49] S. Kourtis, "The initial synchronisation procedure in UMTS W-CDMA," *Proceedings of the 4th IEEE Multiaccess Mobility and Teletraffic conference, Venice*, pp. 97–106, Oct. 1999.

[50] S. Kourtis, "Code planning strategy for UMTS-FDD networks," *Proceedings of the VTC'2000-Spring*, vol. 2, pp. 815–819, May 2000.

[51] A. M. Thurston, "Practical acquisition issues for UMTS," *Proceedings of the IEE 3G2000 mobile comm. technologies, London*, pp. 371–375, 2000.

[52] M. G. El-Tarhuni and A. U. Sheikh, "Application of adaptive filtering to direct-sequence spread spectrum code acquisition," *Wireless Personal Communications*, vol. 8, no.2, pp. 185–203, Sep. 1998.

[53] F. Dominique and J. H. Reed, "Simple PN code sequence estimation and synchronisation technique using the constrained hebbian rule," *Electronics Letters*, vol. 33, no.13, pp. 1119–1120, Jan. 1997.

[54] M. Salih and S. Tantaratana, "A closed-loop coherent acquisition scheme for PN sequences using an auxiliary sequence," *IEEE Journal on Selected Areas in Comms.*, vol. 14, no.8, pp. 1653–1659, Oct. 1996.

[55] J. Iinatti and P. Leppanen, "Performance analysis of DS signal code acquisition using the matched filter and the median filter," *Wireless Personal Communications*, vol. 8, no.2, pp. 93–111, Sep. 1998.

[56] M. Eric and M. Obradovic, "Subspace-based joint time-delay and frequency-shift estimation in asynchronous DS-CDMA systems," *Electronics Letters*, vol. 33, no.14, July 1997.

[57] E. G. Strom, S. Parkvall, S. L. Miller, and B. E. Ottersten, "DS-CDMA synchronisation in time-varying fading channels," *IEEE Journal on Selected Areas in Comms.*, vol. 14, no.8, pp. 1636–1642, Oct. 1996.

[58] K. K. Chawla and D. V. Sarwate, "Acquisition of PN sequences in chips synchronous DS/SS systems using a random sequence model and the SPRT," *IEEE Trans. Comms.*, vol. COM-42, no.6, pp. 2325–2334, June 1994.

[59] Y. Ikai, M. Katayama, T. Yamazato, and A. Ogawa, "A new acquisition scheme of a ds/ss signal with transmit and receive antenna diversity," *Proceedings of the ICC'99, Vancouver, Canada*, pp. 1256–1261, 1999.

[60] M. E. Tarhuni and M. A. Landolsi, "The effects of chip waveform shaping on the synchronisation performance of DS-CDMA signals," *Proceedings of the VTC'99*, vol. 3, pp. 2427–2431, 1999.

[61] G. Wetzeker and F. Jondral, "Incoherent acquisition of DSSS in presence of doppler shifts," *IEE conf. satellite systems for mobile communications and navigation*, vol. 1, pp. 166–170, May 1996.

[62] S. S. Soliman and R. A. Scholtz, "Synchronization over fading dispersive channels," *IEEE Trans. Comms.*, vol. COM-36, no.4, pp. 499–505, Apr. 1988.

[63] H. S. Lee, H. S. Oh, and C. E. Kang, "Code acquisition for the DS-CDMA RAKE receiver in a multipath fading channel," *Proceedings of the IEEE Singapore International Conference on Networks, 1995, Theme: Electrotechnology 2000: Communications and Networks*, pp. 215–219, 1995.

[64] E. R. Adams, M. Gouda, and P. C. J. Hill, "Detection and characterisation of DS/SS signals using higher order correlation," *Proceedings of the ISSSTA'96*, vol. 1, pp. 27–31, 1996.

[65] A. Kajackas, "On synchronization of communication networks with varying channel delays," *IEEE Trans. Comms.*, vol. COM-28, no.8, pp. 1267–1268, Aug. 1980.

[66] F. D. Gardner, "Self-noise in synchronizers," *IEEE Trans. Comms.*, vol. COM-28, no.8, pp. 1159–1163, Aug. 1980.

[67] T. L. Ngoc and K. Feher, "A digital approach to symbol timing recovery systems," *IEEE Trans. Comms.*, vol. COM-28, no.12, pp. 1993–1999, Dec. 1980.

[68] Y. A. Miyagaki, N. Morinaga, and T. Namekawa, "Double symbol error rates of M-ary DPSK in a satellite-aircraft multipath channel," *IEEE Trans. Comms.*, vol. COM-31, no.12, pp. 1285–1289, Dec. 1983.

[69] G. Bilardi, R. Padovani, and G. L. Pierobon, "Spectral analysis of functions of markov chains with applications," *IEEE Trans. Comms.*, vol. COM-31, no.7, pp. 853–860, July 1983.

[70] C. R. Cahn, D. K. Leimer, C. L. Marsh, F. J. Huntowski, and G. L. Larue, "Software implementation of a PN spread spectrum receiver to accommodate dynamics," *IEEE Trans. Comms.*, vol. COM-25, no.8, pp. 832–839, Aug. 1977.

[71] S. Burley, M. Darnell, and P. Clark, "Enhanced PN code tracking and detection using wavelet packet denoising," *Proceedings of IEEE international symposium on time-frequency and time-scale analysis*, pp. 365–368, 1998.

[72] R. D. Gaudenzi, F. Giannetti, and M. Luise, "Signal recognition and code acquisition in CDMA mobile packet communications," *IEEE Trans. Veh. Tech.*, vol. VT-47, no.1, pp. 196–208, Feb. 1998.

[73] F. Vatalaro, G. E. Corazza, C. Caini, and C. Ferrarelli, "Analysis of LEO,MEO and GEO global mobile satellite systems in the presence of interference and fading," *IEEE Journal on Selected Areas in Comms.*, vol. 13, no.2, pp. 291–300, Feb. 1995.

[74] S. G. Glisic, R. Pickholtz, and W. Wu, "Issues in CDMA applications for mobile LEO satellite communications," *IEE conf. satellite systems for mobile communications and navigation*, vol. 3, pp. 913–919, May 1996.

[75] K. P. Phillips, "An overview of propagation factors influencing the design of mobile satellite communication systems," *Electronics & Communication Engineering Journal*, vol. 9, no.6, pp. 281–288, Dec. 1997.

[76] G. E. Corazza and F. Vatalaro, "A statistical model for land mobile satellite channels and its application to nongeostationary orbit system," *IEEE Trans. Veh. Tech.*, vol. VT-43, no.3, pp. 738–742, Aug. 1994.

[77] I. K. Hwang and L. Kurz, "Digital data transmission over nonlinear satellite channels," *IEEE Trans. Comms.*, vol. COM-41, no.11, pp. 1694–1702, Nov. 1993.

[78] L. M. Davis, I. B. Collings, and R. J. Evans, "Estimation of LEO satellites channels," *Proceedings of the ICICS'97 Singapore*, vol. 1, pp. 15–19, Sep. 1997.

[79] Y. T. Su and R. C. Wu, "Frequency acquisition and tracking for mobile LEO satellite communications," *Proceedings of the VTC'97*, vol. 3, pp. 1738–1742, 1997.

[80] J. R. Pierce and R. Kompfner, "Transoceanic communication by means of satellite," *Proceedings of the IRE*, vol. 85, no.6, pp. 372–380, Mar. 1959.

[81] L. Wood, "Network performance of non-geostationary constellations equipped with intersatellite links," *MSc thesis, Univ.Surrey*, 1995.

[82] M. A. Sturza, "The Teledesic satellite system," *IEEE national telesystems conference*, pp. 123–126, 1994.

[83] B. Miller, "Satellites free mobile phone," *IEEE Spectrum*, vol. 35, no.3, pp. 26–35, Mar. 1998.

[84] A. Azzarelli and R. Manohar, "Visibility of non-GSO satellites from a terrestrial station and applications to inter-system interference," *IEE conf. satellite systems for mobile communications and navigation*, pp. 106–109, May 1996.

[85] J. E. H. I Ali, N Al-Dhahir, "Predicting the visibility of LEO satellites," *IEEE Trans. Aerospace and Electronic Systems*, vol. 35, no.4, pp. 1183–1190, Oct. 1999.

[86] J. E. H. I Ali, N Al-Dhahir, "Doppler characterization for LEO satellites," *IEEE Trans. Comms.*, vol. COM-46, no.3, pp. 309–313, Mar. 1998.

[87] J. Restrepo and G. Maral, "Analysis and comparison of satellite constellation configurations for global single permanent visibility," *IEE conf. satellite systems for mobile communications and navigation*, pp. 102–105, May 1996.

[88] W. Zhao, R. Tafazolli, and B. G. Evans, "Positioning assisted inter-segment handover for integrated GSM-satellite mobile system," *IEE conf. satellite systems for mobile communications and navigation*, pp. 124–128, May 1996.

[89] K. Narenthiran, R. Tafazolli, and B. G. Evans, "Evaluation of location tracking schemes for satellite umts," *Proceedings of the IEE 3G2000 mobile comm. technologies, London*, pp. 381–386, 2000.

[90] G. R. Cooper and C. D. McGillem, *Modern communications and spread spectrum*. McGraw-Hill, 1 ed., 1986.

[91] R. C. Dixon, *Spread spectrum systems with commercial applications*. Wiley interscience, 3 ed., 1994.

[92] H. Meyr, M. Moeneclapy, and S. Fechtel, *Digital communication receivers*. Wiley interscience, 1 ed., 1998.

[93] S. Haykin, *Communication systems*. Papasotiriou, 1 Greek ed., 1994.

[94] J. Proakis and M. Salehi, *Communication systems engineering*. Prentice-Hall, 1 ed., 1994.

[95] J. Proakis and D. G. Manolakis, *Digital signal processing*. Maxwell Macmillan internatinal editions, 2 ed., 1992.

[96] A. V. Oppenheim and R. Schafer, *Digital signal processing*. Prentice-Hall, 1 ed., 1975.

[97] A. Papoulis, *Probability,random variables and stochastic processes*. McGraw-Hill, 3 ed., 1991.

[98] L. F. Heinrich, *Correlation techniques*. Iliffe books ltd, 1 ed., 1967.

[99] G. Maral and M. Bousquet, *Satellite communication systems*. John Wiley and sons, 2 ed., 1993.

[100] M. Richharia, *Satellite communication systems design principles*. MacMillan press ltd, 1 ed., 1995.

[101] G. Gordon and W. L. Morgan, *Principles of communication satellites*. John Wiley and sons, 1 ed., 1993.

[102] I. A. Glover and P. M. Grant, *Digital communications*. Prentice-Hall, 1 ed., 1997.

[103] F. J. Tischer, *Basic theory of space communications*. D Van Nostrand company,INC, 1 ed., 1965.

[104] G. Maral, *VSAT networks*. John Wiley and sons, 1 ed., 1996.

[105] R. E. Blahut, *Principles and practice of information theory*. Addison-Wesley, 1 ed., 1987.

[106] A. Leick, *GPS satellite surveying*. John Wiley and sons, 2nd ed., 1995.

[107] R. Deutch, *Orbital dynamics of space vehicles*. Prentice Hall, 1 ed., 1963.

[108] "http://atlantic.evsc.virginia.edu/," *web page on earth rotation*.

[109] "http://hpiers.obspm.fr/," *web page on earth rotation*.

[110] S. J. Mason, "Feedback theory-some properties of signal flow graphs," *Proceedings of the IRE*, vol. 41, no.9, pp. 1144–1156, Sep. 1953.

[111] S. J. Mason, "Feedback theory-further properties of signal flow graphs," *Proceedings of the IRE*, vol. 44, no.7, pp. 920–926, July 1956.

[112] D. M. DiCarlo and C. L. Weber, "Multiple dwell serial search: performance and application to direct sequence code acquisition," *IEEE Trans. Comms.*, vol. COM-31, no.5, pp. 650–659, May 1983.

[113] H. Meyr and G. Polzer, "Performance analysis for general pn spread spectrum acquisition techniques," *IEEE Trans. Comms.*, vol. COM-31, no.12, pp. 1317–1319, Dec. 1983.

[114] H. Urkowitz, "Energy detection of unknown deterministic signals," *Proceedings of the IEEE*, vol. 55, no.4, pp. 523–531, Apr. 1967.

[115] M. Abramowitz and I. A. Stegun, *Handbook of mathematical functions, with formulas, graphs and mathematical tables*. Dover publications, 1972.

[116] V. M. Jovanovic and E. S. Sousa, "Analysis of non-coherent correlation in DS/BPSK spread spectrum acquisition," *IEEE Trans. Comms.*, vol. COM-43, no.2/3/4, pp. 565–573, Feb./Mar./Apr. 1995.

[117] I. S. Gradshteyn and I. M. Ryzhik, *Table of integrals, series and products*. Academic Press, 5th ed., 1994.

[118] J. H. Lindholm, "An analysis of the pseudo-randomness properties of subsequences of long m-sequences," *IEEE Trans.Inform.Theory*, vol. IT-14, no.4, pp. 569–576, July 1968.

[119] M. G. El-Tarhuni and A. U. Sheikh, "Adaptive synchronisation for spread spectrum systems," *Proceedings of the VTC'96*, vol. 1, pp. 170–174, 1996.

[120] G. E. Corazza and A. Polydoros, "Code acquisition in CDMA cellular mobile networks, part I," *Proceedings of the ISSSTA'98*, vol. 2, pp. 454–458, Sep. 1998.

[121] E. Sourour and S. C. Gupta, "Direct-sequence spread-spectrum parallel acquisition in a fading mobile channel," *IEEE Trans. Comms.*, vol. COM-38, no.7, pp. 992–998, July 1990.

[122] E. Sourour and S. C. Gupta, "Direct-sequence spread-spectrum serial acquisition in a nonselective and frequency selective Rician fading channel," *Proceedings of the MILCOM '90*, vol. 1, pp. 171–175, 1990.

[123] E. Sourour and S. C. Gupta, "Direct-sequence spread-spectrum parallel acquisition in nonselective and frequency selective Rician fading channel," *IEEE Journal on Selected Areas in Comms.*, vol. 10, no.3, pp. 535–544, Apr. 1992.

[124] H. Moon, "Performance of double dwell acquisition with continuous integration detector in a Rician fading channel," *Proceedings of the ISSSTA'98*, pp. 111–115, Sep. 1998.

[125] J. Simsa, "On DS-SS code acquisition time probability distribution-serial search by multiple dwell detector in fading channel," *Proceedings of the ISSSTA'98*, vol. 2, pp. 464–468, Sep. 1998.

[126] J. Iinatti, "Performance of DS code acquisition in static and fading multipath channel," *submitted to IEE Proc.Comms.*, personal communication with the author 2000.

[127] J. Iinatti, "Mean acquisition time of DS code synchronisation in fixed multipath channel," *Proceedings of the ISSSTA'98*, vol. 1, pp. 116–120, Sep. 1998.

[128] N. D. Wilson, S. S. Rappaport, and M. M. Vasudenav, "Rapid acquisition scheme for spread spectrum radio in a fading environment," *IEE Proceedings*, vol. 135, Pt.F, no.1, pp. 95–104, Feb. 1988.

[129] Y. T. Su and R. C. Wu, "Code acquisition in a class of time-varying channels," *Proceedings of the VTC'98*, vol. 3, pp. 2431–2435, 1998.

[130] M. G. El-Tarhuni and A. U. Sheikh, "Code acquisition of DS/SS signals in fading channels using an lms adaptive filter," *IEEE Communications Letters*, vol. 2, no.4, pp. 85–88, Apr. 1998.

[131] M. G. El-Tarhuni and A. U. Sheikh, "Adaptive filtering based DS/SS code acquisition in frequency selective and flat Rayleigh fading channels," *Proceedings of the VTC'97*, pp. 1624–1628, 1997.

[132] G. Wetzker, C. Sieborger, U. Kaage, and F. Jondral, "Maximum likelihood DSSS code acquisition in the presence of multipath propagation, Doppler shift and data modulation," *Proceedings of the ISSSTA'98*, vol. 2, pp. 441–445, Sep. 1998.

[133] M. Ardebilipour and R. Tafazolli, "A novel implication of reverse link acquisition," *Proceedings of the IEE 3G2000 mobile comm. technologies, London*, pp. 367–370, 2000.

[134] G. E. Corazza and V. Degli-Esposti, "Acquisition of synchronism in direct sequence CDMA mobile networks," *Proceedings of the VTC'94*, vol. 1, pp. 68–72, 1994.

[135] Y. H. You, T. H. Moon, J. H. Kim, and C. E. Kang, "Threshold decision technique for direct sequence code synchronisation in a fading mobile channel," *IEE Proc.Comms.*, vol. 144, no.3, pp. 155–160, June 1997.

[136] H. D. Schotten, H. Elders-Boll, and A. Busboom, "Optimisation of spreading sequences for DS-CDMA systems and frequency selective fading channels," *Proceedings of the ISSSTA'98*, vol. 1, pp. 33–37, Sep. 1998.

[137] E. Sourour, G. E. Bottomley, and R. Ramesh, "Direct sequence spread spectrum acquisition with sample accumulation in fading channels," *Proceedings of the VTC'99*, vol. 4, pp. 2198–2202, 1999.

[138] H. S. Lee, H. S. Oh, and C. E. Kang, "Code acquisition for the DS-CDMA RAKE receiver in a multipath fading channel," *Proceedings of the IEEE Singapore international conference on networks and information engineering*, pp. 215–219, 1995.

[139] G. L. Turin, "Introduction to spread spectrum antimultipath techniques and their application to urban digital radio," *Proceedings of the IEEE*, vol. 68, no.3, pp. 328–353, Mar. 1980.

[140] R. L. Pickholtz, D. L. Schilling, and L. B. Milstein, "Theory of spread-spectrum communications-A tutorial," *IEEE Trans. Comms.*, vol. COM-30, no.5, pp. 855–884, May 1982.

[141] B. Sklar, "Rayleigh fading channel in mobile digital communication systems part I and part II," *IEEE Comms.Mag.*, vol. 35, no.9, pp. 136–155, Sep. 1997.

[142] M. Patzold, U. Killat, F. Laue, and Y. Li, "On the statistical properties of deterministic simulation models for mobile fading channels," *IEEE Trans. Veh. Tech.*, vol. VT-47, no.1, pp. 254–269, Feb. 1998.

[143] K. Borsuk, *Multidimensional analytic geometry*. Polish Scientific Publishers, 1 ed., 1969.

[144] D. M. Y. Sommerville, *Analytical geometry of three dimensions*. Cambridge University Press, 1st ed., 1934.

[145] R. Bix, *Topics in geometry*. Academic Press, 1st ed., 1994.

[146] J. B. Fraleigh, *Calculus with analytic geometry*. Addison-Wesley, 2nd ed., 1985.

[147] L. A. Pipes, *Matrix Methods for engineering*. Prentice-Hall, 1st ed., 1963.